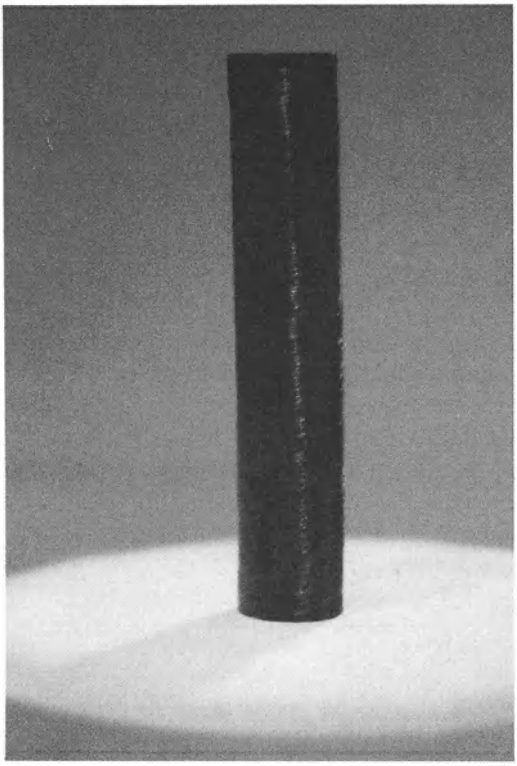

Fig. 4.20 Filament-wound carbon–carbon tube.

precursors. While some attention has been given to the use of thermoplastics (such as PEEK) the majority of work has been carried out with thermosetting systems.

For the fabrication of carbon–carbon the resin should give a high carbon yield on pyrolysis, exhibit low shrinkage and cure rapidly at low temperature (without the evolution of volatiles). It should also be possible to prepare prepreg that exhibits good tack and drape properties from the resin.

Among the commercial high-temperature polymer systems available polyimide has received the most attention as a possible carbon source. As with phenol/formaldehyde and furan resins, extensive data on the properties and processing of polyimides exist. Burger *et al.* [20] prepared carbon–carbon using a series of polyimides as matrix precursors. The polymers had carbon yields of approximately 60% but exhibited high shrinkage and had poor plastic flow on carbonization. The mechanical properties of the polyimide-derived composites were only slightly superior to those prepared from a pitch binder. Generally, polyimides have not been

widely used for production of carbon–carbon because of a combination of high costs and problems associated with their processing such as the use of non-volatile aggressive solvents and evolution of volatiles during polymerization.

Poly (*p*-phenylene) has long been recognized as one of the most stable of organic structures, while it possesses an extremely high carbon content (95%). Numerous attempts to prepare composites from polyphenylene have been made but little success has been achieved as the material is an infusible powder that is insoluble in known solvents. Even if a composite could be prepared, the absence of a means of cross-linking the polymer chains results in the loss of oligomeric phenylene units on carbonization. This leads to a much reduced carbon yield (*c.* 72%) over the theoretical when pyrolysed at atmospheric pressure [60].

Recently studies have been concentrated on the use of soluble precursors that can be easily processed, then converted to polyphenylene *in situ* [61].

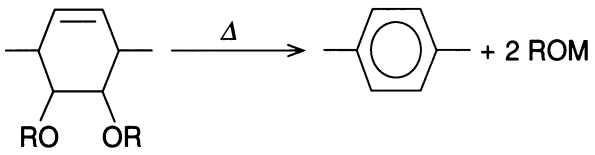

While this approach allows the preparation of prepreg it suffers from a number of drawbacks. The prepolymer is only soluble in high boiling solvents that are difficult to remove. The decomposition to give polyphenylene proceeds at low temperature but generates volatile by-products. In common with previous polyphenylenes the lack of a cross-linking mechanism results in carbon yields of *c.* 70% while the precursor polymer is at present only available on a small scale at a high cost.

Oligomers containing the acetylenic (ethynyl) group (–C≡C–) have recently been the subject of considerable research [62]. These materials can be cured thermally to give cross-linked products having good physical and mechanical properties, coupled with good solvent and moisture resistance. A key feature of acetylene-containing systems is that curing proceeds without the evolution of volatiles, thus making the fabrication of thick void-free laminates considerably easier. A number of efforts to utilize acetylene containing reins as carbon–carbon matrix precursors have been made. These have usually consisted of acetylene-substituted benzenes or oligomeric materials derived from them. Some of the more common routes used to prepare acetylene-containing materials are as follows:

1. from an aryl acetyl compound by treatment with the Vilsmeyer reagent followed by basic cleavage;
2. from olefins by a halogenation–dehydrohalogenation procedure;
3. from an aryl acetyl compound by a halogenation–dehydrohalogenation strategy;

4. from an aryl halide via a palladium–copper catalysed coupling reaction with acetylene.

All of these methods have one or more limitations associated with them. Vilsmeyer chemistry is extremely sensitive to reaction conditions and has often proved difficult to scale up. Both this route and the reactions in (3) frequently give poor yields. Method (2) not only assumes the aryl olefin is readily available but also involves an elimination step where the choice of base and reaction conditions can be critical. The first three methods all tend to produce tar-like materials along with the desired acetylenic compound. These are usually separated by distillation, although aryl acetylenes can decompose explosively at elevated temperatures.

The coupling reaction in (4) is usually carried out with a mono-protected acetylene, with the protecting group being subsequently removed. The main drawbacks to this route are the expense of the catalyst and the starting aryl halides, difficulties in the removal of the protecting groups and problems in the removal of final traces of catalyst. A residual catalyst has a detrimental effect on the long-term thermo-oxidative stability of the resin.

Of the resins used as carbon precursors most work was carried out with so-called H-Resins produced by Hercules. These consisted of acetylene-terminated oligomers derived from diethynyl benzoene such as (X) [63].

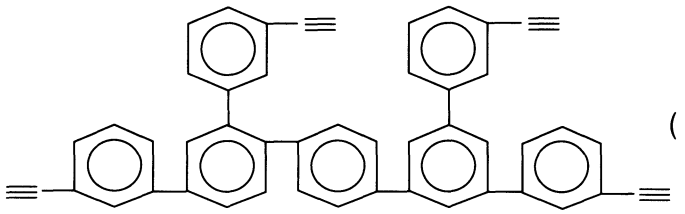

(X)

These resins have very high carbon contents which on curing give a highly cross-linked solid with a carbon yield of *c.* 80%. Despite these favourable properties H-Resins were withdrawn due to a combination of processing difficulties (H-Resins consisted of a fine powder that proved difficult to prepreg) and high cost.

Subsequent to the withdrawal of H-Resins sporadic attempts to develop a carbon precursor based on acetylene resins have been reported.

The use of low-melting diethynyl aromatic compounds of general formula (Y) was described by workers at Hughes Aircraft [64].

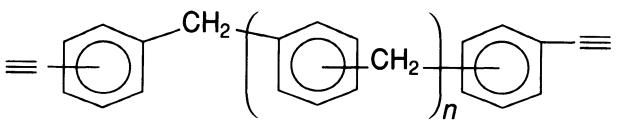

(Y)

These are low-viscosity melts that can easily impregnate fibrous preforms and then undergo rapid polymerization on curing. In the case of 4,4′-diethynyldiphenylmethane (Y, n = 0) the carbon yield was reported as 91%.

As the carbon obtained from acetylene resins is derived from a thermoset it usually exhibits only short-range order (glassy, isotropic carbon). The preparation of 'graphitizable' carbon from acetylenic materials has been described by Bilow [65]. This used a low-melting mixture of diethynyl benzene and ethynyl pyrene which could be polymerized in a controlled manner (without risk of a violent exotherm) at moderate pressure, while still retaining a high carbon yield.

Most recently, Hyperion Catalysis International have introduced a carbon precursor resin. Little detailed information is available but it appears to be an acetylene-containing polyphenylene.

Despite the wide range of resins available, no acetylenic materials have gained wide acceptance as carbon precursors. Problems such as lack of prepreggability, highly exothermic cure reactions, porosity and type of carbon microstructure generated are all potentially soluble, but as yet no cost-competitive system has emerged. The methods of synthesis of acetylene groups described above (along with other more esoteric routes) [66] all suffer from the use of either expensive starting materials or reagents, poor yields or multi-step procedures. Many of the routes are difficult to scale up for bulk resin production.

In conclusion, while none of the 'exotic' resins described above can yet fulfil all the requirements of a carbon matrix precursor the highly desirable prospect of reducing carbon–carbon fabrication costs via a high char precursor will ensure continued research in this area.

REFERENCES

1. Kobayashi, K., Sugawara, S., Toyoda, S. and Honda, N. (1968) *Carbon*, **6**, 359.
2. Mackay, H. A. (1970) *Carbon*, **8**, 517.
3. McAllister, L. E. and Taverna, A. R. (1971) *Proc. 10th Biennial Conf. on Carbon*, Bethlehem, Pa, Paper no. FC-40.
4. Lewis, J. C., Redfern, B. and Cowlard, F. C. (1963) *Solid State Electronics*, **6**, 251.
5. Cowlard, F. C. (1970) *Design Eng.*, March, 49.
6. Bokros, J. C., Atkins, R. J., Shim, H.S., Hanbold, A. D. and Agarwal, N.K. (1976) Carbon in prosthetic devices, in *Petroleum Derived Carbons* (eds M. L. Deviney and T. M. O'Grady) Chem. Soc., Washington DC, p. 237.
7. Kaae, J. L. (1975) *Carbon*, **13**, 246.
8. Kaae, J. L. (1971) *J. Nucl. Mat.*, **38**, 42.
9. Yamada, S. (1968) *A Review of Glass-like Carbons*, Battelle Memorial Institute, Columbus, Ohio.

10. Kawarmura, K. and Jenkins, G. M. (1972) *J. Mat. Sci.*, **7**, 1099.
11. Kaae, J. L. (1972) *J. Biomed. Mat. Res.*, **6**, 279.
12. Stanitski, C. L. and Mooney, V. (1973) *J. Biomed. Mat. Res.*, **7**, 97.
13. Savage, G. M. (1985) PhD thesis, Univ. London.
14. Cowlard, F. C. and Lewis, J. C. (1967) *J. Mat. Sci.*, **2**, 507.
15. Madorsky, S. L. J. (1953) *Res. Nat. Bur. Stds*, **51**, 327.
16. Mackay, H. A. (1969) *Sandia Labs Report, no. SC-RR-68-651.*
17. Kotlensky, W. V. (1973) *Chem. Phys. Carbon*, **9**, 173.
18. Fitzer, E. and Gkogkdis, A. (1986) in *Petroleum-derived Carbons ACS Symp Se no. 303* (eds J. C. Bacha, J. W. Newman and J. L. White, Am. Chem. Soc., Washington, DC. p. 347.
19. Fitzer, E., Heym, M. and Karlisch, K. (1974) *Proc. 4th Lond. Int. Conf. on Carbon*, p. 172.
20. Burger, A., Fitzer, E., Heym, M. and Terwiesch, B. (1975) *Carbon*, **13**, 149.
21. Jenkins, G. M. and Kawamura, K. (1976) *Polymeric Carbons, Carbon Fibre, Glass and Char*, Cambridge Univ. Press.
22. Lum, R., Wilkins, C. W., Robbins, M., Lyons, A. M. and Jones, R. P. (1983) *Carbon*, **21**(2), 111.
23. Conley, R. T. (1967) *J. Macromol. Sci.*, **A1**, 81.
24. Kumar, A. Kulshershtha, A. K. and Gupta, S. K. (1980) *Polymer*, **21**, 317.
25. Zinke, A. (1951) *J. App. Chem.*, **1**, 257.
26. Ouchi, K. and Honda, H. (1956) *J. Chem. Soc. Jap.*, **77**, 147.
27. Ouchi, K. and Honda, H. (1959) *Fuel (London)*, **38**, 429.
28. Ouchi, K. (1966) *Carbon*, **4**, 59.
29. Fitzer, E., Schafer, W. and Yamada, S. (1969) *Carbon*, **7**, 643.
30. Billmeyer, F. W. Jr (1970) *Text Book of Polymer Science*, 2nd edn, Wiley-Interscience, New York, p. 486.
31. The Quaker Oats Company, *Technical Bulletin 131-A.*
32. Delmonts, J. (1969) Furan resins in *Modern Plastics Encyclopedia*, McGraw-Hill, New York, p. 138.
33. Downing, P. A. (1978) *The Chemical Engineer*, April, 272.
34. Dunlop, A. P. and Reineck, E. A. (1947) *Proc. Tech. Conf. Am. Chem. Soc., Chicago Sect.*, North Western Univ., 24 Jan.
35. The Quaker Oats Company, *Technical Bulletin 205-B.*
36. Madorsky, S. L. J. (1964) *Thermal Degradation of Organic Polymers*, Interscience, New York.
37. Fitzer, E. and Schafer, W. (1970) *Carbon*, **8**, 597.
38. Ozanne, N. (1968) PhD thesis, Univ. Grenoble.
39. O'Neill, H. J., Boquist, G. W., Putcher, R. E. and Griffith, J. S. (1964) *Wadd Tr. 81–72*, Vol. XL.
40. Braun, W. (1970) PhD thesis, Univ. Karlsruhe.
41. Yamada, S., Saks, H. and Ishi, T. (1965) *Carbon*, **3**, 253.
42. Delmonte, J. (1981) *Technology of Carbon and Graphite Fibre Composites*, Van Nostrand Reinhold, New York.
43. Manocha, L. M. (1982) *J. Mat. Sci.*, **17**, 3039.
44. Fitzer, E., Geigl, K. H. and Huettner, W. (1980) *Carbon*, **18**, 265.
45. Manocha, L. M., Yasuda, E., Tanabe, Y. and Kimura, S. (1988) *Carbon*, **26**, 333.
46. Bradshaw, W. G. and Vidoz, A. E. (1978) *Am. Ceram. Soc. Bull.*, **57**, 193.

47. Boyne, L. (1974) *Proc. 4th Lond. Int. Carbon and Graphite Conf.*, p. 215.
48. Manocha, L. M. (1988) *Composites*, 19 (4), 311.
49. Kimura, S., Yasuda, E., Tanaka, H. and Yamada, S. (1975) *J. Ceram. Soc. Jap.*, **83**, 122.
50. Hishiyama, Y., Inagaki, M., Kimura, S. and Yamada, S. (1974) *Carbon*, **12**, 249.
51. Kamiya, K. and Inagaki, M. (1973) *Carbon*, **11**, 429.
52. Noda, T. and Kato, H. (1965) *Carbon*, **3**, 289.
53. Kamya, K., Inagaki, M., Mizutani, M. and Noda, T. (1968) *Bull. Chem. Soc. Jap.*, **41**, 2169.
54. Nakamura, S., Ishii, T. and Yamada, S. (1964) *Proc. Symp. on Carbon*, Tokyo.
55. Saxena, R. R. and Bragg, R. H. (1978) *Carbon*, **16**, 373.
56. Yasuda, E., Kimura, S. and Shibusa, Y. (1980) *Trans. Jap. Soc. Comp. Mat.*, **6**, 14.
57. Payne, R. S., von Bradsky, G., Gray, G. and Savage, G. M. (1990) *Proc. Int. Conf. Adv. in Elec. Mic.*, Seattle., p. 1024.
58. Agarwol, B. D. and Broutman, L. J. (1980) *Analysis and Performance of Fibre Composites*, Wiley, New York.
59. Freeman, W. T. and Stein, B. A. (1985) *Aerospace America*, **44**, Oct. p. 44.
60. Fewell, L. (1976) *Chromatog. Sci.*, **14**, 564.
61. Ballard, D. G. H., Courtis, A., Shirley, I. M. and Taylor, S. C. (1983) *J. Chem. Soc. Chem. Commun.*, 954.
62. Hergenrother, P. (1985) in *Encyclopedia of Polymer Science and Engineering*, **1**, 2nd edn, Wiley, New York p. 61.
63. Fitzer, E. (1987) *Carbon*, **25**, 163.
64. Austin, W. B. and Bilow, N. US patent, 4,284,834.
65. Bilow, N. US patent, 4,369,297.
66. Anderson, C. US patent, 4,665,246.

Thermoplastic Matrix Precursors

5

5.1 INTRODUCTION

It has been discussed, thus far, how the fabrication of carbon–carbon composites is achieved by the impregnation of fibre tows, weaves or skeletons (3-D structures or felts) with thermosetting resins or by chemical vapour infiltration with gaseous hydrocarbons. All of the processes presently practised are slow and expensive, and fail to exploit fully the strength of the reinforcing fibres [1]. Vapour infiltration methods require low reaction rates to maintain a uniform deposition throughout a porous body.

The resin-based process, on the other hand, requires a number of cycles of impregnation and carbonization to attain useful levels of density because the carbon yield is limited and/or the matrix may be exuded, in part, by pyrolysis. Carbon–carbon components are used in critical applications where no other material can serve, but serious constraints of cost, processing time and reliability of manufacture limit their use in other systems for which their properties are also well suited.

A great deal of work has been carried out to investigate the suitability of pitches, derived from coal tar or petroleum, and polyaromatic thermoplastic resins as matrix precursors. The aim is to realize the advantages of high carbon yield and ease of graphitizability characteristic of these materials to achieve lower processing costs. Upon pyrolysis, aromatic polymerization drives the majority of pitches through a liquid crystalline state known as the 'mesophase' in which the graphitizability of the coke is established by parallel alignment of the large aromatic molecules [2]. Pitch-based carbons are thus almost unique among structural materials in forming their microstructures by liquid crystal mechanisms [3–5]. The only other notable structural material formed via a liquid crystal precursor are 'Kevlar' polyaramid fibres manufactured by Du Pont [6].

Table 5.1 Typical coal-tar distillation data

Product	*Boiling range* (°C)	*Weight* (%)
Light oil	Below 200	1
Naphthalene oil	200–230	12
Creosote oil	230–300	6
Anthracene oil	Above 300	20
Pitch	Residue	61

5.2 PITCH

The use of pitches as matrix precursors in carbon–carbon composites is an extension of the technology used in the graphite electrode processing industry. A large data base, covering impregnation, carbonization and graphitization of both coal-tar and petroleum pitches, is therefore readily available. Pitches have a low softening point, low melt viscosity, high carbon yield and tend to form graphitic carbon structures. Pitches used as carbon–carbon precursors are a refined oligomeric mixture of polynuclear aromatic hydrocarbons which are thermoplastic in behaviour.

5.2.1 Coal-tar pitch

Coal-tar is a by-product of the coking of bituminous coals to produce cokes. Metallurgical cokes are produced at high temperatures (900–1100 °C) while low temperatures (≈600 °C) yield domestic smokeless fuels. The low-temperature process gives a smaller amount of tar than the high-temperature process. Pitch is obtained from the coal tar by distillation and heat treatment processes. Typical coal-tar distillation data are given in Table 5.1.

Pitch is the residue which follows the removal of the heavy (creosote or anthracene) oil fractions. Pitches are complex mixtures containing many different individual organic compounds, and the precise compositions and properties vary according to the source of tar and the method of removal of low molecular weight fractions. Smith *et al.* [7] report that roughly two-thirds of the compounds so far isolated from coal-tar pitch are aromatic, the remainder being heterocyclic. Many of the compounds are substituted, with the methyl group being the most prevalent. The great majority of the coal-tar pitch components contain between three and six rings, with boiling-points in the range 340–550 °C. Coal-tar pitch can therefore be considered to consist predominantly of carbon and hydrogen with small amounts of nitrogen, oxygen and sulphur. An estimate of the degree of aromacity within the pitch may be made from its C/H ratio.

Table 5.2 Characteristics of typical carbon matrix precursor pitches from three different feedstocks

		Petroleum Pitch		*Coal-tar pitch*	
Property	*Steam cracker tar*	*1*	*2*	*1*	*2*
Softening point (°C)	110	117	110	101	113
Coking value (wt% at 550 °C)	52	54	56	57	60
Aromatic C (%)	78	82	80	89	88
C/H ratio	1.37	1.44	1.57	1.77	1.76

5.2.2 Petroleum pitch

Petroleum pitch is a readily available product and may be obtained from the bottom of catalytic crackers. It is the heavy residue obtained from a catalytic cracking process, from steam cracker tar, a by-product of the steam cracking of naphtha or gas oils to produce ethylene or any residues from crude oil distillation or refining. A number of processes may be used to manufacture pitch from the aforementioned feedstocks, including thermal treatment, vacuum or steam stripping, oxidation, simple distillation or a combination of these [8]. In common with coal-tar pitch, the chemical and physical characteristics of petroleum pitch are very dependent on the process and conditions employed, especially the process temperature and heat treatment time. Generally, longer times and higher temperatures produce pitches with increased aromacity and higher anisotropic contents. Petroleum pitches are usually less aromatic than coal-tar pitch. Typical properties of the various types of pitch are shown in Table 5.2.

5.3 CHARACTERIZATION OF PITCHES

Fundamental to the understanding of the properties of carbon–carbon composites derived from pitch is an accurate chemical characterization of the precursor. Solvent fractionation and extraction are used to divide the pitch into a broad range of constituents which can be further subdivided using more sophisticated techniques as the need arises. As is normally the case in carbon science, a system of nomenclature has existed for many years describing the various fractions obtainable. Unfortunately, the coal-tar and petroleum industries use their own naming routines which do not correspond. The petroleum industry defines the following species:

Carboids are insoluble in CS_2.
Carbenes are soluble in CS_2 but insoluble in CCl_4.
Asphaltenes are insoluble in light paraffinic hydrocarbons (n-pentane, for example) but usually soluble in CS_2, CCl_4 and C_6H_6 – they are condensed, highly aromatic molecules.

Pre-asphaltenes is the term used to describe the fraction which is insoluble in solvents such as benzene, but soluble in pyridine.

Despite a degree of variation in the nomenclature used by different workers in the field [9], carbon–carbon matrix precursor pitches are most often fractionated using the following solvents:

1. The fractions which are insoluble in *quinoline* or *pyridine* are very high molecular weight aromatic compounds and solid impurities known as the 'C' component QI or 'α resins'.
2. *Benzene* or *toluene* insoluble material, which is soluble in quinoline or pyridine, is known as the 'C_2' component or 'β resins'.
3. Material which is insoluble in *petroleum ether* or *n-hexane* but soluble in benzene (or toluene) is referred to as the 'resinoid' fraction and is identified with asphaltenes, while the soluble material is called the 'crystalloid' fraction.

The solubility spectrum for a pitch can be very useful in its characterization especially in understanding the fundamentals of carbonization. Separation procedures, such as distillation [10], solvent fractionation [11,12] and column chromatography [13], have been coupled with various constitutional methods including elemental [14] and molecular weight analysis [15], IR [16] and UV [17] spectroscopy to show that pitches are highly complex mixtures of predominantly aromatic compounds. Figure 5.1 illustrates the type and percentage of structures identified in a typical coal-tar pitch [18]. Despite the fact that over the last two decades substantial progress has been made in the application of new methods for separation and characterization of carbonaceous materials [19], impregnating pitches remain a poorly understood 'hotch-potch' of compounds.

Gas chromatography (GC) is a useful tool with which to study the low molecular weight and volatile components of pitch. Greinke and Lewis [20] used GC to identify aromatic hydrocarbon components containing up to six condensed rings in the distillates collected from both coal-tar and petroleum pitches. Larger molecular components may be separated using high pressure liquid chromatography (HPLC). The separation is based on the presence of functional groups as well as on molecular size [21]. The method most applicable to the analysis of the larger molecular components of pitch is gel permeation chromatography (GPC). The technique involves separation of a solution of the sample on a porous polymer gel and is used to measure size and molecular weight distribution of high polymers. Edstrom and Petro [22] used GPC to measure the molecular size distribution within a number of pitches, using tetrahydro-furan as a solvent. The work was augmented by Tillmans *et al.* who employed quinoline as a solvent, allowing a larger fraction of the pitch to be measured [23].

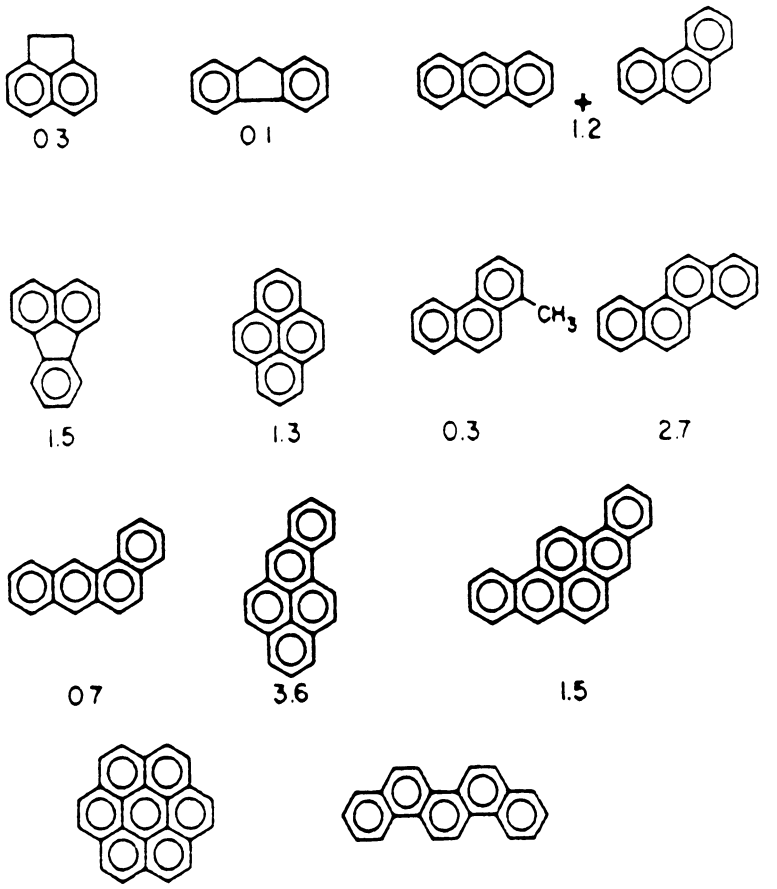

Fig. 5.1 Polynuclear aromatic components of pitch [18].

Quantitative information concerning the distribution of hydrogen and carbon in pitch molecules can be obtained using nuclear magnetic resonance (NMR). Dickinson [24] combined H and C^{13} NMR with other molecular constitutional data to produce average structures for various petroleum pitches. A number of other structural analysis techniques such as mass spectroscopy, X-ray diffraction, neutron inelastic scattering and electron spin resonance (ESR) have been used to study the reaction mechanisms during the carbonization of pitch.

5.4 PYROLYSIS OF PITCH

Pitch is converted to carbon by a process of pyrolysis. The mechanism of carbonization is one of aromatic growth and polymerization [25]. Figure 5.2 shows a schematic representation of the carbonization process whereby a small aromatic structure may ultimately attain the three-dimensional

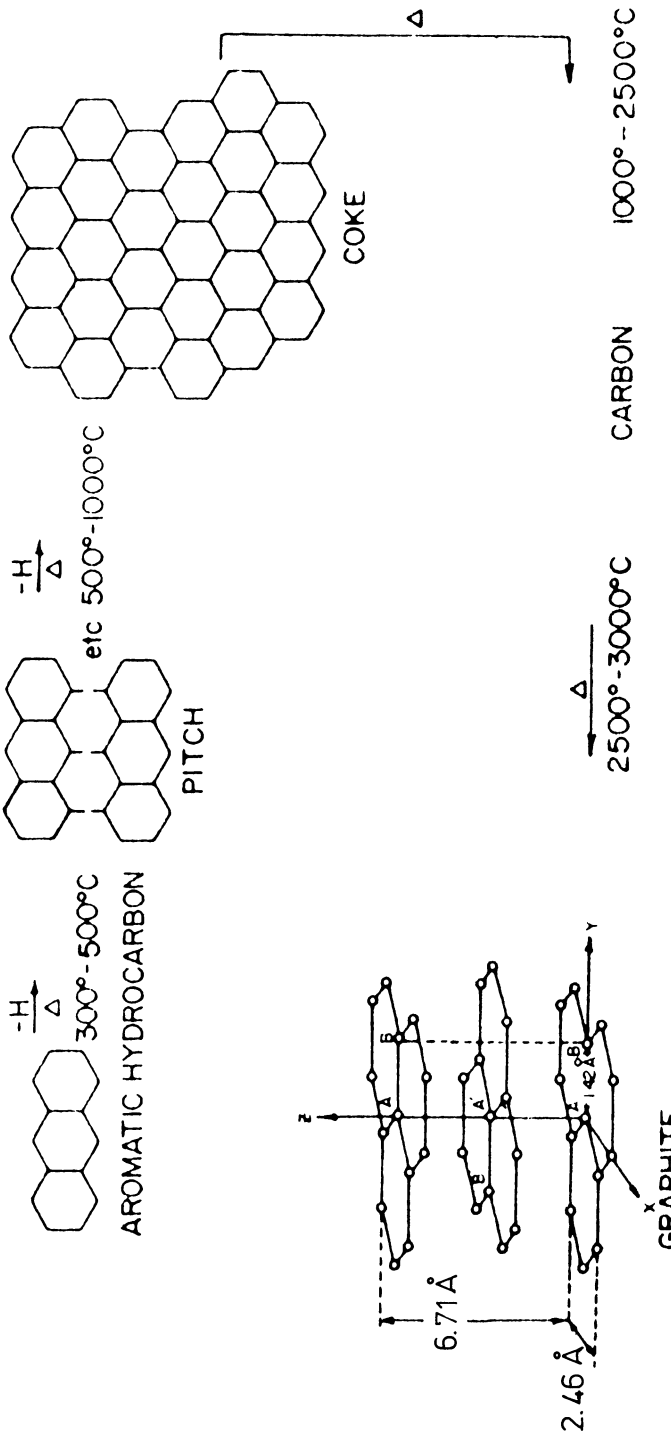

Fig. 5.2 Schematic diagram for the pyrolysis of pitch.

order of graphite via an aromatic polymeric structure. Before the carbonization process commences, non-aromatic structures are converted to aromatics, the key building blocks for carbon. Some polymers also degrade into tar-like liquids in the early stages of pyrolysis, PVC being a prime example. The overall process of carbonization is extremely complex. One may, however, consider individually a number of processes representative of the major reactions involved:

1. C–H and C–C bond cleavage to form reactive free radicals;
2. molecular rearrangement;
3. thermal polymerization;
4. aromatic condensation;
5. elimination of side chains and hydrogen.

All of the above processes can occur in parallel during the heat treatment but may be studied separately from a mechanistic viewpoint.

The initial thermal reaction is the carbonization process; although poorly understood, it is believed to involve the formation of a free radical intermediate. Two types of radical may be formed by bond cleavage of the aromatic molecule. The σ radical is produced by the breaking of an aromatic C–H bond. The reaction is a high-energy process since a bond dissociation energy of $\approx$420 kJ mol^{-1} must be overcome [26]. The σ radical intermediate is very unstable and the free electron localized. The second, π, radical is rather more stable, with much less energy ($\approx$325 kJ mol^{-1}) being required to break the methyl C–H bond. The unpaired electron is resonance stabilized and simple π radicals such as the benzyl radical have been detected by ESR [27]. Stein *et al.* [28,29] predicted the initial stages in the pyrolysis of polynuclear aromatic hydrocarbons using the 'radicals approach'. The addition polymerization of anthracene was proposed to proceed by the reactions delineated in Fig. 5.3 [30]. The π radical (I) could be generated by a small amount of the anthryl σ radical. More detailed observations of unstable radicals are required, however, before the initial reactions of carbonization are clarified.

Thermal rearrangement is another important step in the early stages of carbonization. Figure 5.4 shows examples of thermal rearrangement for (a) acenaphthylene and (b) bifluorene, which can transform unstable five-membered rings into more stable six-membered ring systems without the loss of carbon atoms. Example(c) methylene–phenanthrene, illustrates a similar rearrangement which involves the loss of carbon atoms. Either the rearranged or starting molecule serves as the building block in carbonization. One of the factors making carbonization so complex is the presence of so many possible polymerization sites in an aromatic molecule. Anthracene, for example, may form 11 different reaction products from the simple dimerization reaction [31].

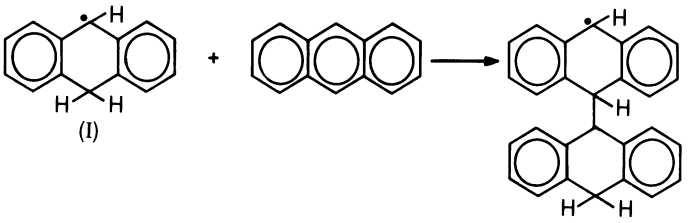

Fig. 5.3 Initial reactions in the pyrolysis of anthracene.

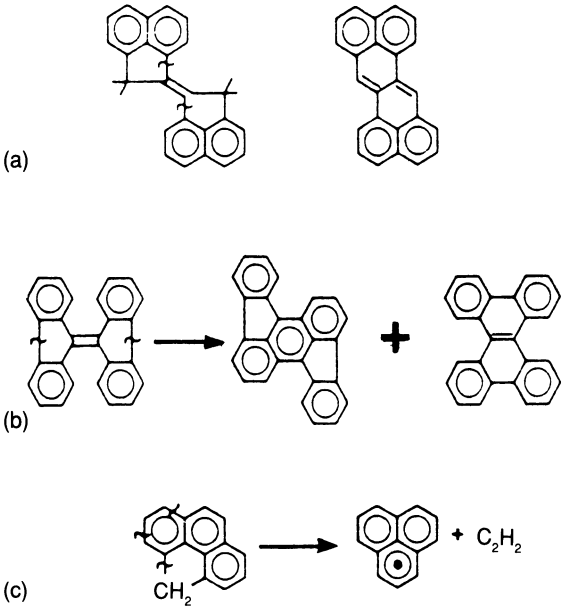

Fig. 5.4 Thermal rearrangement reactions during pyrolysis of polyaromatics.

Once formed, the reacting intermediate can undergo direct polymerization as shown in Fig. 5.5, illustrating the thermal polymerization of naphthalene to form naphthalene polymer. These initial polymerization reactions involve the loss or redistribution of hydrogen which can often be accomplished through internal hydrogen transfer. Figure 5.6 lists the major condensable volatile materials identified during the pyrolysis of several polynuclear aromatic hydrocarbons and illustrates the importance of hydrogen transfer. The products all consist of hydrogenated derivatives of the original compound with hydrogen added at the most reactive position in the molecule.

It can be seen in Fig. 5.7 that the polymerization process may occur in two stages, giving rise to either non-condensed or condensed polymers. In the case of naphthalene, the loss of two hydrogen atoms between two

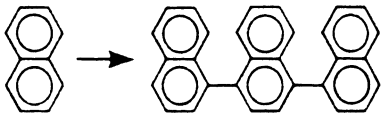

Fig. 5.5 Thermal polymerization of naphthalene.

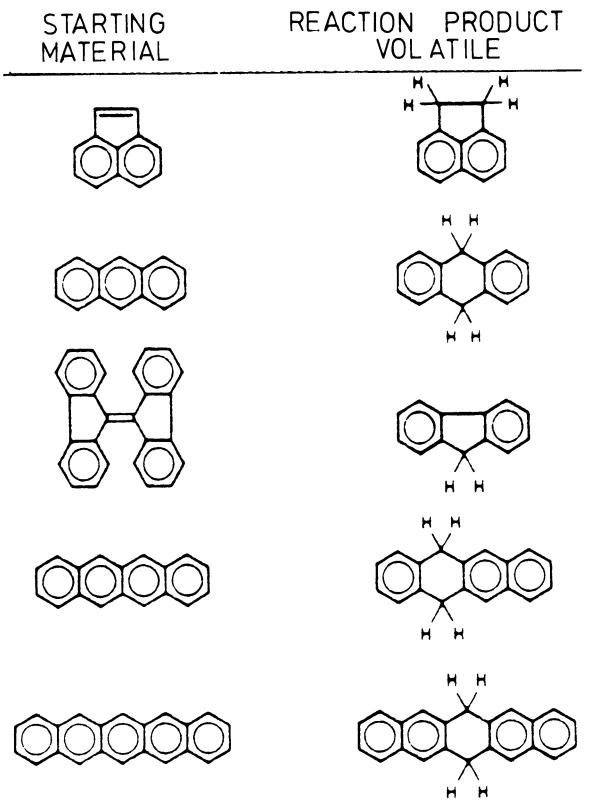

Fig. 5.6 Hydrogenated reaction products from the pyrolysis of aromatic hydrocarbons.

reacting molecules results in polymers in which the units are linked by single bonds. An additional loss of two hydrogen atoms produces a fully condensed polymer. Despite the non-condensed and condensed polymers having virtually the same molecular weights, they vary considerably in structure and properties. The non-condensed polymers are non-planar and their reactivities and ionization potentials change very slowly with increasing degree of polymerization. The condensed polymers, on the other hand, are fully planar and show marked changes in reactivity and ionization potential with increasing size. The relative role of these two processes is critical in the carbonization of pitch.

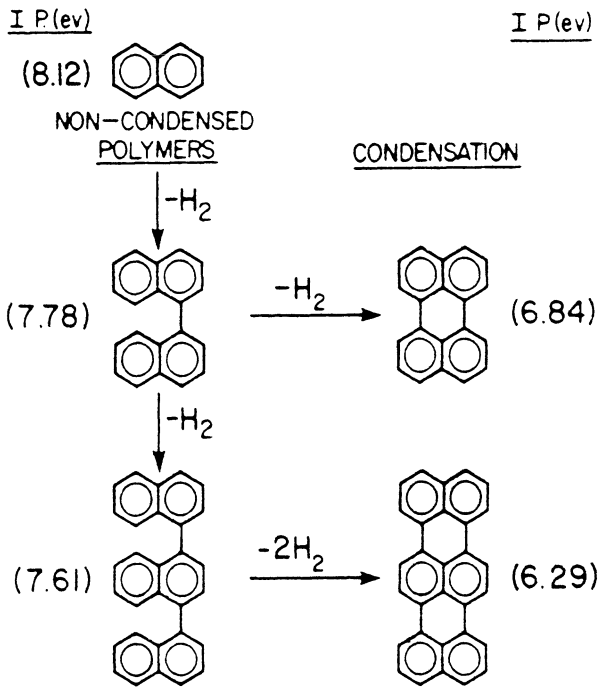

Fig. 5.7 Polymerization–condensation process in carbonization.

Lewis and Singer used the reaction scheme in Fig. 5.8 to show how odd-alternate radicals are involved in the polymerization condensation process in carbonization [32]. The polynuclear aromatic radicals produced are relatively reactive, as is illustrated for naphthalene. A non-condensed polymer (III) is formed by rapid polymerization. This polymer contains 3 non-condensed naphthalene units and a total of 30 carbon atoms. The loss of a single hydrogen atom from the polymer results in the formation of a free radical (IV) containing 30 carbon atoms with a single sp^3 tetrahedral carbon. The loss of an additional hydrogen from the π radical compound would create a fully condensed molecule.

The carbonization process is further complicated because the eventual polymerization to carbon occurs in two dimensions. Of paramount importance is how well the aromatic building blocks polymerize to develop a perfect graphitic network. The molecule zethrene (Fig. 5.9(a)) has the perfect shape and reactivity to polymerize in two dimensions to a planar graphitic structure whereas the compound tetrabenzonaphthalene shown in Fig. 5.9(b) has a non-planar structure, cannot polymerize without creating vacancies and is therefore poorly graphitizing.

The most significant feature of liquid phase pyrolysis is the development of a liquid crystal phase in the pyrolysing liquid prior to the formation of carbon [2]. Above around 400 °C spheres, initially around 0.1 μm

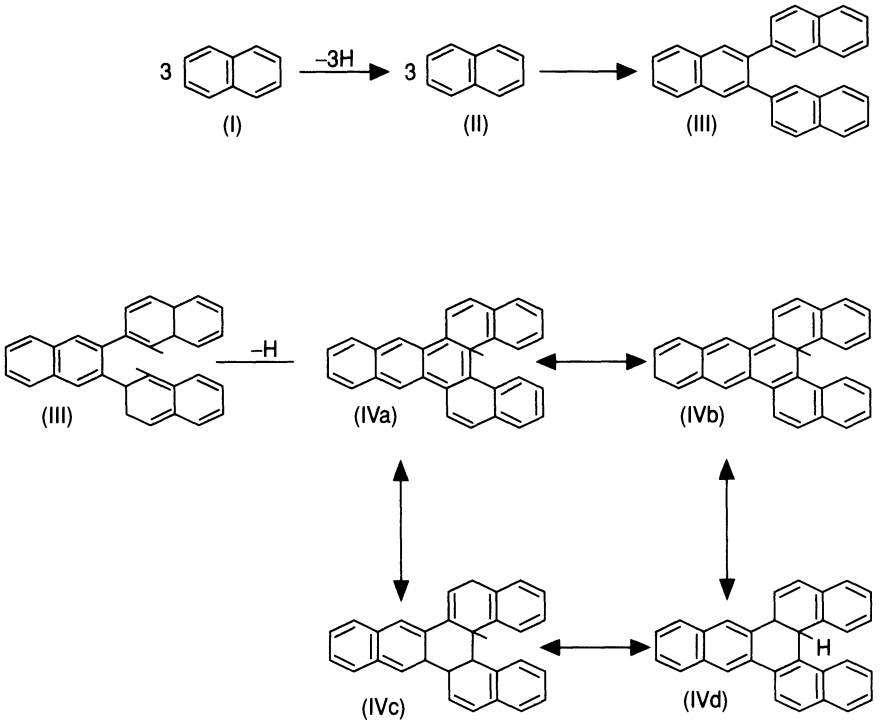

Fig. 5.8 Formation of stable odd-alternate free radical structures in carbonization.

in diameter, are observed in the isotropic liquid pitch. The spheres exhibit a highly oriented structure and are known as 'mesophase' [33]. The mesophase comprises polynuclear aromatic species which are stacked in approximate parallel array to form a discotic nematic liquid crystal system. The lamellar molecular structure formed within this temperature region (400–450 °C) may be considered as the 'embryonic graphite'. Figure 5.10 shows a schematic diagram of the type of molecular arrangement one would expect to find within the mesophase [4]. Under prolonged heating the spheres coalesce to form larger regions of extended order. The volume fraction of the mesophase in the two-phase emulsion gradually increases as pyrolysis proceeds, until the whole liquid is transformed to the anisotropic phase (Fig. 5.11) which subsequently solidifies to form carbon at around 500–600 °C. The structure of the domains of preferred orientation within the mesophase is determined by a number of factors. The reactivity of the precursors and the viscosity of the isotropic parent phase from which the mesophase grows control the nucleation and growth phenomena. The mesophase may be oriented by shear (Fig. 5.11). As a consequence, the shear history during pyrolysis, especially in the latter stages when the system is highly viscous and relaxation times are long, is of great significance in

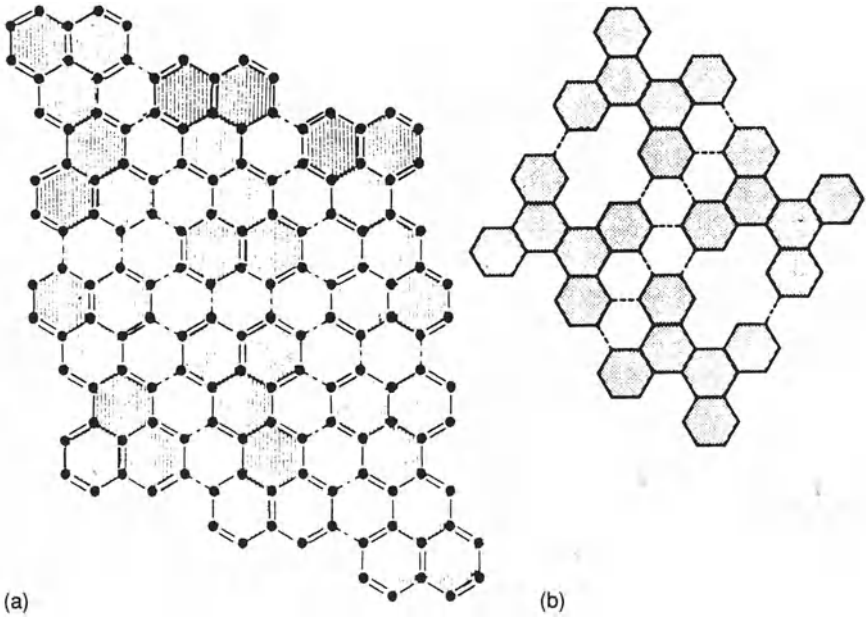

Fig. 5.9 Two-dimensional polymerization scheme for (a) zethrene and (b) tetrabenzonaphthalene.

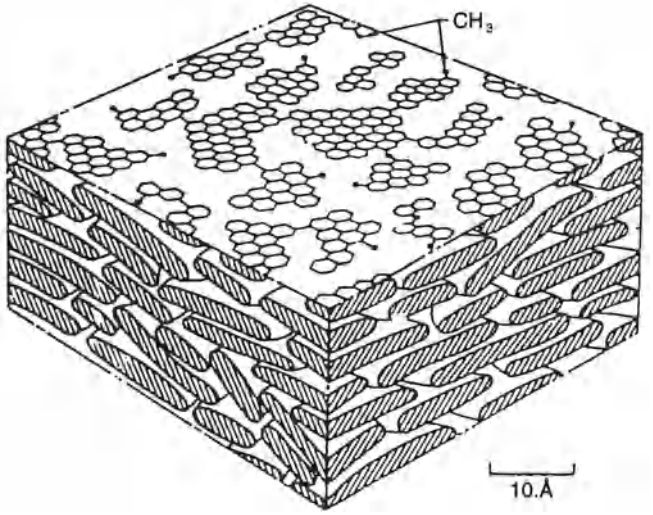

Fig. 5.10 Schematic representation of the molecular arrangement within the mesophase [4].

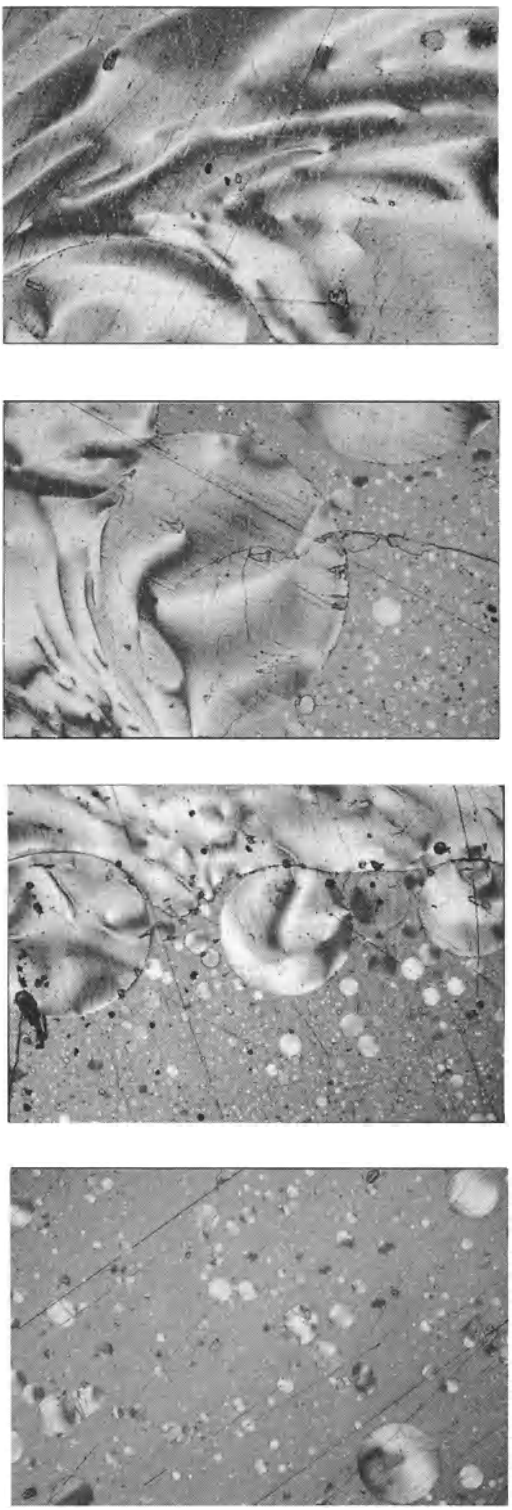

Fig. 5.11 Polarized light micrographs showing the development of mesophase during liquid phase pyrolysis of pitch between 400 and 500 °C (Courtesy Tonen Ltd).

the development of the microstructure of the carbon–carbon composite. Recent work [34] has shown how the mesophase may be aligned using a magnetic field. The polynuclear aromatic molecules of the mesophase have a disc-like shape which tends to align parallel to an applied magnetic field. It is suggested that this technique could be used to improve the mechanical properties of the matrix but, as yet, no conclusive results have been presented.

At high temperatures (>2300 °C) the lamellar arrangement within the pitch-derived carbon favours the formation of a graphitic crystal structure. The high density and small layer spacing measured in pitch-derived matrices of carbon–carbon (Fig. 5.12) is indicative of such a graphitic structure [35].

5.5 CARBON YIELD FROM PITCH

Pitch is a suitable matrix precursor for carbon–carbon composites only under the precondition that high carbon yields are obtainable. The yield depends very much on the composition of the precursor pitch and the conditions of pyrolysis. Decreasing the heating rate, the application of pressure or the use of chemical additives prior to the thermal decomposition of the pitch will all increase its carbon yield. Each of the aforementioned pyrolysis variables serves to improve the yield by restricting the evolution of volatile molecules present in the original pitch. The retention of these species in the carbonizing liquid as the temperature is raised allows them to participate in the aromatic growth and polymerization processes. For a fixed set of pyrolysis conditions, the carbon yield is influenced very strongly by the proportion of β resins and quinoline insolubles. The carbon yield thus generally increases with increasing amounts of high molecular weight compounds. Impregnating pitches are often fractionated to increase their content of those components which provide the highest carbon yield. It should be remembered, however, that this will result in higher viscosities which will affect the final microstructure (Section 5.7) and make processing more difficult. A balance often requires to be struck between the adventages and disadvantages of increasing the content of high molecular weight species in the pitch.

Bhatia and co-workers [36,37] have been able to show that a coal-tar pitch of higher softening point (SP) and β resins content exhibited a superior carbon yield to that of a conventional binder pitch.

High values of the molecular weight related properties of SP, benzene or toluene insolubles (BI), quinoline insolubles (QI) and β-resins (BI-QI) were found to be of significance in the pitch's suitability as a carbon matrix precursor since they are known to influence strongly properties such as viscosity and C/H atomic ratio. They were further able to show a remarkable

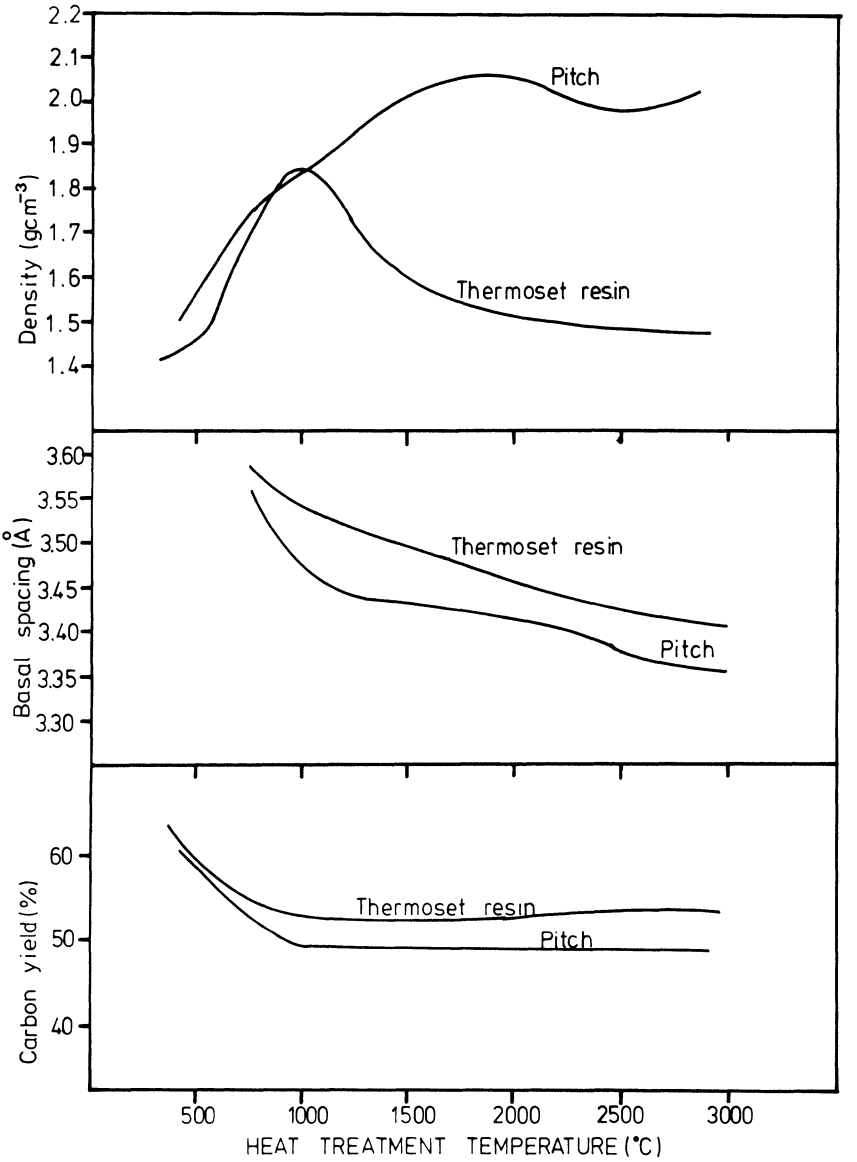

Fig. 5.12 Characteristics of resin and pitch as a function of HTT [35].

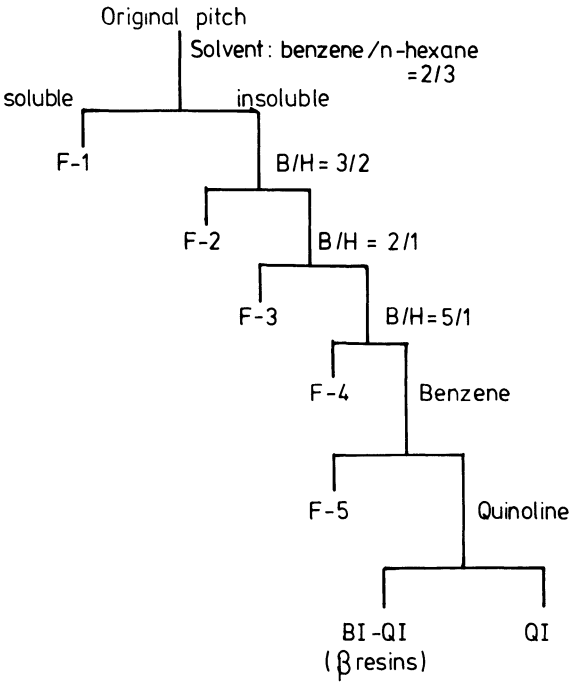

Fig. 5.13 Solvent fractionation of a coal-tar pitch.

agreement between the experimentally measured carbon yields of a number of pitches and those calculated theoretically [38].

The theoretical evaluation of the carbon yield of a pitch is based on the law of mixtures. That is to say, the carbon yield of a pitch is the sum total of contributions of its three components, namely, QI, β resins and benzene solubles (BS) obtained by solvent fractionation as shown in Fig. 5.13. The carbon yields of QI and β-resin fractions are believed to be almost constant and independent of the origin of the pitch [39,40] being ≈95 and 85% respectively [41]. The carbon yield of the BS fraction is known to vary from 30 to 55% depending on the SP of the pitch. The higher the SP of the pitch the higher will be the average molecular weight of the BS fraction and, as a consequence, the higher will be its contribution towards the carbon yield of the pitch. The relationship for the carbon yield of a pitch can be written as [38]

$$CY = QI \times 0.95 + (BI\text{-}QI) \times 0.85 + BS \times K, \quad (5.1)$$

where CY is the carbon yield, QI and BI are quinoline insoluble and benzene insoluble fractions respectively, and K a constant such that $0.3 < K < 0.55$, which is dependent on the SP of the pitch.

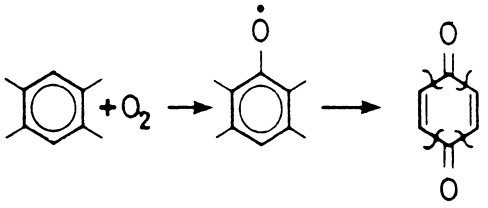

Fig. 5.14 Reaction of oxgen with aromatic hydrocarbons [46].

5.6 THE INFLUENCE OF ADDITIVES ON CARBONIZATION

The *carbonization reactions* of pitches can be considerably altered by the use of reactive additives, the most widely used of which is oxygen [42]. Oxidation treatment is used to 'thermoset' the pitch in order to prevent bloating during carbonization and to increase its carbon yield by retarding the volatilization of low molecular weight compounds. Severe oxidation has been found to reduce significantly the graphitizability of the pitch [43,44] and inhibit mesophase development [45]. Mild oxidation has been demonstrated to induce dehydrogenative polymerization without necessarily adversely affecting graphitizability [45]. Electron spin resonance studies of the oxidation of aromatic hydrocarbons in air identified aryloxy radicals (Fig. 5.14) as polymerization intermediates [46,47]. The decrease in graphitizability symptomatic of extensive oxidation, was believed due to the formation of quinones (Fig. 5.14) which pyrolyse with the loss of CO to produce non-planar radicals.

Sulphur has also been extensively used as an additive to improve carbon yield [48,49]. The final structure of the carbon may be related to the amount of sulphur added. High sulphur contents produce non-graphitizing carbons whereas for lower levels the reverse is true. Sulphur-containing radicals have been proposed as intermediates in these reactions [50]. The reaction of sulphur with aromatic hydrocarbons is thought to produce sulphur-containing polymers in which the sulphur is stable to high temperatures [51]. A number of other additives, such as $AlCl_3$ [52], alkali metals [53], anhydrides [54] and $FeCl_3$ [55], have also been used to convert low molecular weight aromatic hydrocarbons to carbon and improve the carbon yield of pitch, with varying degrees of success.

5.7 CONTROL OF MICROSTRUCTURE IN PITCH-DERIVED CARBON–CARBON COMPOSITES

There are three basic methods for the production of carbon–carbon composites, namely infiltration by CVD (Chapter 3) , impregnation with

a thermosetting resin (Chapter 4) and impregnation with pitch. The microstructure of the matrix carbon produced by CVD may be controlled by the deposition temperature and partial pressure of the hydrocarbon gas to obtain isotropic, rough laminar and smooth laminar textures. The microstructure of the matrix derived from a thermosetting resin is mainly isotropic at HTTs below 1500 °C and coaxially aligned above 2300 °C.

Control of the microstructure is necessary to optimize thermomechanical properties [56]. The microstructure of a pitch-derived carbon matrix is generally dominated by the character of the pitch [57]. The complex polycylic aromatic nature of pitch results in detailed information with respect to carbonization being difficult to obtain. It is possible, however, to subdivide a pitch into a number of fractions of similar molecular weight distributions as defined by their solubility in certain solvents. It is apposite to break down the pitch into three groups: quinoline insolubles, β resins and benzene solubles. Kimura *et al.* [56] report approximate molecular weight ranges for the QI fraction of 1500 and above, 500–1500 for the β resins and between 300 and 460 for the benzene solubles. Carbonization of the benzene solubles produces a strongly anisotropic coarse-flow microstructure texture (Chapter 1), β resins carbonize to a 'coarse mosaic' texture with an average anisotropic domain size of ≈100 μm, whereas the QI fraction produces an isotropic carbon [58]. The BS, β resin and QI fractions are observed to be carbonized in a liquid phase, a more viscous liquid phase and a solid phase respectively. The extent of the orientation of the basal plane of the resultant carbon is proposed to be strongly affected by the difference in the mobility of polycyclic aromatic molecules during the carbonization, suggesting that the microstructure is governed by the viscosity of the pitch. A fractionation and mixing technique can be used to control the viscosity of the pitch by variation of the molecular weights and by the mixing-in of non-fused fine particles. Both techiques are therefore useful methods in the microstructure control of carbon–carbon composites formed from pitch.

A difference is observed between carbons derived from BS fractions themselves and those in fibre-reinforced composites [56]. A longer range of preferred orientation is observed in the composites compared with pitch alone. This is believed to result from a combination of preferred growth of mesophase spherules on carbon fibres, the frictional force near the fibres during mesophase movement and the shear force due to the shrinkage of the matrix. The carbon produced from the β resins, on the other hand, displays a decrease in the size of anisotropic domains when combined with carbon fibres, perhaps due to the fibres increasing the fraction's viscosity by acting as an obstacle to molecular movement. The microstructure of QI-derived carbon shows no changes in the presence of fibres.

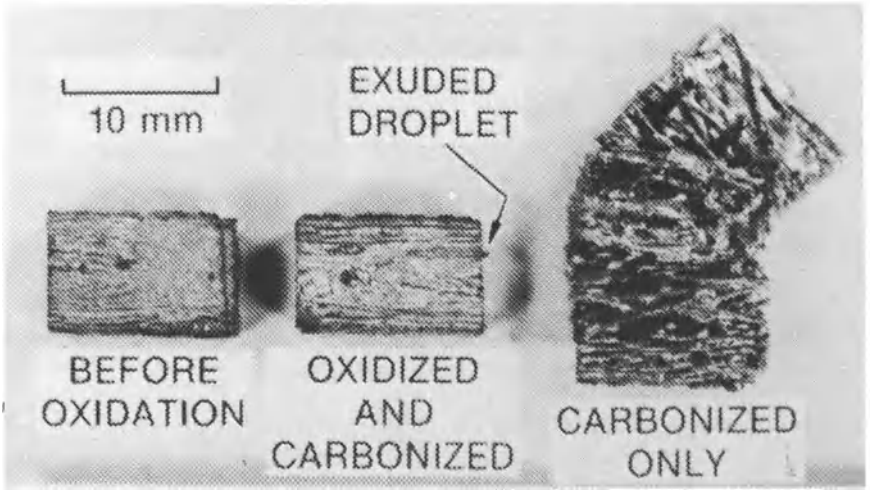

Fig. 5.15 The effect of prior oxidation on the carbonization of 2-D pitch-based carbon–carbon [61] (reproduced from *Carbon, an International Journal*, by kind permission of Pergamon Press).

5.8 LOW-PRESSURE COMPOSITES PROCESSING

Mesophase pitches are known to bloat seriously upon carbonization even under substantial applied pressure. Studies of petroleum coking have shown foaming to commence with the coalescence of bulk mesophase [59, 60]. If carbon–carbon composites are to be efficiently processed from pitch matrix precursors it is paramount that the matrix be stabilized in place prior to carbonization [61]. White and Sheaffer [61] carried out an investigation into the feasibility of stabilizing the pitch matrix by an oxidation process analogous to that used to stabilize pitch fibres prior to carbonization [62]. They postulated that it would be possible to stabilize the pitch within a fibre preform provided the shrinkage cracks, resulting from the severe mismatch in thermal expansivities between fibre and unhardened mesophase, allowed sufficient connected access for the entry of oxygen and evolution of gaseous oxidation products. Their initial work utilized orthogonal 3-D fibre preforms impregnated with Ashland A240 petroleum pitch. Specimens were oxidized in oxygen for up to 100 h at 222 °C followed by carbonization to 1100 °C. Subsequent microscopic investigation revealed that oxidation not only prevented bloating of the samples but also retained the mesophase spherules. Further experiments were carried out using 2-D woven fabric preforms, such materials being highly vulnerable to bloating due to lack of reinforcement in one direction. Matrix bloating destroyed unoxidized samples whereas those treated as before remained intact (Fig. 5.15).

White and Sheaffer concluded that oxidation processing of pitch-based composites was able to prevent bloating during carbonization, preserve the matrix microstructure established while the pitch was fluid or deformable and, by restriction of the volatilization of low molecular weight compounds, increase the carbon yield. An obvious application of this technique would be the ability to produce large 2-D pitch-based structures hereto impossible due to the size limitations of the HIP machines (Section 5.9) presently used in their fabrication.

5.9 HIGH-PRESSURE PROCESSING OF PITCH-DERIVED CARBON–CARBON

At atmospheric pressure the carbon yields obtained from pitches are only around 50% by weight, i.e. similar to those from high-yield thermosetting resins, although oxygen-stabilized pitches are reported to produce carbon yields in excess of 70% [61]. Yields as high as 90% can be obtained, however, by carbonizing the pitch under high pressure [63]. The effect of carbonization pressure on carbon yield is illustrated in Fig. 5.16 [64].

Pressure applied during pyrolysis also affects the matrix microstructure formed. Figure 5.17 shows micrographs of a petroleum pitch carbonized under an applied pressure of 6.89 and 68.9 MPa respectively followed by heat treatment to 2200 °C [35]. The coke formed at the lower pressure is needle-like, possibly due to deformation of the mesophase by gas bubble percolation. The higher the pressure the more coarse and isotropic will be the microstructure. This is thought to be due to the suppression of gas formation and escape during the carbonization reaction. High pressures are also observed to lower the temperature at which mesophase formation occurs. At very high pressures (≈200 MPa) coalescence of mesophase does not occur, so that an optimum of around 100 MPa is generally chosen for high-pressure processing of carbon–carbon [65].

The characteristics of pitches when chosen as matrix precursor for carbon–carbon processing may be summarized as follows:

1. Carbon yields at atmospheric pressure are about 50% by weight. Carbonization under high pressure (≈100 MPa) can result in yields in excess of 90% for some pitches.
2. Carbon microstructures are graphitic.
3. Matrix density is high (≈2 g cm^{-3}).
4. Applied pressure affects matrix microstructure.

5.9.1 Hot isostatic pressure impregnation carbonization

As a result of the low carbon yields generally obtained, all liquid impregnation techniques essentially follow three steps to completion:

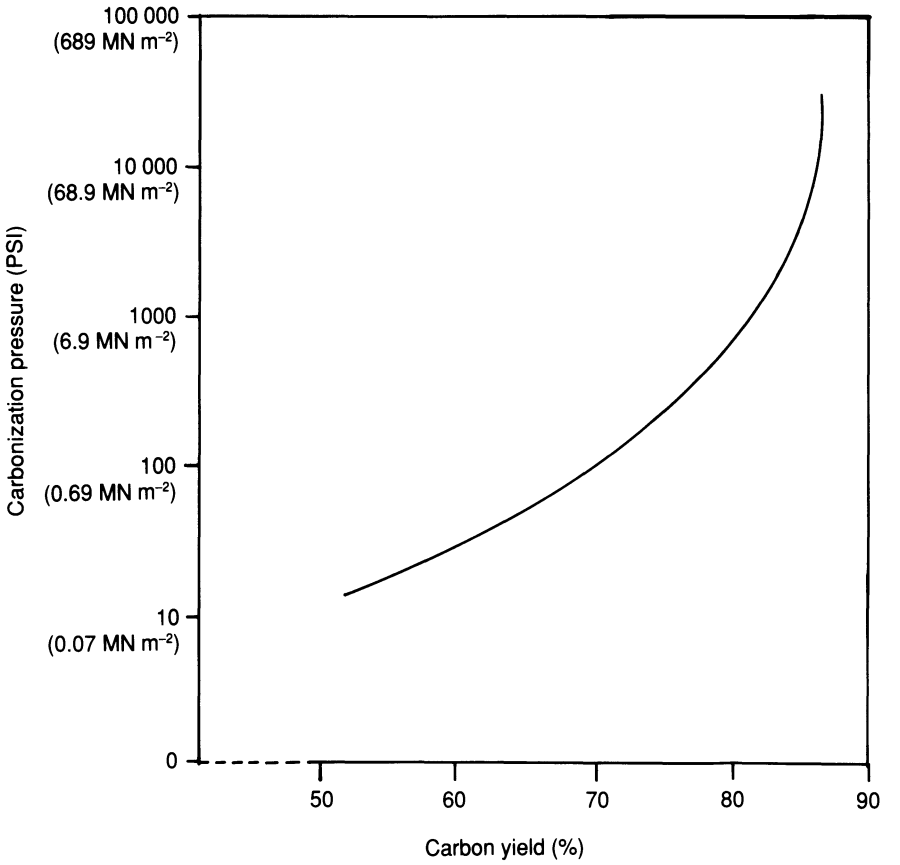

Fig. 5.16 Effect of carbonization pressure on carbon yield from petroleum pitch.

1. Impregnate fibres and form basic shape.
2. Carbonize to form porous carbon structure.
3. Reimpregnate/carbonize to improve density and hence properties, this can involve multiple steps before the component is complete.

It is thus fairly easy to conclude that the cost of carbon–carbon is not controlled by material costs as in carbon-fibre reinforced plastics, but that the greatest cost lies in fabrication. Carbon yields of 50–60% achieved with thermosetting resins, although low, represent a conversion efficiency of around 95% of the carbon actually available.

The only practical route available to lowering the cost of carbon–carbon fabrication is to attempt to improve the carbon yield and processability of pitches or other high-carbon-content compounds.

As shown in Fig. 5.16, the application of pressure during the carbonization of pitch can increase the carbon yield from 50% at ambient pressure to over 90% at 100 MPa. This pressure effect on the carbon yield of

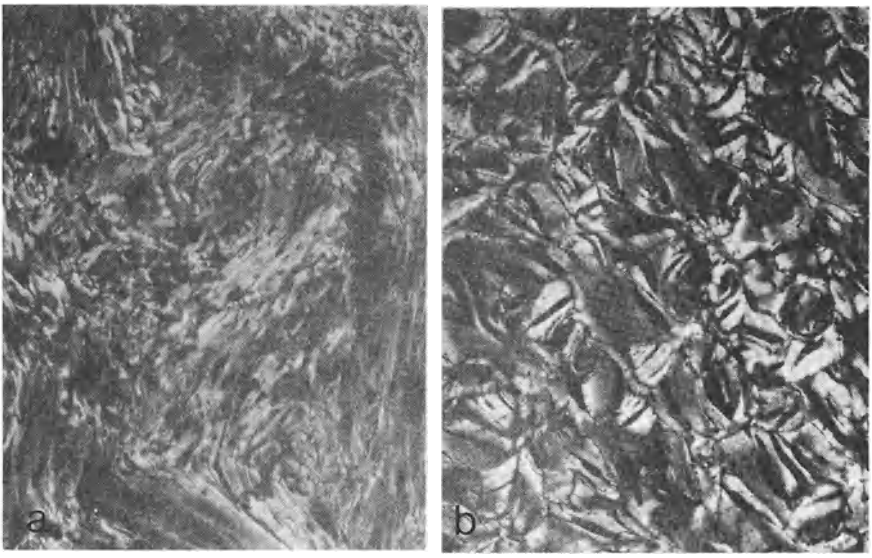

Fig. 5.17 Microstructure formed by petroleum pitch carbonized under (a) 6.89 and (b) 68.9 MPa applied pressure – subsequently graphitized to 2700 °C [35] (reproduced by kind permission of Elsevier Science Publishers).

pitches has become the basis of a process for the densification of carbon–carbon composites known as hot isostatic pressure impregnation carbonization, or HIPIC for short. The technique uses high isostatic inert gas pressure effectively to impregnate and densify carbon–carbon composites during the melting and carbonization stages of the pyrolysis cycle [66,67]. A schematic diagram of a complete HIPIC densification cycle is shown in Fig. 5.18.

5.9.2 Equipment and process requirements

The traditional hot isostatic press (HIP) design consists of a large externally water-cooled pressure vessel within which is situated a furnace surrounded by thermally insulating material referred to as a thermal barrier (see Fig. 5.19). In this design, pressurizing hot zone gases and reaction products have free access to all areas within the pressure vessel.

During the carbonization stage of the HIPIC process, reaction products which fall into one or more of the following categories are produced:

1. carbonaceous materials forming 'sooty' deposits which are otherwise chemically inert and present no threat to the mechanical integrity of the pressure vessel, e.g. condensed carbon black and soot particles;
2. chemically active materials which may produce a corrosive environment within the pressure vessel, e.g. ammonia;

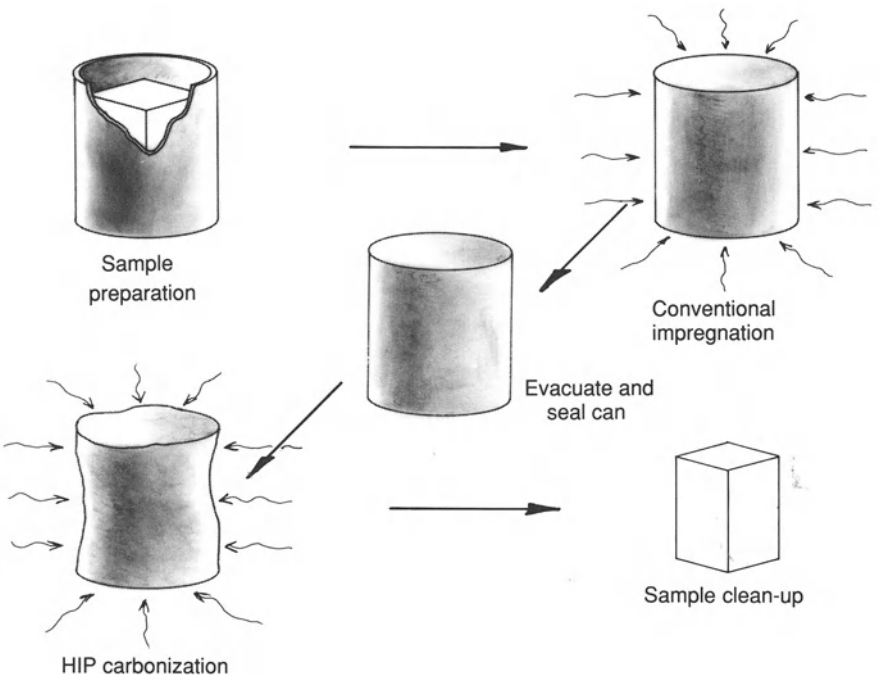

Fig. 5.18 Schematic diagram of HIPIC process.

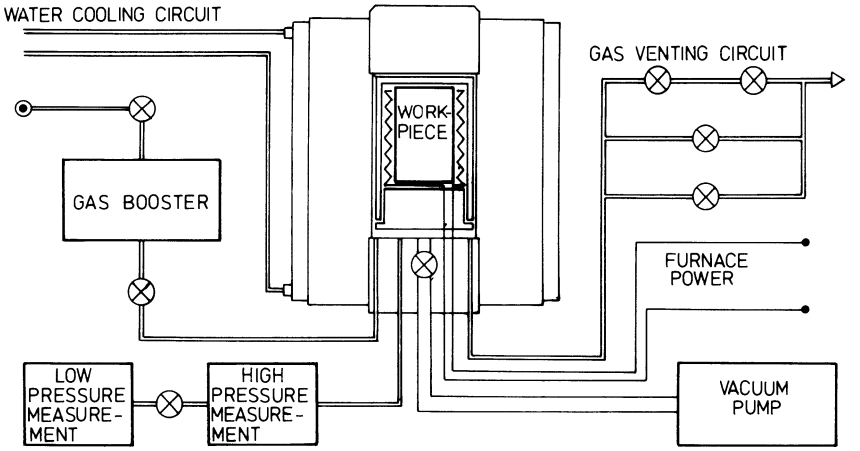

Fig. 5.19 Schematic diagram of standard HIP unit.

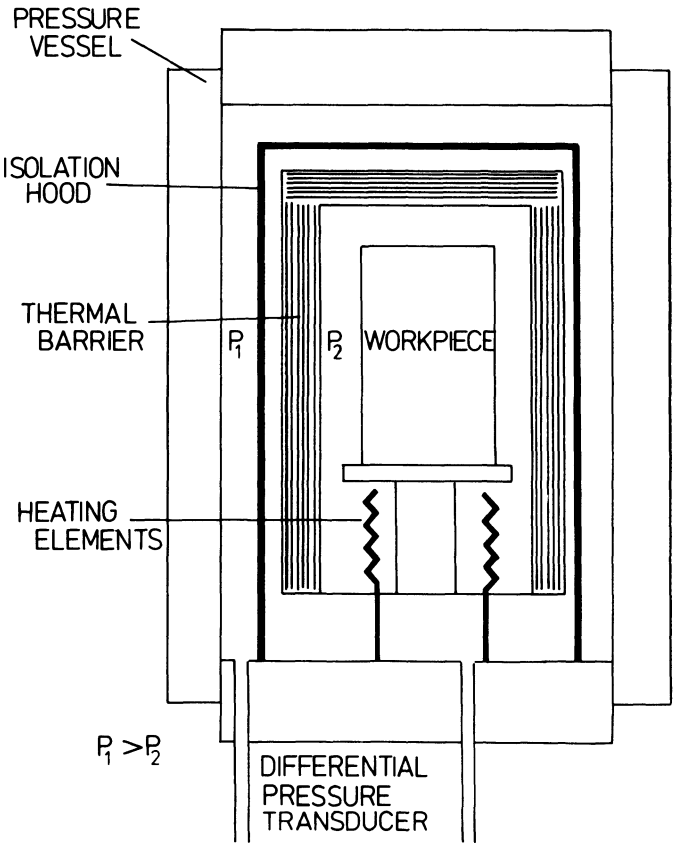

Fig. 5.20 Schematic diagram of the two gas isolation hood and differential pressure transducer gas management system developed for HIPIC processing.

3. atomic and/or molecular hydrogen which under certain conditions can result in embrittlement of the mild steel pressure vessel [68].

The risk of hydrogen embrittlement is small but nevertheless deserves attention. The effects of the reaction products in groups 1 and 2 present more of a cleanliness and good operating procedure problem. In order to combat these problems, the HIPIC process must be carried out in a specially designed HIP fitted with a novel gas management system [69], a schematic of which is shown in Fig. 5.20. Gas control depends upon the establishment of a differential pressure between the work zone and the pressure vessel inner wall. A differential pressure transducer operating at a system pressure of up to 2000 bar establishes and maintains a slight overpressure of 1.5 bar on the outside of the isolation hood. This has the effect of isolating the hot zone gases, and causing all gas movement to be from the outside in. Careful differential pressure control by a microprocessor

leads to a clean, reliable and inherently safer impregnation and carbonization cycle. A dry fibre preform or porous carbon–carbon laminate is vacuum-impregnated with molten pitch, placed inside a metal container, or can, and surrounded by an excess of pitch. The can is then evacuated and sealed (preferably using an electron beam weld).

The sealed can is placed within the work zone of the HIP unit and the temperature raised, at a programmed rate, above the melt point of the pitch, but not so high as to result in weight loss due to the onset of carbonization. The pressure is increased and maintained at around 100 MPa (1.5 kbar).

The pitch initially melts, expands within the can and is forced by isostatic pressure into the pores in the sample. A sealed container will act like a 'rubber bag' and aid the pressure transference to the workpiece. As the pitch begins to carbonize the high isostatic pressure will maintain the more volatile fractions of the pitch impregnant in a condensed phase. The pressure not only increases the carbon yield but also prevents liquid from being forced out of the pores by pyrolysis products [64]. After processing the preforms are removed from their container and cleaned up by removing any excess carbonized liquid from the surface. The matrix may be graphitized by controlled heating to temperatures above 2300 °C [69]. The complete cycle as shown in Fig. 5.18 must be repeated until the required composite density is achieved.

In order to fabricate high-quality composites with good mechanical properties it is essential that the carbonization process be carried out slowly (over 1–3 days) and under strict process control. The control subsystem of an HIP unit used in carbon–carbon technology must integrally link, monitor and maintain all of the time temperature and pressure conditions intrinsic to the process. Because of the long time periods involved it is requisite that the entirety of the operation be controlled by a micro- or minicomputer from a detailed program input by the operator. In the interests of product quality, it is preferable to have the capability to log all of the data with respect to each carbonization cycle. Small irregularities introduced into the composites during the various fabrication subcycles may be very detrimental to the properties of the final component.

5.10 THERMOPLASTIC POLYMER MATRIX PRECURSORS

Recent work [70] has demonstrated the capability of fabricating carbon–carbon composites from a variety of exotic polyaromatic thermoplastic resin precursors such as polyetherether ketone (PEEK) and polyetherimide (PEI) using HIP technology. Over the last 5 or 6 years a novel enabling technology has evolved for the processing of composites made from the aforementioned resins reinforced with carbon fibres [71]. A family of carbon

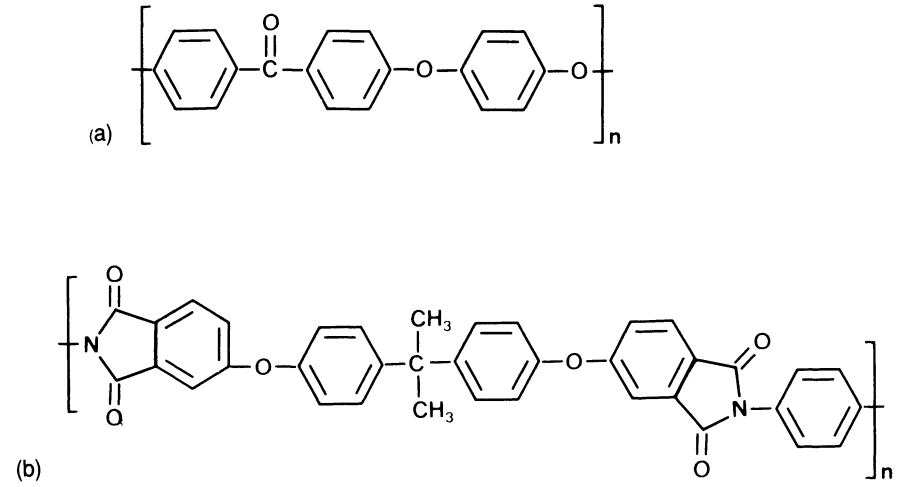

Fig. 5.21 'Exotic' thermoplastic carbon matrix precursors: (a) PEEK; (b) PEI.

fibre/thermoplastic prepregs is produced commercially ICI under the trade name 'APC', which stands for Aromatic Polymer Composite [72], as an intermediate to component manufacture in applications such as the aerospace industry, where weight saving is of paramount concern. Such materials are of interest as carbon–carbon precursors because of the attractive C/H ratios of the resin matrices resulting from a high degree of aromacity (Fig. 5.21). There is thus the potential of high carbon yields (i.e. >70%).

The thermoplastic nature of the precursors, whilst aiding component fabrication [71], requires the application of pressure during carbonization to maintain the integrity of the sample [70]. It has been found that good quality carbon–carbon materials can be made by hot isostatic pressing of these precursors without the need of the encapsulation essential when pyrolysing pitch precursors. It is, as yet, not fully clear what is the precise mechanism behind the achievement of such results. It is believed, however, that the resin precuror, being thermoformable, flows sufficiently during the initial part of the process to form an effective seal around and/or throughout the workpiece whereby the isostatic pressure is applied to the whole of the workpiece, yet enabling volatiles generated in the pyrolysis to diffuse out without significant distortion.

Although expensive (the prepreg costs from £120 kg^{-1} upwards) the properties observed in carbon–carbon from the 'APC' family of materials is generally superior to those derived from phenolic matrix composites even after multiple reimpregnation/carbonization cycles (Table 5.3).

The microstructures observed in these composites differ considerably from their more 'conventional' counterparts. The matrix component of the composites, heat treated to 1000 °C, although isotropic in nature, retains many of the characteristics of the polymer from which it was derived (Fig. 5.22) as indicated by the relatively 'strong' bonding observed between

Table 5.3 Mechanical properties of unidirectional carbon–carbon composites

Precursor	*Density* (g cm^{-3})	*Flexure strength* (MN m^{-2})	*Flexure modulus* (GN m^{-2})	*Transflexure strength* (MN m^{-2})
Carbon/PEEK	1.55	900	190	10
Carbon/PEI	1.47	563	135	4
Carbon/phenolic	1.40	630	130	10
Carbon/phenolic after 4 impregnation cycles	1.46	950	178	10

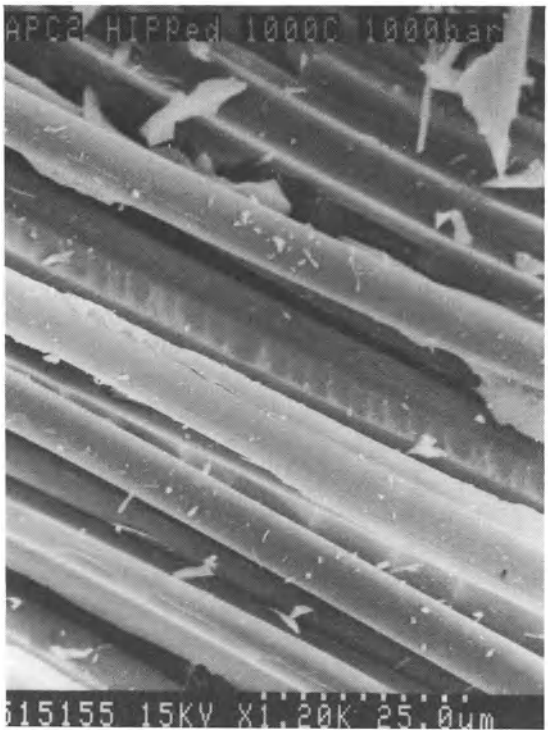

Fig. 5.22 Fracture face of carbon–carbon made from APC-2 precursor.

fibre and matrix. A number of techniques may be employed to improve the bonding between fibre and matrix (Table 5.4) such as pre-oxidation of fibres, heat treatment to 'pseudo-cross-link' the polymer matrix and/or the addition of heterogeneous cross-linking agents to the materials such as sodium. It is possible to obtain a very strong, almost 'polymeric' type of bonding at the fibre/matrix interface (Fig. 5.23). Unfortunately, when inducing such bonds, one is confronted by the classic brittle fibre/brittle matrix problem; cracks propagating through a brittle matrix under

Table 5.4 Effect of precursor–pretreatment on the fibre/matrix interface in UD carbon–carbon produced from CF/PEEK

Pre-treatment to precursor	*Transflexure strength* (MPa)
Unoxidized carbon fibres	4
Standard fibre oxidation treatment (APC 2)	10
4 × standard fibre oxidation treatment	12
Resin cross-linked by heat treatment	17
Resin cross-linked by chemical additions	25
Resin cross-linked by chemical addition and heat treatment	32

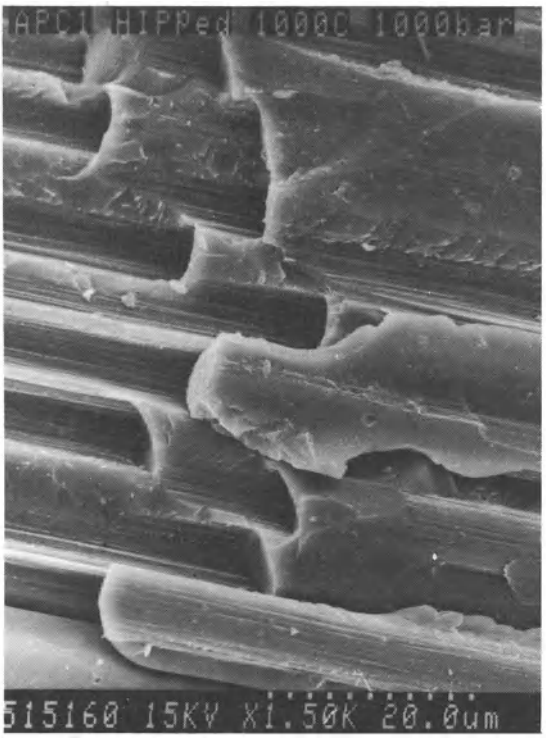

Fig. 5.23 Transflexure fracture face of cross-linked carbon/PEEK derived carbon–carbon showing strong 'polymeric' fibre/matrix interface.

Table 5.5 Comparison of ultra-high modulus carbon–carbon with that made from other precursors

Precursor	*Density* (g cm^{-3})	*Transflexural strength* (MN m^{-2})	*Flexural strength* (MN m^{-2})	*Flexural modulus* (GPa)
APC-2	1.55	10	900	190
P75/PEEK	1.83	16	600	325
Phenolic	1.40	10	630	130

mechanical stress are not deflected at a strong interface and carry straight on through the brittle fibre resulting in catastrophic failure at relatively low levels of loading. A weak interface, on the other hand, diminishes the efficiency of the transfer of load from matrix to fibres. Carbon–carbon composites will thus always exhibit lower strengths than the materials from which they were derived. A balance must therefore be struck between effective load transfer and tendency to brittle failure. The interface in thermoplastic-derived materials may be 'engineered' with a good degree of accuracy and reproducibility, thus allowing the required optimization.

In space applications, such as satellite structures, the most important design parameter is specific stiffness, i.e. modulus per unit weight. To attack that market niche, several products have been developed which are composites reinforced with ultra-high modulus carbon fibres made from mesophase pitch precursors [73–75]. In that area, ICI have developed a prepreg material similar to APC-2 but which employs high modulus (517.5 GPa) Thornel P75 fibres [76]. Since APC-2 had proved a very useful carbon–carbon precursor, it was a logical step to investigate the possibility of forming similar materials using the ultra-high modulus product.

Table 5.5 shows a comparison of the properties of carbon–carbon from P75/PEEK with those from other precursors. The long flexure fracture faces in Figs. 5.24 and 5.25 show a transition between pull-out and transverse cracking modes of failure. What is most apparent when viewing the micrographs is the very low level of voidage as confirmed by the high density obtained (although some of the increase is due to the higher fibre density). The matrix, although glassy and isotropic in nature, again exhibits a 'polymeric' type fracture behaviour in that it is not catastrophically cracked away from the fibres during testing. The flexure strength of the P75-based material represents a drop of only 25% over its polymeric 'parent', whereas the APC-2 derived material is more than 50% lower than that of its precursor, indicating a more efficient stress transfer at the fibre/matrix interface.

It is known that graphitization can be induced in a thermoset-based matrix for carbon–carbon and that thermoplastic polymers and pitches

Fig. 5.24 Axial flexure fracture face of P75/PEEK carbon fibre reinforced carbon.

form a graphitizable carbon. The transition between amorphous and crystalline carbon occurs slowly up to 2000 °C. Above this temperature defects become highly mobile, resulting in a dramatic increase in the rate of ordering. It has been suggested that graphitization, in sheaths oriented along the fibre axis, results from a combination of thermally activated processes and stress induced by the difference in thermal expansion coefficients between the fibre and matrix. This process is usually thought to commence at around 2000 °C. Observations made during TEM studies indicate that the process begins at temperatures below 1600 °C when PEEK is HIPed [77]. It is

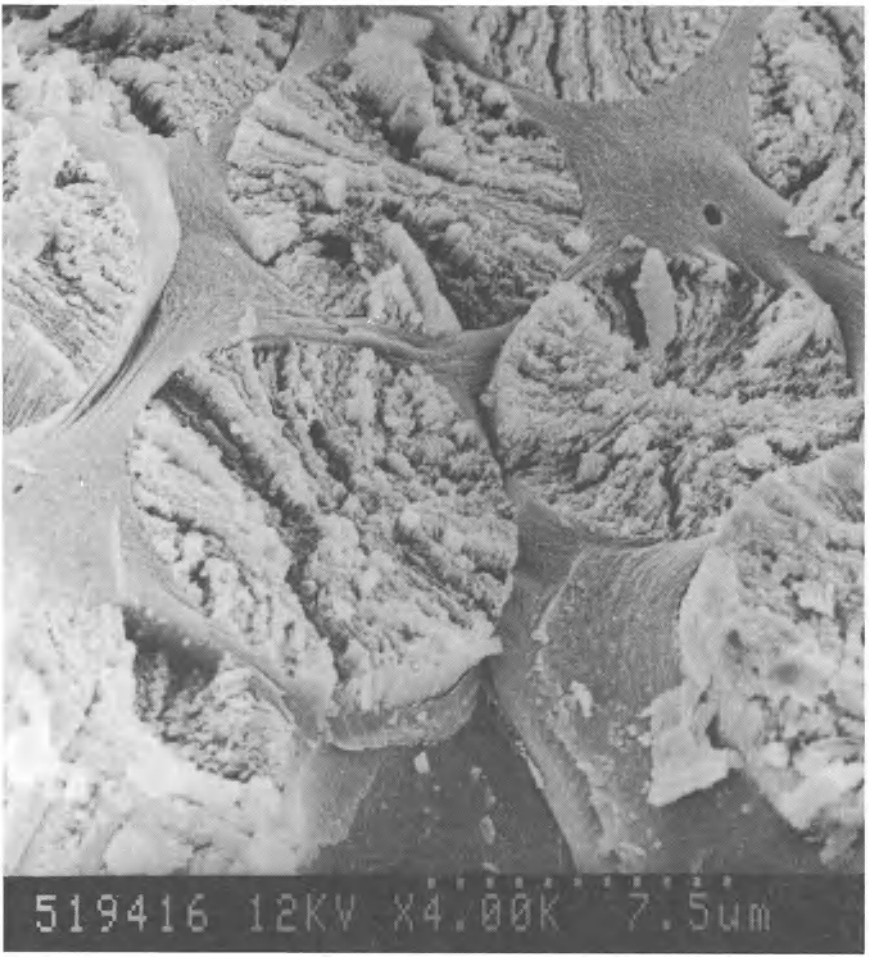

Fig. 5.25 Texturing of carbon microstructure in P75/PEEK derived carbon–carbon composite indicative of ordering of matrix microstructure at higher temperatures (HTT 1600 °C).

possible that the application of external pressure during pyrolysis aids crystallographic alignment. One can detect a gradual texturing of the matrix structure in the electron micrograph in Fig. 5.25.

5.11 SUMMARY

The fabrication of carbon–carbon composites from thermosetting resin precursors is severely limited due to the relatively low carbon yields obtainable from resins such as phenolics and furans. Acetylene-terminated

resins, although possessing high potential carbon yields, are beset by prohibitively high raw materials costs. The use of pitches as matrix precursors is an extension of the technology used in the graphite electrode processing industry. A large data base covering impregnation, carbonization and graphitization of both coal-tar and petroleum pitches is therefore readily available. Pitches have a low SP, low melt viscosity, high carbon yield and tend to form graphitic carbon structures. The complex oligomeric nature of pitches results in their being difficult to categorize with any great degree of accuracy, thus presenting a severe problem of quality control in the final product. It is, however, possible to divide the pitch into three subgroups: QI, β-resins and benzene solubles, dependent on their molecular weight as 'defined' by solubility in certain solvents. As a general rule of thumb, the greater the proportion of the high molecular weight species the higher will be the carbon yield. The SP of the pitch is another indication of carbon yield; the higher the SP the greater the average molecular weight of the pitch and thus the higher will be its carbon yield. As an example, one may consider the Ashland series of refined petroleum impregnation pitches A240, A400 and A420 where the figures represent the pitches' SPs in °F, A420 having the highest carbon yield.

Pitch-based matrices thus offer higher yields than do the phenolic resins conventionally used in 2-D composites, and are generally much lower in cost than polymer systems of equivalent yield. Furthermore, pitch-based systems exhibit the potential for a wider variety of matrix microstructures, ranging from glassy carbon to fully graphitizable mesophase microstructures. The thermoplastic nature of the pitches results in severe bloating and loss of low molecular weight compounds when carbonized under ambient conditions. Oxidation treatment to cross-link the pitch can be used to eliminate the bloating problem and increase the carbon yield. The true potential yields of pitches can, unfortunately, only be achieved by the application of high pressure in specially designed HIP apparatus. Exploitation of the HIP process is limited by the physical size of the equipment and the high initial capital investment requirement to set up a production facility, but it is probably the most efficient route to the manufacture of good quality, thick sectioned, high density artefacts such as rocket nozzles and re-entry vehicle nose cones. Pitches are also useful as reimpregnants in thermoset-based processing when they are often blended with the resin to improve carbon yield.

Recently it has been shown that an HIP is capable of converting thermoplastic resin matrix composites to carbon–carbon. Furthermore the materials so formed have generally exhibited superior properties (density, strength, stiffness, etc.) to those derived from the more 'traditional' phenolic precursors. These observations are particularly true when the precursor material is a combination of fibres derived from the mesophase pitch (Thornel P75) and a PEEK matrix. Microstructural observations have shown that

the carbon–carbon composites formed by HIPing this relatively novel precursor retain a good deal of their 'polymeric' characteristics (e.g. 'well wetted' fibre/matrix interfaces and low porosity), while acquiring the high-temperature properties unique to 'all-carbon' systems.

The properties measured for the HIPed materials compare favourably and often exceed those of competitive materials (even after those competitors have been subject to a series of densification cycles). It is fair to say then that the composite produced, and particularly those from the P75/PEEK precursor, may be considered as near-finished materials and therefore ready for exploitation as prototype components. Although the properties of carbon–carbon from the APC genre of composites have good properties they will be prohibitively expensive for many applications because of the high cost of raw materials. It is therefore important to target applications requiring 'high-added-value' artefacts. Applications where further research effort could/should be placed are: fasteners, biomedical implants and, most especially, space structures where high costs can be justified by the reduction of launching costs.

REFERENCES

1. Fitzer, E. (1987) *Carbon*, **25**, 163.
2. Brooks, J. D. and Taylor, G. H. (1968) *Chem. Phys. Carbon*, **4**, 243.
3. White, J. L. (1975) *Prog. Solid-State Chem.*, **9**, 59.
4. Zimmer, J. E. and White, J. L. (1982) *Adv. in Liq. Cryst.*, **5**, 157.
5. White, J. L. and Buechler, M. (1986) in *Petroleum-derived Carbons*, **303**, Am. Chem. Soc. Symposium Series, Washington DC, p. 62.
6. Blades, H. (1972) US Patent 3,767,756.
7. Smith, F. A., Eckle, T. F., Osterholm, R. J. and Stichel, R. M. (1966) in *Bituminous materials*, Vol. **3** (ed. A. J. Hoiberg), Interscience, New York, p. 57.
8. Newmann, J. (1976) in *Petroleum Derived Carbons* (eds M. L. Deviney and T. M. O'Grady,) AC5 Sym. Ser. 21. p. 52.
9. McNeil, D. (1966) in '*Bituminous Materials*, **3** (ed. A. J. Hoiberg), Interscience, New York, p. 139.
10. Franck, H. G. (1963) in *Chemistry and Coal Utilization*, supplementary vol. (ed. H. H. Lowry), Wiley, New York, p. 592.
11. Smith, J. W. (1966) *Fuel*, **45**, 233.
12. Halleux, A. and de Greef, H. (1963) *Fuel*, **42**, 185.
13. Vahrman, M. (1950) in *Progress in Coal Science*, (ed. D. H. Bangham), Interscience, New York, p. 60.
14. Van Krevelen, D. W. (1950) *Fuel*, **29**, 269.
15. Phillips, G. and Wood, L. J. (1955) *J. App. Chem. (Lond.)*, **5**, 326.
16. Brooks, J. D. and Steven, J. R. (1964) *Fuel*, **43**, 87.
17. Friedel, R. A. (1966) in *Applied Infrared Spectroscopy*, (ed. D. N. Kendall), Wiley, New York, p. 312.

18. Lewis, I. C. and Singer, L. S. (1969) Preprints of fuel division, *Am. Chem. Soc.*, **13**, 86.
19. Friedel, R. A. (ed.) (1970) *Spectrometry of Fuels*, Plenum Press, New York.
20. Greinke, R. A. and Lewis, I. C. (1975) *Anal. Chem.*, **47**, 2151.
21. Bartle, K. D., Collin, G., Stadelhofer, J. W. and Zander, M. (1979) *J. Chem. Tech. Biotechnol.*, **29**, 531.
22. Edstrom, T. and Petro, B. A. (1968) *J. Poly. Sci. Part C*, **21**, 171.
23. Tillmanns, H., Ulsamer, W. and Pietzka, G. (1976) *Carbon 76*, Int. Carbon Conf. Preprints, 2nd p. 557.
24. Dickinson, E. M. (1980) *Fuel*, **59**, 290.
25. Lewis, I. C. (1982) *Carbon*, **20**(6), 519.
26. Badger, G. M. (1965) *Prog. Phys. Organ. Chem.*, **3**, 1.
27. Carrington, A. and Smith, I. C. P. (1965) *Mol. Phys.*, **9**, 137.
28. Stein, S. E., Golden, D. M. and Benson, S. W. (1977) *J. Phys. Chem.*, **81**, 314.
29. Stein, S. E. (1981) *Carbon*, **19**, 421.
30. Livingstone, R., Zeldes, H. and Conradi, M. S. (1979) *J. Am. Chem. Soc.*, **101**, 4312.
31. Lewis, I. C. (1980) *Carbon*, **13**, 191.
32. Lewis, I. C. and Singer, L. S. (1981) *Chem. Phys. Carbon*, **17**, 1.
33. Brooks, J. D. and Taylor, G. M. (1967) *Carbon*, **3**, 185.
34. Zimmer, J. E. and Weitz, R. L. (1988) *Carbon*, **26**(4), 579.
35. Burns, R. L. and McAllister, L. E. (1976) *Proc. 12th Propulsion Conf.*, Palo Alto.
36. Manocha, L. M., Bhatia, G. and Bahl, O. P. (1982) *Proc. 1st Indian Carbon Conference*, New Delhi, December, p. 325.
37. Bahl, O. P., Manocha, L. M., Singh, Y. K., Bhatia, G., Aggarwal, R. K. and Dhami, T. L. (1986) *Proc. 4th Int. Carbon Conf.*, Baden-Baden, June, p. 38.
38. Bhatia, G., Aggarwal, R. K. and Bahl, O. P. (1987) *J. Mat. Sci.*, **22**, 3847.
39. Blackley, T. H. and Earp, F. K. (1958) *Industrial Carbon and Graphite*, Soc. of Chem. Ind., London.
40. Chari, S. S., Bhatia, G. and Aggarwal, R. K. (1978) *J. Sci. Ind. Res.*, **37**, 502.
41. King, L. F. (1978) in *Analytical Methods for Coal and Coal Products*, **2** (ed. C. Karr), Academic Press, New York.
42. Fitzer, E., Meuller, K. and Schaffer, W. (1971) in *Chemistry and Physics of Carbon*, **7** (ed. P. L. Walker jr), Marcel Dekker, New York, p. 237.
43. Kipling, J. J., Sherwood, J. N., Shooter, P. V. and Thompson, N. R. (1964) *Carbon*, **1**, 315.
44. Otani, S. (1965) *Carbon*, **3**, 31.
45. Barr, J. B. and Lewis, I. C. (1978) *Carbon*, **16**, 439.
46. Lewis, I. C. and Singer, L. S. (1981) *J. Phys. Chem.*, **85**, 354.
47. Lewis, I. C. and Singer, L. S. (1969) *Proc. 9th Biennal Conf. on Carbon*, Boston, USA, June, p. 120.
48. Christie, N., Fitzer, E., Kalka, J. and Schafer, W. J. (1969) *Chem. Phys. Physicochem. Biol.*, p. 50.
49. Fitzer, E., Huttner, W. and Manocha, L. M. (1980) *Carbon*, **18**, 291.
50. Kipling, J. J., Shooter, P. V. and Yound, R. N. (1966) *Carbon*, **4**, 333.
51. Lewis, I. C. and Greinke, R. A. (1982) *J. Polym. Sci. Chem. Ed.*, **20**, 1119.
52. Mochida, I., Inoue, S., Maeda, K. and Takeshita, K. (1977) *Carbon*, **15**, 9.

53. Mochida, I., Nakamura, E., Maeda, K. and Takeshita, K. (1976) *Carbon*, **14**, 123.
54. Evans, S. and Marsh, H. (1971) *Carbon*, **9**, 747.
55. Otani, S. and Oya, A. (1972) *Bull. Jap. Chem. Soc.*, **45**, 623.
56. Kimura, S., Yasinda, K., Inagaki, M. and Yasuda, E. (1984) *Rpt. Res. Lab. Eng. Mats. Tokyo Inst. Tech. no. 9.*
57. Kamramura, K. Kimura, S., Yasuda, E. and Inagaki, M. (1982) *Tanso*, **109**, 46.
58. Sanda, Y. (1978) *Nenryokokaishi*, **57**, 117.
59. White, J. L. (1976) in *Petroleum-derived Carbons*, **21**, Am. Chem. Soc. Symp. Series, Washington DC, p. 282.
60. Weinberg, V. A., White J. L. and Yen T. F. (1983) *Fuel*, **62**, 1503.
61. White, J. L. and Sheaffer, P. M. (1989) *Carbon*, **27**(5), 697.
62. Singer, L. S. (1977) US patent 4,005,183.
63. Fitzer, E. and Terwiesch, B. (1973) *Carbon*, **11**, 570.
64. Lachmann, W. L., Crawford, S. A. and McAllister, L. E. (1978) *Proc. Int. Conf. on Composite Mats*, Met. Soc. of AIME, New York.
65. Gray, G., Hunter, A., Payne, R. S. and Savage, G. M. (1990) *Powder Met. Rept*, **45**(4), 290.
66. Burns, R. L. and Cook, J. L. (1974) *Petroleum-derived Carbons*, **21**, ACS Symp. Series, Am. Chem. Soc.,Washington DC, p. 139.
67. Chard, W., Conaway, M. and Neizz, D. (1974) *Petroleum-derived Carbons*, Vol. 21, ACS Symp. Series, Am. Chem. Soc., Washington DC, p. 155.
68. Gangloff, R. P. and Wei, R. (1977) *Metallurgical Transactions, A, USA*, 1043.
69. Dietrich, H. and McAllister, L. E. (1978) *Am. Ceram. Soc. 80th Ann. Meeting, Detroit.*
70. Norton-Berry, P., Savage, G. M. and Steel, (1990) M. L. Eur. Patent App. H35016/EP.
71. Gray, G. and Savage, G. M. (1989) *Metals and Materials*, Sept; 513.
72. ICI Fiberite Corp. (1986) *APC 2 Data Sheet no. 2*, (1986) Orange.
73. Silverman, E. M. and Jones, R. J. (1988) *Proc. SAMPE. Int. Symp.*, **33**, 1418.
74. Silverman, E. M. and Jones, R. J. (1988) *SAMPE J.*, **24**(4), 33.
75. Silverman, E. M., Sathoff, J. E. and Forbes, W. C. (1989) *SAMPE J.*, **25**(5), 39.
76. Barnes, J. A. and Cogswell, F. N. (1989) *SAMPE Quart.*, **20**(3), 22.
77. Payne, R. S., von Bradsky, G. Gray, G. and Savage, G. M. (1990) *Proc. Conf. Adv. in Elec. Mic.*, Seattle, Sept. p. 1024.

Oxidation and oxidation protection

6

6.1 INTRODUCTION

Over the past decade the development of structural carbon–carbon materials has received a great deal of attention. Potential uses have been cited in future generation military aircraft, missile systems and a number of proposed hypersonic aerospace vehicles. All of the possible applications take advantage of the excellent high-temperature properties of carbon and the benefits of fibre reinforcement, most especially high strength and strength retention at temperatures in excess of 2000 °C. It is important to note that all such applications involve operation for extended periods of time in oxidizing environments. Since the composites have already demonstrated the mechanical requirements, it is generally concluded that the development of reliable oxidation protection is crucial to carbon–carbon attaining its full potential. The method accepted as the most feasible way to protect carbon–carbon composites involves **coating** of the outer surfaces of the material with appropriate refractory materials in order to prevent oxygen attacking the substrate. Additionally, protective compounds, known as **inhibitors**, may be placed within the composite.

The provision of oxidation protection for carbon materials has been the subject of intense research over the last 50 years. The first noteworthy patent to be granted in this field was issued to the National Carbon Company in the USA in 1934 [1]. Up until roughly 25 years ago, the major driving force for oxidation protection was for polycrystalline graphite used as electrodes in the steel industry or for furnace heating elements.

In the 1960s, the 'space race' demanded ablation and oxidation-resistant graphites for rocket propulsion and as re-entry components. The emphasis in present-day studies is firmly on carbon–carbon composites. The first efforts in oxidation protection of carbon–carbon were conducted in the

early 1970s and the stimulus was provided by the requirements of the space shuttle programme. The components involved, leading edges and nose-cap, used low-performance rayon-based fibre composites [2]. The investigation of methods for providing oxidation protection for high-performance structural carbon–carbon has only been ongoing over the last 10 or so years. A 'potted history' of the development of carbon oxidation protection systems is given in Fig. 6.1.

The earlier mentioned National Carbon Company patent claimed a dual protection system based on an inner silicon carbide layer and an outer glaze of B_2O_3. It has since been recognized that glassy materials are an important constituent of oxidation protection systems for carbon, a whole host of patents having been granted using variations of this theme. The original patent also exemplifies the possible use of P_2O_5 and SiO_2 glasses. P_2O_5 glasses can be effective but are limited in operation by volatilization to fairly low temperatures, while silica glasses do not generally possess the required wetting characteristics to afford protection. B_2O_3 glasses, on the other hand, have the ability to provide protection over a wide range of temperatures both in the form of surface coatings and inhibitors within the body of the composite. This ability arises from a combination of thermal stability and appropriate viscosity and wetting properties.

A prominent milestone in the ongoing 'saga' of oxidation protection of carbon was the development of JTA graphite by Union Carbide and a number of related materials [3–5]. Developed for the production of re-entry components for the US space programme, these materials contained non-oxide ceramics of boron, silicon, zirconium and hafnium. Oxidation produced a borate glass coating capable of providing protection for periods of several hours at temperatures of up to 1700 °C. A pure borate glass is only able to give primary protection for limited times above around 1100 °C due to the volatility of B_2O_3. Although limited in application, the work clearly demonstrated the effectiveness of boron additions (preferably in unoxidized form – to ease processing) to the body of a carbon in laying the foundations for further development.

A great many coatings, other than glasses and glass formers, have been added to carbon–carbon for high-temperature operation in oxidizing environments. Chown and his team investigated the suitability of coatings of SiC, produced both by CVD and direct reaction with molten silicon [6]. A number of other refractory carbide and boride coatings have also been investigated by Chown [6] and Fitzer *et al.* [7]. The results obtained indicated that silicon carbide was capable of providing reliable protection for long time periods, provided the temperature remained below 1700 °C and flaws in the coatings could be eliminated. SiC coatings are found to decompose rapidly above 1700 °C, whereas a sintered coating of zirconium carbide and boride (ZrC and ZrB_2) will allow short-term protection up to temperatures of roughly 2200 °C.

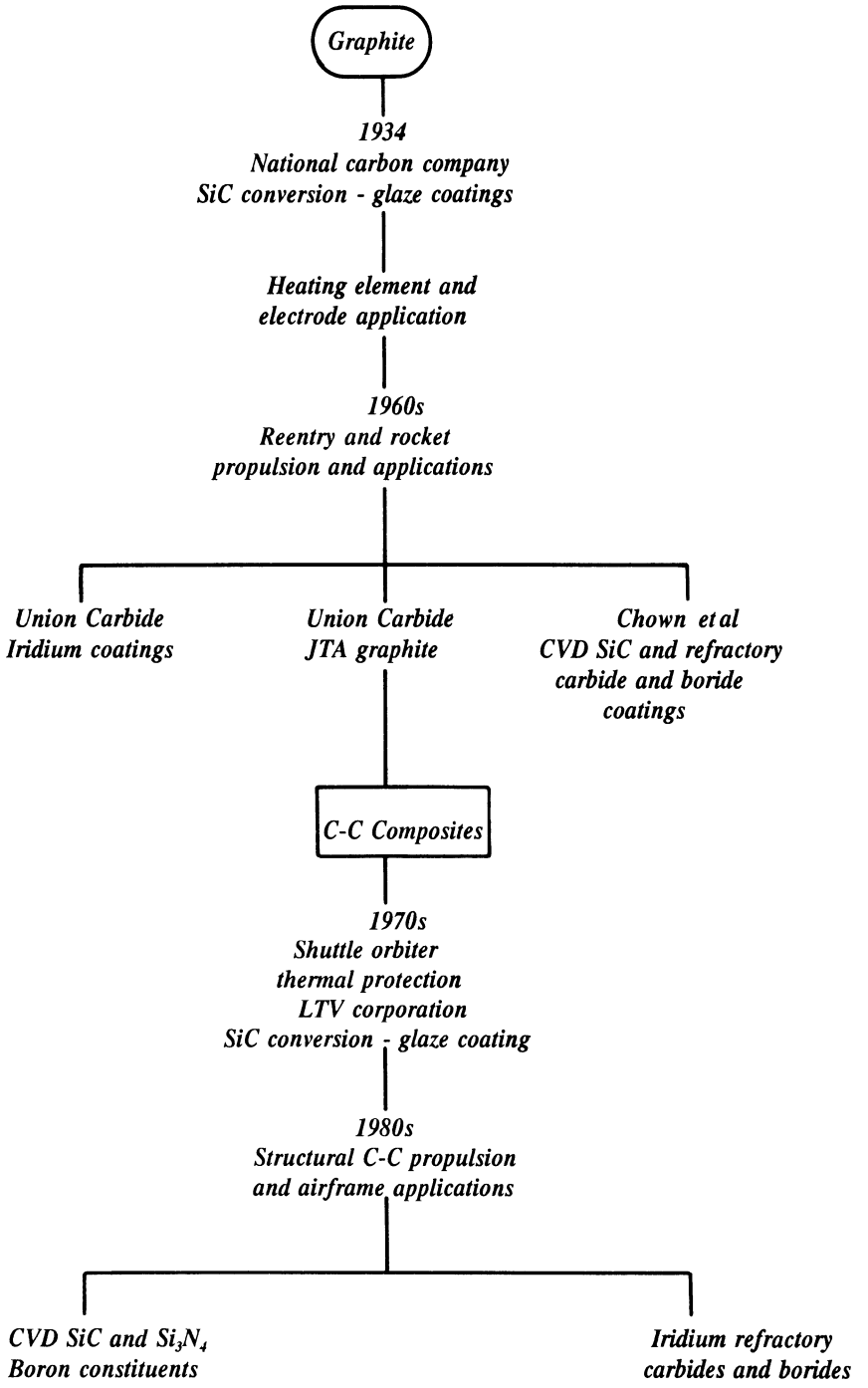

Fig. 6.1 Development of oxidation protection for carbon materials.

The temperature limit observed for SiC appears to apply to all silicon-based materials used in oxidation protection. Molybdenum disilicide ($MoSi_2$) and silicon nitride (Si_3N_4) also show this limitation which is probably endemic to the silicon family of materials. Higher-temperature refractories based on zirconium and hafnium are able to operate at temperatures well above silicon, but only for limited periods of time as a result of the rapid rates of diffusion of oxygen through these oxides.

In the middle of the 1960s iridium coatings were used to protect graphite for short periods of time in the 2000–2100 °C temperature range [8, 9]. Iridium melts at 2440 °C, has very low permeability to oxygen up to 2100 °C, does not react with carbon below 2280 °C, and forms an effective barrier to the diffusion of carbon. It is thus an attractive material for the basis of a high-temperature protection system. The problems associated with iridium include erosion due to the formation of a volatile oxide, a relatively high coefficient of thermal expansion and poor adhesion to carbon. At 2000 °C, in flowing air, an iridium coating has been observed to erode at a rate of $\approx$0.13 mm h^{-1} [10]. The erosion problem could, perhaps, be averted by combining the iridium with a refractory oxide coating, with an inner carbide layer to improve adhesion. Despite showing promise, iridium has never been deployed to any great extent due to high costs and limited availability.

The driving force for research into the protection of carbon–carbon arose in the 1970s with the development of leading edges and nose-caps for the space shuttle programme (Fig. 6.2). The carbon–carbon parts for the shuttle are made by the low-pressure resin technique from rayon-based fabric and a phenolic resin. Following three reimpregnation cycles with a phenolic resin, a ceramic coating of silicon and aluminium is added by pack cementation. The part is packed both inside and out with ceramic powder and fired to 1650 °C. A silicon carbide coating is formed on the top two layers of the laminate. To protect the coating from spallation, due to differential thermal cracking, the surface is impregnated with tetraethyl-orthosilicate (TEOS). The TEOS is cured to leave a silicon residue throughout the coating, further reducing the area of exposed carbon and providing a glass sealant for cracks in the carbide layer.

The coefficient of thermal expansion (CTE) of the rayon-based fibres used in the shuttle's re-entry parts is roughly twice that of the PAN-based fibres used in today's structural or 'advanced' carbon–carbon (ACC). Rayon-based carbon–carbon has a CTE closer to that of SiC or Si_3N_4 and thus has less mismatch than PAN systems. New structural applications require PAN-based materials which tend to amplify the problems of thermal shrinkage mismatch. Applications in jet engines demand longer and longer operating times at higher and higher temperatures. Exhaustive research is ongoing, developing newer materials and combinations of materials in an attempt to meet these new demands. The oxidation

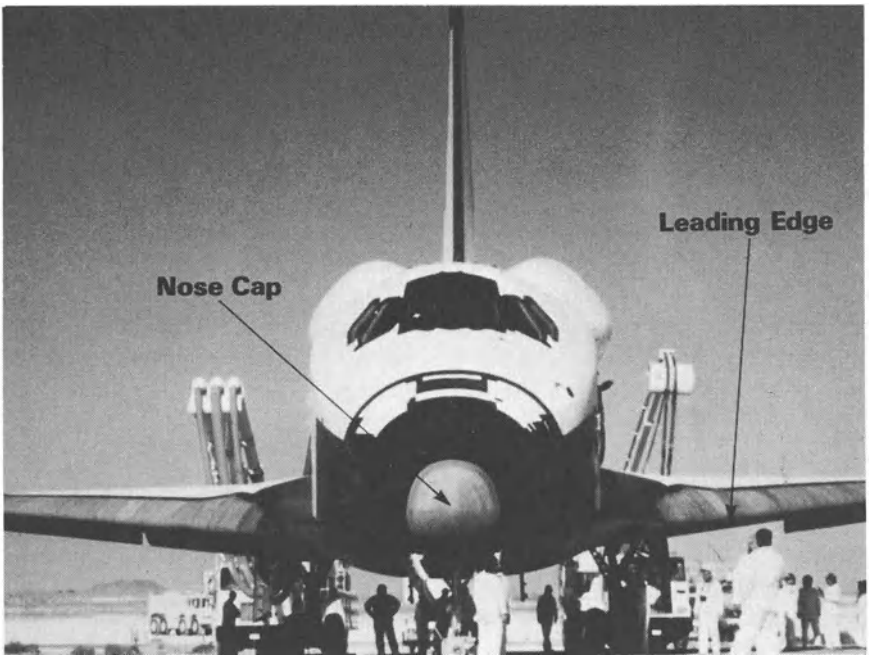

Fig. 6.2 Oxidation-protected carbon–carbon re-entry components of US space shuttle.

protection systems presently in use are generally modifications of the earlier silicon-based systems, using boron [11–13].

All of the contemporary protection systems successfully operating at temperatures of 1500 °C or below, for extended time periods, use boron in one form or another. The benefits obtained from the inclusion of boron and its compounds in carbon–carbon composites are disclosed in a number of recent patents and papers [14–18]. Oxidation protection at temperatures above 1500 °C requires higher refractories as a result of the volatilization of B_2O_3. Short-term protection has been demonstrated at temperatures in excess of 2000 °C, but long-term protection above 1500 °C requires materials systems which have yet to be identified, let alone introduced into service. It is possible, however, to define some of the parameters and problems needing to be addressed in order to achieve the goal of a truly reusable high-temperature (>1500 °C) protection system.

6.2 OXIDATION BEHAVIOUR OF CARBON–CARBON

The oxidation of carbon has been studied, historically, in terms of the combustion of coal. 'Bouduard's reaction' and the steam gasification

reaction have been used to describe carbon's oxidation by CO_2 and H_2O gases. At low to moderate temperatures, the rate-controlling steps of the following two reaction schemes are known to be chemical in nature [19,20]:

$$C(s) + CO_2(g) \rightarrow 2CO\ (g) \tag{6.1}$$

$$C(s) + H_2O(g) \rightarrow CO(g) + H_2(g). \tag{6.2}$$

Catalysts are thus effective in the acceleration of these oxidation reactions.

The rates of oxidation are found to increase exponentially with temperature. Above 700 °C the rate-controlling step generally changes to the diffusion of gaseous species through the boundary layer close to the solid carbon [21]. By contrast, carbon–carbon composites are usually used in air. The oxidation reaction therefore proceeds according to

$$2C(s) + O_2(g) \rightarrow 2CO(g). \tag{6.3}$$

The above reaction has a large driving force, even at very low oxygen partial pressures, as a result of the large negative value of Gibbs free energy change. The rate of oxidation is thus controlled not by the chemical reaction itself, but rather by the transport of the gaseous species to and from the reaction front.

Over a number of years, the Japanese workers Kimura and Yasuda have studied the oxidation behaviour of carbon–carbon between 650 and 850 °C using a thermobalance [22]. The relationship between percentage weight loss and time at a number of different temperatures for the oxidation of a 67% by weight of fibres composite (HTT 2800 °C) is shown in Fig. 6.3. The rate of oxidation increases with temperature but decreases with time. Yasuda *et al.* [22] found the matrix to be more reactive, with a slower oxidation of the fibres. Figure 6.4 shows the effect of composite HTT on the rate of oxidation. The rate clearly decreases with increase in HTT, despite a higher oxidation temperature. A number of other workers have observed the same phenomena independently. In Fig. 6.4, the rate of oxidation, as defined by the slope of the curves, is increasing with time.

An Arrhenius plot (log gasification rates versus $1/T$) for several carbon–carbon materials shows the rate of oxidation to decrease with increase in HTT (Fig. 6.5). At the lower temperatures (below around 600–800 °C) oxidation is controlled by the reaction of oxygen with active sites on the carbon surface [23]. At higher temperatures the rate-limiting step is the diffusion of oxygen through the boundary layer at the surface of the composite [24]. The reaction-controlling steps of the oxidation of carbon–carbon are thus very similar to that of graphite [23].

The general rate of reaction dw/dt, in the zones of the chemical and diffusion-controlled steps respectively, may be expressed as follows [23]:

$$\frac{dw}{dt} = \frac{R}{n} K_s S_v C_r^m \phi + C_r^m K_s f \tag{6.4}$$

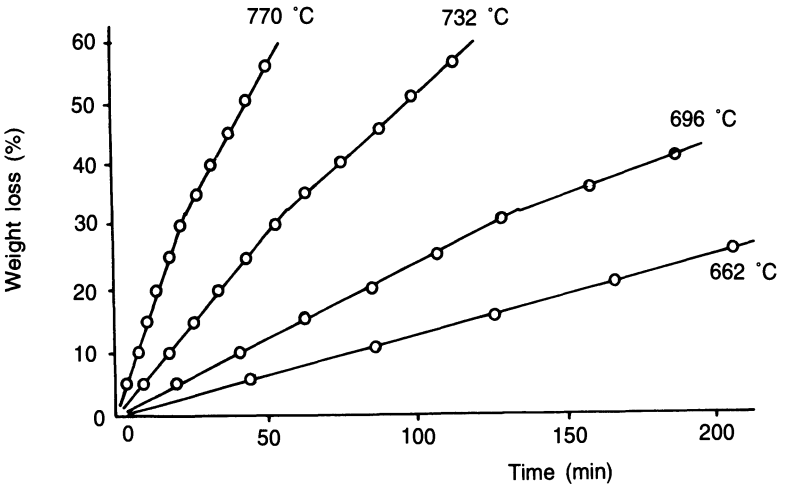

Fig. 6.3 Oxidation of carbon–carbon composite in air [22].

$$\frac{dw}{dt} = \frac{(C_g - C_r)}{\delta} D_f, \tag{6.5}$$

where R is the thickness for a planar sample and radius for a cylinder or sphere, n is 1, 2 or 3 for a plane, cylinder or sphere respectively, K_s the rate constant per unit of reacting surface, S_V the specific internal surface area expressed per unit volume, C_r the concentration of reactant gas at the exterior surface of the reacting specimen, m the true order of reaction, ϕ Thiele modulus, defined as the ratio of the actual rate of reaction to that which would occur if the reacting gas concentration were uniform throughout the material, f a 'roughness' factor of the exterior surface, C_g the concentration of reactant gas in the gas stream, and D_f the diffusion coefficient of the reactant through the boundary layer of thickness S.

The first term on the right-hand side of equation (6.4) represents the reaction occurring **within** the solid, while the second term describes the reaction occurring on the exposed exterior surface. The change in surface area (ΔS_v) is generally proportional to the square of the change in length $(\Delta l)^2$ [25], i.e.

$$\Delta S_v = \alpha(\Delta l)^2 \tag{6.6}$$

where α is a constant. Neglecting the surface oxidation terms in equation (6.4) it becomes

$$\frac{dw}{dt} = \frac{R}{n} K_s S_v C_r^m \phi. \tag{6.7}$$

Inserting equation (6.6) into (6.7)

$$\frac{dw}{dt} = \frac{R}{n} K_s C_r^m \phi \alpha (\Delta l)^2. \tag{6.8}$$

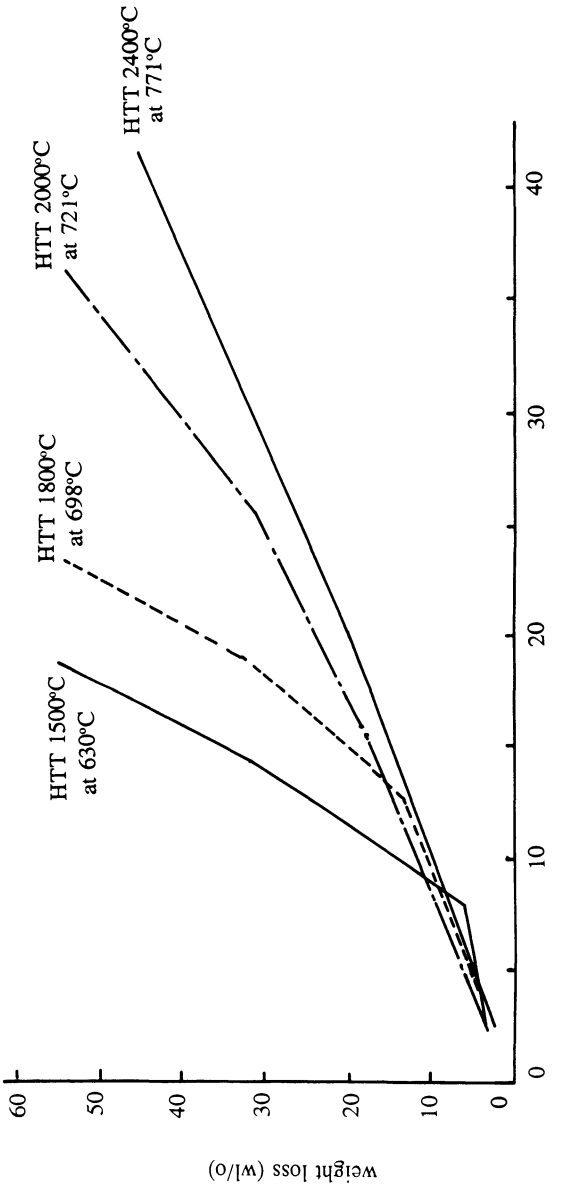

Fig. 6.4 Oxidation of carbon–carbon composites heat treated to different final process temperatures.

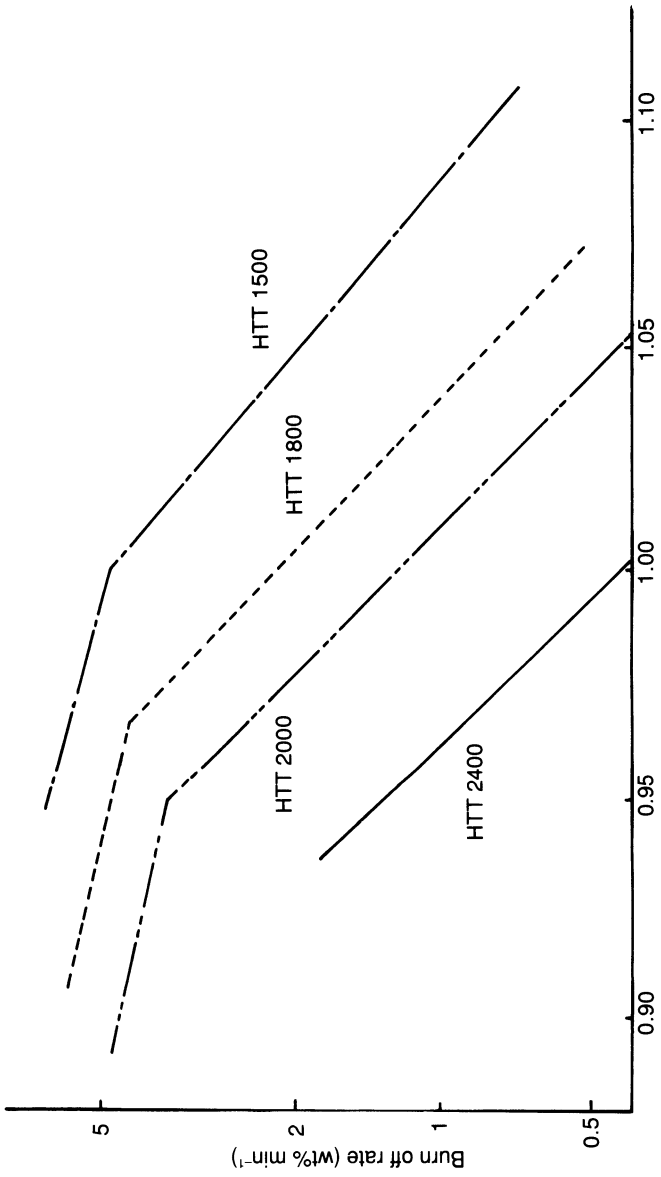

Fig. 6.5 Arrhenius plots of the oxidation of carbon–carbon composites [22].

If it is assumed that Δl is proportional to the square root of time ($t^{\frac{1}{2}}$)

$$\frac{dw}{dt} = \frac{R}{n} K_s C_r^m \phi \alpha' t. \tag{6.9}$$

Differentiation of equation (6.9) yields

$$\frac{d^2w}{dt^2} = \frac{R}{n} K_s C_r^m \phi \alpha', \tag{6.10}$$

showing that the rate of oxidation accelerates with time. If equation (6.9) is integrated

$$W = \frac{R}{n} K_s C_r^m \phi \alpha'' t^2. \tag{6.11}$$

The weight loss due to oxidation is thus proportional to t^2. Curves of oxidation follow a parabola and may be described by a quadratic equation. This result has been illustrated practically by Fischbach and Uptegrove [26] (Fig. 6.6).

The rate of oxidation of carbon fibre/isotropic carbon matrix composites in the region 650–850 °C is quicker than that of both pyrolytic graphite and non-reinforced isotropic (glassy) carbon. As one would expect, oxidation commences at the regions of highest energy, which are manifested as the presence of lots of edge sites and porosity that is to say at the fibre/matrix interface. The reaction then proceeds to regions of laminar, optically anisotropic carbon matrix, optically isotropic 'glassy' matrix, fibre lateral surface, fibre ends and, finally, fibre cores [26].

Microscopic observations indicate that oxidation is governed by the structural defects or by stress accumulation within the matrix as a result of carbonization shrinkage. The general 'rule of thumb' is that the rate of oxidation is increased by increase in operating temperature and reduced by increased HTT of the composite. The latter observation is interpreted as being due to a reduction in the degree of retained impurities, relaxation of carbonization stresses [27] and reduction of reactive edge sites by annealing, despite the increased fraction of open pores. It should be noted that the relative reactivity of the various components of the system do not always follow this idealized pattern. At very high rates of burn-off, for example, the fibres may appear more prone to oxidation than the matrix [24], depending on the type of fibre and matrix.

The surface area S_v increases with the oxidation of carbon–carbon composites as a direct consequence of the preferential oxidation of the matrix. The rate of oxidation therefore accelerates with respect to time in the zone of the chemical rate-controlling step. Equation (6.5), on the other hand, shows that in the zone of the oxygen diffusion-controlling step, the surface area does not affect the rate of reaction. The parameters C_g, C_R,

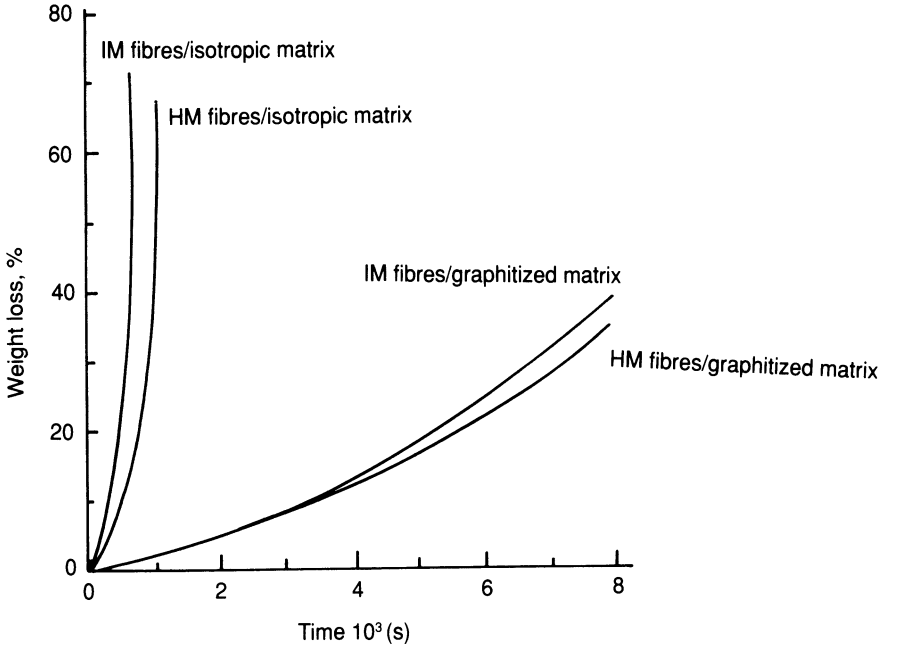

Fig. 6.6 Isothermal oxidation behaviour of carbon–carbon in dry air at 650 °C [26].

D_f and δ are not related to the surface area and may therefore be assumed to be constant. When equation (6.5) is integrated

$$W = \frac{(C_g - C_r)}{\delta} D_f t. \tag{6.12}$$

That is to say, the oxidation loss is proportional to time and may be represented by a linear curve. The oxidation rate does not accelerate with time as shown in Fig. 6.7 [25].

Although investigators generally believe the oxidation of carbon–carbon in air to be controlled by the reaction itself at low temperatures and gaseous transport at higher temperatures, the critical temperature separating the two controlling steps is not well defined or exactly determined. Two very serious problems arise; firstly, the reaction surface changes with time, making it difficult to express the rate of reaction as a simple function of time, temperature and macroscopic surface area of the composite. Secondly, open pores and microcracks are generated during the oxidation process. As a result it is difficult to express the rate of transport of the gaseous species as a simple function of the initial porosity and the labyrinth factor of the composites. Table 6.1, for example, shows the results of Chang and Rhee [27] from their investigation into the increase of the surface area of carbon derived from phenolic resin. The surface area is observed to increase markedly after a 5% loss in weight due to oxidation.

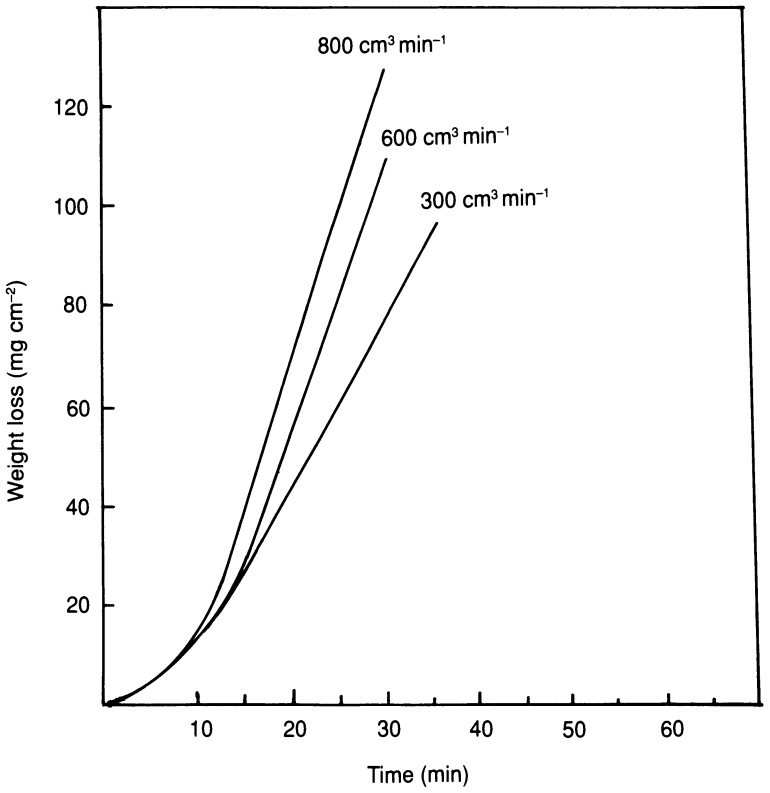

Fig. 6.7 Oxidation of carbon-carbon and the effect of the flow rate of air on the oxidation rates at 600 °C [25].

Table 6.1 Surface area of carbon–carbon ($m^2 g^{-1}$) after 5 and 10% oxidation

HTT (°C)	*Surface loss of carbon–carbon (m^2g^{-1}) after 5 and 10% oxidation* (%)		
	0	*5%*	*10%*
1000	12.6	599	854
1400	1.3	107	114
1800	2.1	24.3	20.5
2400	2.4	4.6	3.1

The rate of increase is clearly very much larger for carbon heat-treated at lower temperatures. Further work by Chang and Rusnak [28], on a carbon–carbon brake material, re-emphasized the general observation that the rate of oxidation increases with increased surface area. The surface area is influenced by the extent of graphitization, degree and shape of porosity, active sites and impurity levels. It is thus virtually impossible to derive a simple relationship between rate of oxidation and surface area.

When the reactant gas flow rate is increased, the thickness of the stagnant layer close to the solid phase is decreased. Chang and Rusnak observed the flow rate to have very little effect on oxidation rate at 650 °C but that the rate of reaction increased significantly with flow rate at 700 °C [28]. When the rate increases with increase of flow rate, diffusion control is generally assumed. They interpreted their results, therefore, as backing up the 'low-temperature chemical/high-temperature diffusion control hypothesis'. In reality, however, the oxidation behaviour is far more complex as illustrated by the results of Thrower and Marx [29]. The oxidation rate of graphite at ≈900 °C was found to be increased by increase in flow rate from 9 to 13 $cm^3\ s^{-1}$ but decreased by further increase to 15 $cm^3\ s^{-1}$. The result was postulated to be due to the change in surface roughness resulting from increased flow rate. What becomes apparent, is that the rate being controlled by diffusion below a threshold temperature and diffusion above is not a general conclusion but rather an empirical observation. Far more detailed work is required before a general rule describing the rate-controlling steps of the oxidation of carbon–carbon composites is established. In either rate-controlling zone, the rate of reaction is found to be proportional to the partial pressures of oxidizing gases.

Thrower and Marx also measured the effect of an applied compressive stress upon the rate of oxidation of graphite. Their results showed there to be no major effect upon oxidation [29]. A tensile stress, on the other hand, was found to accelerate oxidation as a result of the increase in open porosity and microcrack density [30,31]. Peng was furthermore able to show a decrease in tensile strength of polycrystalline graphite as a direct result of oxidation [32]. He attributed his findings to pore enlargement and component debonding.

6.3 FUNDAMENTAL CONCERNS IN THE OXIDATION PROTECTION OF CARBON–CARBON COMPOSITES

In developing a successful oxidation protection system for carbon-based materials there are a number of factors which must be considered, as depicted schematically in Fig. 6.8. The primary aim is to apply a coating system which isolates the composite from the oxidizing environment. This

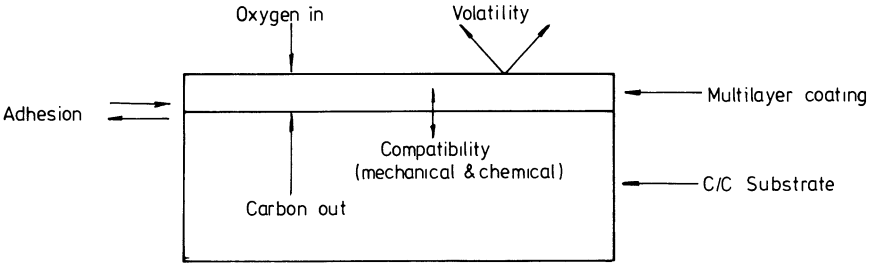

Fig. 6.8 Considerations when designing a carbon–carbon oxidation protection system.

coating system must have at least one major component which acts as an efficient barrier to oxygen. The primary oxygen barrier must ideally exhibit low oxygen permeability and ought to encapsulate the carbon with few or no defects through which the oxidizing species can ingress. Additionally, it must possess low volatility to prevent excessive ablation in high-velocity gas streams. A good level of adherence to the substrate must be achieved without excessive substrate penetration. The internal layers must also prevent outward diffusion of carbon to avoid carbothermic reduction of the oxides in the outermost layers. Finally, all of the various interfaces must exhibit chemical and mechanical compatibility.

In designing protection systems for high-performance, structural carbon–carbon for long periods of operation, mechanical compatibility, i.e. the avoidance of coating spallation, becomes the overriding issue. Figure 6.9 [33,34] compares the thermal expansion behaviour of a number of refractory ceramics with those of carbon–carbon (in-plane). The composite has a considerably lower CTE within fibre-reinforced lamina than any ceramic exhibiting a symmetric crystal structure. Any applied coatings therefore contain microcracks since the coating process is carried out at elevated temperatures. We may therefore schematically represent the relationship between protection requirements and system performance (Fig. 6.10) [35].

The oxidation threshold for carbon–carbon is around 370 °C, which may be improved to approximately 600 °C by the incorporation of refractory particulate inhibitors. The 'intrinsic protection range' of the coating is defined by the microcracking temperature and the limiting use temperature of the coating. In this range, the cracks are mechanically closed and sealed by the oxidation products. Flaws always exist in the primary oxygen barrier due to fabrication imperfections, thermal expansion mismatch with the substrate, or as a result of service stresses. To date, the most successful solution to the cracking problem has been the employment of a sealant glass to fill any cracks in the primary coating. For a successful full range of oxidation protection, the glass sealant must be capable of operating from ≈600 °C to the microcracking temperature of the primary oxygen barrier.

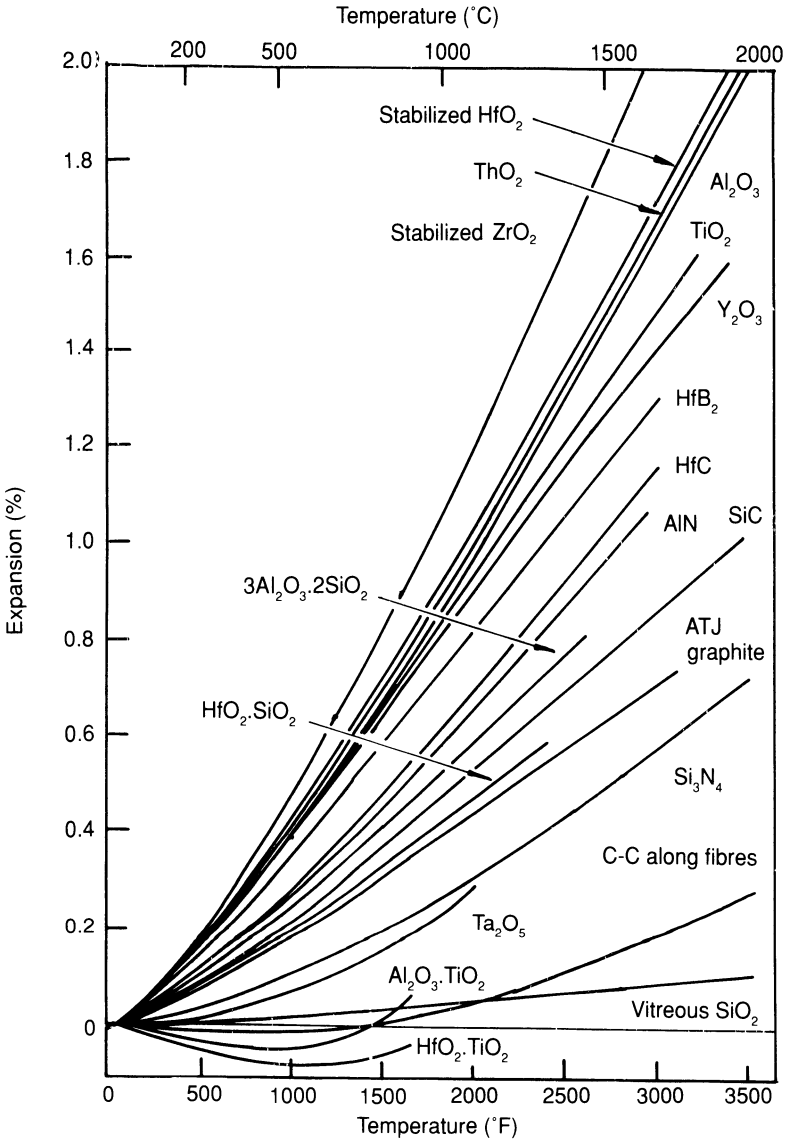

Fig. 6.9 Comparison of the thermal expansion characteristics of a number of refractory materials [33, 34].

In choosing the primary oxygen barrier, one would ideally prefer a material which forms an adherent *in situ* oxide so that oxygen is gettered at free surfaces. The oxidation kinetics of several candidate refractories are compared in Fig. 6.11. The kinetics of oxide growth are considerably slower for the silicon-based ceramics than those based on aluminium, hafnium or zirconium [36–42]. The silicon ceramics exhibit the most attractive thermal expansion compatibility with carbon–carbon and the lowest oxidation rates;

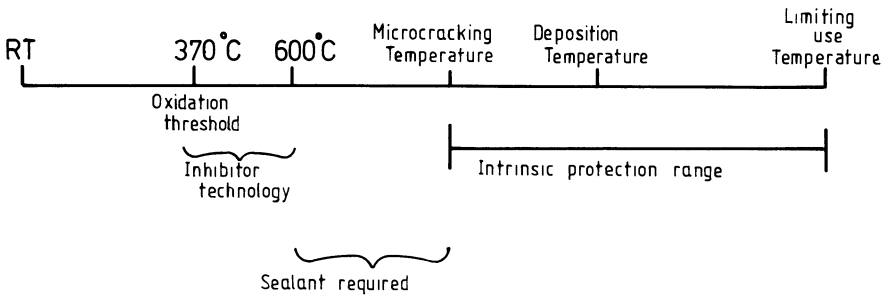

Fig. 6.10 General oxidation behaviour of carbon–carbon composites coated with oxidation protection systems.

thus the amorphous SiO_2 scales which grow during oxidation have very low oxygen diffusivity. Thin films of these materials can thus be utilized for protection without concern for total conversion of the ceramic coating or oxide spallation. They are limited at high temperatures, however (>1700 °C), by dissociation of SiO_2, and at low temperatures because the silica glass is too viscous to flow and effectively seal cracks. It is therefore appropriate to discuss oxidation protection in three different temperature regimes: below 1500 °C, 1500–1800 °C and above 1800 °C.

6.4 PROTECTION AT TEMPERATURES BELOW 1500 °C

Ceramic coatings such as silicon carbide and silicon nitride are excellent primary barriers to oxidation. They are both refractory and oxidation-resistant due to the formation of a silica skin upon oxidation. Silica exhibits a relatively low vapour pressure to temperatures as high as 1650 °C as well as low oxygen diffusivity [43–45]. If cracks develop in the primary coating self-sealing can occur, because the silica skin exhibits a relatively low viscosity at elevated temperatures allowing it to flow effectively into the cracks, preventing oxidation of the underlying substrate. At temperatures below 1150 °C, however, the viscosity of the silica glass is too high for it to afford any crack-sealing properties. Additionally, thermal cycling of the composite results in cracking and spallation of the oxidation protection system as a result of the mismatch in the thermal expansion of the substrate and coating.

The most successful approach to solving this problem, to date, involves the introduction of boron or a boron-containing additive into the carbon–carbon substrate. The addition of boron has been found to retard the oxidation kinetics of a number of carbon materials including carbon–carbon composites [46,47]. Oxidation of boron results in the formation of boric oxide, B_2O_3, which has a lower melting-point and viscosity than silica [48]. Additives such as zirconium boride, boron and boron carbide particles,

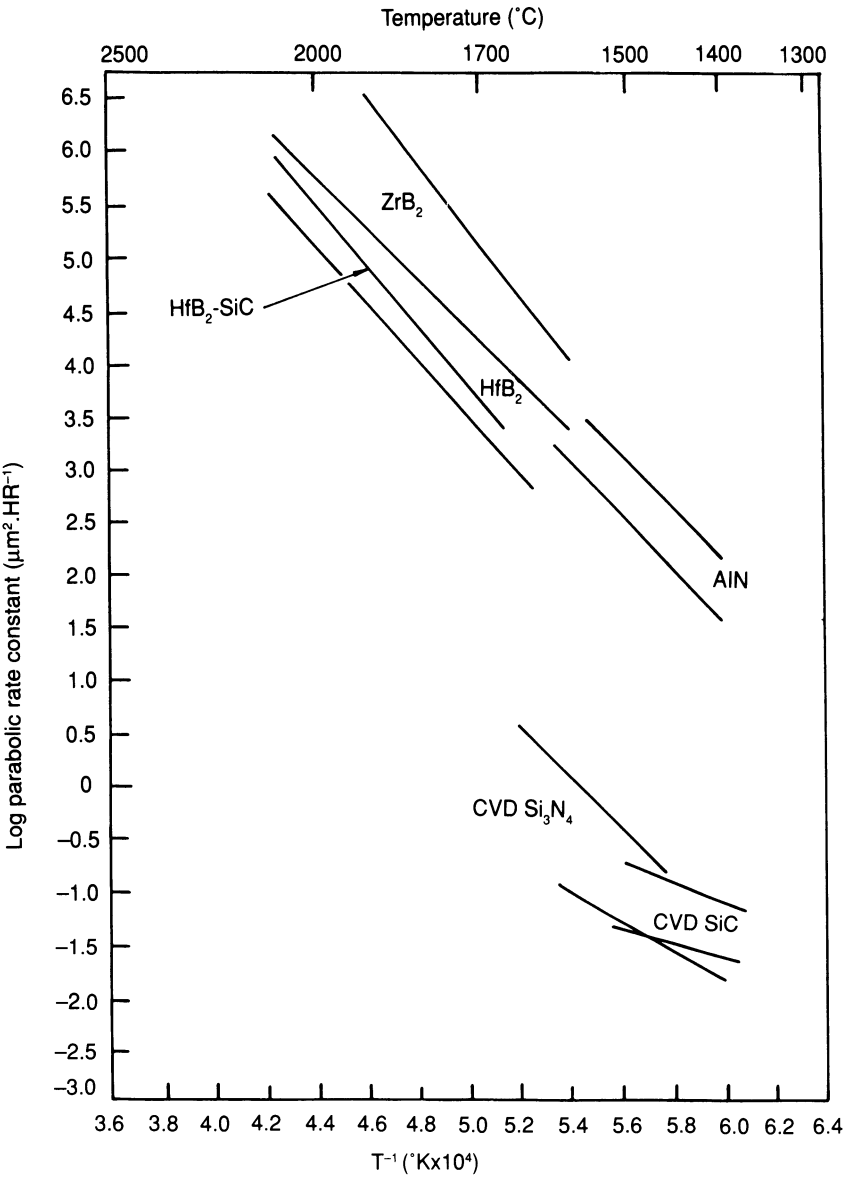

Fig. 6.11 Oxidation of refractory ceramics [36–42].

oxidize in air spreading a borate glass within the composite. A number of so-called 'inhibited' prepregs, for example, are available commercially for this purpose. The inhibitors only become effective, however, after appreciable fractions of the carbon have been gasified [49]. Furthermore, boric oxide exhibits higher vapour pressure and oxygen diffusivity than silica [18,50,51]. It is thus generally used as a secondary oxidation barrier beneath the primary coating which acts to minimize its depletion.

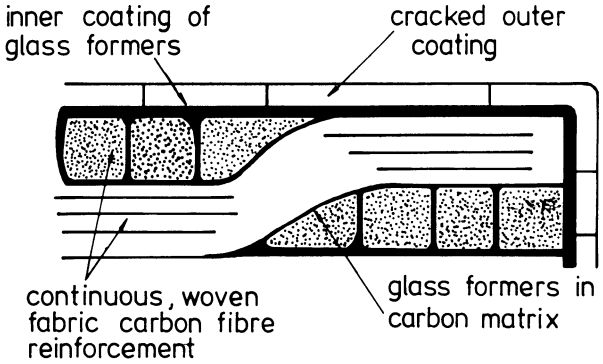

Fig. 6.12 Schematic diagram of carbon–carbon oxidation protection system.

A protection system, based upon the aforementioned principles, has been developed by GA Technologies in the USA. The material, denoted VLG-25/IMCC-3, has shown oxidation resistance for hundreds of hours of cycling between room temperature and 1370 °C and is shown schematically in Fig. 6.12 [10].

The composite materials system has also been successfully operated in stressed oxidation tests in the same temperature regime, and high flow rate burner and rig tests at temperatures of up to 1540 °C gave no indication of failure. It consists of a carbon–carbon composite substrate with borate glass former inhibitors, an inner coating of borate glass formers and an outer coating of CVD-deposited silicon carbide.

The problems associated with oxidation-protected carbon materials of this genre are moisture sensitivity of borate glasses, spallation of the carbide coating under thermal cycling and the long-term chemical compatibility between SiC and the borate glass. The exposure of borate glasses to ambient moisture in the air causes a gradual hydrolysis, resulting in swelling and crumbling of the glass. Hydrolysis of the borate glass sealant may cause coating spallation at room temperature due to glass swelling, and spallation during heating as a consequence of the rapid release of mositure. The high volatility of hydrated borates can add to the disruption on heating, resulting in glass depletion at relatively low temperatures in moist environments.

The solution generally employed is to modify the borate glass composition to improve moisture durability while retaining its attractive viscosity and carbon-wetting characteristics. As an example, it has been shown that additions of alkali significantly reduce the ambient moisture sensitivity of B_2O_3 [52,53]. Lithium appears to have a particularly strong effect [10]. In addition, lithia Li_2O is the most thermodynamically stable alkali oxide and is compatible with carbon in the same temperature range as boric oxide [54]. Studies show that lithia tends to reduce the viscosity of B_2O_3 at high

temperatures, although this may be corrected by the addition of a third oxide which will also improve moisture resistance [48,52,55]. Li_2O additions also increase the surface tension of B_2O_3 so that the carbon wetting may be somewhat impaired as compared with a 'pure' borate glass [52,56].

Spallation of the silicon carbide primary oxidation barrier occurs as a result of its thermal expansion mismatch with the carbon–carbon substrate. The problem may be alleviated slightly by replacing SiC with a coating of silicon nitride which has a lower CTE (3.2 as opposed to 4.9×10^{-6} °C^{-1}). It is further possible to reduce the thermal expansion coefficient by vapour depositing a modified primary coating of either SiC or Si_3N_4 containing a dispersion of low expansion particulates of, for example, silica or boron nitride (BN). The first carbon–carbon composites to be deployed in service consisted of rayon-based fibres as the reinforcing phase. As discussed earlier, thermal mismatch was not such a great problem with the rayon fibres as those derived from PAN as they have around double the CTE. It is not inconceivable that one ought to be able to 'engineer' both PAN fibres and carbon matrix to increase the CTE of the substrate, but it is doubtful whether this could be done without adversely affecting mechanical properties. If one has a highly oriented carbon fibre – PAN or pitch – it will have a low, or negative CTE. Only poor orientation fibres have a high CTE and hence poor mechanical properties.

At high temperatures, a chemical incompatibility arises between the borate glass and the outer coating as a result of fluxing of the protective layer of SiO_2, formed on the primary protective coating, by the glass. Additions of silica and lithia, etc., used to improve moisture durability and increase the high-temperature viscosity of the borate glass, will also serve to retard the interaction with the outer layer by lowering the chemical driving force for interdiffusion.

The factors governing oxidation protection below 1500 °C are well understood and based on proven scientific principles backed up by experimental evidence. A number of systems have been employed in service with a good deal of success, the most notable being that on the space shuttle. A great deal of optimization and development work remains to be done, however, and one would certainly expect a number of improvements in the future.

6.5 PROTECTIVE COATINGS FOR THE 1500–1800 °C RANGE

The reduction of borate glasses by carbon limits oxidation protection systems of the type developed by General Atomic (VLG-25/IMCC-3) to temperatures below 1500 °C. Thermodynamic analysis (Fig. 6.13) [54], shows the total CO pressure for the reduction of B_2O_3 by carbon, to form B_4C and CO, to be approximately 0.1 MPa (1 atm). Since CO pressures at higher temperatures are greater than the total ambient pressure, 1500 °C may be considered as the upper limit for boric oxide in contact with carbon.

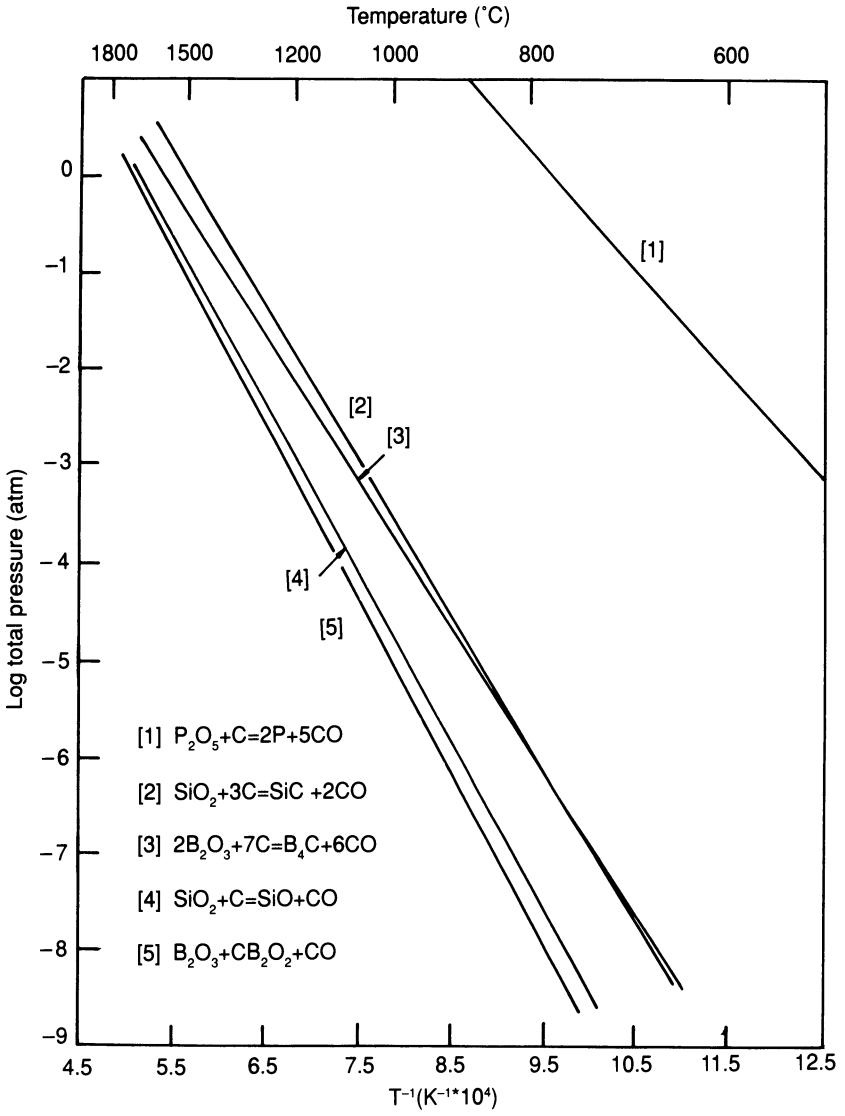

Fig. 6.13 Carbothermic reduction of glasses [54].

It is important to note that the data presented in Fig. 6.13 show this same temperature limit to exist for the reaction of silicate glasses with carbon.

In discussing oxidation protection at elevated temperatures it is first necessary to define the upper temperature limit of silicon-based ceramic coatings. Experimental work has shown the upper use temperature of CVD coatings of SIC and Si_3N_4 to be defined by reactions at the interface between the SiO_2 scale and the underlying ceramic [36,57]. A thermodynamic analysis of the stability temperature of SiC and Si_3N_4 is shown in Fig. 6.14

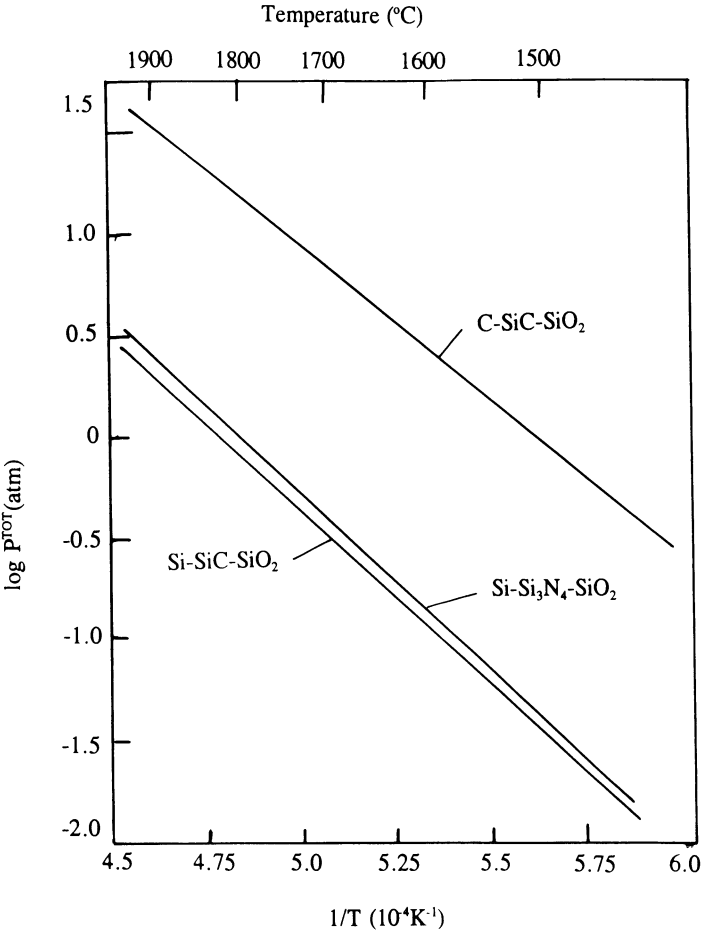

Fig. 6.14 Total gas pressures at three equilibrium conditions in Si–O–C and Si–O–N systems [35].

[35]. It can be seen that, if the silicon activity is maintained at unity, SiO_2 films will be stable on SiC or Si_3N_4 up to approximately 1800 °C. At higher temperatures the reaction product gas exceeds 1 atm, thus disrupting the protective scale. Strife and Sheehan [35] have clearly demonstrated, in the case of silicon nitride vapour-deposited films, that exposure to flowing air at 1760 °C produced a stable SiO_2 scale growth, whereas oxidation at 1840 °C caused gas generation and bubble formation in the silica. It has further been shown that the temperature limit for the stability of B_2O_3 on B_4C with unit boron activity is roughly 1760 °C [10]. One may conclude, therefore, that the temperature limit of the protective oxide coatings may be enhanced by several hundred degrees provided they are in contact with carbides rather than carbon.

Borate glass sealants are employed in oxidation protection systems to

provide protection below the intrinsic protection range by the sealing of microcracks in the outer protection layer. This is an especially important consideration in the case of components which are subject to thermal cycling between ambient and their designed operating temperature. From the standpoint of chemical compatibility, it ought to be possible to use borate glass sealants in conjunction with boron carbide inner coatings up to temperatures of 1760 °C. The use of borate glasses at such high temperatures is unfortunately not possible due to volatilization, high oxygen permeability and poor compatibility with SiC and Si_3N_4 outer coatings.

The glass, despite being primarily contained beneath the outer coating, would be very prone to volatilization over extended periods at temperatures above about 1300 °C. It is difficult to imagine a useful protection period of over 10 h using borate glasses at or above this temperature. Furthermore, as one may easily deduce from Fig. 6.15 [44,50]. B_2O_3 has a relatively high permeability to oxygen while silica forms an excellent barrier to the diffusion of oxygen. It thus becomes apparent why silicon ceramics, which oxidize to produce protective layers of SiO_2, are oxidation resistant to temperatures above 1650 °C, whereas boron carbide and nitride are limited to much lower temperatures. Indeed, it is postulated that the rates of oxidation of SiC and Si_3N_4 remain very slow up to temperatures at which the stability of the oxide is the performance-limiting factor [36].

The high-temperature limitations of borates require that they be replaced for operation in the 1500–1800 °C region. The obvious choice is to use a refractory silicate glass in contact with a silicon carbide inner coating. The vapour pressure of SiO_2 is several orders of magnitude lower than that of B_2O_3 in this region [10]. Silica also offers lower oxygen permeability and improved chemical compatibility with the outer CVD coatings. The major problem associated with silicate glasses is their high viscosity at low temperatures. The viscosity of 'pure' SiO_2 glass is generally an order of magnitude or more higher than pure B_2O_3 and borate glasses, thus limiting the flow necessary to allow for effective crack sealing and spreading on internal surfaces.

A logical approach to the viscosity problem is to use highly fluxed silicate glasses. The obvious choices for additions are lithia and boric oxide, since their strong fluxing action is coupled with thermodynamic stability. Alkali additions are the stronger flux, reducing the viscosity of SiO_2 into the borate range at temperatures above 800 °C. All silicate glasses are found to exhibit viscosities which are strongly dependent on temperature, being very high below 800 °C. The viscosity behaviour at 800 °C achieved by fluxing SiO_2 with Li_2O therefore probably represents the best achievable from this glass system.

As is often the case in materials science, altering or blending a material to improve one property must be done to the detriment of another. The fluxing of silicate glasses with oxide additions such as B_2O_3 and Li_2O is no

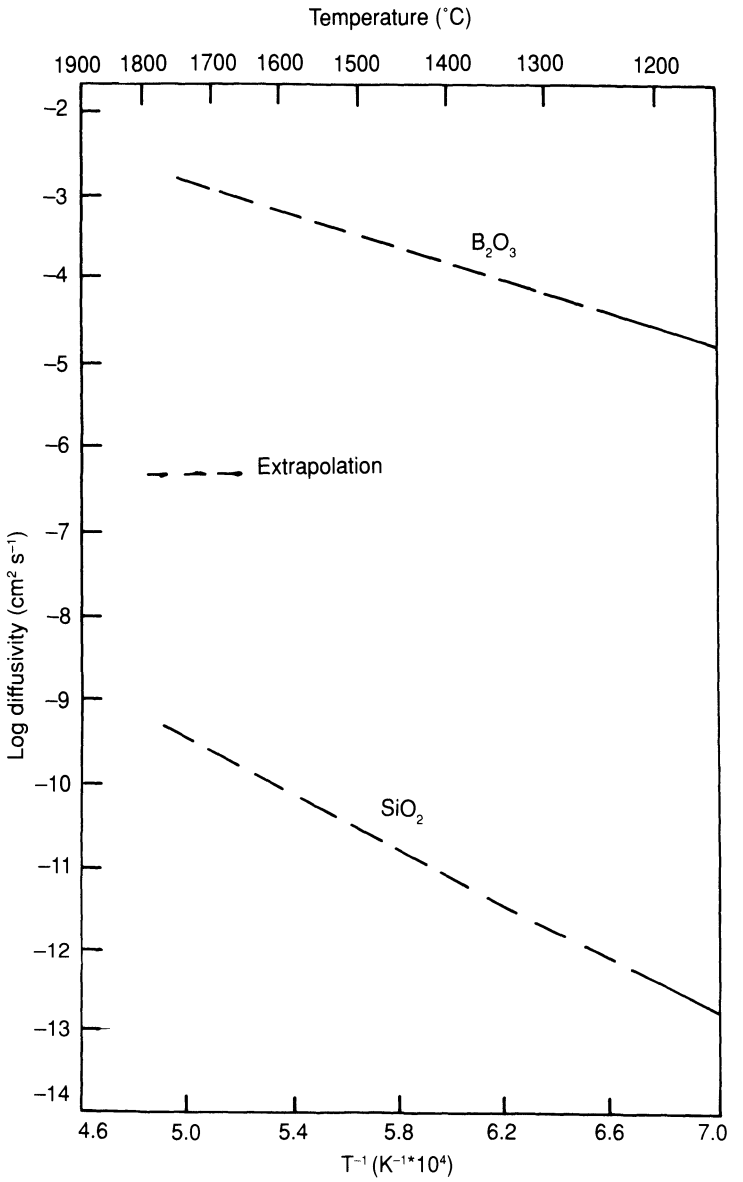

Fig. 6.15 Oxygen diffusivity in SiO_2 and B_2O_3 glasses [44,50].

exception to this rule. Both additions compromise the advantages pure SiO_2 presents over borate glasses in that they reduce moisture durability and increase oxygen permeability. Damage due to mositure uptake, chemical incompatibility with outer coatings and accelerated oxygen transport to the substrate might therefore result. Both B_2O_3 and Li_2O have significantly higher vapour pressures than SiO_2 (although that of Li_2O is

an order of magnitude lower than that of B_2O_3) and thus may present volatility problems over long periods at high temperatures.

The silicon ceramics generally favoured as outer coatings in carbon–carbon oxidation protection systems are limited in temperature of operation to around 1800 °C. Glass sealants employed to repair cracks in the outer coating are reduced by the carbon–carbon substrate at temperatures of 1500 °C and above, but may be used to higher temperatures provided a carbide inner layer is employed. Borate glass sealants ought to be chemically compatible with such interfacial carbide layers up to around 1760 °C, but the relatively high vapour pressure of B_2O_3 tends to dictate a limit of 1650 °C or lower. Borates tend to be protective down to the temperatures generally associated with the onset of carbon oxidation. Glasses based on silica provide a temperature advantage over borates, the limit again being set by volatility and/or chemical compatibility. Additionally, silicate glasses are thought to possess improved moisture durability, oxygen permeability and chemical compatibility with outer coatings. The major drawback with silicate glasses is a high viscosity at low temperatures which reduces protection at those temperatures. Fluxing the silicate with oxide additions can reduce the low-temperature viscosity but at the expense of high-temperature performance.

6.6 OXIDATION PROTECTION AT TEMPERATURES IN EXCESS OF 1800 °C

Outer coatings of silicon ceramics cannot be used in long-term protection of carbon–carbon at temperatures above 1800 °C because reaction product gases disrupt the protective SiO_2 layer whence oxidation resistance is derived. Glass sealants cannot be used in contact with the composite substrate or interfacial carbide layers for the same reason. Protection of carbon to very high temperatures thus requires the understanding of the fundamental principles governing behaviour of materials at those temperatures. This will necessitate the development of coating systems very different and far more sophisticated than those employed at lower temperatures.

The most oxidation-resistant refractory materials at temperatures in excess of 1800 °C, identified to date, are hafnium boride (HfB_2) and mixtures of the same with silicon carbide [37, 38]. A great deal of research is presently under way, assessing these materials in short-term protection applications at temperatures in which silicon ceramics cannot operate. Figure 6.11 shows hafnium boride materials to oxidize in a parabolic manner but at a fairly rapid rate. Calculations have shown that 100 h at 1927 °C would produce approximately 2 mm of oxide scale on the surface of a CVD-deposited HfB_2–SiC material [41,42]. An outer coating of this

material would therefore oxidize through and become an oxide coating within a very short period of time. Similar observations are made for refractory carbides such as HfC.

The high rates of oxidation of refractory carbides and borides preclude their use in long-term protection above 1800 °C. The only viable solution is to use refractory oxides as the primary oxidation barrier. The use of these oxides will, however, create problems of physical and chemical compatibility. When selecting an oxide coating it is necessary to consider its melting-point, vapour pressure and coefficient of thermal expansion. The vapour pressures of a number of appropriately high melting oxides are compared with those of selected carbides and nitrides in Fig. 6.16 [10]. The data show zirconia (ZrO_2), hafnia (HfO_3), yttria (Y_2O_3) and thoria (ThO_2) to possess the necessary thermal stability for long-term use above 2000 °C, while alumina (Al_2O_3) could be used in the 1800–2000 °C range.

Figure 6.9 shows how all but a few oxides have large CTE mismatches with carbon materials. The spallation of coatings during thermal cycling therefore presents a serious problem [33]. A number of hafnium, zirconium and thorium titanates and silicates exhibit both high-temperature stability and low CTE [33,34]. All of these materials have highly anisotropic crystal structures and microcrack at low temperatures. Pure silica glass has a very low CTE but devitrifies in the 1000–1650 °C temperature range. The resulting cristobalite phase transforms to a modified structure at low temperatures with an associated volume contraction of around 3% [58]. Such disruptive behaviour, when combined with viscosity and vapour pressure characteristics, indicates silica to be an inappropriate choice as outer coating since it would erode rapidly in high gas flow conditions.

The rapid oxidation of HfB_2 makes the choice of effective oxygen barrier a serious concern. The high refractory oxides all have high oxygen permeabilities (Fig. 6.17). Silica, on the other hand, is one of the least permeable oxides [45,59]. One might therefore propose a dual system, consisting of a refractory oxide outer coating to act as an erosion barrier, with an inner SiO_2 glass coating as an oxygen barrier and sealant for cracks in the outer coating. Iridium has been used for some time to protect graphite from oxidation [8, 9], being an efficient barrier to both oxygen and carbon diffusion at temperatures up to 2100 °C. The noble metal is, as previously discussed, impractical, except in low-volume specialized applications, due to high costs and limited availability.

The dual coating of refractory oxide over silica glass will, unfortunately, be chemically incompatible with carbon or carbides. The SiO_2 would require to be separated from the substrate by a layer of refractory oxide. The inner oxide layer, to ensure carbon compatibility, ought to be in contact with a refractory carbide interlayer between it and the carbon–carbon composite. Figure 6.18 shows the carbides of tantalum (TaC), titanium (TiC), hafnium (HfC) and zirconium (ZrC) to have appropriately low

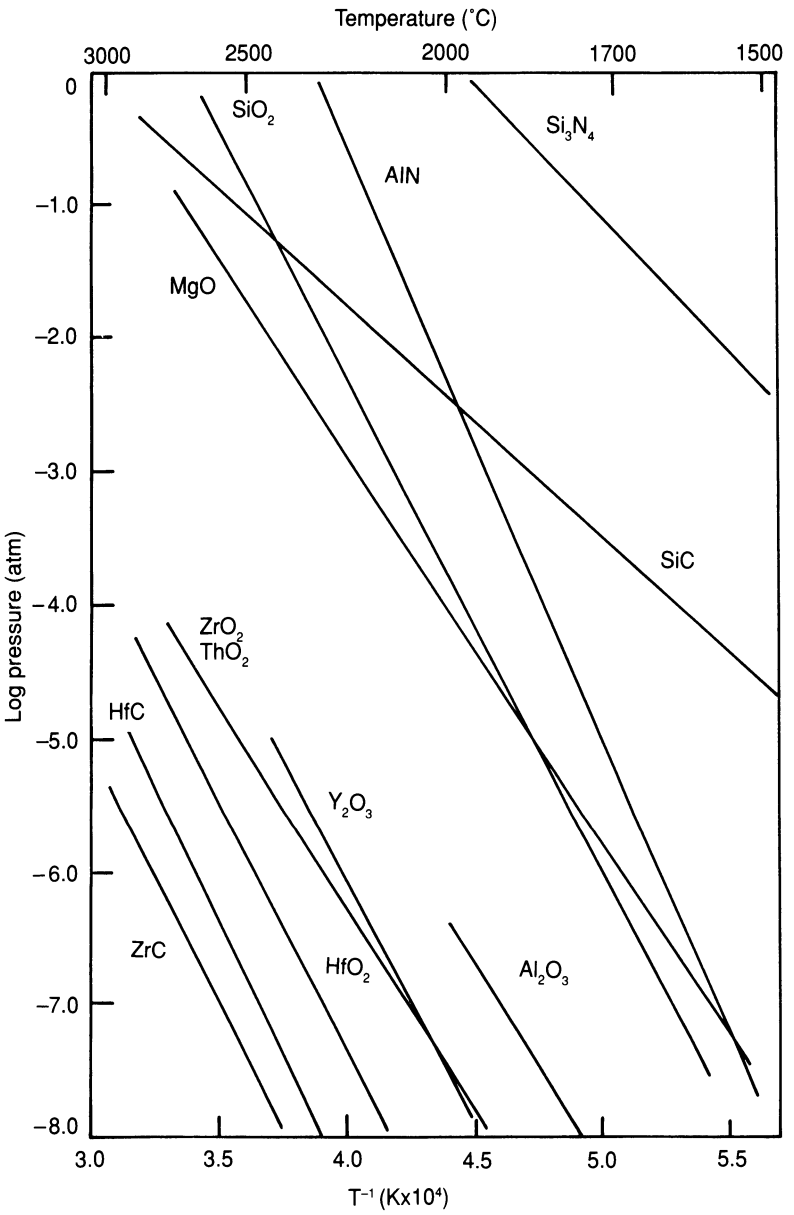

Fig. 6.16 Vapour pressures of ceramic materials [10].

carbon diffusivities [60]. The four-layer protection system would therefore consist of: refractory oxide/modified SiO_2 glass/inner refractory oxide/ refractory carbide (Fig. 6.19). A multi-layer coating such as this, while possessing the required chemical stability, would present serious problems in deposition of consistent quality. In addition, the high CTE of the

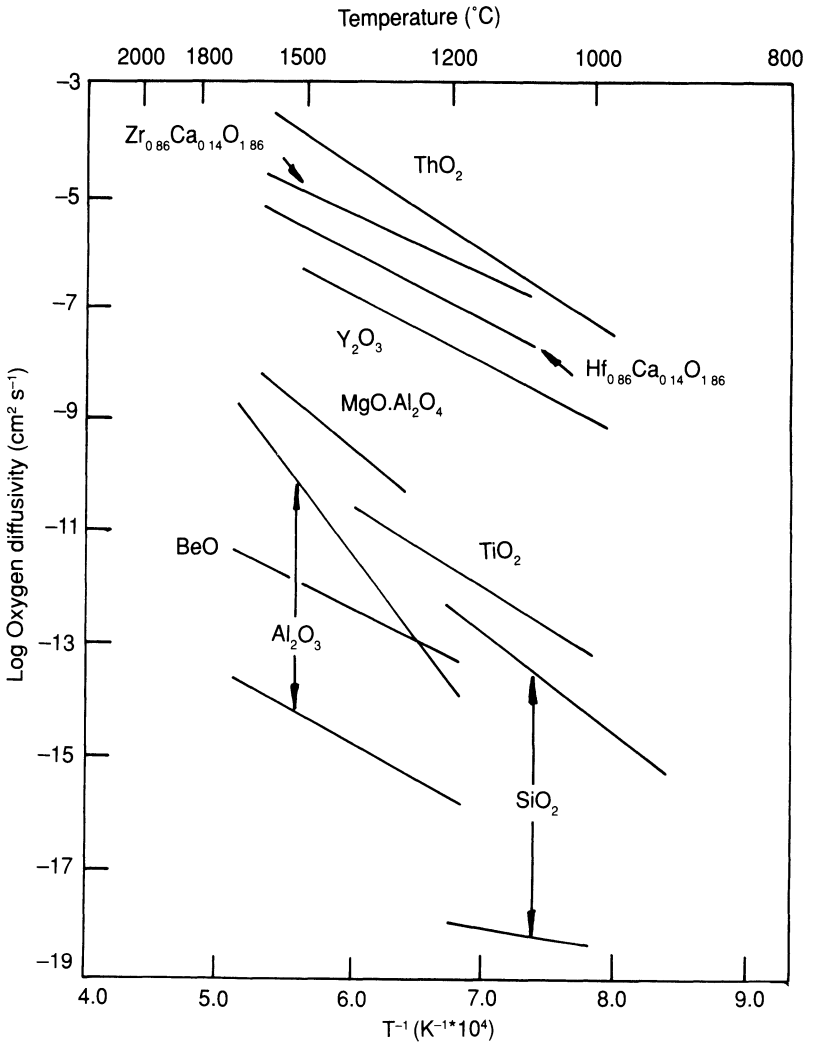

Fig. 6.17 Apparent oxygen diffusivities in silica glass and polycrystalline oxides [45,59].

protection system compared to the substrate will create severe problems of mechanical compatibility in thermal shock situations.

6.7 SUMMARY

The excellent high-temperature properties of carbon–carbon composites make them prime candidates for use in a whole host of refractory engineering structures. A great number of these applications, such as jet engines, require the component to operate in an oxidizing environment. Their

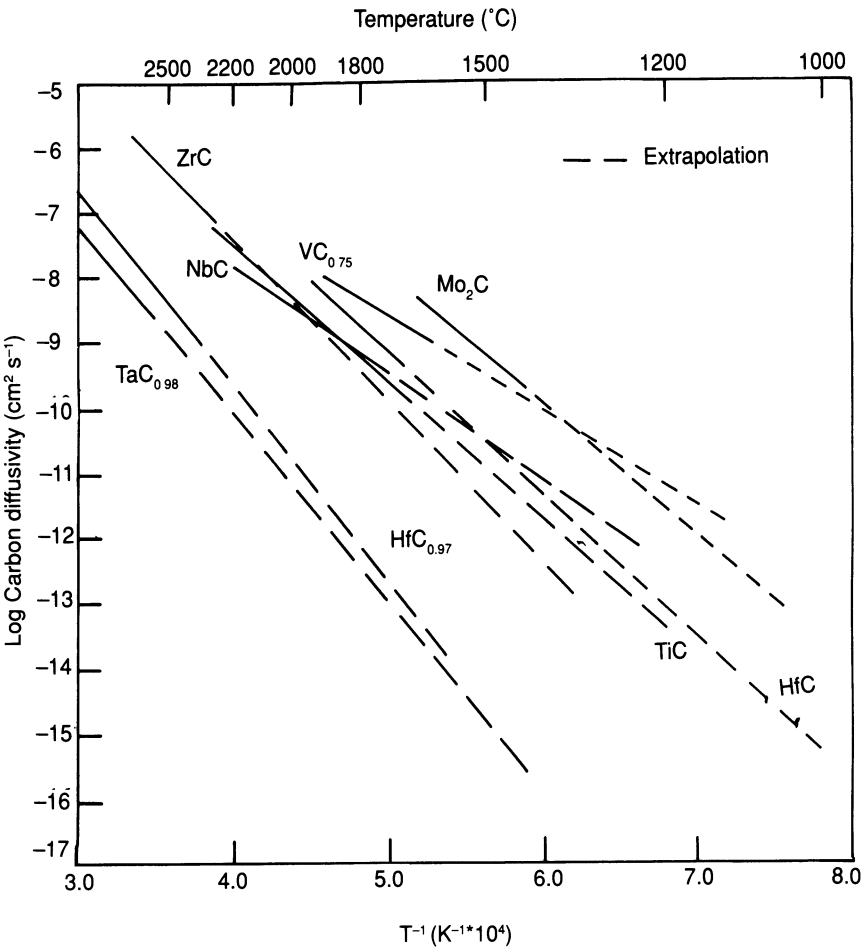

Fig. 6.18 Apparent carbon diffusivities in polycrystalline carbides [60].

usage is thus grealty limited unless they can be protected in some way from oxidation. Carbon–carbon will oxidize at temperatures as low as 370 °C in air. Experimental work has shown the oxidation reaction at low temperatures to be controlled by the reaction of oxygen with active sites on the carbon's surface. At higher temperatures, the rate-limiting step is the diffusion of oxygen through the boundary layer at the surface of the composite. The temperature at which the reaction changes to being governed by one regime or the other varies considerably from material to material within the 600–800 °C range. The oxidation mechanisms which occur, in what are extremely complex multiphase materials, are virtually impossible to model to any degree of accuracy with simple mathematical relationships. The majority of information tends, therefore, to be empirical, based on experimental observations. Oxidation attack tends to occur

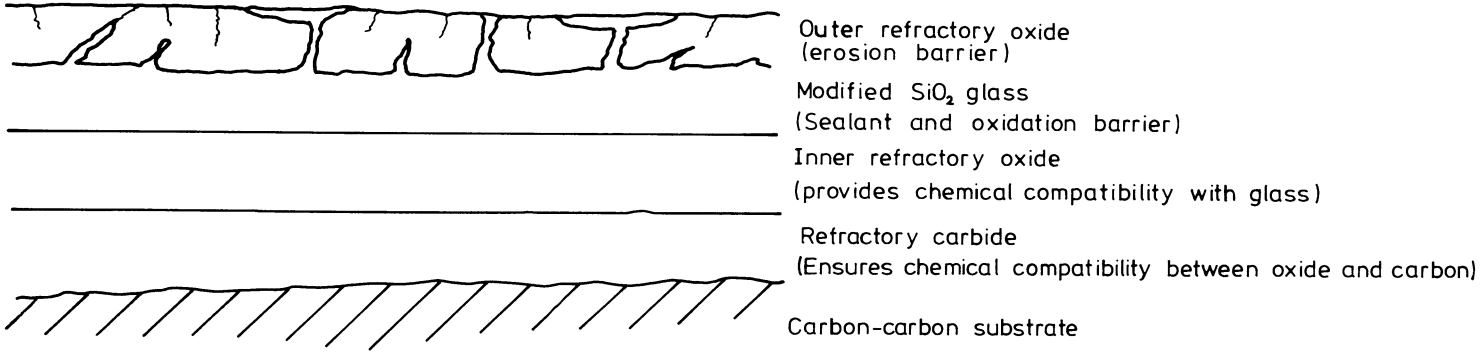

Fig. 6.19 Idealized coating system for long-term oxidation protection of carbon–carbon at temperatures of 1800 °C and above.

preferentially in high-energy regions such as the fibre/matrix interface, proceeding to laminar, isotropic and finally fibrous carbon. Increasing the HTT of the composite increases the temperature of the onset of oxidation and decreases the oxidation rate. This is believed to occur as a result of a reduction in reactive edge sites, defect concentration and residual carbonization stresses.

The only solution to the problem of carbon oxidation is to isolate the material from the high-temperature gas. This is achieved by encapsulating the composite in a refractory coating system. The coating must possess low permeability to oxygen, chemical compatibility with the substrate, good adhesion without excessive penetration and a comparable CTE to avoid spallation under thermal cycling. The onset of oxidation of carbon–carbon can be extended to around 600 °C by the use of inhibitors. These are ceramic materials placed within the composite substrate. Upon oxidation, oxide glasses are formed which flow within the structure forming an oxygen barrier, the most widely used being borates. Inhibited carbon–carbon is limited to 600 °C by the volatilization of the protective glass. Furthermore, some of the carbon is always lost because of the finite time period prior to the glass becoming effective, which depends upon its viscosity.

The driving force for the oxidation protection of carbon–carbon composites was the development of the leading edges and nose cone of the space shuttle. All of the successful systems which have evolved use a primary protective coating of a silicon ceramic. Coatings such as silicon carbide or nitride, when oxidized, form a protective surface scale of SiO_2 which acts as a barrier to the diffusion of oxygen. The coatings are applied by CVD, pack cementation or direct reaction with the substrate. All of the materials used as coatings exhibit higher coefficients of thermal expansion than the carbon–carbon substrate.

The problem of thermal mismatch between the composite and its protection system has been exacerbated in recent years with the move from low strength and modulus rayon-based fibres towards PAN fibres which generally possess a CTE of around half that of their predecessors. Oxidation-protective coatings are therefore generally flawed and cracked as a result of differential thermal expansion between themselves and the composite on cooling from the coating temperature. Borate glass forming materials are placed within the substrate and coating to enable cracks and other flaws within the coating to be sealed. This is done in order to prevent loss of carbon and reduce spallation of the outer coating during thermal cycling. Systems of this type have been successfully tested for hundreds of hours of operation. Much optimization remains to be done however as, for example, in the modification of the borate glass sealants to reduce their susceptibility to moisture and volatilization, and the lowering of the CTE of silicon ceramics with particle additions.

Oxidation protection at temperatures above 1500 °C demands more

sophisticated materials systems to be effective. At this temperature both silicate and borate glasses, used as sealants, are reduced by the carbon substrate. To increase the temperature of operation it is necessary to introduce an inner protective layer of a carbide between the carbon and the glass. Borate glasses are prone to volatilization at around 1500 °C and require to be replaced. Silicate glasses offer lower oxygen diffusity and better chemical compatibility over borates at high temperatures, but a high viscosity at low temperatures reduces their effectiveness as sealants. Additions of alkali or B_2O_3 can lessen this problem but at the expense of moisture vulnerability and high-temperature performance.

Silicon protective coatings are limited in temperature of operation to ≈1800 °C. At or above this temperature the products of reaction disrupt the protective oxide scale, thus rendering long-term protection impossible. Much research is ongoing into addresssing the fundamental scientific and engineering problems posed at such high temperatures. Just how effective the work has been is difficult to assess owing to the extremely classified nature of the military research undertaken. The solution demands complex multi-component systems of four or more different coatings to permit protection against oxidation and erosion while maintaining chemical compatibility of the system not only with the substrate but also with itself.

One of the major obstacles to long-term protection and a truly 'reusable' composite materials system, is the spallation of coatings due to thermal mismatch with the substrate under cyclic conditions. The most feasible way to avoid this occurrence would be to replace the discrete coating/composite interface with a functionally graded system. In such an artefact, there would be a hybrid region between protection and composite, thus minimizing thermal expansion differences.

REFERENCES

1. Johnson, H. V. (1934) US Patent 1,948,382.
2. Klein, A. J. (1986) *Adv. Mat. Proc. inc. Metal Prog.*, **11**, 64.
3. Zeitsch, K. J. (1967) Oxidation resistant graphite base composites, in *Modern Ceramics* (eds J. E. Hove and W. C. Riley), Wiley, New York, p. 314.
4. Bortz, S. A. (1971) Testing of graphite composites in air at high temperatures, in *Ceramics in Severe Environments* (eds W. W. Kriegel and H. Palmour), Plenum, p. 49.
5. Gloedstein, E. M., Carter, E. W. and Klutz, S. (1966) *Carbon*, **4**, 273.
6. Chown, J., Dencon, R. F., Singer, N. and White, A. E. S. (1963) Refractory coatings on graphite, in *Special Ceramics* (ed. P. Popper), Academic Press, p. 81.
7. Fitzer, E. (1978) *Carbon*, **16**, 3.
8. Criscione, J. M., Mercuri, R. A., Schram, E. P., Smith A. W. and Volk, H. F. (1974) *Rpt ML-TDR-64–173 Part II*, US Army, Washington, DC.

9. Nat. Acad. Sci. and Eng. (1970) *Pub. no. 15BMO-309–01769–6.* Washington, DC.
10. Sheehan, J. E. (1987) *Proc. 4th Ann. Conf. 'Recent Research Into Carbon–Carbon Composites'*, Southern Illinois Univ., 5 May.
11. NASA (1981) *Tech. Briefs*, **6** (2), MSC-18898.
12. Shuford, D. M. (1984) US patent 4,471,023.
13. Shuford, D. M. (1984) US patent 4,465,777.
14. Ehrenreich, L. C. (1978) US patent 4,119,189.
15. Saito, M. K. and Kogo, Y. L. (1980) US patent 4,197,279.
16. Holzl, R. A. (1985) US patent 4,515,860.
17. Vasilos, T. (1986) US patent 4,559,256.
18. McKee, D. W. (1986) *Carbon*, **24**, 737.
19. Taylor, H. S. and Neville, H. A. (1921) *J. Am. Chem. Soc.*, 2055.
20. Jalan, B. P. and Ras, Y. K. (1978) *Carbon*, **16**, 175.
21. Jalan, B. P. and Ras, Y. K. (1972) *Met. Trans.*, **3**, 2465.
22. Yasuda, E., Kimura, S. and Shilsusa, Y. (1980) *Trans. JSCM*, **6**(1), 14.
23. Walker, P. L., Rusinko, F. and Austin, L. G. (1959) *Adv. in Catalysis*, **11**, 164.
24. Goto, K. S., Han, K. H. and St Pierre, G. R. (1986) *Trans. Iron Steel Inst. Jap.*, **26**, 597.
25. Han, K. H., Ono, H., Goto, K. S. and St Pierre, G. R. (1987) *J. Electrochem. Soc.*, **134**(4), 1003.
26. Fischbach, D. B. and Uptegrove, D. R. (1977) *Proc. 13th Biennial Conf. on Carbon.*
27. Chang, H. W. and Rhee, S. K. (1978) *Carbon*, **16**, 17.
28. Chang, H. W. and Rusnak, R. M. (1979) *Carbon*, **17**, 407.
29. Thrower, P. A. and Marx, D. R. (1977) *Proc. 13th Biennial Conf. on Carbon.*
30. Knefeld, R., Linkenheil, G., Glaude, P. and Karcher, W. (1972) *Proc. Carbon 72 Conf.*, Baden-Baden, FRG.
31. Knefeld, R., Linkenheil, G. and Karcher, W. (1973) *ORNL-CONF – 730601*, 88.
32. Peng, T. C. (1977) *Proc. 13th Biennial Conf. on Carbon.*
33. Lynch, J. F., Ruderer, C. C. and Duckworth, W. H. (1966) *US Air Force Mat. Lab. Tech. Rpt no. AFML-TR066–52.*
34. Lynch, J. F. and Morosin, B. (1972) *J. Am. Ceram. Soc.*, **55**(8), 409.
35. Strife, J. R. and Sheehan, J. E. (1988) *Am. Ceram. Soc. Bull.*, **67**(2), 369.
36. Schriroky, G. H., Price, R. J. and Sheehan, J. E. (1986) *GA Technologies Rpt no, GA-A18696.*
37. Bock, P., Glandus, J. R., Jarrige, J., Lecompte, J. P. and Mexmain, J. (1982) *Ceram. Int.*, **8**, 34.
38. Laurenko, V. A. and Alexeev, A. F. (1983) *Ceram. Int.*, **9**, 80.
39. Hirai, T., Niihara, K. and Goto, T. (1980) *J. Am. Ceram. Soc.*, **63**, 708, 419.
40. Costello, J. A. and Tressler, R. E. (1986) *J. Am. Ceram. Soc.*, **69**(9), 674.
41. Kaufman, L., Clougherty, E. V. and Berkowitz-Mattuck, P. J. (1967) *Trans. Met. Soc. AIME*, **239**, 458.
42. Clougherty, E. V., Pober, R. L. and Kaufman, L. (1968) *Trans. Met. Soc. AIME*, **242**, 1077.
43. Schick, H. L. *Chem. Rev.*, **1960**, 331.
44. Sucov, E. W. (1963) *J. Am. Ceram. Soc.*, **46**, 14.

45. Harrop, P. J. (1968) *J. Mat. Sci.*, **3**, 206.
46. Woodley, R. E. (1968) *Carbon*, **6**, 617.
47. McKee, D. W., Spiro, C. L. and Lainby, E. J. (1984) *Carbon*, **22**, 507.
48. Napolitano, A., Mucedo, P. B. and Hawkins, E. G. (1965) *J. Am. Ceram. Soc.*, **48**, 613.
49. McKee, D. W. (1988) *Carbon*, **26**, 659.
50. Grigorev, A. I. and Polishchuk, D. I. (1973) *Fiz. Aerodisp. Sist.*, **8**, 87.
51. Greene, F. T. and Margrave, J. L. (1971) *J. Phys. Chem.*, **70**, 2112.
52. Mazurin, O. V., Streltsina, M. V. and Shavaiko-Shavaikovskaya, T. P. (eds) (1985) *Handbook of Glass Data*, Elsevier, Amsterdam.
53. Adams, P. B. and Evans D. L. (1978) *Mat. Sci. Res.*, **12**, 525.
54. Stull, D. R. and Prophet, H. (eds) (1971) *JANAF Thermochemical Tables*, 2nd edn, Nat. Bur. Stds Pub. NBS 37.
55. Riebling, E. F. (1964) *J. Am. Ceram. Soc.*, **47**, 478.
56. Kingery, W. D. (1959) *J. Am. Ceram. Soc.*, **42**, 6.
57. Schiroky, G. H. Kaae, J. L. and Sheehan, J. E. (1985) *Am. Ceram. Soc. Bull.*, **64**(3), 447.
58. Fleming, J. D. (1964) *Fused Silica Manual*, Final Rpt AEC Proj. B-153, Georgia Inst. Tech.
59. Freer, R. (1980) *J. Mat. Sci.*, **15**, 803.
60. De Poorter, G. L. and Wallace, T. C. (1971) Diffusion in binary carbides, in *Advances in High Temperature Chemistry*, (ed. L. Eyring), Academic Press, New York, p. 107.

Laboratory scale production and evaluation of carbon–carbon

7

7.1 INTRODUCTION

In earlier Chapters the principles and processing involved in the various industrially exploited methods of carbon–carbon manufacture have been discussed. The aim of this Chapter is to detail the production, testing and evaluation of the materials on a laboratory scale for research purposes.

7.2 RAW MATERIALS

Carbon fibres are produced by a large number of companies from the three basic precursors, rayon, PAN and pitch. Research quantities may be obtained relatively easily, especially from the larger organizations. The American company Amoco, for example, produce fibres from all three types. Having taken over the capacity of Union Carbide, one of the pioneers in this field, the most impressive products marketed by Amoco are their family of ultra-high modulus fibres made from pitch. Hercules in the USA and Toray in Japan specialize in very high quality intermediate and high modulus PAN-based fibres. Both companies market equivalent products and may be considered the leaders in the field. The Mitsubishi Chemical Corporation of Japan is unique in being the only major producer of fibres from coal-tar pitch, all other organizations in the pitch-based fibre business using petroleum pitch.

A large number of companies weave carbon fibres into a variety of felts, fabrics and 3-D preforms. The business is split between specialist weavers

and larger companies such as Fiberite who perform weaving operations as a prelude to subsequent processing such as prepregging. The world leaders in the production of three-dimensionally woven stock and preforms are Aerospatiale/Hercules who produce both orthogonal and polar woven products which they subsequently densify.

The overwhelming majority of commercially operated chemical vapour deposition (CVD) operations use methane as the feedstock. In the laboratory a number of other sources of carbon may be used, such as propane and benzene. Bottled hydrogen is generally used as the diluent. One of the most common resin precursors used for structural carbon–carbon is the phenolic resol SC 1008 originally developed by Monsanto which can be readily obtained from Borden Resins. Furan resins such as those produced by the Quaker Oats Chemical Corporation are often used in reimpregnation/densification processes. Prepregs and moulding compounds are produced by a number of companies, Fiberite and BP Chemicals/US Polymeric being the most notable.

A whole host of impregnating carbon precursor pitches which are available for use in the 'conventional' carbon and graphite industries are equally apposite in carbon–carbon fabrication. Of special interest are the series of fractionated pitches produced by Ashland in the USA, for which a considerable experimental data base exists in the open literature on carbon–carbon use. Finally, for those interested only in the evaluation of existing products, a number of 'finished' materials may be obtained from the various manufacturers. A more complete listing of the companies involved in the various stages of carbon–carbon production can be obtained from Chapter 10. A number of 'exotic' thermoplastic precursors such as PEEK and PEI may be obtained commercially, while high char yield resins and oxidation inhibitors are generally proprietary, and must be synthesized in the laboratory.

7.3 DENSIFICATION OF COMPOSITES BY CVD

Chemical vapour deposition has been used for over 20 years for depositing carbon matrices in carbon–carbon composites. The same technology is appropriate for depositing silicon carbide or other matrices in ceramic–ceramic composites or carbon–ceramic composites. Furthermore, CVD is a well-developed technique for applying the graded oxidation-resistant coatings required for carbon–carbon to be subjected to long-time exposure to oxidizing environments.

Figure 7.1 shows a schematic diagram of a furnace capable of producing carbon–carbon and ceramic composite materials and coatings by CVD.

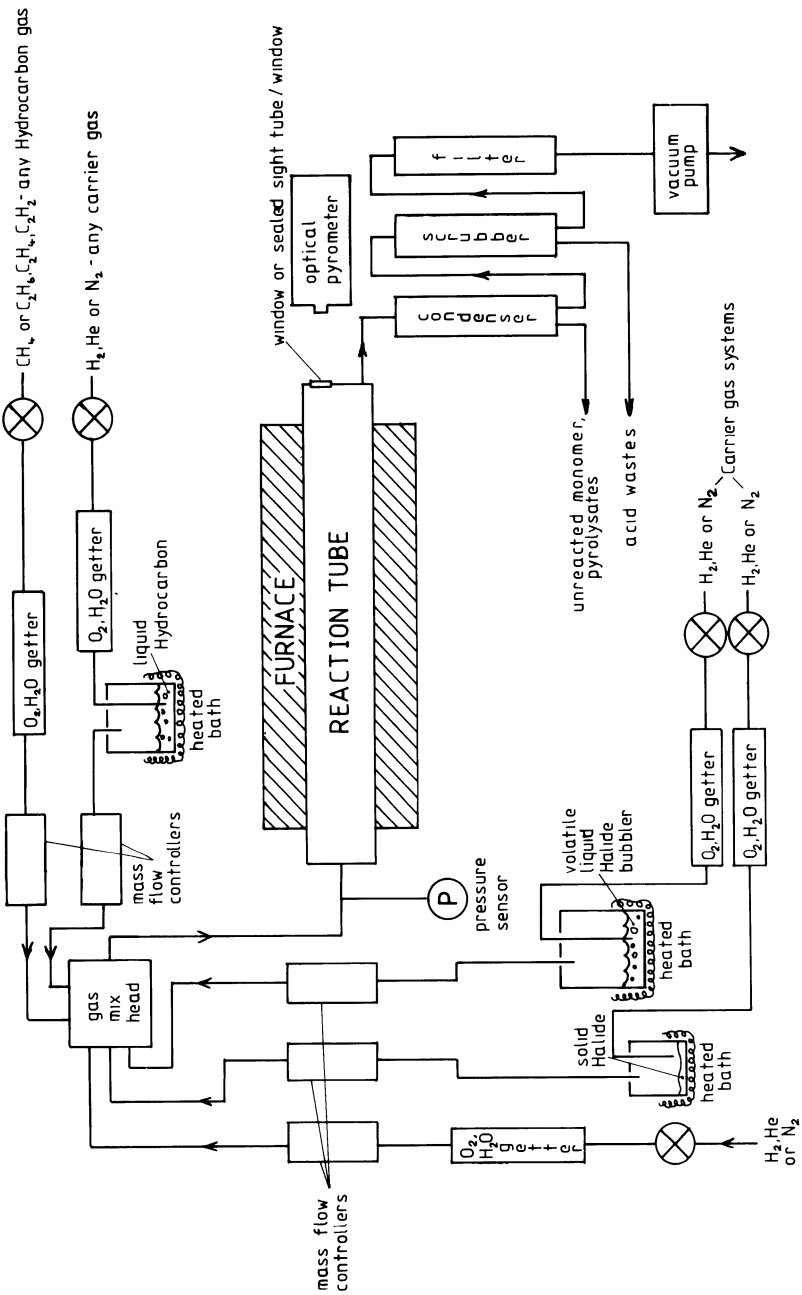

Fig. 7.1 Schematic diagram of CVD equipment suitable for research.

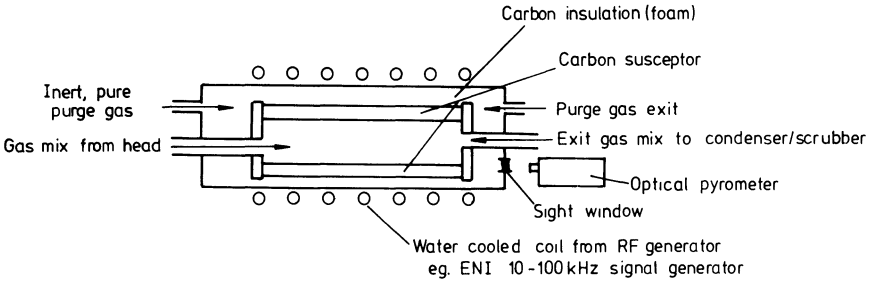

Fig. 7.2 Induction-heated furnace for use with CVD apparatus.

Starting materials can be a carbon felt preform or a pre-carbonized porous component made by resin/carbonization. The furnace contains five input lines to give flexibility for carbon deposition from gaseous/liquid hydrocarbon precursors and ceramic deposition from liquid/solid precursors such as ZrC–SiC alloys from $ZrCl_4/CH_3SiCl_3$, $/H_2$ and ZrB_2 from $ZrCl_4/BCl_3/H_2$. A conventional resistive heated tube furnace can be substituted by an induction-heated tube furnace of similar structure to the design in Fig. 7.2. A thermocouple such as W/WRe can be used to control the temperature in situations where only carbon is being deposited. Thermocouples cannot be used when acid halide gases are used for ceramic deposition, necessitating the use of a pyrometer/window system.

All of the parts, furnaces, mass flow controllers and valves, etc. are standard components and easy to obtain. It is possible therefore to construct such equipment from scratch although it is probably wiser to consult a specialist supplier. Modern instrumentation allows many variations in properties to be made which had been impossible in the past. All of the mass flow controllers/valves and furnace temperature settings should therefore be computer interfaced. A sophisticated computer program can then be used to control and operate the equipment using dual screen displays. Finally, an appropriate warning and alarm system is required to identify malfunctions, especially those which may result in permanent damage or safety concerns.

Most CVD technology has evolved empirically. Very little is known about the mechanisms of deposition and the relationships between reaction conditions, product microstructures and final properties. Furthermore, all of the proprietary information generated on low-pressure CVD of protective coatings and commercial products is zealously guarded by the various organizations involved. A great deal of 'trial and error' research will therefore be required of anyone entering this field, both at the R&D level and when scaling up to form a business.

7.4 FABRICATION OF THERMOSET RESIN LAMINATED PRECURSORS

7.4.1 Hand lay-up

The majority of composite structures, such as motor car body panels and racing kayaks, still use hand lay-up as the method of production. In the laboratory it is possible to use a variation on the process to make good quality 2-D precursor laminates. Using a rectangular matched metal mould, a woven fabric laminate plaque may be laid up using an excess of resin between two PTFE-coated aluminium sheets. Consolidation is best carried out under heat and pressure using a heated platen press. The resin content may be controlled using the applied pressure. Application of pressure via the platens results in excess resin being squeezed out of the mould. Experimentation allows the evaluation of pressure/resin content relationships, from which the desired laminate can be produced. The technique, for obvious reasons, is known as the 'leaky-mould' method.

7.4.2 Prepregging and filament winding

Virtually all of the structural carbon–carbon produced commercially by the thermoset resin route is of the 2-D lamellar type. In the laboratory, on the other hand, unidirectional (UD) material is often produced in order to minimize the number of variables in materials evaluation. A number of companies produce simple inexpensive machines for making UD carbon fibre prepregs. They all essentially consist of a drum winder with an impregnation system as shown in Fig. 7.3. The cylinder or drum is typically a 38 cm diameter steel tube with closed ends, driven by an electric motor with variable speed control, allowing approximately 1 m^2 batches of prepreg to be prepared. Thyristor heat controllers are used to vary the drum's temperature to allow the volatilization of solvents. The impregnation system relies on gravity or a positive pressure pump to deposit the resin on to the fibre just before the impregnation wheel (Fig. 7.3). The whole unit can be traversed along the length of the drum by a controlled-speed electric motor.

The 'wet winding' prepreg process is essentially a form of filament winding in which the tows are laid parallel to one another to produce a sheet material. Filament-winding machines facilitate the arrangement of impregnated tows at various orientations over a mandrel to form cylindrical or regular polygonol cross-sectional composite tubes. Structures so formed may be cured under ambient pressure at elevated temperatures or consolidated with a vacuum bag and autoclave cure.

Woven prepregs may be produced relatively easily by pultrusion through a solution bath (Fig. 7.4). Resin content is controlled by the process variables

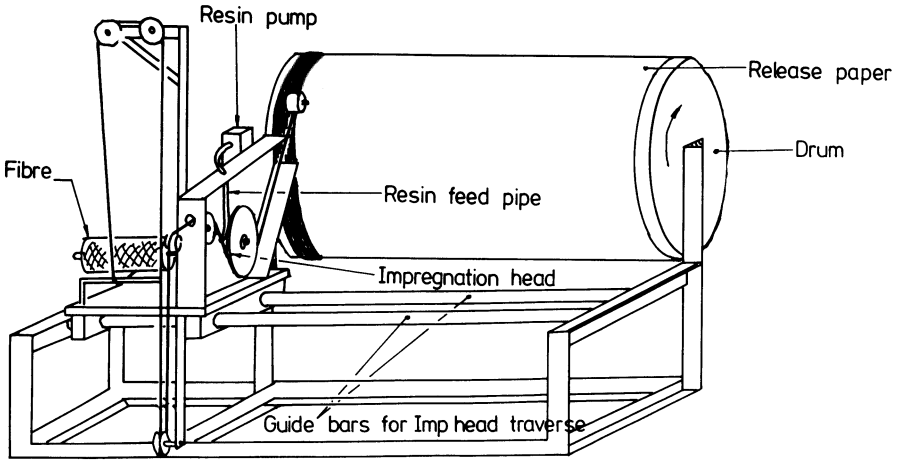

Fig. 7.3 Simple UD laboratory-scale prepregger.

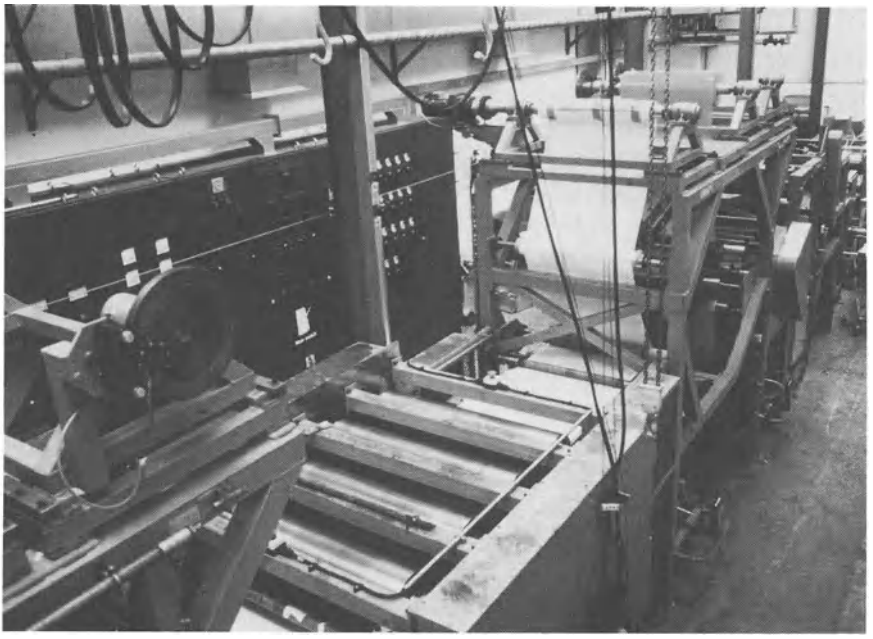

Fig. 7.4 Solution prepregging of carbon fibre fabric (courtesy Ciba-Geigy).

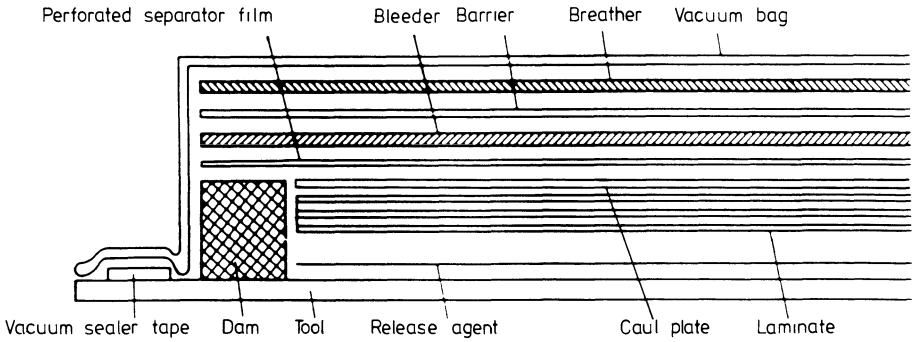

Fig. 7.5 Vacuum bag preparation.

of solution strength and line speed, etc. the most difficult parts of the operation being the provision of a consistent resin solids and volatile content, and subsequent removal and recovering of the generally flammable solvents. Finally, short-fibre brake-moulding compounds are made by a similar solution process save that two UD tows are pultruded through a circular die and then cut into approx 35 mm lengths. The composite is formed by compression moulding in a matched die and elevated temperature curing. All of the prepreging and winding processes lend themselves to the incorporation of additional phases such as particulate fillers and oxidation inhibitors.

7.4.3 Processing of thermoset prepregs

In the curing of thermosetting materials the prepreg resin is transformed from a semi-solid to a viscous liquid by the applied heat and the excess resin is squeezed out by the action of the applied pressure prior to the formation of a three-dimensional cross-linked molecular network known as gel. The chemical reactions which occur during curing are always exothermic. An applied pressure provides the force necessary to consolidate the plies and to compress vapour bubbles in order to obtain a product with minimum void content; alternatively, the voids diffuse out of the lay-up during resin flow. The vacuum bag lay-up sequence for a typical thermoset matrix composite (phenolic, epoxy, etc.) is shown in Fig. 7.5, which illustrates the fabrication of a flat plate laminate for materials evaluation. A shaped component would follow the same process save that a contoured male or female tool would replace the flat baseplate. The mould tool, or aluminium baseplate, is first thoroughly cleaned using acetone or some other degreasing agent. The surface is then 'released' twice with mould-release agent. A number of such products are available in the market-place; while their composition is generally proprietary, all operate as a suspension which leaves a thin coating of PTFE or silicone particles over the moulding

surface. From experience of a number of different release agents, and lengthy discussions on the subject, it is suggested that the 'Frekote' range produced by the Dexter Corporation is one of the best available, especially the 'Frekote 44' product which may be considered as an 'industry standard'.

When making large numbers of laminates for mechanical property, etc. determination it is advisable to use a 'pre-released' baseplate. This is achieved by covering the metal with a self-adhesive film of PTFE-impregnated glass fibre fabric. Such a product can be obtained from Courtaulds or Airtech, Richmond in the USA. After each lamination the plate can be quickly cleaned and reused without the need for further release agent. The mould for a plate laminate is made in the form of a 'picture frame' using a self-adhesive rubber gasket material [1] specifically designed for the purpose. A rubber 'wall' is built up around an aluminium 'caul plate' cut to the same size as the prepreg sheets. The plate is removed and the laminate stack laid inside the mould. Two glass fibre cords are laid into the asssembly to facilitate removal of air once the vacuum is applied (see Fig. 7.5). The caul plate, a sheet of aluminium coated similarly to the baseplate, is then dropped into the mould above the laminate. In the case of curved mouldings the plate is replaced by a PTFE-coated glass fabric. The caul plate is secured to the rubber gasket using high-temperature 'tacky tape' to prevent movement during cure and damage to the vacuum bag. A continuous vent cloth is placed on top of the lay-up and extended over the vacuum line attachment. The purpose of the porous vent or 'breather' cloth is to provide a path for volatiles to escape in the applied vacuum and to achieve a uniform distribution of vacuum. A nylon bagging film is placed over the entire plate and sealed against the bagging adhesive, allowing enough material to permit conformation to all contours without being punctured. Finally, the vacuum line is attached and the bag checked for leaks.

Curing of the laminate takes place in an autoclave under vacuum. The autoclave is generally a large pressure vessel equipped with a microcomputer-interfaced temperature and pressure control system. The elevated temperature and pressure conditions are created by electrically heating a pressurized gas (usually air or nitrogen). Once locked in the autoclave the part is left under vacuum for around 30 min to recheck for leaks in the bag. Curing conditions are either provided by the manufacturer or may be determined experimentally. Research has shown that the best results (in terms of matrix properties and carbon yield) are obtained if the laminates are post-cured in an oven prior to pyrolysis in order to increase the degree of cross-linking [2,3] and removal of water in condensation polymerized resins. A large degree of matrix shrinkage occurs during pyrolysis of the composites which may result in delamination. In addition, delamination may occur due to pore pressures in post-cure. It is imperative,

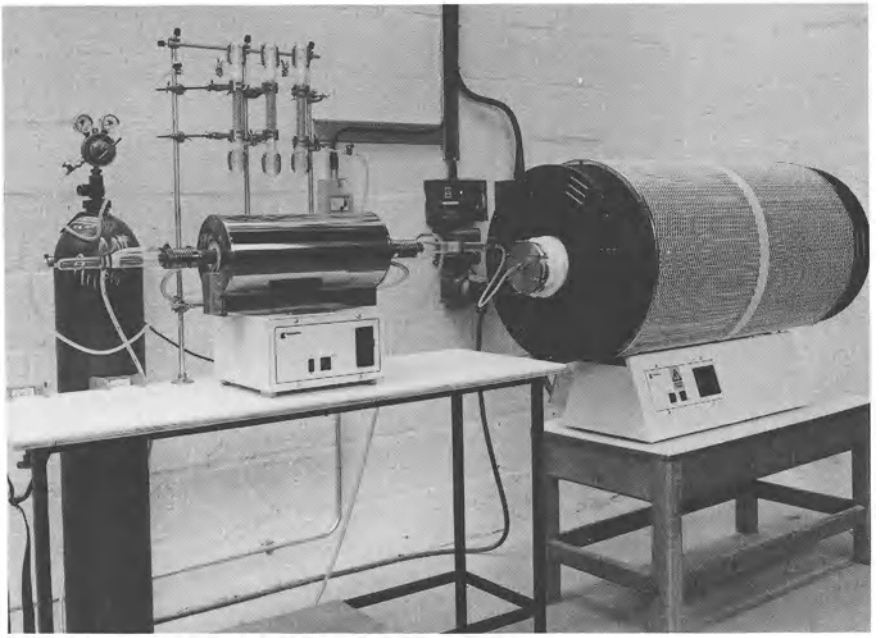

Fig. 7.6 Low-pressure pyrolysis furnace for carbon–carbon production showing gas purification equipment.

therefore, that the precursor laminates be of the highest quality in order to minimize this effect. It is recommended that, after a panel is cured, it should be non-destructively inspected by the Ultrasonic C Scan [4] method. Should any material contain delaminations or an unacceptably high void content it should be rejected and a replacement produced.

7.4.4 Pyrolysis of carbon fibre reinforced thermosets

Carbon fibre reinforced thermoset laminates may be converted to carbon–carbon by controlled pyrolysis in an inert atmosphere. Figure 7.6 illustrates a furnace system capable of performing such a task on a laboratory scale. The furnace consists of a heated reaction tube through which a flow of inert gas (generally nitrogen or argon) may be passed (Fig. 7.7). A typical laboratory temperature profile would consist of heating at a linear rate of, say, 10 °C min^{-1}, holding for 2 h at the carbonization temperature (850–1200 °C) followed by a linear cooling at around the same rate. Larger components may require cycles of 5–10 days to 900 °C or more. Control is thus relatively easy to achieve using a simple three-term controller/programmer operating via a thermocouple. Within reason, it is preferable

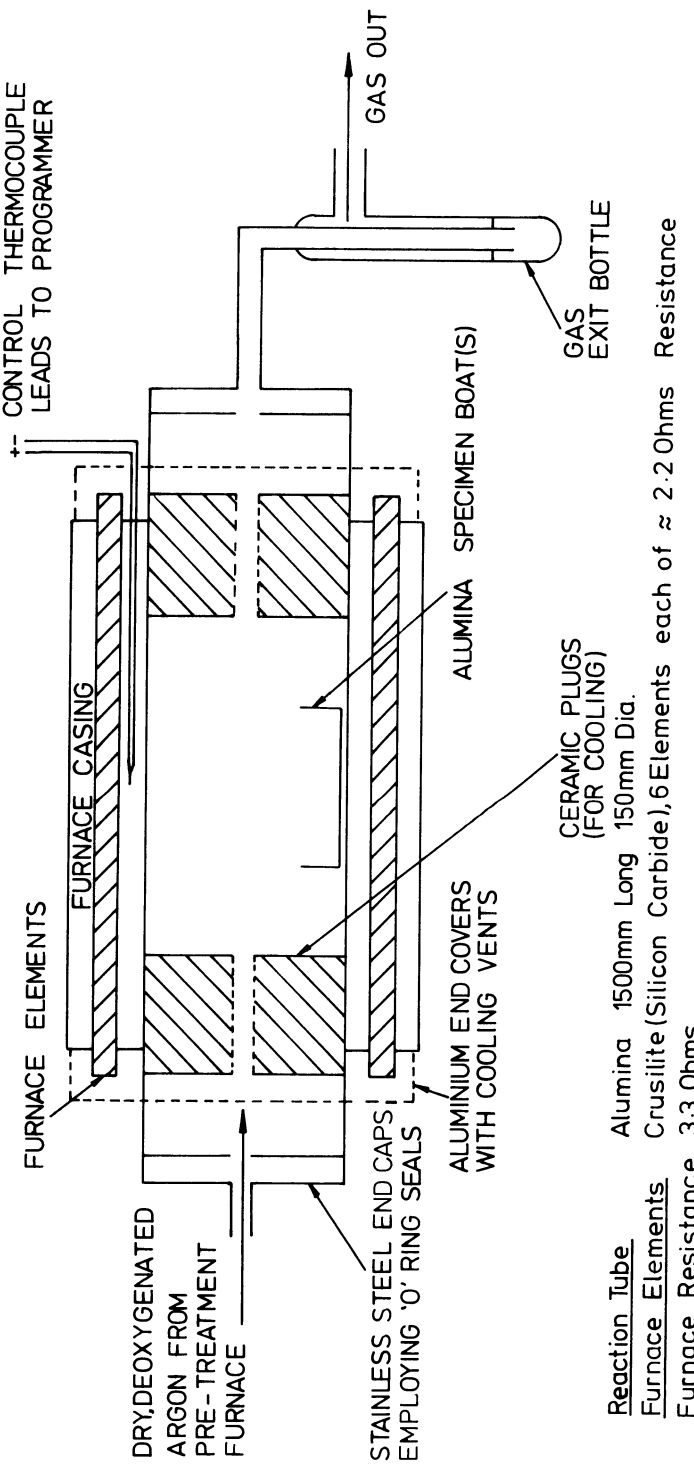

Fig. 7.7 Schematic diagram of ambient pressure carbonization furnace.

to use as slow a heating and cooling rate as possible to minimize the effects of shrinkage, cracking and thermal stresses which may build up during carbonization.

The presence of oxygen during processing is, as one would expect, extremely damaging to the carbon–carbon product. Despite bearing the tag of 'high purity', many of the gases supplied by manufacturers contain moisture and oxygen contamination in amounts which may be quite significant when the time period of the processing is considered. It is advisable, therefore, to ensure that gas is dry and free of oxygen before it enters the furnace. This is achieved by allowing it to pass through a series of drying columns containing a molecular sieve and into a pre-treatment furnace. This device is a simple tube furnace, held at around 900 °C using a single-term controller, containing titanium granules which act as an oxygen getter. Both gas purification devices can be clearly seen in Fig. 7.6. Other room-temperature oxygen getter systems can be used as well, such as supported catalysts.

7.4.5 Reimpregnation/densification cycles

The carbon yields obtained from the pyrolysis of thermosetting resins generally fall in the range 50–65% by weight. As a result, the carbon–carbon produced by this route contains large amounts of porosity, is of low density and hence possesses poor mechanical properties. To obtain a useful engineering material it is necessary to densify the cabonized material. Densification may be carried out by CVD of the porous laminate, or by vacuum reimpregnation with a resin or resin/pitch mixture followed by a further carbonization cycle. The process is repeated until the desired density is attained. Intermediate graphitization (Section 7.6) is often used to open up porosity and aid reimpregnation. A simple and inexpensive densification unit may be constructed in the laboratory using a vacuum desiccator, a one-way stopcock, a polyethylene funnel and a short length of tubing. The unit is assembled as shown in the sketch in Fig. 7.8. The desiccator may be made of glass or some form of polymer. Should a plastic unit be used, great care must be taken to ensure that it will resist the solvents which tend to splash around inside during the resin introduction step. Such a unit is only good for vacuum impregnations at room temperature with rather small parts such as mechanical test pieces, although scaling-up should not present too many problems.

7.5 PROCESSING THERMOPLASTIC PRECURSORS

The processing of thermoplastic composites involves heating the matrix to a temperature above its melting-point, application of a consolidation

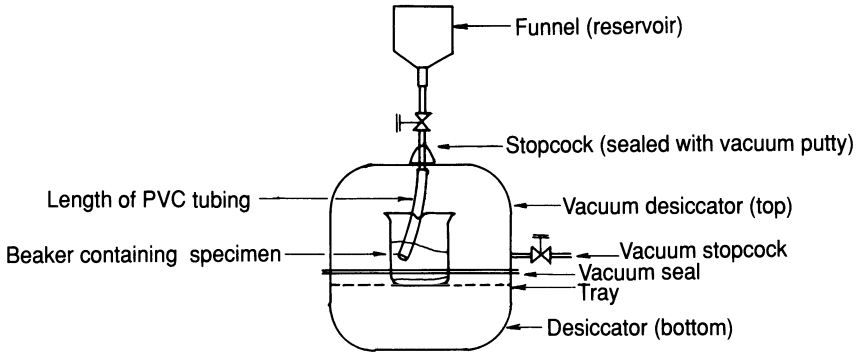

Fig. 7.8 Simple vacuum reimpregnation unit.

pressure and cooling. In the case of semi-crystalline polymers such as PEEK it is important to achieve the optimum degree of crystallinity and thus the cooling rate may be critical [5]. The cooling rate is not of concern when processing amorphous polymers such as PEI or pitches [6].

7.5.1 Impregnating with pitches

A woven or multi-directional carbon fibre structure may be vacuum impregnated with a molten pitch [7,8]. In some cases pressure is applied as part of the impregnation cycle to ensure penetration of all available porosity in the composite structure. The impregnated parts may be subjected directly to carbonization in an inert atmosphere to temperatures in the range 650–1100 °C [9]. The atmospheric pressure carbonization of pitch and other thermoplastics is extremely inefficient, as discussed in Chapter 5. The processing of such precursors is far better suited to the HIPIC process. In preparation for the HIPIC process, impregnation of the fibre preform structure is achieved by a hot pitch transfer technique [10]. The pitch is melted under vacuum in a heated reservoir. The fibre performs are placed in metal canisters and heated to the same temperature, again under vacuum, in an adjacent tank. Connecting pipes are employed to transfer the molten pitch to the metal cans containing the performs. The pitch transfer can be achieved with relative ease by backfilling the reservoir tank with nitrogen. Once the cans are full of liquid pitch the pressure is equalized by backfilling the preform tank with nitrogen in order to stop the transfer. The cans are closed off under vacuum by applying metal lids and then sealed with an electron-beam weld (Fig. 7.9).

Fig. 7.9 Electron-beam welded HIP can ready for processing.

7.5.2 Thermpolastic prepregs

Thermoplastic polymers are most easily prepregged in the molten state by a simple pultrusion process. A UD web of fibre tows, or a woven fabric is pulled through a 'melt pool' of the matrix material and then between 'nip' rollers which effect the impregnation. A scraper bar or similar device is used to remove any excess melt. The solidified material may then be collected by winding on to a spool. A schematic diagram of the process is shown in Fig. 7.10. Control of the process is achieved via the tension in the fibres, speed of pultrusion, matrix melt viscosity and the spacing between the nip rollers. A number of polymers may be prepregged in a simple melt condition. The materials useful in carbon–carbon production are generally high-temperature engineering resins. Polymers such as PEEK, Polyether sulphone (PES) and PEI, for example, have a melt consistency rather like chewing gum and must be 'thinned' with some form of solvent. The solvents needed and the dilution required are usually proprietary information.

Pitch has a very low melt viscosity and may be prepregged with ease. When solid, however, it is extremely friable and easily cracked off the fibres. The room-temperature toughess of pitch may be improved by adding graphite powder and milled carbon fibres to the melt. Such additions as well as making the prepreg handlable will also increase the carbon yield. A variation on the prepregging process involves the pultrusion of single or double tows through a circular die rather than nip rolls. The

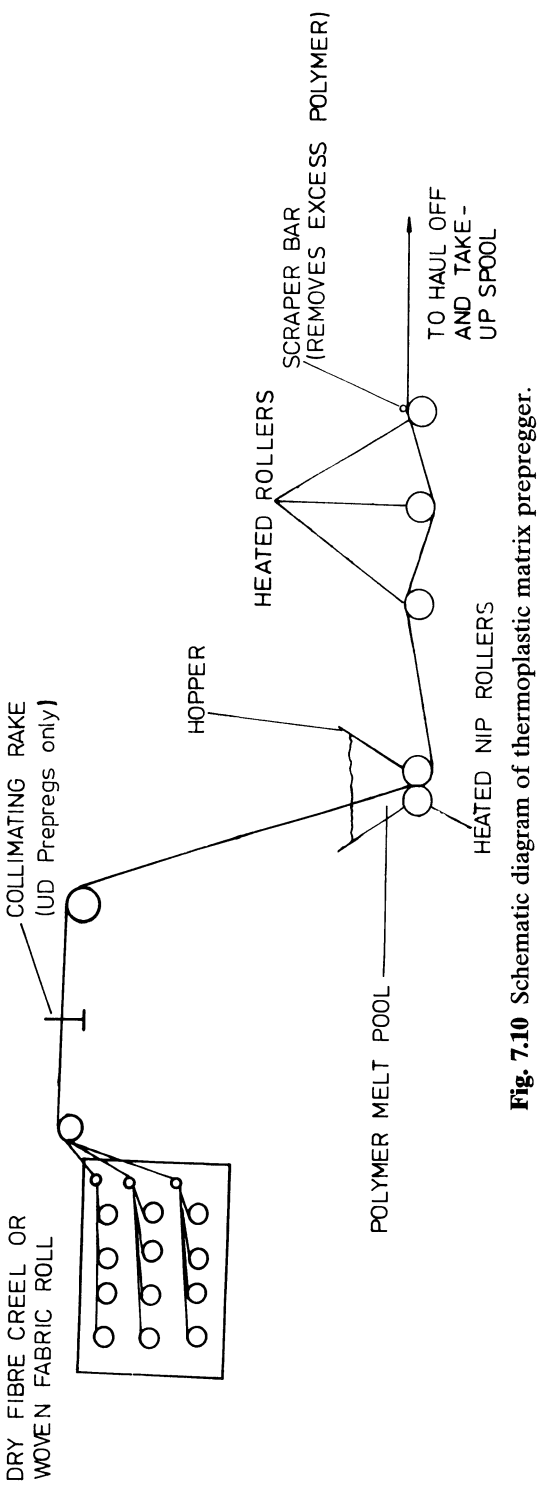

Fig. 7.10 Schematic diagram of thermoplastic matrix prepregger.

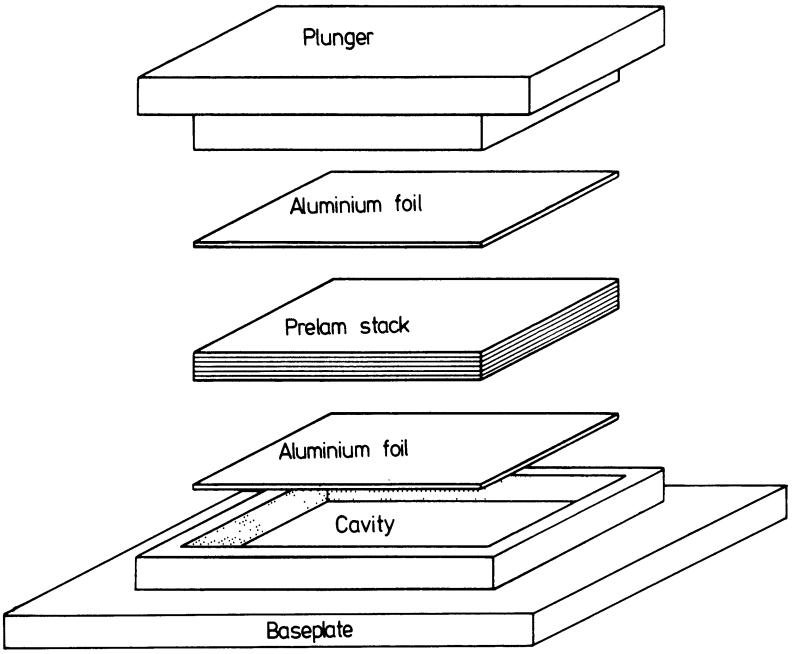

Fig. 7.11 Matched die moulding of thermoplastic.

product may then be chopped up to produce a thermoplastic equivalent of the thermoset 'matchstick' moulding compounds.

7.5.3 Lamination of thermoplastic composites

The production of laminates involves stacking layers of the prepreg which are then placed in a press, heating to above the melting temperature of the matrix under a low pressure, application of a consolidation pressure, and cooling rapidly. A prepreg stack is formed by cutting pieces of the prepreg in the desired orientation. Once the required number of plies have been produced they are laid up into a stack of layers and tacked together with a soldering iron. The preferred method for producing flat thermoplastic composite laminates is the matched-die moulding technique. The matched die is made of stainless or mild steel and consists of a female mould cavity and a male plunger (Fig. 7.11). The plunger fits into the cavity with the standard die-mould clearance. The moulding stack is then made up of the mould cavity, two pieces of aluminium foil in between which are placed the prepreg stack or moulding compound, and the plunger. The die and aluminium foil are liberally coated with release agent prior to processing. A slight variation on the above technique is the 'film stacking' process which can be used to manufacture woven reinforced laminates. The prepreg

stack is replaced by a 'sandwich' of woven carbon fibre fabric interspaced with the matrix in the form of a film. The consolidation process is the same as before, save that longer time is required in order to allow for the melting of the film and impregnation of the fibres. Film stacking is a useful technique in making laminates to assess a fibre/resin combination not yet available in prepreg form, but is time-consuming and tends to produce poorer laminates due to incomplete impregnation and damage to the surface of the fibres during processing. Resin content of the composite is controlled by the relative amounts of fibre and film and the applied pressure. A number of technologies may be applied to produce curved geometry thermoplastic composites [11].

7.5.4 High-pressure carbonization

The majority of a HIPIC densification process is the same as that of an ambient pressure cycle save for the use of pressure during carbonization. A number of manufacturers such as ASEA and National Forge market laboratory-scale HIPs suitable for the processing of carbon–carbon (Fig. 7.12). A schematic of a complete HIPIC densification cycle using pitch is shown in Fig. 7.13. The major difference between an ordinary (if such a thing exists!) HIP unit and one suitable for carbon–carbon production arises from the severely corrosive nature of the outgassing which occurs during carbonization. This, coupled with a small but nevertheless noteworthy risk of hydrogen embrittlement of the pressure vessel, necessitates a special isolation chamber with a differential pressure control system (Chapter 5). The gas-pressure vessel is usually water-cooled with an internal furnace. The remainder of the system consists of gas storage, high-pressure gas transfer lines, compressor and controls (Fig. 7.14) [12]. Computer control via a PC interface is essential to maintain product quality [13].

The sealed metal can containing preform and excess pitch is placed in the pressure vessel. The temperature and pressure are raised at a programmed rate to effect the conversion to carbon–carbon. The thin metal can allows the isostatic gas pressure to be transferred to the workpiece in a cycle which may take typically 1–3 days. Once the cycle is complete the cans are removed and the sample machined to clean it up. The carbon–carbon artefact may be graphitized and/or reimpregnated and sealed in another can to undergo further cycles. Usually three or four HIPIC cycles are required to reach optimum density. Thermoplastic polymer matrix materials may be HIP carbonized without the need of metal cans as they have been shown to form their own hermetic seal [14]. Laminates based on PEEK, for example, may be processed to high-quality carbon–carbon in two or, in some cases only one, cycle.

Fig. 7.12 Laboratory scale HIP unit suitable for making carbon–carbon composites.

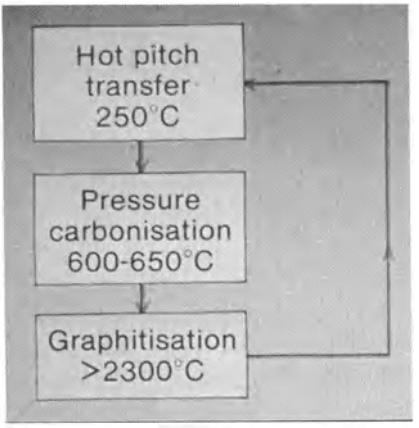

Fig. 7.13 Flow diagram of a complete HIPIC process.

7.6 GRAPHITIZATION OF CARBON–CARBON

The graphitization of materials which have passed through a liquid state on carbonization or the 'stress-induced' graphitization of fibre-reinforced isotropic carbon, is achieved by a controlled heat treatment to temperatures above 2300 °C. The furnaces to perform such a task consist of a heavy wall, seamless extruded aluminium or stainless steel chamber,

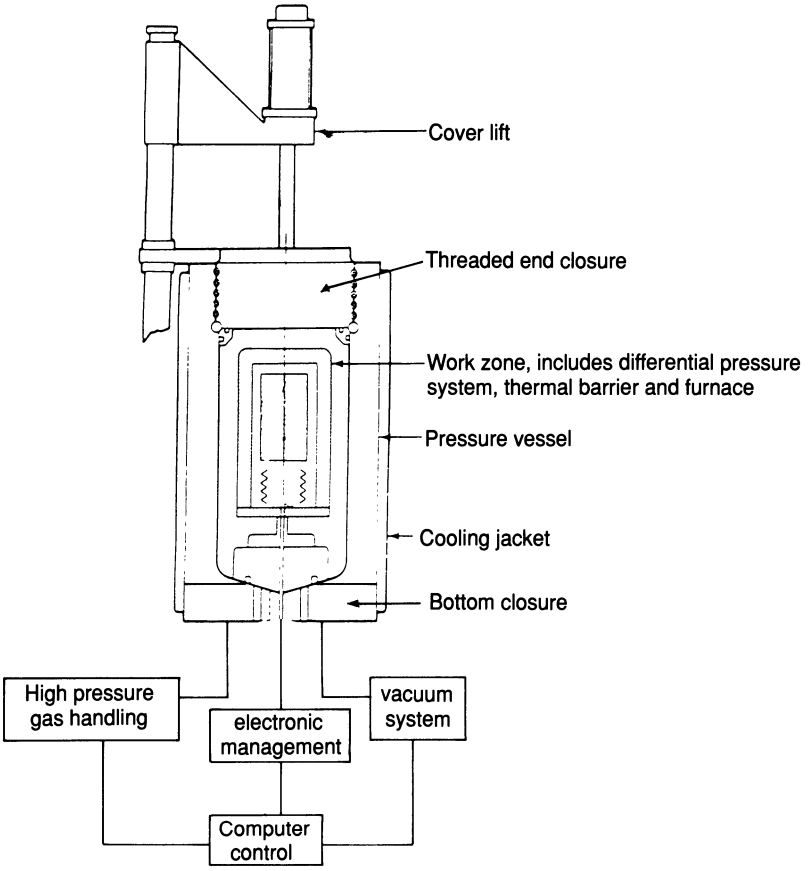

Fig. 7.14 Schematic diagram of laboratory-scale HIPIC unit.

water-cooled with an opening door (Fig. 7.15). The hot zone may be cylindrical, rectangular or cubic depending on the geometry of the perceived payload. Heating is achieved using graphite strip electrical elements or inductively heated graphite susceptors, which will allow continuous operation at temperatures of up to 2750 °C and short time usage at up to 3000 °C. A temperatures above 2800 °C the elements begin to sublime and their lifetime will therefore be finite at these temperatures. Operating environments are inert or dry reducing atmospheres with a maximum over pressure of 1 bar and full vacuum. The addition of a ceramic muffle tube permits working in oxidizing or wet atmospheres compatible with aluminium oxide (max. temperature ≈1850 °C) and zirconia (≈2200 °C). High-purity graphite felt is used as thermal insulation (Fig. 7.16). Temperature control is generally achieved using a three-term programmer/controller operating via a thermocouple at lower temperatures (<1400 °C) and a two-colour optical pyrometer over the high-temperature range. For maximum

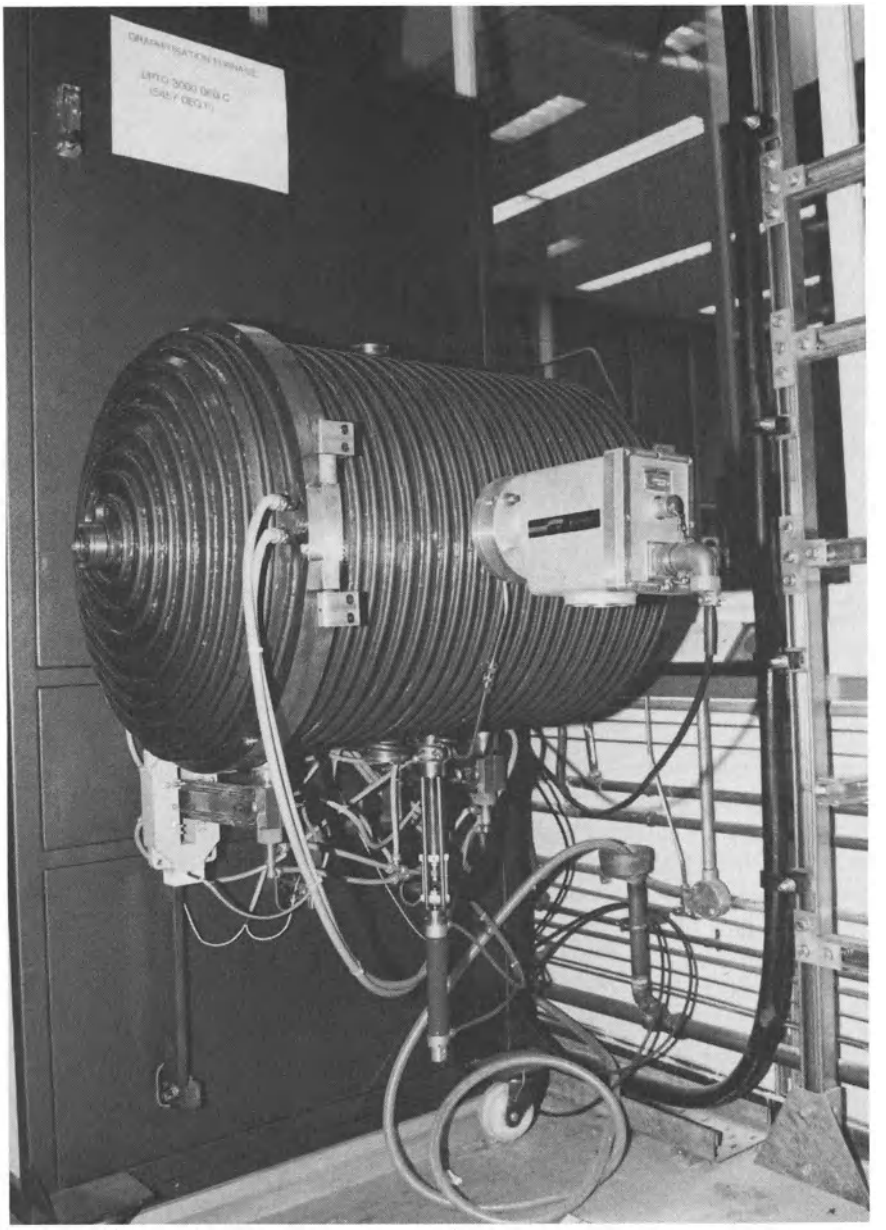

Fig. 7.15 3000 °C capability graphitization furnace showing optical pyrometer, thermocouple retracting device and water-cooling coils over the main chamber.

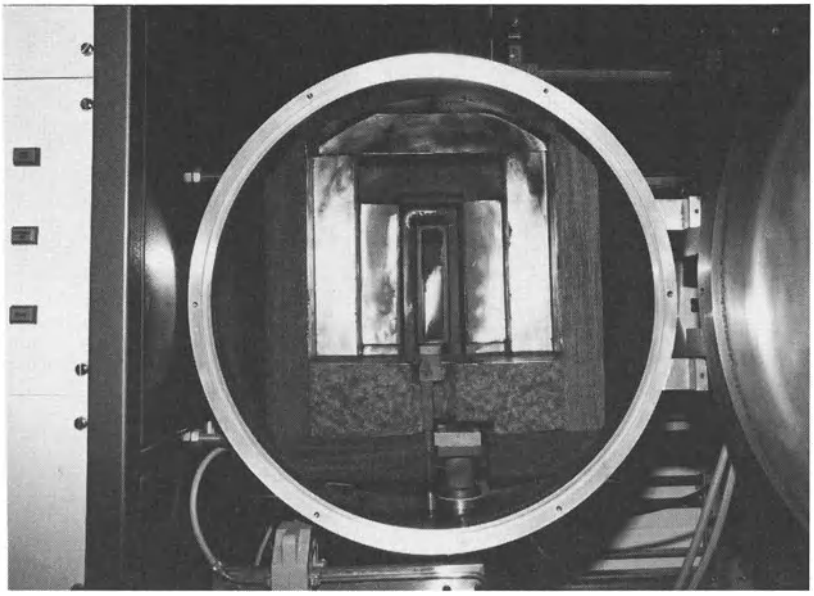

Fig. 7.16 End view of graphitization furnace with a rectangular hot zone.

accuracy it is advisable to place the thermocouple as close to the working zone as possible. To prevent damage to the thermocouple at high temperatures a retracting device is fitted which also triggers a 'bumpless transfer' to pyrometer control. A pneumatically operated device of this type can be seen underneath the furnace in Fig. 7.15. Prior to operation, air is removed from the furnace using a rotary pump capable of producing a vacuum of 10^{-2} bar followed by backfilling with an inert gas (argon or helium). This process must be repeated three or four times to ensure all traces of air are removed, thus preventing oxidation damage to furnace and workpiece during operation. Alternatively, the air can be displaced by flushing for extended times with nitrogen. The temperatures of operation involved make a furnace of this type potentially an extremely dangerous piece of apparatus. It is advisable therefore to install a safety interlock system coupled with water supply, inert gas supply, furnace body and contents over-temperature and over-pressure trips as 'fail-safe' devices.

7.7 MECHANICAL TESTING OF CARBON–CARBON

7.7.1 General considerations

All of the applications of carbon–carbon composites are either structural or require at least a degree of strength and stiffness to be successful. It is important therefore to determine the mechanical properties of the material. There are no standard procedures for the testing of carbon–carbon.

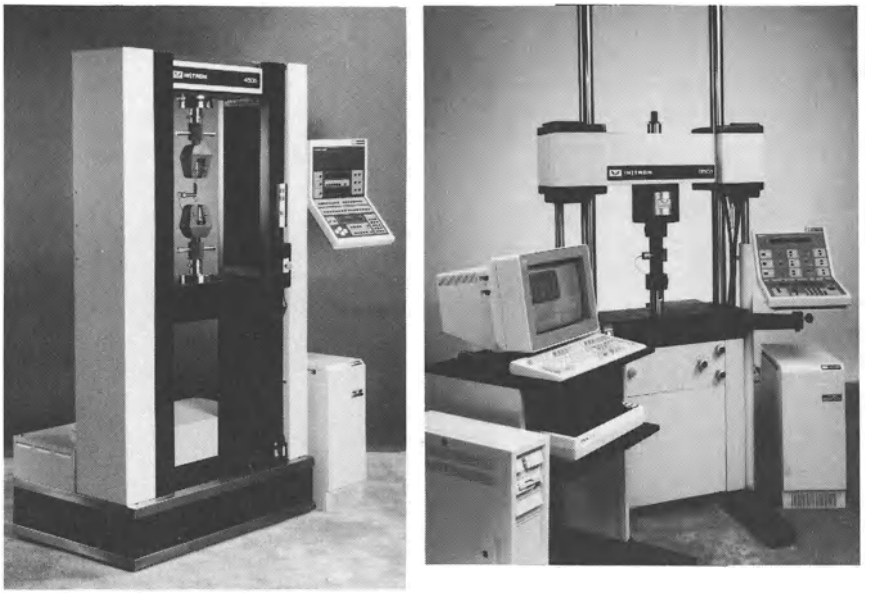

(a) (b)

Fig. 7.17 Servomechanical (a) and Servohydraulic (b) universal test machines (courtesy Instron Ltd).

Having said that, a number of the tests detailed for the evaluation of fibre-reinforced polymer composites may be used [15,16]. Testing is carried out using a universal testing frame. Two types of frame are available, servohydraulic and servomechanical. Servohydraulic machines apply the load by means of a hydraulic actuator controlled by a servovalve and are best suited to dynamic testing of materials and components. A servomechanical tester applies the load via cross-head movements driven by one or two large screws. The servomechanical device is generally preferred in the 'static' testing of materials as a result of its inherently high degree of accuracy. This is especially true when testing extremely low strain-to-failure materials such as carbon–carbon. A number of manufacturers supply equipment of one or both types (Fig. 7.17) which are required to conform to the calibration standards BS 1610 [17] and/or ASTM E4 [15] and be equipped to record load, and deflection rate via cross-head or actuator movement. Accurate load alignment and position control are essential for satisfactory testing. Continuous or 'ramp' loading is preferred, with continuous load and strain recording.

The measurement of strain may be carried out using electrical resistance strain gauges or an extensometer. Foil strain gauges with 350 Ω resistance and a gauge length of 3–6 mm are preferred. Typically, two gauges, one each in the longitudinal and transverse direction, are bonded to the

specimen using a cyanoacrylate adhesive [18]. Many researchers believe strain gauges to be far more accurate than extensometers. The technology of the latter has evolved considerably of late, such that they are now extremely precise especially when interfaced with the test equipment via a computer. Extensometers are far more easily attached to the specimen than strain gauges and can be used at very high temperatures. They are required to conform to ASTM E83 [15]. Universal testing frames are often known by the generic term of an 'Instron' machine after one of the best known companies in the field, in the same way that in the UK vacuum cleaners tend to be called a 'Hoover' irrespective of manufacturer. The company's model 4505 servomechanical and 8502 servohydraulic machines have a load capacity of 100 kN and can be used in load, displacement and strain control, operating via a well-researched software package through a personal computer, and are ideally suited to the testing of composites in general and carbon–carbon in particular.

7.7.2 Sample preparation

Considering their 'ceramic' nature, carbon–carbon composites are extremely tough. It is well known that a 2-D carbon–carbon material can be 'nailed' without fracturing. Photos of carbon–carbon composites with nails driven through them have, unfortunately, become something of a cliché in the literature so the author shall refrain from using one! Despite their apparent toughness carbon–carbon and indeed polymer matrix composites are extremely susceptible to damage during machining. Great care must be taken to avoid fraying and disorientation while preparing mechanical test pieces. Specimens are best cut using water-cooled, high-speed diamond-impregnated grinding wheels (Fig. 7.18). It is advantageous to secure the laminate to a backing plate of acrylic sheet using double-sided sticky tape. The acrylic plate serves as a carrier for the composite laminate, avoiding the fraying out of fibres, and allows the diamond saw to cut through the carbon–carbon without damaging the blade.

Alignment of the composite laminate is an important issue since the mechanical properties of these anisotropic materials are strongly dependent on the orientation of the fibres. Should the particular test piece require the fitting of end-tabs (Section 7.7.4) they should be bonded prior to machining.

7.7.3 Statistical analysis

Composite materials are notorious for their variability in mechanical properties. The variability is even more prevalent in carbon–carbon composites due to their inherent flaws and inhomogeneities. It is important, therefore,

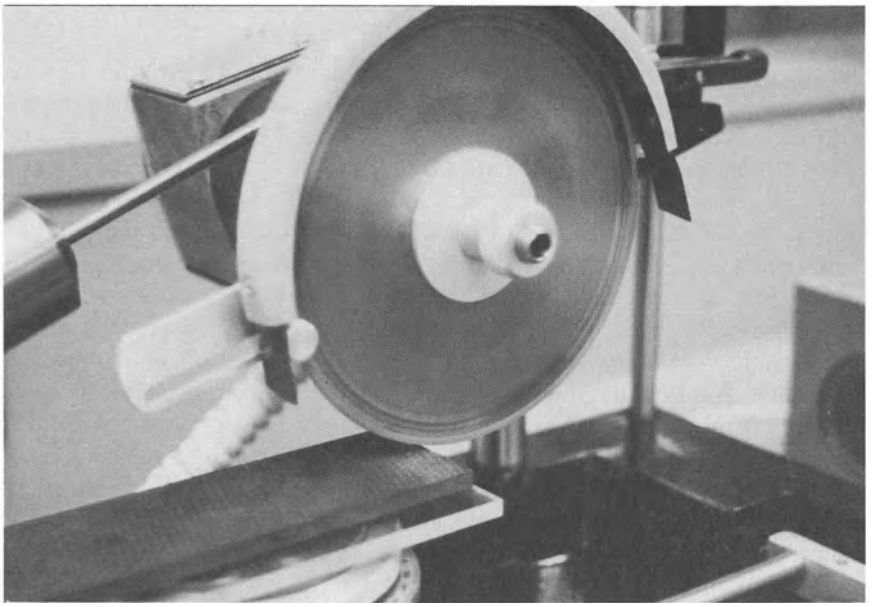

Fig. 7.18 Machining a carbon–carbon composite using a water-lubricated diamond saw.

to present the spread of results which is in itself a property of the material. Mechanical properties are given as the arithmetic mean ($\bar{x}$) of a sample of n specimens, where n must be greater than 10 and preferably around 30; then

$$\bar{x} = \sum^{n} \frac{x_n}{n}. \tag{7.1}$$

The standard deviation σ_{n-1} is then calculated using the following formula:

$$\sigma_{n-1} = \left(\frac{\sum^{n} (x_n - \bar{x})^2}{n-1} \right)^{1/2}. \tag{7.2}$$

The spread of results may then be expressed in terms of the 'coefficient of variation' which is defined as a percentage:

$$C_v = \frac{\sigma_{n-1}}{\bar{x}} \times 100\%. \tag{7.3}$$

7.7.4 Static testing

Static testing is used to evaluate the 'ultimate' or failure properties of materials in various configurations.

Tensile testing

The principal engineering properties of a carbon–carbon laminate are determined using a tensile test. The test may be carried out using either 0° UD or woven materials, providing the sample is axially orthotropic to obviate bending. Chamfered 'end-tabs' (Fig. 7.19) are attached to each end of the tensile specimen to ensure a uniform loading and prevent damage to the surface. A 30° taper is used to relieve the stress at the end-tab and ensure that failure occurs in the centre of the test piece. Tabs are made from a commercially available woven glass-cloth epoxy laminate sheet, typically 3.2 mm thick. The surfaces to be bonded are degreased using trichloroethane and are then lightly abraded using a grit-blasting technique. A pure aluminium oxide grit, of particle size range 80–120 mesh and free from contaminants, is employed at a low blast pressure of around 0.6 MPa. Loose particles are removed from the abraded surfaces by a short immersion in an ultrasonic cleaning bath followed by another degreasing operation. The end-tabs are attached using a suitable adhesive following the manufacturer's instructions [19].

The specimens must be carefully aligned in the jaws of the test machine to avoid induced bending of the specimen (this is best achieved using hydrautically operated grips) (Fig. 7.20). Width and thickness (w and t respectively) are be to measured at five positions on the specimen to an accuracy of 0.01 mm. Axial strain is measured using a 50 mm gauge length extensomether and width strain using a lateral extensometer at the centre of the gauge length. Alternatively a biaxial extensometer may be used. Tensile load, P, should be increased uniformly at a constant displacement of 1 mm min^{-1} or, more preferably, should the apparatus allow, a constant strain rate of 0.5% min^{-1}. Longitudinal tensile strength σ_{11} is given by

$$\sigma_{11} = \frac{P}{wt}. \tag{7.4}$$

The stress versus strain curve is sometimes non-linear with modulus changing slowly with increasing strain. The axial tensile modulus of the material is thus calculated as a spot value at a specified level of strain. The longitudinal tensile modulus is thus defined as

$$E_{11} = \text{secant modulus at } S\% \text{ longitudinal strain} \tag{7.5}$$

(cf. Fig. 7.21). Similarly, the major Poisson's ratio may be defined as

$$\nu_{12} = \frac{\text{transverse strain}}{\text{longitudinal strain}} \text{ at } S\% \text{ longitudinal strain}. \tag{7.6}$$

The data recorded should include longitudinal tensile strength (failure stress) modulus, the stress/strain curve to failure, strain to failure, major

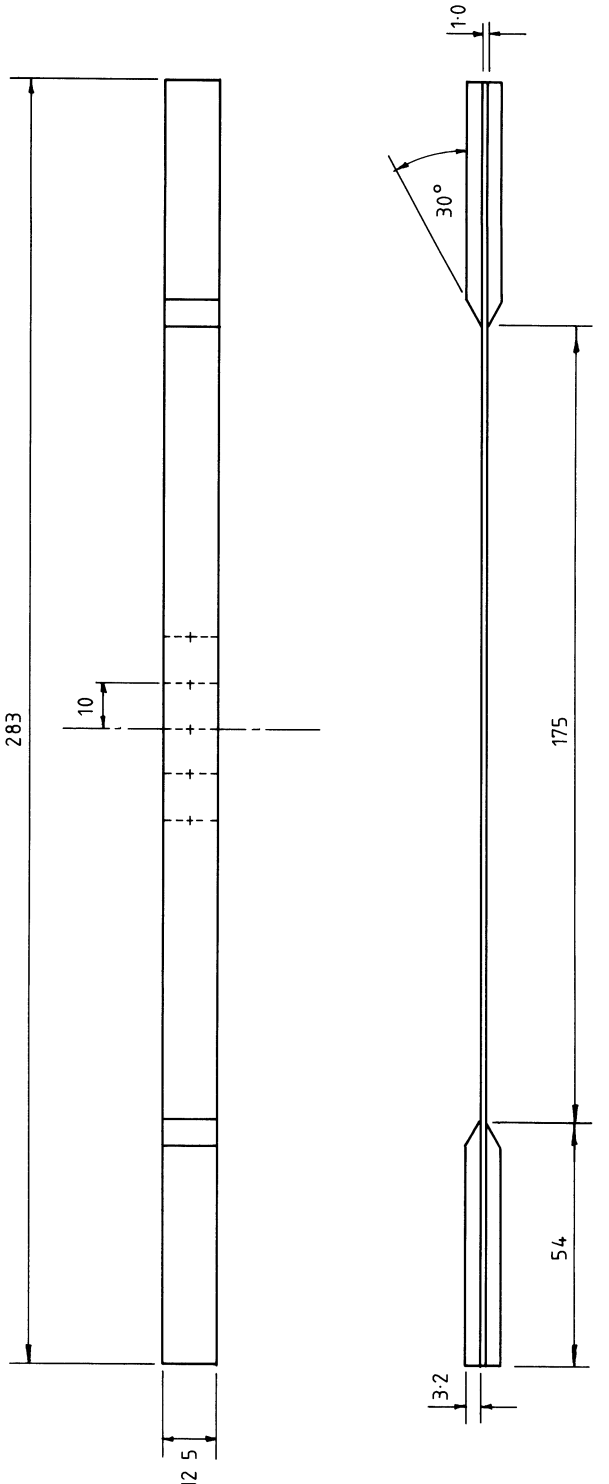

Fig. 7.19 Tensile test specimen showing dimensions and end-tabs.

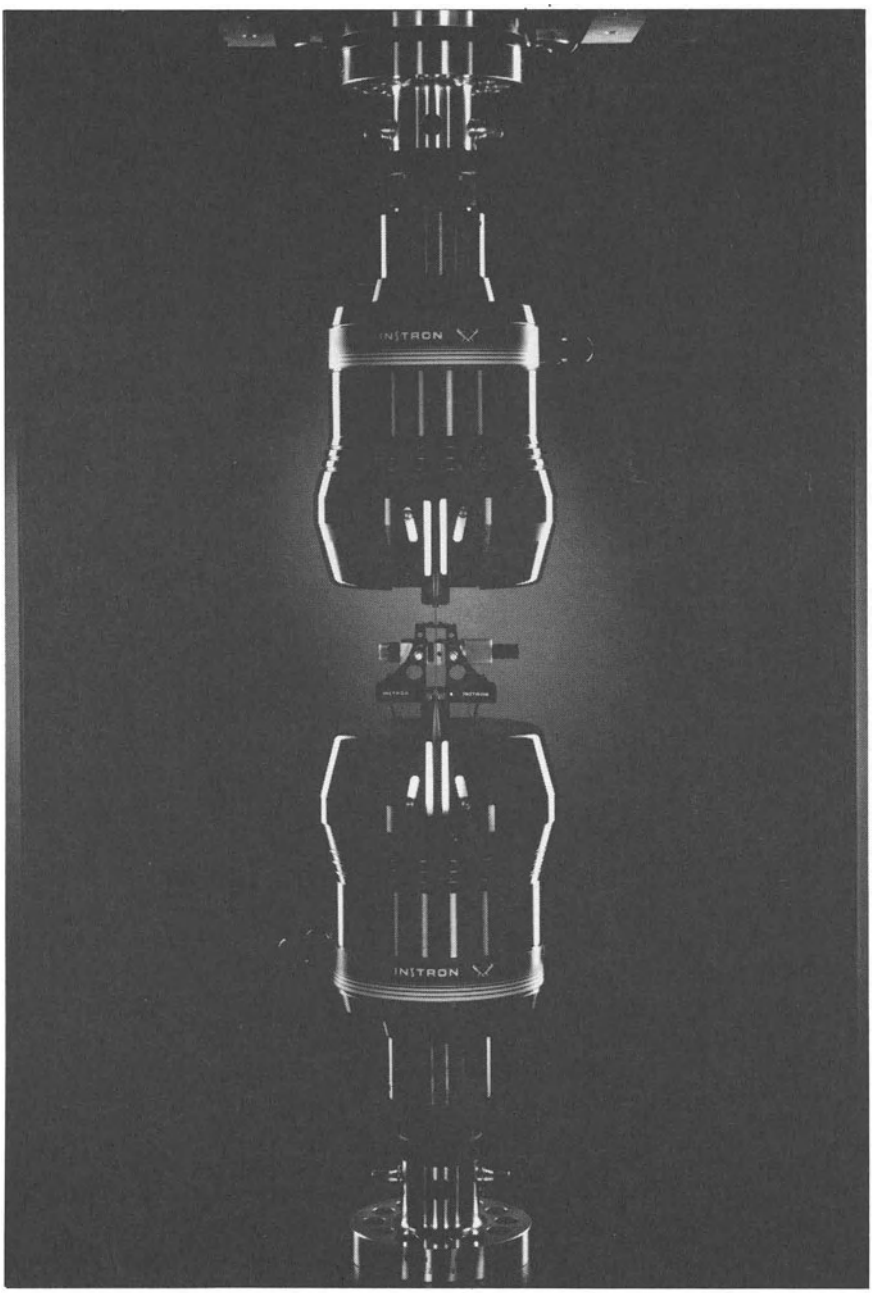

Fig. 7.20 Properly tabbed and aligned tensile specimen just prior to testing, complete with axial, averaging extensometer (courtesy Instron Ltd).

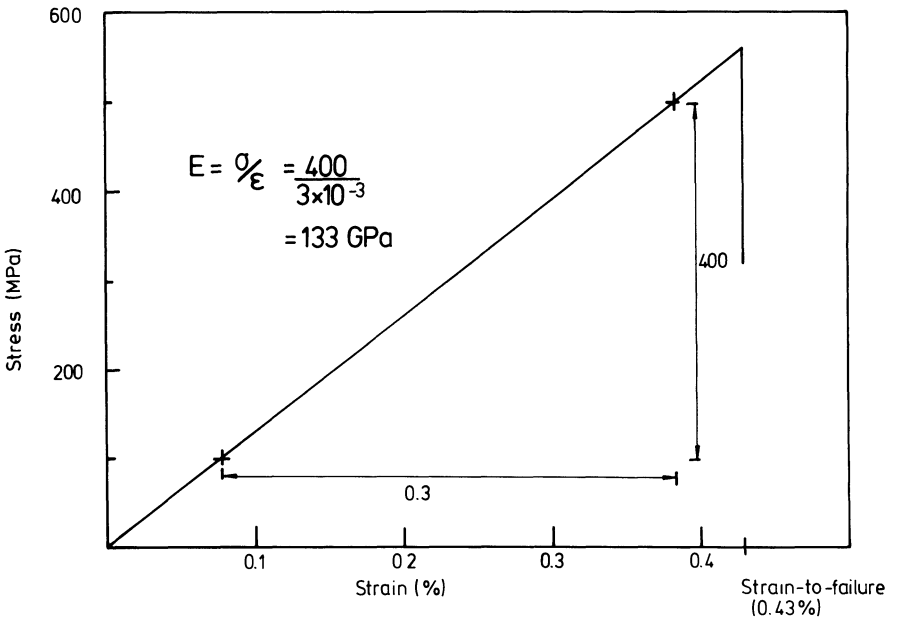

Fig. 7.21 Typical carbon–carbon composite stress–strain curve showing modulus calculation.

Poisson's ratio, and nominal and actual specimen depth and thickness. To be valid as design data, failure must occur in the central region of the specimen.

Flexure testing

The flexural properties of carbon–carbon laminates are evaluated using a three- or four-point test fixture. For a high modulus material such as this the three-point (Fig. 7.22) is generally preferred as the most direct and simplest technique to use. The procedure can be found in ASTM D-790 [15]. Flat specimens, machined with the same care and precision as previously described for tensile testing, are selected for measurements. The test may be carried out on either UD or woven material. The material direction under investigation must be orientated along the length dimension of the specimen. The test pieces require a span/depth (l/d) ratio high enough to minimize the influence of interlaminar shear deformation and to achieve failure in bending rather than shear [20]. The minimum l/d ratios for each specimen geometry are shown in Table 7.1. Woven fabric reinforced materials should be tested in both warp and fill directions. The 90° aligned specimens may be used as a qualitative/comparative estimate of the fibre/matrix bond strength.

The three-point flexure fixture should be properly mounted and aligned

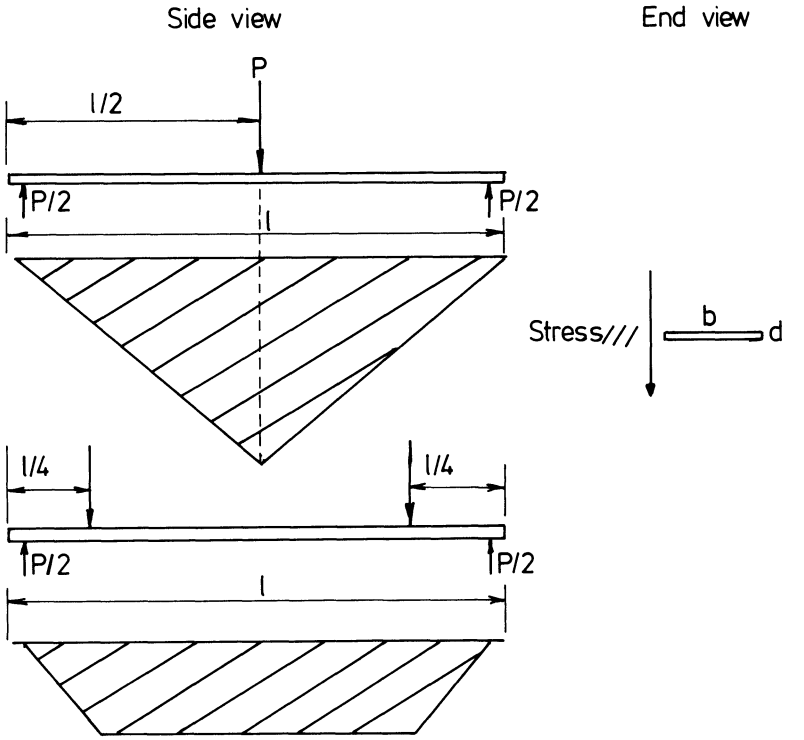

Fig. 7.22 Three- and four-point flexure test geometries showing stress distributions at the bottom surface.

Table 7.1 Span/depth requirements in flexure testing

Composite reinforcement	*Alignment of fibres to beam axis*	*Minimum l/d*
Unidirectional	0°	40/1
Unidirectional	90°	25/1
Woven	0°/90°	25/1

within a calibrated test frame (Fig. 7.23). Testing is carried out at a displacement of 1 mm min^{-1}. Strain readings are recorded continuously, being calculated from the displacement. The ultimate flexural strength σ_f, i.e. the stress in the outer fibre at failure, and the flexure modulus (Ef) are calculated as follows:

$$\sigma_f = \frac{3Pl}{2bd^2} \tag{7.7}$$

$$E_f = \frac{l^3 m}{4bd^3} \tag{7.8}$$

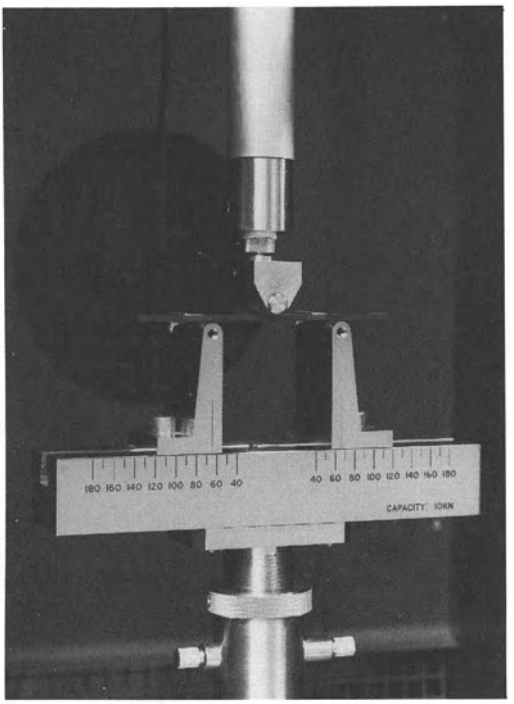

Fig. 7.23 Apparatus and sample set-up for three-point flexure test (courtesy Instron Ltd).

where the symbols represent the specimen dimensions in Fig. 7.22 and m is the slope of the tangent to the initial straight line portion of the load–deflection curve.

Shear deflections can seriously reduce the apparent modulus of highly anisotropic composites when tested at low span to depth ratio. It is recommended, therefore, that 0° UD specimens be tested at l/d of 50 : 1. Flexure testing imposes tension, compression and a degree of shear loading on the sample simultaneously. While the flexure specimens cannot therefore provide data suitable for design purposes, such tests are valuable in performing comparisons between materials or the effects of different processing and environmental conditions, etc. The four-point flexure test (Fig. 7.22) is sometimes used when testing carbon–carbon in order to minimize the local crushing between the central loading nose of the three-point loading procedure and to provide a uniform maximum stress field between the upper loading points. Loading at one-quarter of the span distance from each support is recommended [15].

In four-point flexure:

$$\sigma_f = \frac{3Pl}{4bd^2} \tag{7.9}$$

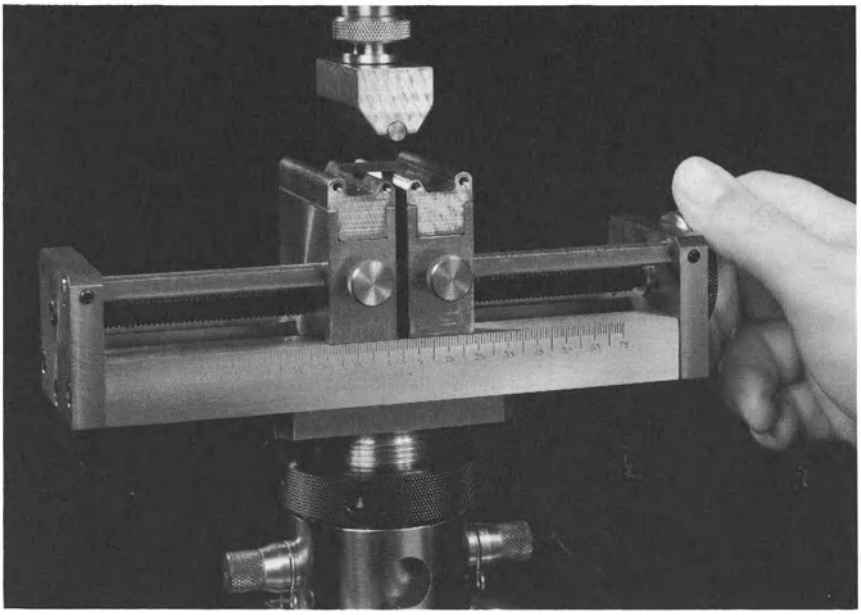

Fig. 7.24 Interlaminar shear test configuration (courtesy Instron Ltd).

$$E_f = 0.21 \frac{l^3 m}{bd^3}. \tag{7.10}$$

Interlaminar shear strength

The interlaminar mode of fracture has aroused a great deal of attention in laminated composites since the early 1970s [21]. Since the introduction of fibre-reinforced composite materials subjected to severe service loading, it has become increasingly apparent that the interlaminar fracture mode is potentially the major life-limiting failure process [22].

One test frequently referred to in the literature (cf. ASTM D2344 [15]), which may be used to evaluate the interlaminar properties of composites, is the short beam interlaminar shear strength. Using a shortened span on a three-point flexural test fixture, with a span to depth ratio of 4 : 1, testing is performed as shown in Fig. 7.24. The short beam shear strength is calculated as follows:

$$\text{ILS} = \frac{3P}{4bd}, \tag{7.11}$$

where ILS is the shear strength, P the breaking load, b the width of specimen and d the thickness. For the result to be meaningful, the failure

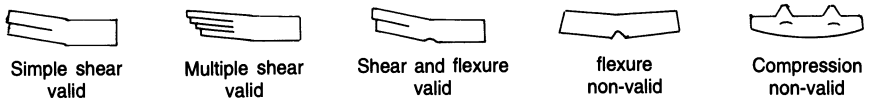

Fig. 7.25 Validity of the various failure modes possible in the short beam shear specimens.

mode must be either single or multiple shear, or plastic deformation with evidence of shear failure. The mode of failure must be recorded. Should failure occur by a non-shear mechanism, the result should be quoted as the 'short beam' rather than interlaminar shear strength. The various possible failure modes and their validity are shown in Fig. 7.25.

The interlaminar shear strength determined by this test method is useful for quality control and specification purposes. The data generated cannot be used as design criteria, but may be used in comparative testing. Carbon–carbon, especially that made by the resin pyrolysis route, in the 1- or 2-D form is extremely prone to interlaminar failure. The ILS test is therefore a useful method of characterizing the material. It should be remembered though, that flaws and defects in test specimens would generally disqualify the specimen from the test [23]. Since carbon–carbon composites usually contain an inordinate number of various types of flaws and inhomogeneities, the validity of such testing will always tend to be very questionable.

Iosipescu test

The major problem in shear testing, particularly in the determination of strength, is the influence of non-shear stresses on the properties measured. Such stresses are introduced by the specimen geometry and the test fixture. Iosipescu [24] proposed a test technique employing a double edge-notched test specimen. A region of pure shear stress is induced at the mid-point of the specimen by the application of two counteracting moments procured by two force couples (Fig. 7.26). A state of constant shear force is induced through the middle section of the test specimen, with the induced moments cancelling exactly at the mid-length, thereby producing a pure shear load at that point.

The average shear stress is given by

$$\tau = P/A, \tag{7.12}$$

where A is the cross-sectional area between the roots of the notches. The thickness of the specimen is not considered to influence the results of the test but practically it is found that specimens less than 4 mm thick are prone to instability due to twisting.

For UD specimens the fibres may be orientated either along the beam or perpendicular to the beam axis. The latter case provides the preferred configuration for an unambiguous failure as total separation occurs on

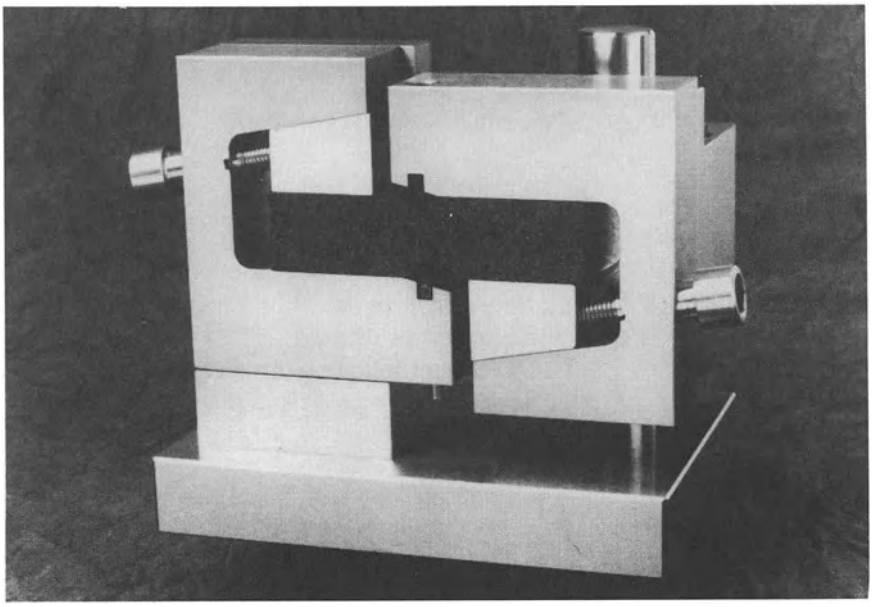

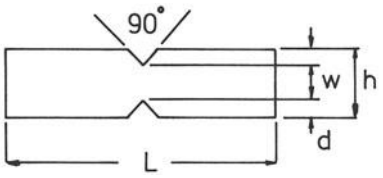

w = 12mm d = 4mm
h = 20mm L = 80mm

Fig. 7.26 Iosipescu fixture and test specimen geometry.

shear cracking. Despite great care being taken in diamond machining it is almost inevitable that sharp starter cracks will be introduced into the specimen at the roots of the v-notches. These microcracks will raise the local stress and introduce non-shear components. As a consequence, UD fibre orientation is observed to generate low strength results, although shear modulus data, calculated from the slope of the straight line portion of the stress–strain curve, should be identical to tests on beams with axial fibres.

Failure in specimens with axial fibres is harder to identify. Since small cracks may initiate at the roots of the v-notches running along the fibre direction. A small but definite load drop may be identified on the load deflection plot. A similar but smaller phenomenon is observed in composites with woven reinforcement.

Additional notes on shear testing

In all shear testing it is the matrix that is dominant in controlling the behaviour of the material. There are two principal classes: in-plane shear and interlaminar shear. A state of pure shear can rarely be established and the relatively low strength of the matrix and the interface renders the composite vulnerable to any extraneous local normal stress. The failure mode in a shear test therefore may not be a genuine shear failure. A further complication is the existence of areas and planes of weakness along which a specimen may fail preferentially, irrespective of the principal axes of the stress field. In most test situations those complications result in the measured property being notional rather than genuine.

When studying carbon–carbon composites, many of the techniques developed for polymer matrix materials are inappropriate due to the extreme brittleness of the matrix and weakness of the fibre/matrix interface. Unsatisfactory as the short beam ILS test may be, it is the best method currently available for evaluating the interlaminar shear strength of carbon–carbon. The Iosipescu test is considered to yield accurate modulus data and relatively good strength data. The procedure is likely to emerge as an ASTM standard for in-plane shear measurements in the near future, and is relatively easy to execute for carbon–carbon specimens. With this in mind an empirical set of acceptable and unacceptable failure modes has been produced (Fig. 7.27). Recent research has identified shear stress concentrations at the root of the v-notches, with the magnitude of the stress concentration being a function of the anisotropy ratio in the material. This will most likely lead to the introduction of correction factors for strength measured using this method [25].

7.7.5 Dynamic testing

Fatigue is a dangerous form of fracture which occurs in materials when they are subjected to cyclic or otherwise fluctuating loads [26]. It occurs by the development and progressive growth of a crack and is characterized by two equally unfortunate features. Firstly, as reported by Gotham [27], fatigue is a progressive weakening of a test piece or component with increasing time under load, such that loads which would be supported satisfactorily at short times produce failure at long times. Secondly, during the lengthening period of time that is required for fracture to propagate to the point of final failure, there may be no obvious external indication that internal fracture is occurring. Fatigue fracture is most familiar with respect to metals but no material is immune to this form of failure.

Fluctuating stress is generally far more harmful to a specimen than a steady stress of the same amplitude. Failure in fibre-reinforced composite materials proceeds in a progressive manner, similar to metals, though more complicated because of the extreme dissimilarity of the properties of the

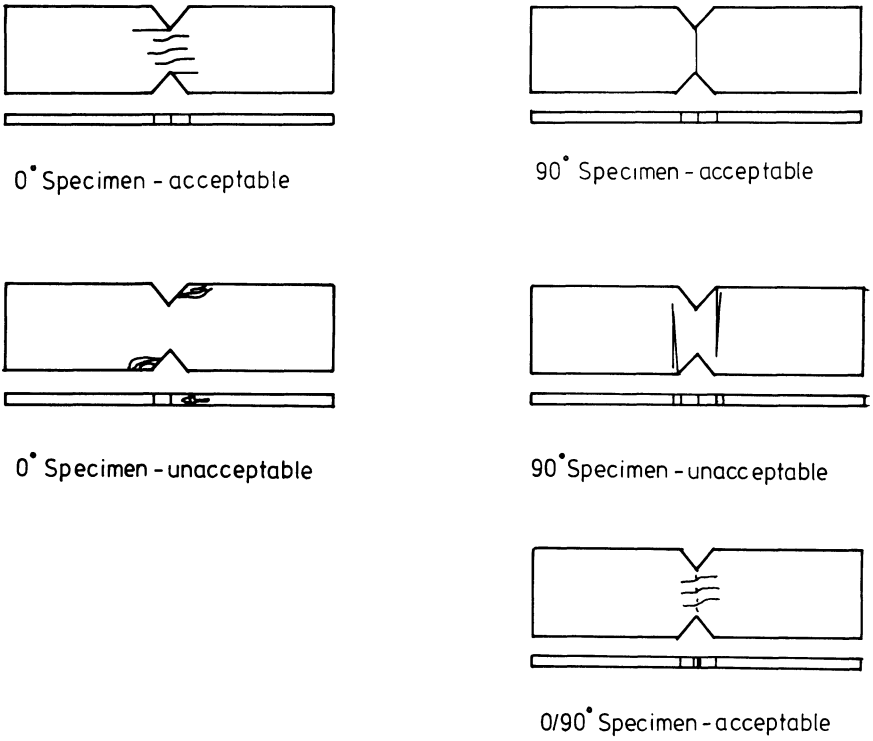

Fig. 7.27 Acceptable and unacceptable failure modes for Iosipescu four-point bend test.

constituents. There are at least three possible modes of failure. Matrix fracture, separation at the fibre/matrix interface and homogeneous fracture of both the matrix and fibres may all occur. In the case of brittle fibre/brittle matrix composites such as carbon–carbon, failure under dynamic loading is manifest in powdering ('dusting out') of the matrix. The appearance of the fracture surface depends on the nature of the stress cycle and the type of reinforcement. In laminates reinforced by fabrics or felts, the fracture surfaces produced by cyclic tensile stresses usually have a fibrous appearance and lie approximately normal to the stress axis. Should the stress cycle include compression, the fracture surface is usually fairly smooth and inclined at an angle to the stress axis. Fractures in UD materials are often delaminations, with the filament failure widely separated, producing a brush-like effect [28].

Fatigue data on non-metallic materials are extremely sparse and ill-understood. A considerable amount of work is being done to fill this gap but it is unlikely that designers will be provided with adequate information for many years to come. Only two internationally recognized test methods presently exist for plastic materials, whereas the fatigue testing of metals is well covered in the standards literature. Not surprisingly, there are no tests whatsoever to cover carbon–carbon.

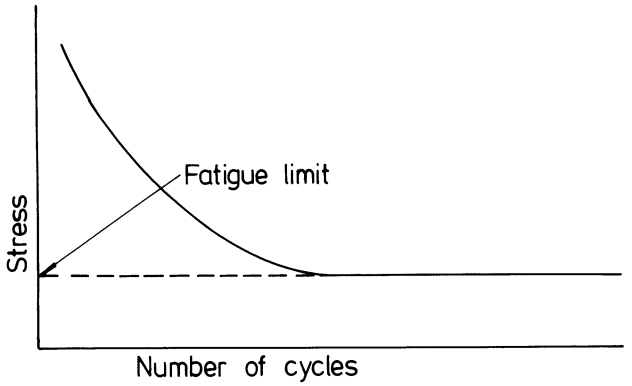

Fig. 7.28 Typical *S–N* fatigue curve.

A large number of cyclic deformation patterns are possible. The data are almost always displayed as the number of cycles to failure at a given maximum stress level. Such plots are known as *S–N* curves (Fig. 7.28). The fatigue life and fatigue limit may be derived from plots such as that in Fig. 7.28. The fatigue life, or endurance, is the number of cycles to failure at a specified level of stress. The greater the applied stress, the fewer cycles are needed to break the test piece. The fatigue limit is the stress condition below which the material may endure an infinite number of stress cycles without failure. The fatigue limit is not, unfortunately, as clear-cut as depicted in Fig. 7.28 and estimates based on statistical analysis are all that can be obtained for real materials.

The applied load may be tensile, compressive, flexural, shear or any combination of these. A sinusoidally varying stress is generally used as it is the easiest to generate. Modern testing equipment such as the Instron 8500 series of servohydraulic test machines operate an accurate system of 'closed loop' control allowing the generation of triangular and square-wave functions with ease. Testing may be carried out at constant cyclic stress amplitude or constant amplitude of cyclic strain. The latter method offers the advantage of ease in setting up the experiment but may create problems in that stiff materials are subjected to higher stresses than materials of low modulus. The constant strain test is therefore a more severe test for composite materials. Furthermore, once cracks develop the imposed stresses lessen such that the number of cycles to failure may become very large indeed. Once cracks start to develop in a constant stress test, on the other hand, failure usually follows very quickly.

Fatigure testing of carbon–carbon is best evaluated in tension or flexure. Flexure tests are the easiest to set up but will, of course, suffer from the usual problems associated with this test of mixed stress modes and tensile surface defect sensitivity. It is advisable that tensile tests are carried out such that all of the applied stress is tensile since the application of a compressive component would require unrepresentative short, squat

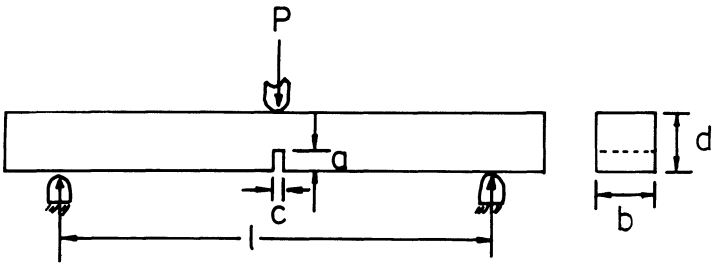

Fig. 7.29 Single edge notched beam fracture toughness test geometry.

specimens to eliminate buckling. As will be seen in Chapter 8, very little work has been carried out on the fatigue of carbon–carbon. For those who embark on this path it should be noted that the fatigue performance in contrast to metals is likely to be very dependent on the frequency of the applied stress as a result of the extreme brittleness of the matrix and weakness of the fibre/matrix interface.

7.7.6 Fracture toughness testing

Carbon–carbon composites have internal voids and flaws as a consequence of their fabrication processes. Fracture toughness is therefore a property which ought to be considered in the evaluation of a material for a specific application [29]. The toughness is best described as the ability of a material to resist crack propagation from a pre-existing flaw. Two fracture toughness parameters have been developed from linear elastic fracture mechanics, both of which deal with the onset of instability or crack initiation near the tip of a pre-existing flaw in ideally elastic and elastic–plastic materials [30, 31]. The toughness can be represented by the stress parameter known as the notch toughness K_c, or by the characteristic energy parameter known as the critical strain energy release rate, G_c.

The stress intensity factor describes the state of stress in the vicinity of the tip of a crack as a function of the specimen geometry, the crack geometry and the applied load. An analytical expression for K_{Ic} (K_c in mode I fracture) may be derived from a rectangular beam specimen tested in three-point flexure. The test (Fig. 7.29) 'borrowed' from monolithic ceramics testing employs a pre-machined crack, approximately half the depth of the specimen [32].

The crack is formed using a slow speed diamond wire saw [33]. K_{Ic} is then given by [34]

$$K_{Ic} = \left(\frac{Pl}{bd^{3/2}}\right) y, \tag{7.13}$$

where P is the load at failure, l the span, b the specimen breadth, d the specimen depth, a the crack length and y is an experimentally determined geometrical factor depending on specimen geometry and (a/d) ratio:

$$y = 2.9(a/d)^{1/2} - 4.6(a/d)^{3/2} + 21.8(a/d)^{5/2} - 37.6(a/d)^{7/2} + 38.7(a/d)^{9/2}$$

and

$$0 \leq (a/d) \leq 0.6. \tag{7.14}$$

When a crack is machined into a brittle material such as carbon–carbon there will inevitably be a degree of crack growth ahead of the cutting tool. It is therefore advisable, in the interests of accuracy, to measure the crack length a after the experiment is complete using a microscope.

The critical strain energy release rate is defined as

$$G_c = -\left(\frac{\partial U}{\partial a}\right)\delta_c, \tag{7.15}$$

where U is the strain energy, A the area of the new fracture surface and δ_c the midspan deflection at instability. In the single edged-notched beam (SENB) test geometry, equation (7.15) becomes

$$G_c = -\frac{1}{2bd}\left(\frac{P}{K}\right)^2 \frac{\partial k}{\partial (a/d)}, \tag{7.16}$$

where K is the bending stiffness of the specimen and $\partial K/\partial\ (a/d)$ is the slope of the K versus (a/d) curve evaluated for the crack length a at the onset of propagation. Since P can be measured experimentally and K versus (a/d) obtained by calibration [35], G may be determined directly using equation (7.16).

While the parameters K_c and G_c describe the resistance of a material to a pre-existing flaw, the work of fracture (γ_f) is a measure of the energy absorbed as a crack initiates and propagates through the material. In the case of a notched flexure test, the work of fracture is defined [36] as

$$\gamma_f = \frac{\bar{u}}{2b(d-a)}, \tag{7.17}$$

where $\bar{u}$ is the total area under the load–deflection curve and $2b(d-a)$ is the approximate area of the new surfaces created during fracture. The Linear Elastic Fracture Mechanics (LEFM) parameters K_c and G_c are found to provide an appropriate description of the ability of a material to resist crack propagation of an existing flaw under load. They are found to be independent of the (a/d) ratio, and may be considered 'material constants'. This is only true, however, in the case of 2-D composites tested in the interlaminar mode between the plies. Tests within the fibre plane (Fig. 7.30) and in 3-D composites result in delaminations which invalidate the tests. Having said that, it is the interlaminar failure in 2-D composites which causes the most concern with respect to unstable crack propagation in the matrix. Toughness testing thus offers a useful method of characterizing that behaviour. In the SENB geometry, K_c evaluation is generally preferred because it does not require the experimental determination of compliance curves.

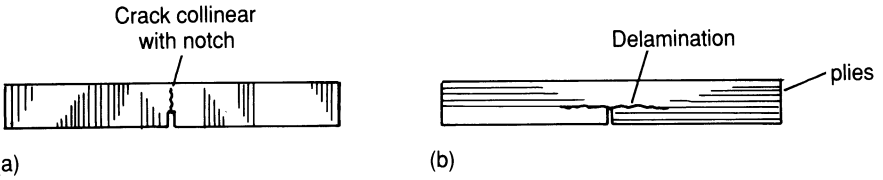

Fig. 7.30 Schematic representation of the failure modes observed in fracture toughness experiments: (a) fibres parallel to notch; (b) fibres perpendicular to notch.

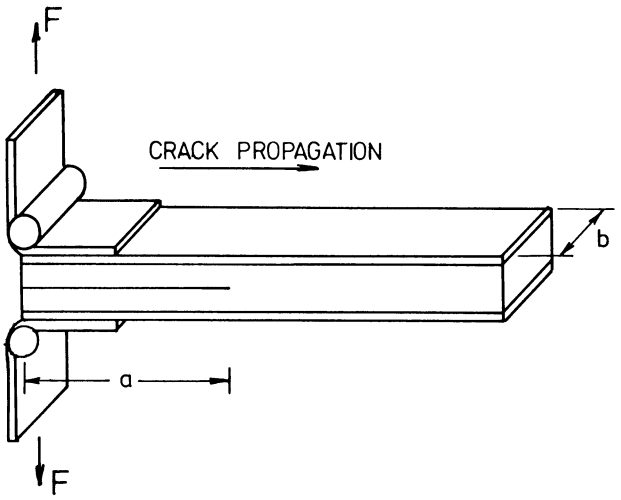

Fig. 7.31 The DCB test geometry.

The work of fracture, γ_f, is not independent of (a/d) and cannot therefore be considered a material constant. Calculated values of γ_f are significant not in a quantitative sense, but as a method of comparison between materials. The fracture toughness parameter G_c has recently been derived for carbon–carbon from an experimental relationship between the compliance and crack length, assuming G_c to be constant during crack propagation [33]. The relationship between fracture toughness and energy release rate during delamination has been investigated in carbon fibre reinforced polymer composite materials [37,38]. Double cantilever beam (DCB) specimens are used in a mode I test (Fig. 7.31). Data reduction is carried out by a compliance method based on elementary beam theory. A DCB test in which an interlaminar crack is propagated generally results in a force deflection trace of the type depicted in Fig. 7.32. With reference to Fig. 7.32, the critical strain energy release rate, calculated using the area method, is given by

$$G_{Ic} = \frac{\Delta U_i}{2b(a_{i+1} - a_i)} = \frac{\frac{1}{2}(F_i\delta_i - F_{i+1}\,\delta_{i+1}) + \int F(\delta)\,d\delta}{2b(a_{i+1} - a_i)} \tag{7.18}$$

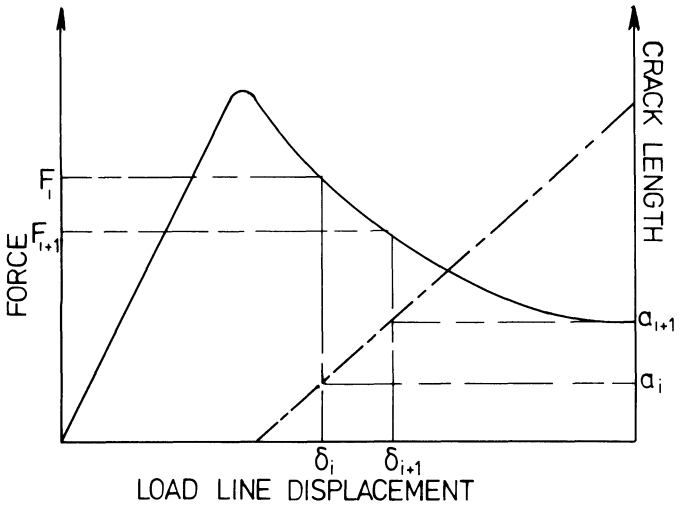

Fig. 7.32 Typical force–displacement–crack length curve recorded during the DCB test.

where U_i is the incremental energy, a the crack length, F the applied force and δ the load line displacement.

In carrying out DCB tests on carbon–carbon it was found that simply attaching hinges to the surface of the 1- and 2-D laminates often resulted in flexural failure of the two half-beams rather than interlaminar crack propagation. The problem can be rectified by bonding a 16-ply UD carbon fibre reinforced polymer composite to both sides of the carbon–carbon before attaching the loading hinges. This serves to restrict the flexural deformation in the beams and cause cracks to propagate along the beams in the required manner. Interlaminar starter cracks are best produced using a diamond-wire saw. Crack length measurement is achieved via resistive crack gauges affixed to one side of the test specimen. The signals from the testing machine and crack length measurement apparatus are interfaced with a microcomputer programmed to carry out calculations of G_{Ic} using equation (7.18).

Values of G_{Ic} are calculated from the gradients of the best-fit lines to the plots of the incremental energy (ΔU_i) versus incremental crack area ($2b(a_{i+1} - a_i)$). An example of such a plot is illustrated in Fig. 7.33. The full line is the least squares fit and the 95% confidence limits are shown dashed.

7.7.7 High-temperature mechanical testing

One of the major advantages of carbon–carbon composites is their excellent high-temperature mechanical properties. It is important therefore to be able to obtain high-temperature design data on the materials such that they may be exploited in refractory engineering applications. The flexural or bend test has been used extensively in evaluating the mechanical

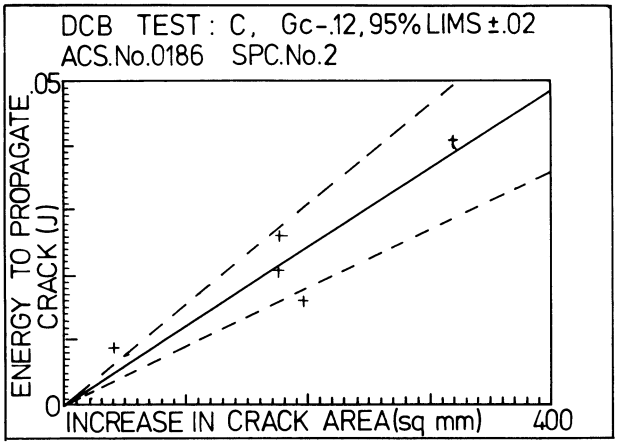

Fig. 7.33 Typical incremental crack energy versus incremental area plot obtained from DCB testing of carbon–carbon.

properties of carbon–carbon and other fibre-reinforced ceramics [39] at high temperatures because of its simple specimen geometry and the relatively inexpensive nature of the test. Testing is fairly straightforward and generally involves some form of three-point test fixture made in ceramic [40]. It has already been discussed how, despite its usefulness for the screening of composite materials, the flexure test cannot be employed to generate the strength and stiffness data required in design calculations.

Fibre-reinforced composites tested under flexural loading may fail in compression, tension, shear or a combination of fracture modes. At high temperatures creep and oxidation effects can further complicate the failure mode. Fracture of the specimen other than in tension results in significant errors in the flexural strength values calculated on the basis of elastic beam theory. Furthermore, flexural testing is more sensitive to surface flaws relative to volume flaws and may not yield the true strength statistics required for the design of components. The majority of the problems associated with the flexural test may be alleviated by uniaxial tensile testing of carbon–carbon. Under uniaxial tensile load the material experiences a uniform tensile stress in the tested volume and fractures when its ultimate tensile strength is reached. High-temperature tensile testing requires unique gripping, heating and specimen design. The stringent requirements of the test procedure result in uniaxial tensile testing being extremely difficult, time-consuming and expensive. Several gripping systems have been developed for testing monolithic ceramics in uniaxial tension [41–43] most of which employ tubular or cylindrical specimens and are unsuitable for flat, laminated carbon–carbon materials. A number of researchers have experimented with pin-grips and 'necked-down' samples, as used in metals testing, to promote failure within the gauge section [44]. Such techniques generally prove unsuccessful when testing carbon–carbon

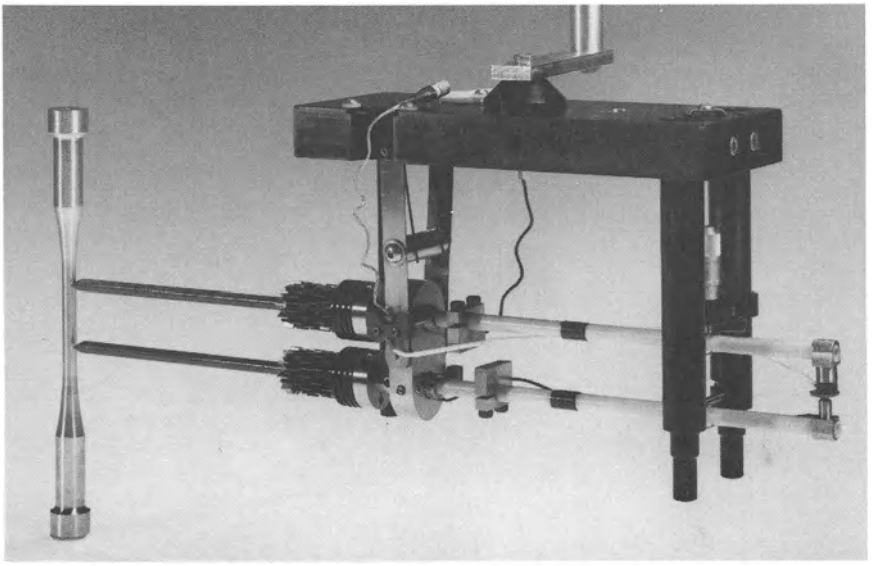

Fig. 7.34 High-temperature extensometer (courtesy Instron Ltd).

as they tend induce premature failure due to shear near the gripped ends of the sample [45,46].

High-temperature testing of carbon–carbon is most successfully carried out using straight section specimens identical to those used in room-temperature testing, but with deformable aluminium tabs bonded to the ends of the specimen, rather than tabs made from a glass reinforced composite. To date, testing has been carried out successfully at temperatures up to and including 1500 °C either in an inert atmosphere or vacuum [47].

A high-temperature tensile test system consists of a universal test machine, a furnace (either inductively heating the specimen, or electrically heated using, preferably, $MoSi_2$ elements), a high-temperature capacitive extensometer (Fig. 7.34) and temperature measuring equipment. A photograph of such a system is shown in Fig. 7.35. When designing the equipment, great care must be taken in the gripping mechanism. Very few materials can tolerate temperatures as high as 1500 °C and those that can are expensive and difficult to machine. They are also prone to failure from thermal cycling to the test temperature, so the lifetime of the equipment is likely to be very low. Chemical interaction may also occur between the grips and material under test, and finally, long extension rods reaching into a furnace make alignment difficult and are impractical for loading in the compression mode where lateral stiffness is important. To combat these difficulties, water-cooled grips that remain outside the furnace can be made of standard metallic materials and are easier to align and preload for tension/compression fatigue testing. The low temperatures also ensure no chemical interaction between the specimen and grip ends.

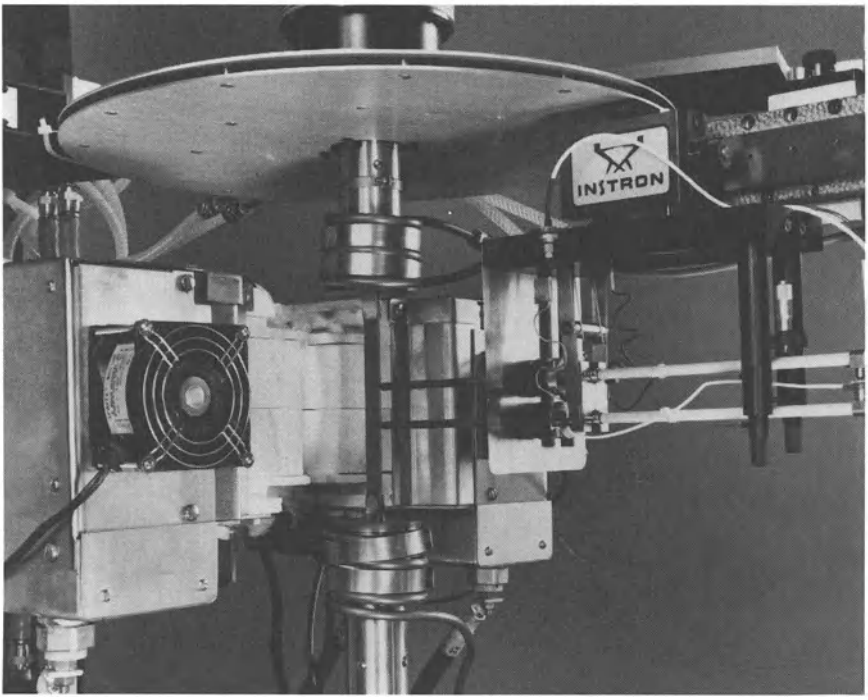

Fig. 7.35 Complete test set-up for high-temperature testing of flat laminated carbon–carbon (courtesy Instron Ltd).

The two main disadvantages of the 'cold' gripping technique are that the specimen must be much longer than the furnace whose design becomes critical in achieving an acceptable temperature gradient across the specimen especially when considering the high thermal conductivity of carbon–carbon. In contrast to the majority of other materials, carbon–carbon tends to increase in strength at high temperature. Great care must therefore be taken to avoid failure in the transition region between the hot and cold zone. Clearly all of the problems associated with the high-temperature testing of carbon–carbon are increased with the tendency towards higher testing temperatures.

7.8 MICROSCOPY

7.8.1 Optical microscopy

Carbon–carbon samples for optical microscopy are prepared by first cutting them to size using water-lubricated diamond-impregnated tools. The

specimen is then mounted in a cold curing plastic resin, of which there are a great number commercially available specifically for this purpose. The specimens are polished to optical flatness using lapping wheels and a range of alumina and diamond pastes of sizes from 240 to 0.05 μm. The prepared specimens possess a surface of high reflectivity with little relief which can be examined using incident light illumination in the optical microscope. Cross-polarized light may be used to highlight areas of anisotropy as described in Chapter 1. A useful technique is to combine the microscope with a CCTV camera input to an image analyser which may be used to provide quantitative and statistical information on the various features observed.

7.8.2 Scanning electron microscopy

Scanning election microscopy (SEM) is best suited to revealing the topography of specimen. As a result it is an invaluable tool in fractography. Fracture faces of carbon–carbon samples used in mechanical testing are sectioned and fixed to aluminium stubs for viewing in the microscope. Despite being an electrical conductor, carbon–carbon materials are often found to produce electron beam charging in the SEM. It is therefore advisable to sputter-coat the specimens with a thin (≈200 Å) layer of gold prior to examination in the SEM. It is very difficult to exploit the increased resolution of the SEM with respect to optical microscopy since the specimens prepared for the latter, by definition, lack any appreciable topography. This problem may be overcome by oxidatively etching the samples prepared for optical microscopy in a manner analogous to the etching of samples in metallography.

A typical etching technique is to remove the specimen from its resin mounting and oxidize it in a chromic acid solution. Etching for 10 min at around 130 °C in nitric acid or, a 10% solution of $K_2Cr_2O_7$ in orthophosphoric acid has been found to be particularly useful [48]. Oxidation treatment of this type will preferentially attack the most thermodynamically unstable regions. A combination of optical and etched SEM microscopy is thus a very useful technique in identifying the various constituents of these complex multiphase materials [49].

7.8.3 Transmission electron microscopy

Transmission electron microscopy (TEM) has been used to characterize carbon–carbon in several modes [50]. Electron diffraction techniques (selected area diffraction, microdiffraction) have allowed the structural characterization of the materials in terms of crystallite size parameters, stack height, L_c, and width, L_a, and the interlayer spacing d_{002} [51,52]. Electron diffraction is useful in cases in which the longitudinal or transverse

structure possesses structural heterogeneity. It is possible to obtain a selected area diffraction pattern from areas as small as 0.8 μm^2. The pattern may be analysed using a scanning densitometer. The diffraction peaks can be analysed by methods similar to those employed in X-ray diffraction [53]. The application of scanning transmission electron microscopy (STEM) permits microdiffraction from an area as small as 4 nm^2, providing an excellent technique for the study of microcrystallinity.

Dark field micrographs using the 002 reflection of the diffraction pattern have been used to estimate the crystallite size [54]. The most useful application of TEM is the study of the extremely complex fibre/matrix interface interactions in carbon–carbon [55].

Preparation of a thin sample of carbon–carbon composite for TEM analysis is an extremely complicated process. Many of the techniques employed such as microtomy are very aggressive and may result in damage to the delicate structures. The subsequent microscopy is thus very likely to be a study of the damage done in specimen preparation rather than the actual structure of the material! Specimens approximately 0.5 mm thick are cut from the bulk composite using a diamond saw. Discs of 3 mm dia. are then cut from the slice using a coring machine. The discs are thinned down by ion bombardment at an initial incidental angle of 45°. A four- or five-stage process is used to thin the specimen down to around 10 μm at the centre, with the milling angle lowered to ≈12° for the final stage. Thin sections of the fibres, matrices and the interface are analysed by electron diffraction, bright and dark field images.

7.9 DENSITY AND POROSITY MEASUREMENTS

The density and, indirectly, porosity of a carbon–carbon composite are generally used as a qualitative measure of the mechanical properties, efficiency of production and quality control. The complex structure of the material with its various phases, open and closed porosity, necessitates the use of a number of techniques to produce the overall 'picture'.

The volume of the bulk specimen may be found using a water displacement technique. The bulk density of the composite is then calculated from

$$\rho = \frac{m}{v}, \tag{7.19}$$

where ρ is the density, m the mass and v the volume. If the carbon–carbon material has appreciable open porosity, however, water will enter it and the 'bulk' density will rise above its proper value.

Mercury porosimetry [56], whereby pressure is applied to force mercury into open porosity at the specimen's surface, is used to measure the size

of the openings to pores and the open pore volume. The limitation of this technique is that it assumes a cylindrical pore geometry.

The true density of the material (i.e. accounting for both open and closed porosity) is obtained by the displacement of liquid helium. This measurement requires approximately 5 g of material for a precision of ± 0.01 g cm^{-3}. The degree of porosity may be calculated from the helium and bulk densities according to

$$V_p = 1 - \frac{\rho_B}{\rho_{He}}, \tag{7.20}$$

where V_p is the volume fraction of pores, ρ_B the bulk density and ρ_{He} helium density.

7.10 OXIDATION AND OXIDATION PROTECTION

7.10.1 Oxidation protection

There are three issues of concern when designing a protective system: these are particulate inhibitors, coatings and sealants.

Particulate inhibitors

The role of particulate inhibitors is to augment the protection provided by the coating which, due to the differential CTE between substrate and coating, generates microcracks. Enough particulate inhibitor is required to generate rapidly a glassy sealant phase at the tip of the cracks in the coating so that excessive erosion of the carbon underneath does not occur. One of the most catastrophic events to occur to an inhibited system is delamination of the coating from the substrate due to loss of carbon at the substrate/coating interface. The type of sealant generated by the particulate inhibitor, e.g. B or $B_4C \rightarrow B_2O_3$, B/SiC $\rightarrow B_2O_3/SiO_2$, gives different viscosity/wetting glass sealants. Key issues with inhibitors include using a fine powder to achieve an even distribution, good reactivity and choice of processing temperatures to avoid detrimental inhibitor–fibre interfaces, and selections of the optimum loading in relation to fibre and matrix to give the best compromise between oxidative and mechanical performance. Inhibitors always increase the cured ply thickness of the materials, hence reducing some in-plane mechanical properties. There is no 'right' inhibitor; the correct choice will depend on the high-temperature application and operating conditions.

Coatings

Coatings are typically applied by pack cementation where a carbon–carbon component is immersed in a mixture of ceramic powders and

subjected to a temperature where vapour phase reaction with the substrates can occur and a diffusion-bonded coating is produced. This method is used on the carbon–carbon parts of the space shuttle. The other technique is CVD, where the coating is deposited via a heterogeneous substrate–gas chemical reaction; CVD is flexible as regards the thickness and stoichiometry of the coating and is in common use.

Again, there is no one 'correct' coating technique. Often multi-layer, multi-technique coating systems are used; multi-layer techniques can minimize the differential CTE problems that plague many coating systems. Different CVD coatings, Si_3N_4 and B_4C/SiC mixed phases, for example, are sometimes used. It is important to mention that coating inspection is an important part of the application process. X-ray non-destructive testing (NDT) techniques are used to check for gross delaminations, and dye penetrometry can be used to investigate the microcrack density of the coating. Unfortunately, most of the information on coatings technology is in classified military reports and are thus inaccessible to the general reader.

Sealants

Sealants are the third method used to provide some oxidation protection for carbon–carbon. Again published literature is hard to find, although there are a number of papers on the LTV space shuttle material describing the TEOS silicate glazes applied to the components. Sealants are typically filled, for example with low-viscosity glasses designed to heal the CTE microcracks in the primary coating.

7.10.2 Testing of oxidation protection systems

This is an extremely complex and difficult issue. The best way to test an oxidation-inhibited substrate is to monitor key properties used as design allowables as a function of time/temperature/gas flow rates/pressures encountered in the real environment of the substrate.

More realistically, the most common test used for screening the oxidation protection system is a weight loss test, either continuously in a thermobalance, or by a series of fixed time exposures at a certain temperature. Absolutely paramount is an awareness of the sensitivity of oxidation rate not just to temperature, but gas flow rates, sample/gas flow geometry, etc. At around 700 °C oxidation kinetics change from being chemically controlled to diffusion dominated. Diffusion-controlled data are extremely difficult to compare unless tests are carried out under identical conditions. For example, static air testing oxidation kinetics at 1000 °C are strongly dependent upon the furnace design in which they are carried out.

Given the need to screen using well-defined test conditions, and test under similar conditions to the desired end use, two further points should

be raised. Most people monitor oxidative stability solely in terms of weight loss/gain. Even for lightly loaded materials, however, the key property is mechanical performance at a given time/temperature oxidation exposure. A very commonly used test is a 'stressed' oxidation test in which the substrate is mechanically loaded while being oxidized. Another important issue, particularly when dealing with inhibited materials, is that of humidity. Often, systems for jet engines which looked promising in simple laboratory test time/temperature cycles have failed when exposed to more humid environments due to the absorption of water. Hydration of a borate glass inhibitor and subsequent (near explosive) dehydration of the rehydrated borate on exposure to temperatures above the boric acid dehydration temperature have caused coating spallation. Given a suitable screening test to evaluate potential candidates, testing under conditions (often cyclic) that accurately duplicate the time/temperature/stress/gas pressure and flow rate conditions of service, a number of other factors must be considered. Many, many replications of the test must be performed, as oxidation testing does not duplicate very well due to inconsistencies in substrate and coatings. Oxidation testing may be carried out in a furnace with a static or flowing atmosphere, a flame such as a gas burner test rig or a plasma arc jet which is used to simulate re-entry, for example.

7.11 MEASUREMENT OF THERMAL CONDUCTIVITY

The object of this section is to provide a brief description of the different methods for experimental determination of thermal conductivity. This is by no means a trivial task, and considerable care in experimental design is called for if meaningful date are to be obtained. There are two basic types of thermal conductivity determination experiments; a steady-state method, where the heat flow in and out of the test piece is constantly balanced (as are the temperature differences from one point of the sample to another), and a non-equilibrium method where the test piece is submitted to thermal pulsing – such as a laser flash – and its thermal response monitored. The simplest concept of experiment is the steady-state method for a rod of defined dimensions, with a known heat flow along its length and a known temperature drop. This method is carried out as follows. The thermal conductivity value (K) for the rod material is defined as

$$K = \frac{-ql}{A(T_2 - T_1)}, \tag{7.21}$$

where q is the heat flux across the test piece (W), l the length of test piece (m), A the cross-sectional area of test piece (m^2) and ($T_2 - T_1$) the temperature difference from one end of test piece to the other and has SI units of W m^{-1} K^{-1}. It is worth pointing out that thermal conductivity values

of carbons are quoted in a plethora of different units. All values may be converted into SI units using tabulated conversion factors [57]. The simple longitudinal steady-state heat flow experiment has to be very carefully performed if meaningful data are to be obtained. Sidewall heating of the test piece has to be provided at just the right level to prevent radiant heat loss from the test specimen. A whole range of different geometry test pieces can be used, from rods to discs and spheres.

One commonly used technique is to use a comparative method, in either a steady-state and non-equilibrium mode, where the test piece is placed directly adjacent to a test piece of known thermal conductivity. This technique is quite simple to perform, but care must be taken to minimize sources of error – the efficiency of thermal contact to the reference and test specimens must be the same, for example. Considerable variations in conductivity values occur in the literature. This may be due, in part, to the inadequacies of the experimental methods used in determining these values. (Recent texts give a full account of the range of possible techniques of thermal conductivity determination. For more detailed information, the reader is referred to them [57].

REFERENCES

1. Pioneer Gasket Inc., Salt Lake City, Utah, USA.
2. Savage, G. M. (1985) PhD Thesis, Univ. London.
3. Savage, G. M. and Williamson, J., Submitted to *J. Mat. Sci.*
4. Wegman R. F. (1989) Non destructive test methods for structural composites, in *SAMPE Handbook*, **1**, Covina, Ca, USA.
5. Belbin, G. R. (1984) *Proc. I. Mech. E.* **198**, 47.
6. Gibbs, H. H. (1984) *SAMPE J.*, **20**, 37.
7. McAllister, L. E. and Taverna, A. R. (1971) *Proc. Am. Ceram. Soc. 73rd Ann. Mtg.*, Chicago.
8. McAllister, L. E. and Taverna, A. R. (1976) *Proc. Int. Conf. on Comp. Mats*, **1**, *Met. Soc. AIME*, New York, p. 307.
9. Mullen, C. K. and Roy, P. J. (1972) *Proc. 17th Nat. SAMPE Symp.*, p. iii–A–2, AZ, USA.
10. Dietric, H. and McAllister, L. E. (1978) *Proc. Am. Ceram. Soc. 80th Ann. Mtg.*, Detroit.
11. Gray, G. and Savage, G. M. (1989) *Metals and Materials Sept.*, 513.
12. Chard, W., Conaway, M. and Neisz, D. (1974) in *Petroleum Derived Carbons*, **21**, (eds M. L. Deviney and T. M. O'Grady), *ACS Symp. Series*, Ann. Chem. Soc., Washington DC, p. 155.
13. Gray, G., Hunter, A., Payne, R. S. and Savage, G. M. (1990) *Met. Pwdr Rpt.*, **45** (4), 290.
14. Gray, G. and Savage, G. M. (1991) *High Temperature Technology (Butterworths)*, **9**(2), May, 102.

15. ASTM (1987) *ASM Standards and Literature References for Composite Materials*, ASTM, Philadelphia, Pa, USA.
16. Curtis, P. J. (ed.) (1988) *Crag Test Methods for the Measurement of the Engineering Properties of Fibre Reinforced Plastics*, RAE Tech. Rpt 88012, Farnborough.
17. BS 1610 Br. Std Inst., (1989) London.
18. *Student Manual for Strain Gauge Technology*, Bull. 309, Measurements Group, PO Box 27777, Raleigh, N. Carolina, USA.
19. Hysol Division, The Dexter Corporation, Pittsburg, California, USA.
20. Whitney, J. M., Daniel, I. M. and Pipes, R. B. (1984) *Experimental Mechanics of Fibre Reinforced Composite Materials*, rev. edn, Soc. for Exp. Mech., Prentice-Hall, Englewood Cliffs, New Jersey.
21. Pipes, R. B. and Pagano, N. J. (1972) *J. Comp. Mat.*, **4**, 538.
22. Wilkins, D. J., Eisenmann, J. R., Canin, R. A., Margolic, W. S. and Benson, J. W. (1980) *ASTM STP* 775.
23. Delmonte, J. (1981) *Technology of Carbon and Graphite Fibre Composites*, van Nostrand Reinhold, New York.
24. Iosipescu, J. (1967) *J. of Materials*, **2**, 537.
25. Kumosa, M. and Hull, D. (1987) *Int. J. Fracture*, **35**, 83.
26. Charles, J. A. and Crane, F. A. A. (1989) *Selection and Use of Engineering Materials*, Butterworths, Harlow.
27. Gotham, K. V. (1969) *Plastics and Polymers*, **37**, 309.
28. Turner, S. (1983) *Mechanical Testing of Plastics* 2nd edn, George Goodwin.
29. Guess, T. R. and Hoover, W. R. (1973) *J. Comp. Mats.*, **7**, 2.
30. Wu, E. M. (1968) Comp. Mats Workshop Techronic.
31. Outwater, J. O. and Murphy, M. S. (1969) *Proc. 24th Ann. Tech. Conf. Reinforced Plastics*, Comp. Div. Soc. of Plastics Ind., Sect. 11-C, p. 1.
32. Kim, H. C., Yoon, K. J., Pickering, R. and Sherwood, P. J. (1985) *J. Mat. Sci.*, **20**, 3967.
33. Savage, G. M. Submitted to *J. Mat. Sci.*
34. Brown, W. F. Jr (1970) *ASTM STP* 463.
35. Brown, W. F. Jr and Srawley, J. E. (1968) *ASTM STP* 410.
36. Tattersal, H. G. and Tappin, G. (1966) *J. Mat. Sci.*, **1**, 296.
37. Russell, A. J. and Street, K. N. (1982) *Proc. ICCM-IV Bordeaux*, p. 279.
38. Wilkins, D. J. (1982) ASTM STP 775, 168.
39. Amaral, J. E. and Pollock, C. N. (1989) in *Mechanical Testing of Engineering Ceramics at High Temperatures* (eds B. F. Dyson, R. D. Lohr and R. Morrell), Elsevier App. Sci. Pub., London, p. 51.
40. Loveday, M. S., Day, M. F. and Dyson, B. F. (eds) (1982) *Measurement of High Temperature Mechanical Properties of Materials*, HMSO, London.
41. Liu, K. C. and Brinkman, C. R. (1985) *Proc. 23rd Automotive Technology Development Contractors' Meeting*, SAE, Detroit, p. 279.
42. Vaidyanthan, R., Shankar, J. and Avva, V. S. (1987) *Proc. 25th Automotive Technology Development Contractors' Coordination Meeting*, SAE, Detroit, p. 175.
43. Herrmansson, L., Adlerborn, J. and Burstrom, D. ASEA CERAMA AB, company literature.

44. Gouila, R. K. (1983) *J. Mat. Sci.*, **18**, p. 307.
45. Sheshadri, S. G. and Chia, K. Y. (1987) *J. Am. Ceram. Comm.*, **70**(10), 242.
46. Gyekenesi, J. Z. and Herrman, J. H. *NASA Contractor Rpt 180888.*
47. Mandell, J. F., Grade, D. H. and Dannerman, K. A. (1986) *Proc ASTM Symp.*, Phoenix Ariz. USA, 3–4 Nov.
48. Markovic, V., Ragan, S. and Marsh, H. (1984) *J. Mat. Sci.*, **19**, 3287.
49. Forrest, M. A. and Marsh, H. (1981) *Proc. Biennial Conf. on Carbon*, Am. Carbon Soc., Univ. Pennsylvania, Philadelphia.
50. Kowbel, W. and Don, J. (1989) *J. Mat. Sci.*, **24**, 133.
51. Wicks, B. J. (1971) *J. Mat. Sci.*, **16**, 173.
52. Oberlin, A. (1982) *J. Mat. Sci.*, **23**, 7.
53. Johnson, D. J. and Crawford, D. (1973) *J. Mat. Sci.*, **8**, 286.
54. Badami, D. V., Joiner, J. C. and Jones, G. A. (1967) *Nature*, **215**, 386.
55. Weizhou, P., Tianyou, P., Hanmin, Z. and Qias, Yu (1988) *Proc. Int. Conf. Compos. Interfa*, Elsevier, p. 399.
56. Sibilia, J. (ed.) (1988) *A Guide to Materials Characterization and Chemical Analysis*, VCH Publishers, Weinheim, Germany.
57. Eckert, E. R. G. and Irvine, T. F. (eds) (1977) *Progress in Heat and Mass Transfer*, **8** Pergamon Press, Oxford.

The Properties of Carbon–carbon Composites

8

8.1 GENERAL CONSIDERATIONS

The microtexture, that is to say the microstructure and morphology, of the various types of carbon–carbon composite will differ according to the type of raw materials and the processing conditions. Further complication will arise from the use of 'subtle' treatments such as surface modification of the fibres and inclusion of oxidation protection. All such differences in microstructure exert a considerable influence on the properties of the materials.

The architecture of the carbon fibre reinforcement can take many forms: random short fibres, unidirectional (UD) continuous fibres, braided structures, laminated fabrics, orthogonal 3-D weaves (in either Cartesian or cylindrical coordinates) or multi-directional structures may be used. Commercial carbon fibres are manufactured from rayon, acrylic and pitch precursors. The mechanical and other properties of these fibres vary considerably, again depending on raw materials and processing conditions. High-strength fibres are usually obtained from acrylic precursors whereas pitch is preferred for the fibres of highest modulus. The carbon fibre is generally post-treated to improve weaving characteristics and/or to modify the bonding of fibre to matrix.

The matrix may vary from an isotropic, glassy carbon produced from the pyrolysis of a thermoset resin, through to a highly oriented anisotropic graphitic carbon arising from mesophase, developed during the carbonization of pitch. A matrix material may also be formed by chemical vapour deposition (CVD) of carbon from the cracking of hydrocarbons. The structure of the CVD matrix depends very much on the processing conditions. All of the production routes used to manufacture carbon–carbon are slow, inefficient multi-step batch processes. As a result, many finished products tend to be made using a variety of methods. Composites fabricated by the

thermoset resin pyrolysis route, for example, are often densified using CVD or a mixture of pitch and a different resin from that used in the initial cycle.

The number of possible combinations of parameters is almost limitless. Rather than provide a complete catalogue of the properties of carbon–carbon, it is intended to present the general trends associated with the different variables. The theme developed, throughout this text, of carbon–carbon as a family of materials whose properties may be tailored to suit a specific application, will thus become apparent.

8.2 MICROSTRUCTURE

8.2.1 CVD-densified composites

The matrix deposited in the CVD process may comprise three different types as discussed in Chapter 3. The first of these, the isotropic type, consists of an optically isotropic morphology of fine particles no more than a few microns in size. The other two matrix types are both optically anisotropic morphologies. The rough laminar structure comprises a combination of layers with strong optical anisotropy, arranged such that the fibres as a whole are surrounded. In the smooth laminar microstructure optically weakly anisotropic layers are oriented so as to surround the fibre uniformly [1]. The principal factors influencing the different microstructures are the concentration, or partial pressure, of the reactant gas and the processing temperature [2]. A simplified representation of the temperature/pressure/microstructure relationships observed in carbon deposition from propane is given in Fig. 8.1 [3–5]. It should be remembered, however, that the mechanisms involved in CVD are extremely complex and as yet poorly understood. Even at the same temperature and pressure, and with the same feedstock gas, the morphologies obtained can be different. The effect of any sizing materials on the fibres can generally be disregarded since deposition is carried out at temperatures in excess of 800 °C at which any such compounds will have been carbonized.

Figures 8.2 and 8.3 are optical micrographs of CVD brake materials produced by the French company SEP for use in aircraft and Formula 1 racing cars. The microstructure in Fig. 3.2 illustrates an important characteristic of CVD-densified material, in that CVD is extremely good at filling small pores, but generally poor at filling large ones.

Figure 8.3 shows a detail of this microstructure in Fig. 8.2. The matrix is optically anisotropic and is highly reflective. Around the fibres the matrix exhibits extinction crosses indicative of the presence of circumferentially stacked, highly graphitic material that has been deposited around individual carbon fibres. The circular cross-sections, characteristic of PAN-based fibres, can be clearly seen. The irregular extinction crosses (blue, yellow and

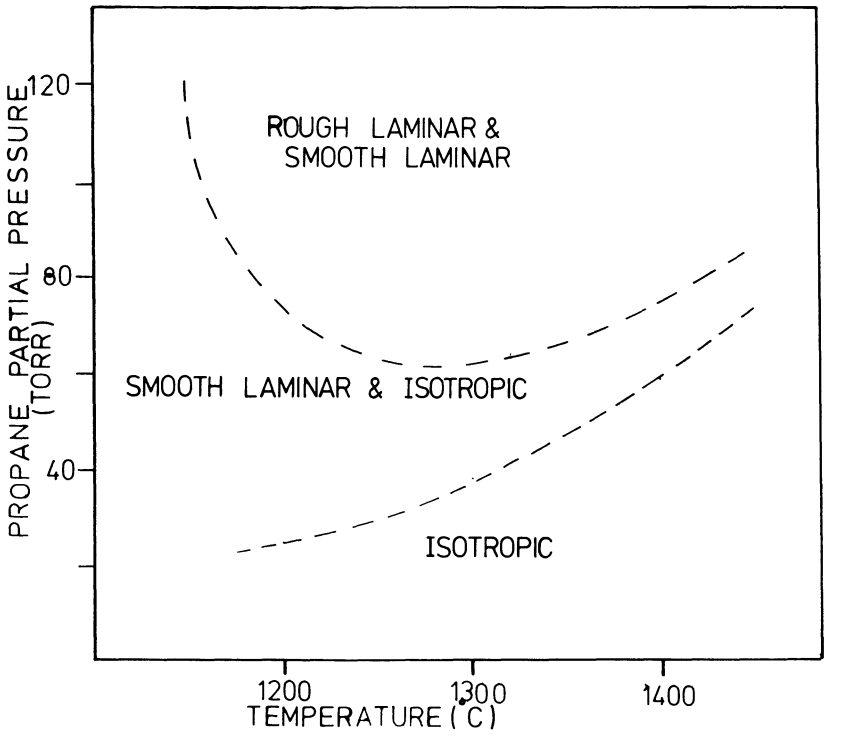

Fig. 8.1 Relationship of CVD matrix microstructure to processing temperature and propane gas partial pressure.

purple under polarized light) are typical of the rough laminar microstructure [6].

8.2.2 Thermoset resin derived material

The microstructure of a composite produced using the thermoset resin pyrolysis route will vary dramatically according to the heat treatment temperature (HTT). When carbonized by itself, a thermoset resin will form a glassy isotropic carbon [7]. X-ray analysis reveals no evidence of the formation of graphite. The material is optically isotropic, very hard, and has a low porosity and permeability. When heat-treated in the form of a composite with carbon fibres on the other hand, graphitic material is observed in the matrix in the region of the interface with the fibres [8]. This effect is most marked in the case of a furan precursor, in which optical anisotropy is seen even at HTTs below 1000 °C. Should the temperature of processing exceed 2200 °C, the domains of anisotropy gradually change to graphite. An HTT of 2800 °C or greater will result in a completely graphitic matrix.

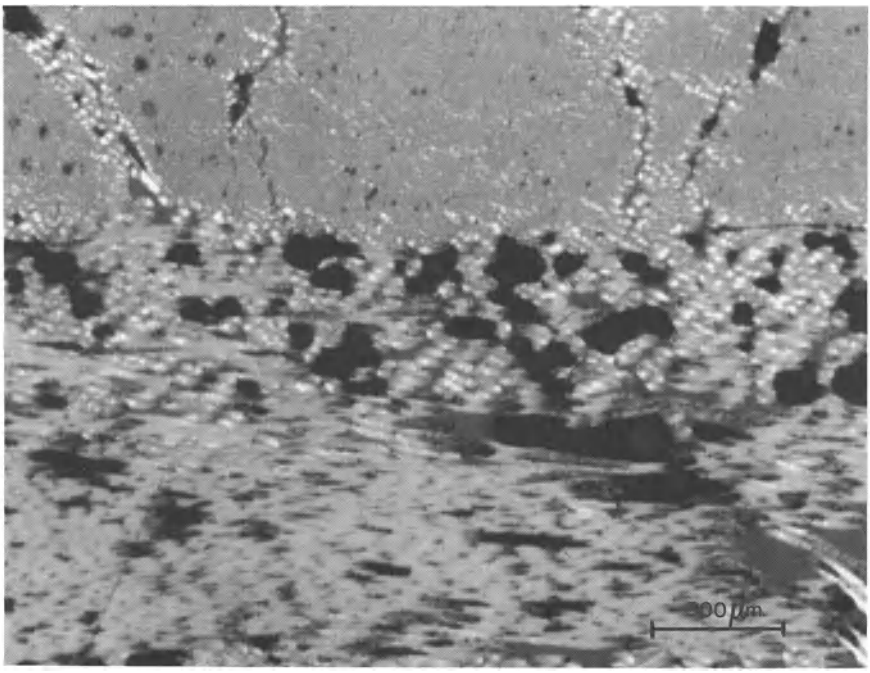

Fig. 8.2 Optical micrograph of SEP brake material.

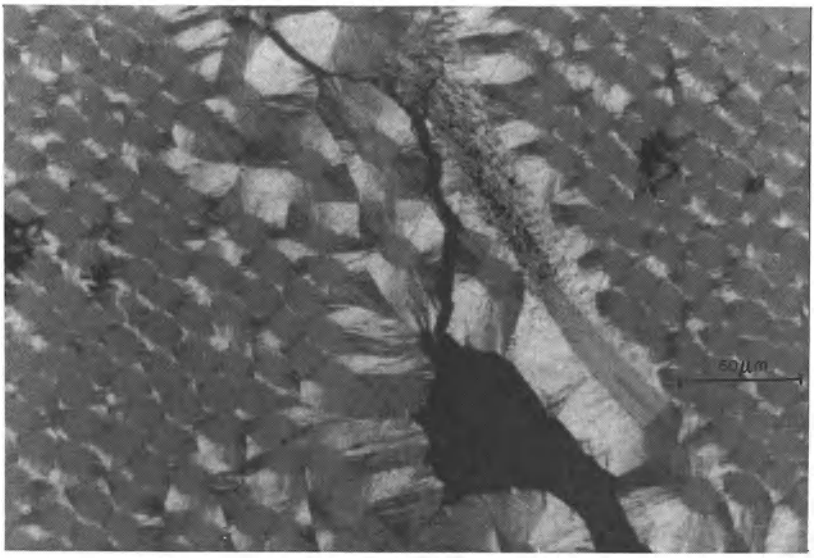

Fig. 8.3 Detailed microstructure of SEP brake material showing rough lamellar matrix morphology.

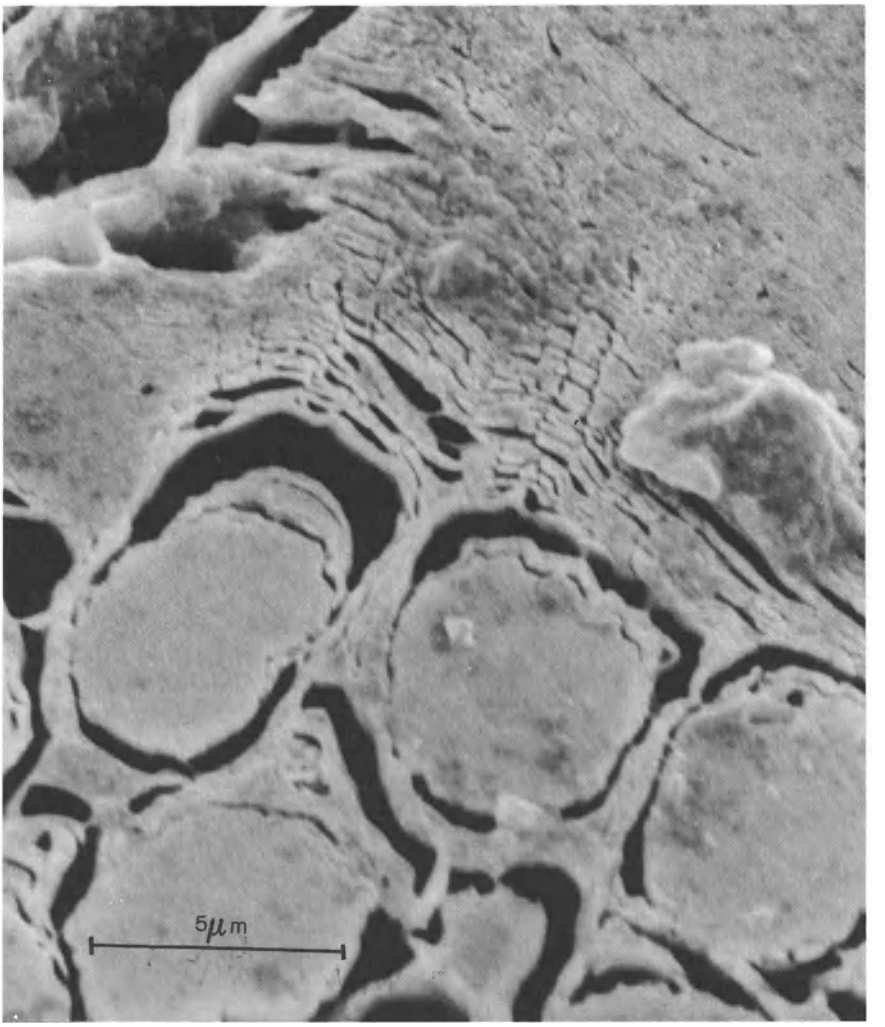

Fig. 8.4 Scanning electron micrograph of a graphitized carbon–carbon composite, acid etched to show the lamellar structure of the matrix in the vicinity of the fibre/matrix interface.

Research suggests that the graphite microstructure in thermoset-derived matrices is oriented in such a way that the graphite planes encircle the fibres [9]. Figure 8.4 is a scanning electron micrograph of a polished surface perpendicular to the fibre axis which has been subjected to acid oxidation. It appears that the graphite layers are divided into a number of domains and, as a whole, envelop the fibre. The graphitization of what are essentially 'non-graphitizing carbons' is believed to be due to the high stresses set up between fibre and matrix as a result of thermal expansion

mismatch at high temperatures. The process is described as 'stress-graphitization' [10,11]. The temperature and rate at which the matrix transformation proceeds depend very much on the type of reinforcing fibre. The higher the modulus of the fibre the lower will be the graphitization temperature range and the quicker the rate of change. A number of studies of stress-graphitization are reported in the open literature [12–14] but the mechanism remains poorly understood.

Very little work has been published relating to the fibre surface treatments which are so important in the polymer composite industry [15]. Fitzer *et al.* reported oxidizing the surface of the fibres, using nitric acid, to result in an increase in the strength of a carbonized composite [16]. Their results indicated an optimum level of pre-treatment since excessive oxidation caused a lowering of strength. The majority of sizing agents carbonize at temperatures lower than that of the matrix precursor with a very poor carbon yield. Their presence is therefore considered deleterious to the properties of the carbon–carbon composite. All weaving lubricants and sizing materials are generally removed, by thermal treatment, prior to processing.

The microstructure of ex-thermoset composites is dominated by large-scale porosity and shrinkage cracks. The porosity results from the volatilization of small molecules and heteroatoms during pyrolysis (Fig. 8.5). Carbonization is generally performed at temperatures up to 1000 °C even though the matrix will retain some percentage of residual hydrogen. The hydrogen content diminishes to below 0.1% with further heat treatment to between 1350 and 1400 °C. Heat treatment above 2000 °C results in significant shrinkage of the carbon matrix as it gradually transforms into a graphite structure. The use of intermediate graphitization cycles is thus observed to improve the efficiency of subsequent impregnation and recarbonization processes by increased access to porosity. Even when fully graphitized composites are not required, it is often standard practice to graphitize the composite after the first carbonization as an aid to sub-sequent densification.

Figure 8.6 shows a polarized light micrograph of a densified carbon–carbon composite produced from a thermoset resin (phenolic) reinforced with intermediate modulus (IM) fibres (Hercules AS4). Following carbonization the sample was heat treated to 2700 °C to open up the porosity and then densified four times with a mixture of pitch and furan resin. Reimpregnation, even after four iterations, has failed to densify fully the composite as may be witnessed by the fact that the reimpregnant carbon tends to line the pores rather than fill them in. A 'matrix rich' region in the same composite is shown in Fig. 8.7.

Optical anisotropy in the phenolic-based matrix can be clearly discerned in the bottom left-hand corner of the micrograph. The graphitic carbon can be seen grading continuously into an isotropic matrix as the distance from the fibre increases. One may thus conclude that the microstructure of the matrix derived from phenolic resins is strongly affected by the presence of fibres and the associated thermal stresses at the interfaces.

Fig. 8.5 Electron micrograph of densified carbon–carbon composite made from phenolic precursor, showing evidence of microcracking and porosity.

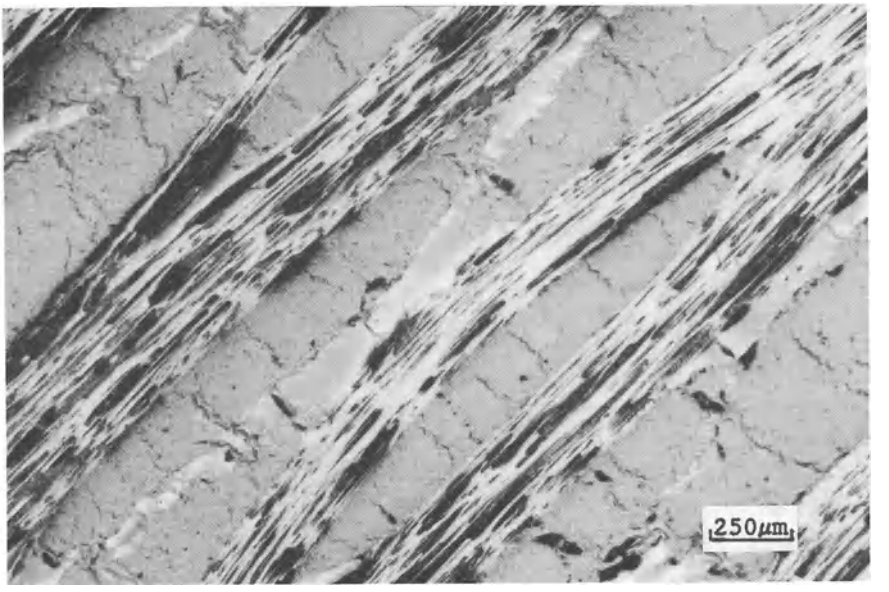

Fig. 8.6 Polarized optical micrograph of densified composite showing optical anisotropy resulting from graphitization and lined but open microcrackes and pores illustrating inefficient reimpregnation.

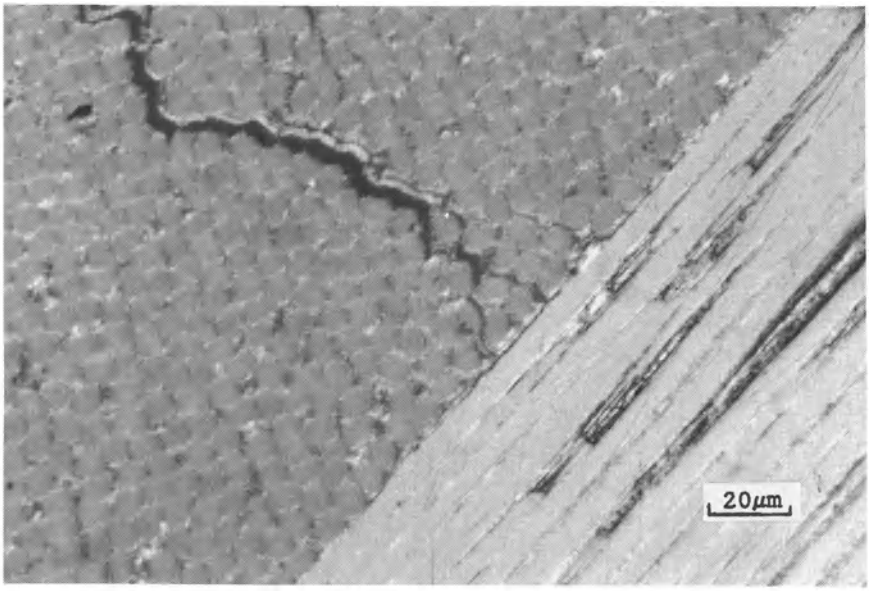

Fig. 8.7 Polarized light micrograph illustrating stress graphitization in phenolic-based matrix.

8.2.3 Thermoplastic-based composites

The microstructure of pitch matrix materials pyrolysed at pressures below 10 MPa is hardly affected by the fibre type. Graphite planes are oriented parallel to the fibre axis at the interface, becoming more and more disordered with distance from the fibre. In Chapter 5 it was shown how the carbon yield from pitch can be substantially increased by the application of pressure during pyrolysis. The suppression of mesophase incorporation occurs at pressures of above 30 MPa such that the matrix as a whole is isotropic, except in very close vicinity to the fibres where the graphite planes are oriented parallel to the fibre axis [17]. A completely isotropic matrix may be obtained if fibres with a thin (0.5 μm) CVD carbon layer are applied to the fibres prior to impregnation with pitch [18,19]. It is considered that the CVD treatment impairs the wetting ability of the pitch. Pitch, however, is never a straightforward and predictable material, examples having been reported in which mesophase incorporation is not suppressed at high pressures [20].

Ambient pressure carbonization of pitch matrix composites results in large-scale open porosity of complex geometry. Pressure carbonization, on the other hand, results in many closed pores which tend to be spherical in shape and of uniform size distribution. Further methods of increasing the carbon yield of pitch involve oxidation (Chapter 5) and the addition of sulphur [21,22]. Both processes essentially serve to cross-link and 'pseudo-thermoset' the pitch in order to prevent the loss of lower molecular weight

Fig. 8.8 Carbon–carbon composite with PEEK-derived matrix showing unique 'polymeric-type' morphology.

compounds as volatiles. A hard/rigid carbon microstructure akin to a glassy carbon tends to result.

The use of engineering thermoplastic polymers, such as PEEK, as matrix precursors is a relatively recent development [23,24]. The microstructures obtained tend to be of the glassy, isotropic type, but with a unique morphology very similar to that of the polymer whence it was derived (Fig. 8.8). Microstructural [25] and electron diffraction [26] evidence suggests that the matrix may be stress graphitized, especially in the presence of ultra-high modulus pitch-based fibres. The materials may be considered as intermediate between those obtained from thermosets and that from pitch. Carbonization at high pressures (≈100 MPa) results in a low porosity and a high density (Fig. 8.9).

8.3 INTERFACES IN CARBON–CARBON COMPOSITES

The nature of the interfaces in carbon–carbon composites and their influences on thermomechanical properties is extremely complex. The type of bonding across the interfaces is not well understood [27]. A number of

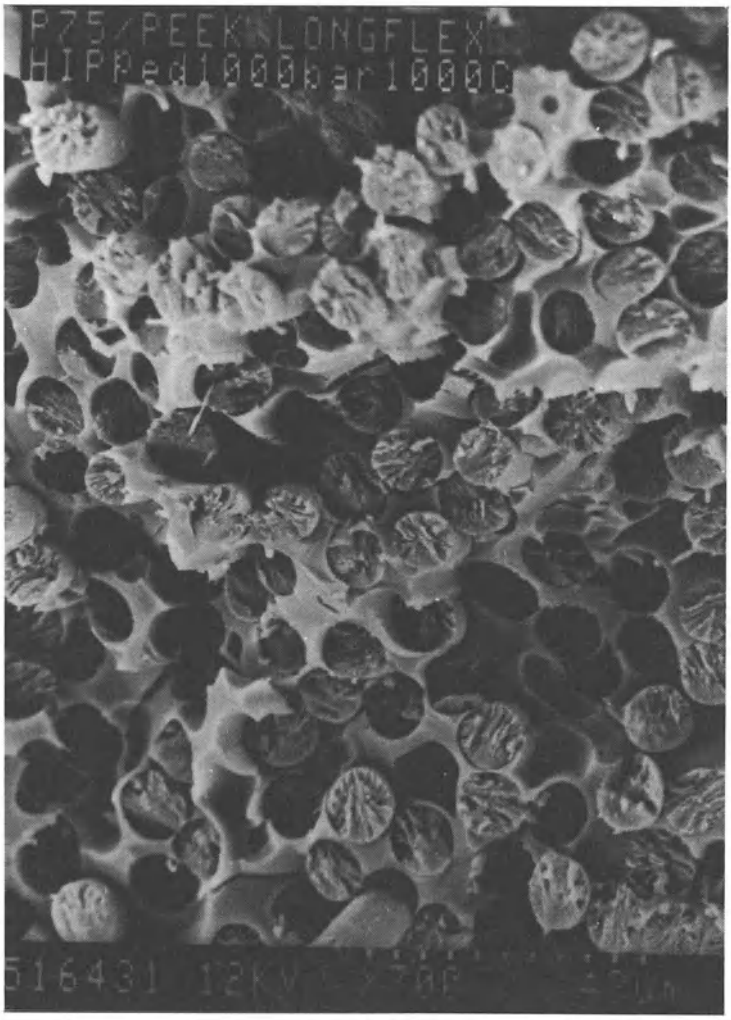

Fig. 8.9 High-density carbon–carbon made from P75 fibres in PEEK matrix.

different types of interface may exist in carbon–carbon: between fibres and matrix, within fibre bundles, between fibre bundles and between the different microstructures which may exist within the matrix. The bonds formed may be strong or weak chemical links, mechanical interlocking and friction couplings. The nature of the interfaces in a particular composite depends, as do so many other properties, on the choice of raw materials and processing conditions.

The possible orientations of the matrix at the interface with the fibres are shown in Fig. 8.10 [28]. The isotropic form is generally seen in the

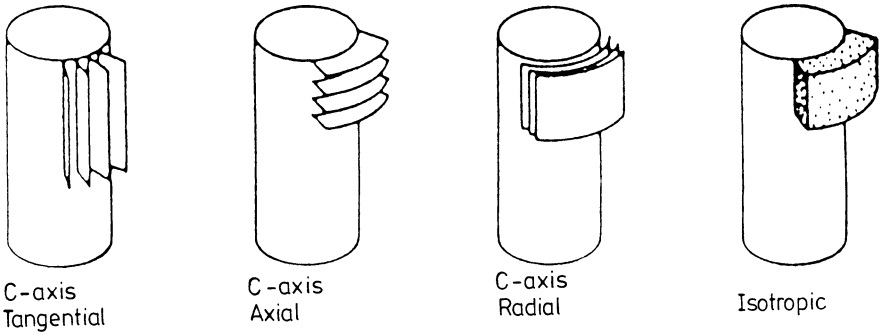

Fig. 8.10 Elementary possibilities for the orientation of the carbon matrix about a carbon fibre [28].

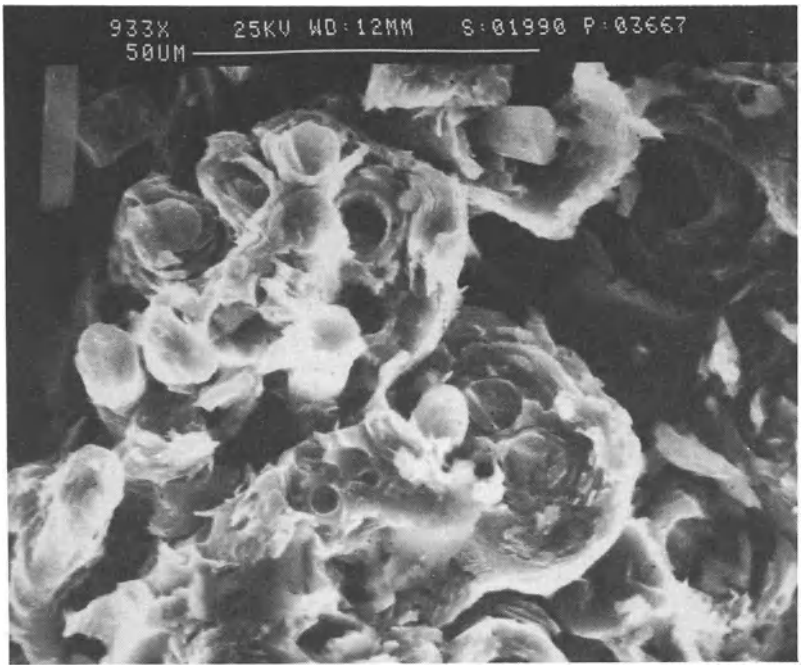

Fig. 8.11 Strong fibre matrix bonding in CVD-densified carbon–carbon.

matrix of ex-thermosetting resin materials although it is sometimes observed in CVD matrix materials [29]. Of the laminar forms, the *c*-axis radial (sheath) and *c*-axis axial (transversely aligned) are the most common. The fibre/matrix bond in CVD-formed composites is extremely strong, having been progressively built up atom by atom (Fig. 8.11). In the case of liquid matrix precursors, strong bonds may form when the fibre substrate has active carbon sites available to which the matrix can attach. The majority

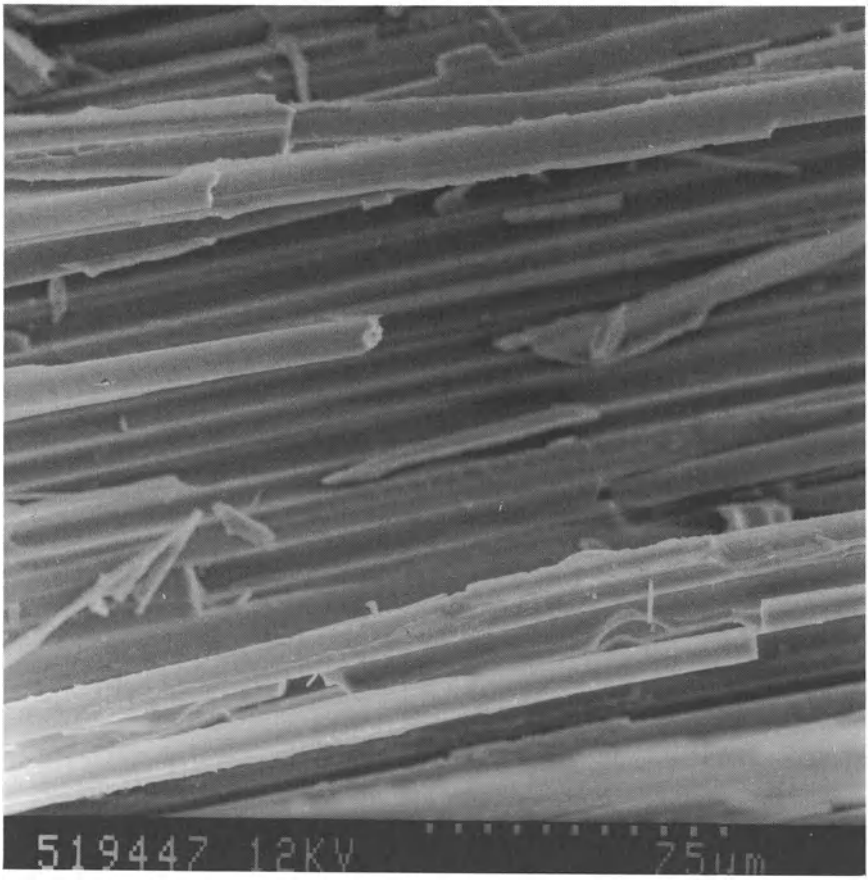

Fig. 8.12 Moderately strong interface around radial texture pitch-based ultra-high modulus fibres.

of PAN-based intermediate or high modulus (HM) fibres possess a skin-core structure with a sheath-like HM skin [30]. One would, therefore, only expect weak fibre–matrix bonds for this material. Ultra-high modulus pitch-based fibres, on the other hand, exhibit a radial texture with an active surface to which the matrix may bond well [31]. Evidence of this can be seen in Fig. 8.12, showing the relatively strong interface which is formed in P75/PEEK-based composites. A pitch matrix, however, tends to form a sheath around such fibres despite the postulated availability of edges to which the mesophase ought to have formed covalent bonds [32]. It is discrepancies such as this which highlight the severe gaps in our understanding of carbon–carbon.

The evidence presented in the literature shows a predominance of weak fibre–matrix bonding in carbon–carbon composites produced from liquid

precursors. Interfacial bonding in CVD materials, on the other hand, is quite strong, the material being limited by the remaining large-scale porosity that is inherent to the process. The exact nature of the fibre/matrix interface in liquid pyrolysed composites remains a subject of some debate. In many respects, the outcome of the discussion is of little concern since if, as is believed, the interfacial bonds throughout the matrix are weak, the predominant failure mode will be a cohesive fracture of the matrix. The effects of such a phenomenon would be closely analogous to adhesive failure at the interface.

Unidirectional carbon–carbon composites exhibit low transverse flexure and shear strengths as a result of their weak matrix and interfaces. Their usefulness in structural applications is thus very limited. Nevertheless, they are extensively studied when researching the fundamental properties of carbon–carbon (Chapter 7). Carbon–carbon components thus tend to be multi-directionally reinforced; 2-D fabric laminates or spatially reinforced *n*-D structures are employed in order to increase damage resistance and reduce the risk of delamination in service.

The fibre to matrix bonding depends on the stresses developed between the two components as a result of matrix shrinkage during processing and by differences in thermal expansion. Increases in the degree of chemical bonding or intimate contact (mechanical interlocking) have been shown to manifest themselves in high tensile and compressive strengths in the fibre direction.

If the interface becomes stronger than the matrix itself, then the load transfer behaviour between fibre and matrix will depend on the mechanical properties of the matrix. Poor interfacial bonding will, conversely, result in failure at the interface. This has been demonstrated in tensile fractures showing fibres pulled out of composites without any discernible matrix adhering to their surface [33]. It is possible to engineer the nature of the interface by the selection of fibre type, the matrix and processing conditions [25]. A 'moderately strong' bond (transverse flexure strength $\approx$16 MPa) is preferred. Too weak an interface impairs stress transfer from matrix to fibres, whereas too strong a bond may promote damage to fibres during heat treatment and brittle fracture behaviour.

The thermal expansion behaviour of carbon–carbon is strongly dependent on the extent of fibre/matrix interaction. The CTE of highly aligned carbon fibres between 0 and 500 °C is negative. In contrast, a glassy carbon matrix will possess a CTE which is both positive and isotropic and is approximately four times the absolute value of that of the fibres. As a result, there will be a thermal mismatch between fibres and matrix which must, by definition, be resisted by the interface [34]. There is evidence, therefore, that the coupling between fibre and matrix may be altered from one of a chemical nature in the precursor into something akin to a 'frictional' type of bond.

In Section 8.2 it was shown how microscopy reveals a myriad of cracks running in a variety of directions within a carbon–carbon composite. This three-dimensional crack network arises due to inefficient penetration in CVD materials, and owing to the shrinkage which occurs from hetero-atom elimination and differences in CTE between fibres and matrix in the case of liquid precursors. It is this network of cracks which permits the further densification of partially processed materials. The crack network enlarges the surface area available to oxidative attack [35]. The cracks do, however, aid the infiltration of the composite with protective compounds. Coatings and inhibitors may thus be anchored to the composite by mechanical interlocking, allowing the material to act as a reservoir for substances which soften at high temperatures and produce a protective barrier (Chapter 6) and also increasing the coating–substrate adhesion/spallation resistance.

Additional microcracking in service is a consequence of the thermal stress cracks, weak matrix and interfaces and the porosity present in all carbon–carbon composites. The resulting effects on thermomechanical properties include inefficient utilization of fibre properties, unpredictable anomalies in thermal expansion behaviour and highly non-linear responses to shear stresses [36]. The understanding of interfacial behaviour in carbon–carbon is paramount to the development of composites with attractive and predictable properties. Much of the behaviour of carbon–carbon may be explained, in part, by assuming that load transfer across interfaces occurs primarily by a friction mechanism. That is to say, much of the thermal and mechanical behaviour of carbon–carbon may be modelled assuming debonded interfaces which are only able to transmit stress in compression across the interface [36].

8.4 MECHANICAL PROPERTIES

The structural properties of continuous fibre 'advanced' composites are generally controlled by the properties, volume fraction and geometry of the fibres. Carbon–carbon composites, however, are by nature very complex as a result of the physical and chemical changes, and interactions that occur during processing. Pyrolysis of an organic precursor, for example, to form a carbon matrix involves a 50% reduction in volume. Shrinkage of this magnitude can create severe damage to the composite by the build-up of large process-related stresses [37]. The transformation from a carbon fibre/organic interface to a carbon/carbon fibre interfacial bond will vary considerably, dependent on materials and process variables. Extended heat treatments, process-induced stresses, and fibre–matrix interactions are very likely to affect adversely the primary properties of the fibre reinforcement [38,39]. Severe thermal stresses, due to thermal expansion mismatches between fibres and matrix, and between different matrix structures, will

result in a time-dependent deterioration of composite mechanical properties during heat treatment and service cycles.

A complete description of how composition and processing influence the properties of carbon–carbon is beyond the current level of knowledge and understanding. The data available are only capable of qualitatively indicating the trends that have been observed. A number of these trends will be reviewed in an attempt to illustrate the factors and principles that influence the mechanical behaviour of carbon–carbon.

In keeping with all fibre-reinforced materials, the mechanical properties of a carbon–carbon composite show marked anisotropy as a result of the anisotropy in the fibres. For the case of UD fibres, the maximum stress theory states that the tensile strength of the fibre will be manifest when the angle (θ) between the applied load and fibre axis is no more than 4°. If θ exceeds 4° the strength (σ_{11}) will be governed by the shear strength (τ) and may be expressed as

$$\sigma_{11} = \tau / \sin \theta \cos \theta. \tag{8.1}$$

Should θ exceed 24°, the strength approaches that of the matrix. The relationship between the angle at which a tensile load is applied and the strength of a UD carbon–carbon composite is shown in Fig. 8.13 [40]. The composite's tensile strength (σ_c) in the fibre axis of a 1-D material can be expressed according to a simple rule of mixture:

$$\sigma_c = \sigma_f V_f + \sigma_m (1 - V_f), \tag{8.2}$$

where σ_f is the fibre strength, σ_m the matrix strength and V_f the volume fraction of fibres. The strength of the matrix can generally be neglected when compared to the strength of the fibres such that the strength of a composite is proportional to the fibre content.

It is very difficult, in practical applications, to realize the theoretical strength of a composite due to twisting and distortion of the fibres, variations in fibre orientation, and stress concentrations associated with the method of test. Furthermore, should the fibre content exceed 70%, uniform impregnation by the matrix becomes impossible, resulting in a fall in strength. The large-scale, irregular porosity, poor fibre/matrix interface, and inherent brittleness of the system have the result that the carbon–carbon never attains its theoretical strength, values of 50–60% being typical. As a general rule of thumb, it is usually assumed that a balanced woven fabric reinforced material (or 0/90° UD lay-up) will have roughly half the strength of a UD material and a quasi-isotropic laminate one-third its strength.

The strength of carbon–carbon composite materials does not generally follow the simple law of mixtures relationship. The weak interfacial bonding results in an inefficient transfer of applied loads on to the fibre reinforcement, such that theoretical strengths are seldom if ever, achieved. Mechanical properties of carbon–carbon tend to vary between 10 and 60%

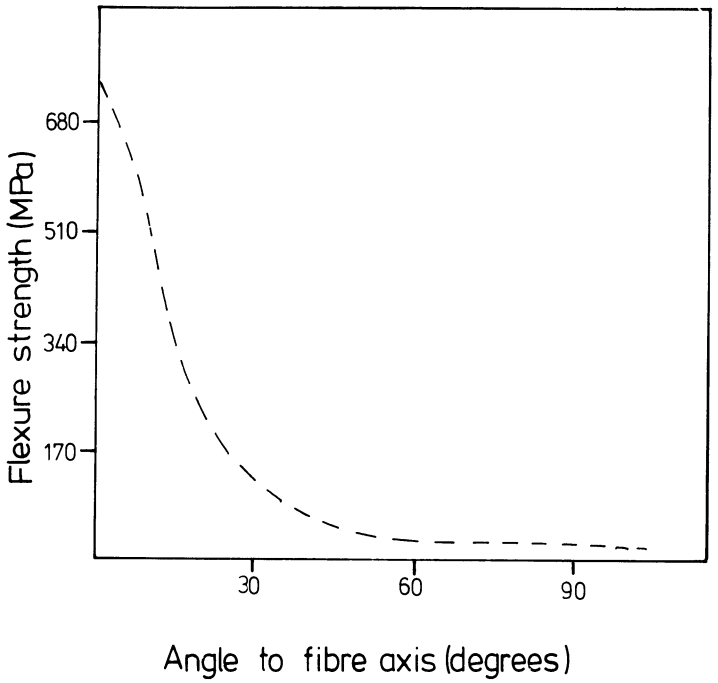

Fig. 8.13 Effect of angle between fibre axis and the load directions on the strength of a carbon–carbon composite.

lower than the values calculated from the rule of mixtures. It is possible to increase the strength of the fibre/matrix interface but, as previously discussed, this manifests itself in extreme brittleness of the composite.

8.4.1 Influence of the fibre microstructure and architecture on mechanical properties

The mechanical properties of carbon–carbon are very much dominated by the properties of the fibres which depend on precursor type and processing conditions (Chapter 2). Microstructural variations in shape, porosity and cross-section can occur within filaments. Variations in fibre architecture on the thermomechanical properties of carbon–carbon are ill-understood, but it is postulated that they may result in a heterogeneous distribution within the composite. Such a distribution may result in understresses in some fibres while overstressing others at adjacent locations [41]. The key factor in optimum fibre utilization is good alignment with respect to the axis of the load [42]. Stress–strain curves in 2- and 3-D composites show reductions in fibre properties and behave non-linearly as a consequence of misalignment [43] due to the 'crimping' which occurs as a result of the weaving process. The fibres are not aligned with the principal stress axis and their effective strengths are thus reduced.

A study has been carried out by Manocha and Bahl [44] on the effect

of fibre type and weave pattern on the mechanical properties of 2-D carbon–carbon. They were able to demonstrate clearly how the choice of reinforcement is paramount to the performance of the composite. The basic properties of the fibre were found to influence the ultimate properties of the composites. The fibre surface affects the fibre/matrix interaction, which in turn adopts a significant role in the densification process.

High modulus fibres are observed to lead to better densified composites than high strength or IM fibres. The weave pattern also contributes to the properties of the 2-D materials. An eight-harness satin weave was found to produce superior composites to those employing a plain weave geometry. The eight-harness weave exhibits fewer 'kinks' in its structure and thus a greater utilization of fibre properties. Furthermore, the kinked plain-weave pattern results in a carbon–carbon composite with heterogeneous matrix pockets.

8.4.2 CVD material

One of the major virtues of carbon–carbon is the non-brittle fracture behaviour exhibited, especially in the case of continuous fibre reinforcement. Schmidt [45] and Cristina [46] have reported a psuedo-plastic failure behaviour under tensile loading. This phenomenon is attributed to matrix cracking and fibre movement to accommodate the applied load. Similar behaviour has been observed under flexural loading [47]. It has been discussed how the fracture behaviour is strongly influenced by the type of interface established between fibre and matrix. The mechanical properties of material formed by the CVD method are strongly influenced by the matrix structure, which in turn depends on the deposition conditions employed. The dependence of the flexural strength of carbon-felt/CVD carbon composites on the matrix has been demonstrated by Pierson and Northrop [48]. A similar result was also observed by Delhaes *et al.* for a carbon-fabric/CVD material [49].

In Chapter 3 it was shown how the structure of the pyrolytic carbon matrix exhibits a systematic variation with changes in the deposition temperature and gas composition. A wide range of structural parameters, such as density and crystallite size, as well as microstructures, is possible. These variations in matrix structure, as one would expect, influence the mechanical properties. The mechanical properties of CVD carbon–carbon composites will be affected by the variations in elastic properties of the matrix which are due to the difference in crystalline perfection and to the presence of defects.

Oh and Lee [50] carried out a series of densification experiments using a reactant gas concentration of 10% propane at temperatures between 1100 and 1440 °C with a carbon fabric. In material processed at 1100 °C, the matrix was observed to be well infiltrated between, and well bonded to, the fibres. By contrast, a great number of pores are observed in

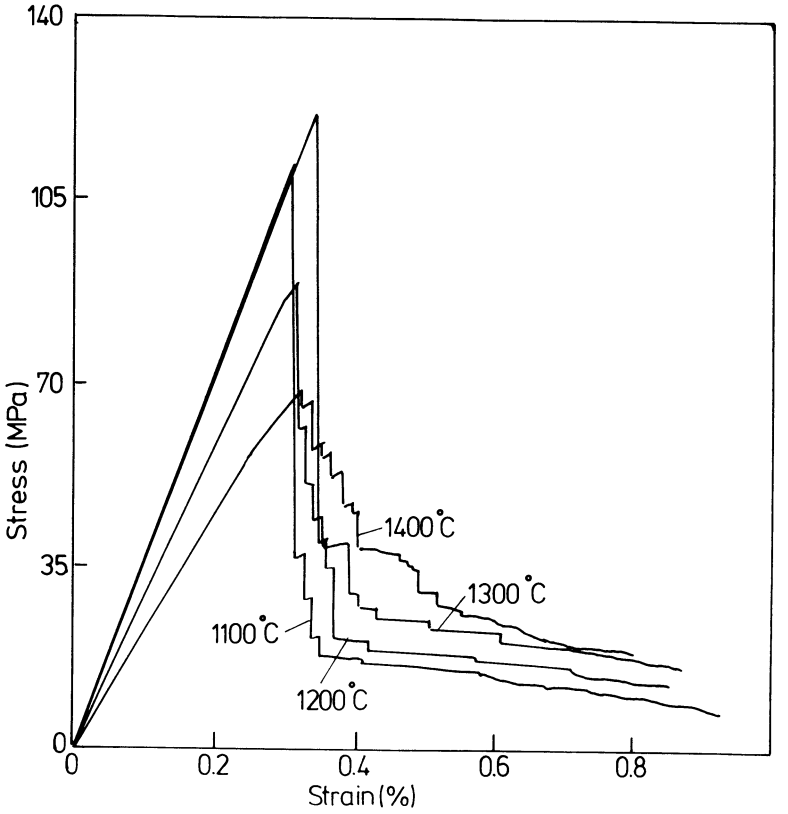

Fig. 8.14 Stress–strain behaviour of CVD carbon–carbon composites prepared from 10% propane at various temperatures [50].

composites made at 1400 °C, the matrix being loosely bound to the fibres. The increased porosity at high temperatures is due to the blockage of the pore channels to reactant gases, which is caused by the deposition of carbon on to the outer fibres before those in the interior are completely infiltrated. The bulk density decreased from 1.79 to 1.37 g cm^{-3} with increasing deposition temperature [51]. This is a consequence of a decrease in matrix density from 1.99 to 1.55 g cm^{-3} and the greater porosity. A decrease in the optical activity is also observed, corresponding to a microstructural change from smooth laminar to isotropic, the arrangement of planar carbon atoms in the matrix being better at lower deposition temperatures [50].

The variation in the stress–strain curves (in flexure) with respect to the deposition temperature is shown in Fig. 8.14 [51]. The stress–strain behaviour of the material deposited at 1100 °C is very linear elastic, representing a near catastrophic failure mode. Increasing the temperature of deposition leads progressively to a stepwise failure behaviour. Both strength and modulus decrease with increasing processing temperature (Fig. 8.15)

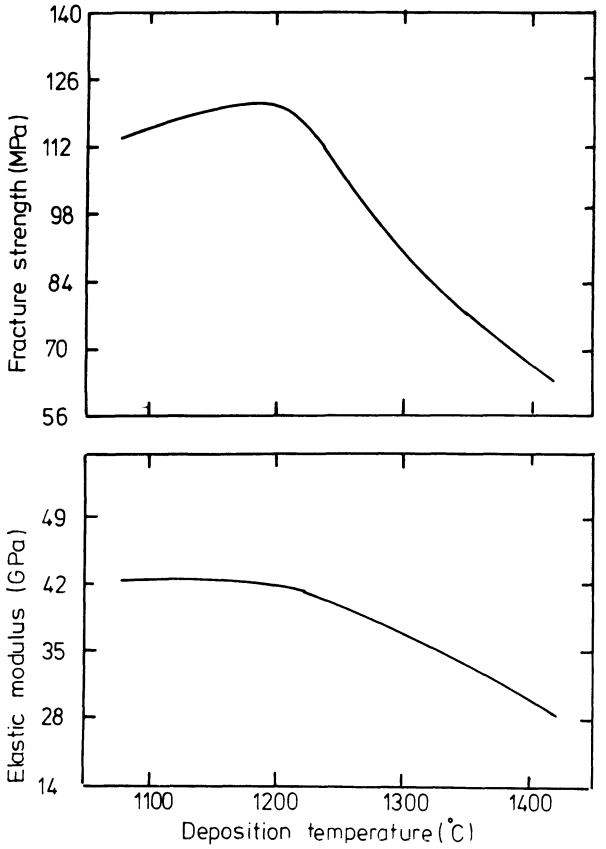

Fig. 8.15 Effect of processing temperature on the mechanical properties of 2-D CVD carbon–carbon using a 10% concentration propane feedstock [50].

due, in part, to the reduced bulk density of the composite and also the increased flow/pore size [52]. The strain to failure, on the other hand, remains almost constant. This observation was made for both fabric and felt reinforcement. The strain to failure of the composite is dominated by that of the matrix, from which one may conclude that the different matrix microstructures have roughly identical failure strains [53].

Microscopical observations on fabric-reinforced material reveal two failure modes: fracture perpendicular to the plane of the reinforcement and delamination. Composites formed at 1100 °C possess a smooth fracture surface with no evidence of fibre pull-out. Material produced at 1400 °C, by contrast, fails predominantly by delamination. Pyrolytic carbon deposited at high temperatures would tend to be more chemically active, having edge atoms with unsaturated C–C bonds as a result of a lower degree of preferred orientation. One would therefore expect a stronger fibre/matrix interface in composites densified at 1400 °C rather than those produced at 1100 °C. Experimental observations, however, reveal the converse to be

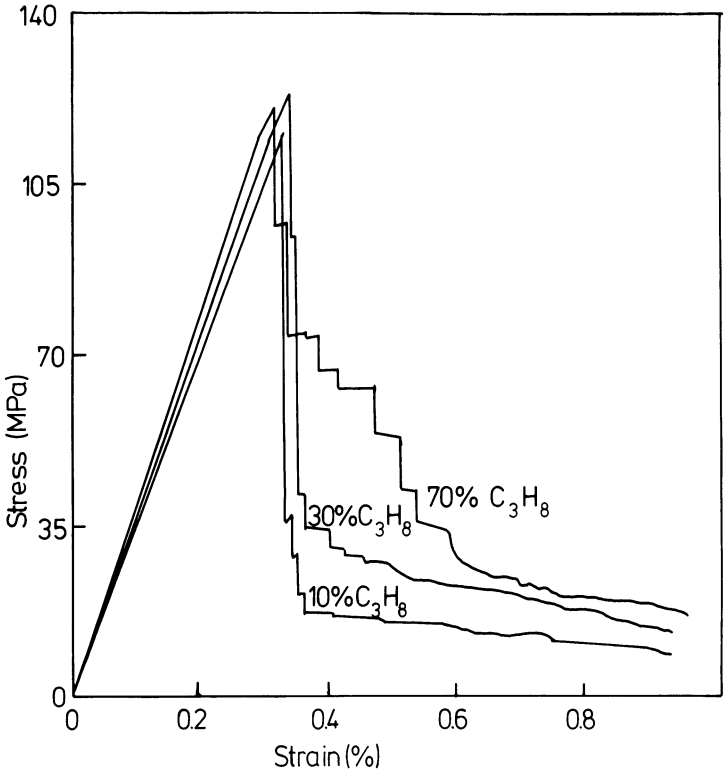

Fig. 8.16 Stress–strain behaviour of CVD carbon–carbon composites with respect to reactant (propane) gas concentration [51].

true. This suggests, then, that the bond between fibres and matrix in CVD composites is one of mechanical interlockings rather than a chemical bond. The strong interface at 1100 °C is most likely due to a compact infiltration of matrix into the pores between fibres. Cracks may propagate through such a microstructure with ease. Fibres may fracture in the primary crack plane, resulting in a catastrophic failure mode devoid of delamination or fibre pull-out. The loosely bound fibre/matrix interface is much less efficient at load transfer but can serve to arrest cracks. Such a material will fail in a stepwise process with fibre pull-out and delamination.

Increasing the concentration of the reactant gas at constant temperature results in an increased optical activity in the microstructure of the carbon–carbon [51]. A higher composite bulk density is observed, caused mainly by the increased matrix density, which in turn results from improved arrangement of planar carbon molecules. Stress–strain curves change from a catastrophic fracture to a stepwise failure with increasing hydrocarbon concentration. The results of Oh and Lee, using propane as the reactant, are shown in Fig. 8.16. The strength and modulus do not, however, vary

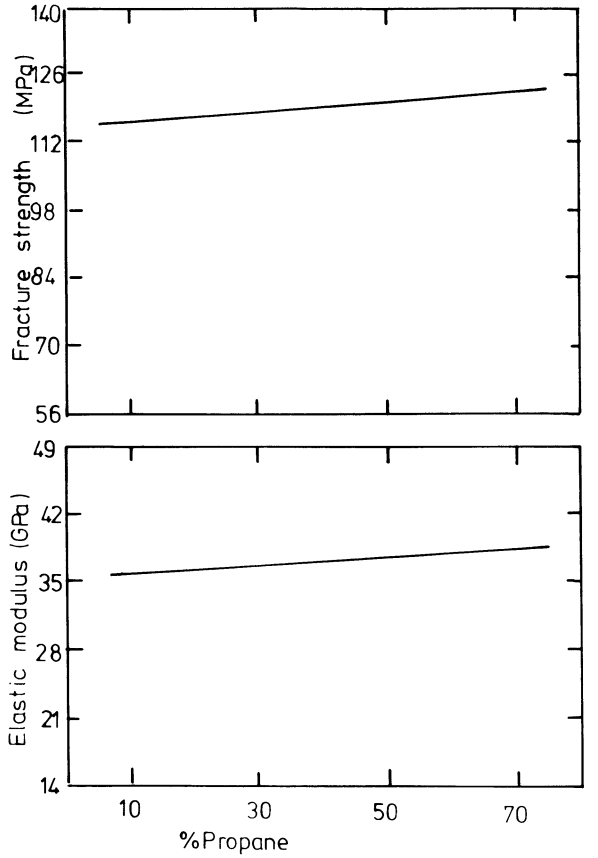

Fig. 8.17 Effect of reactant gas concentration on the mechanical properties of CVD carbon–carbon densified at 1100 °C [51].

significantly but, rather, are slightly increased with increasing reactant concentration (Fig. 8.17). A higher concentration of propane in the system was shown to yield a higher degree of preferred orientation of the matrix with respect to the fibre surface, resulting in a weaker bond between fibre and matrix, and hence a pseudo-plastic fracture behaviour.

To summarize, the lower mechanical properties of an isotropic matrix deposited at higher temperatures are due to its lower density and the formation of closed porosity. A high-density smooth laminar matrix produces composites with high strength and stiffness but brittle fracture behaviour. Rough laminar matrix material shows the highest degree of preferred orientation. It is associated with severe microcracking and has a lower modulus and strength than the smooth laminar structure in spite of their similar densities. Increasing the reactant gas concentration results in a slight improvement in mechanical properties and a pseudo-plastic rather than linear-elastic fracture behaviour. The stepwise failure is believed to

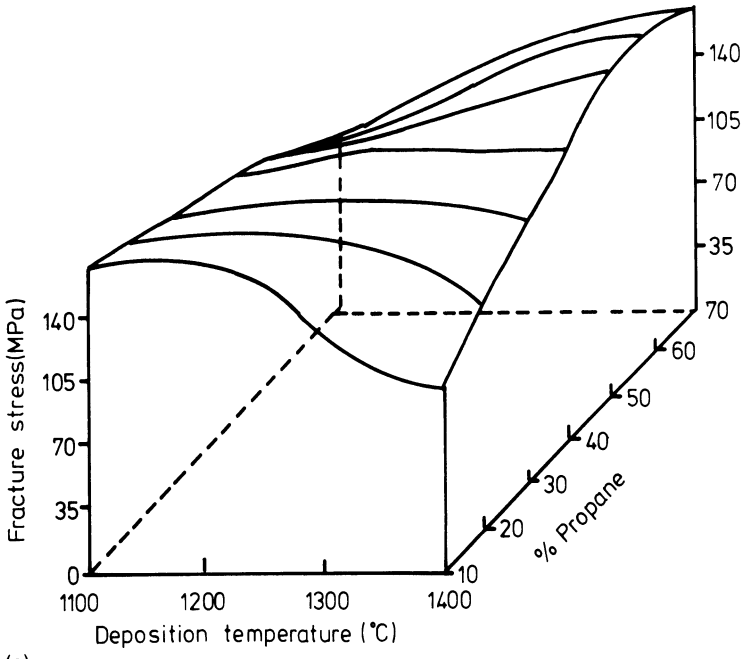
Fracture stress(MPa)
140
105
70
35
0
1100
1200
1300
1400
Deposition temperature (°C)
140
105
70
35
70
60
50
40
30
20
10
% Propane

(a)

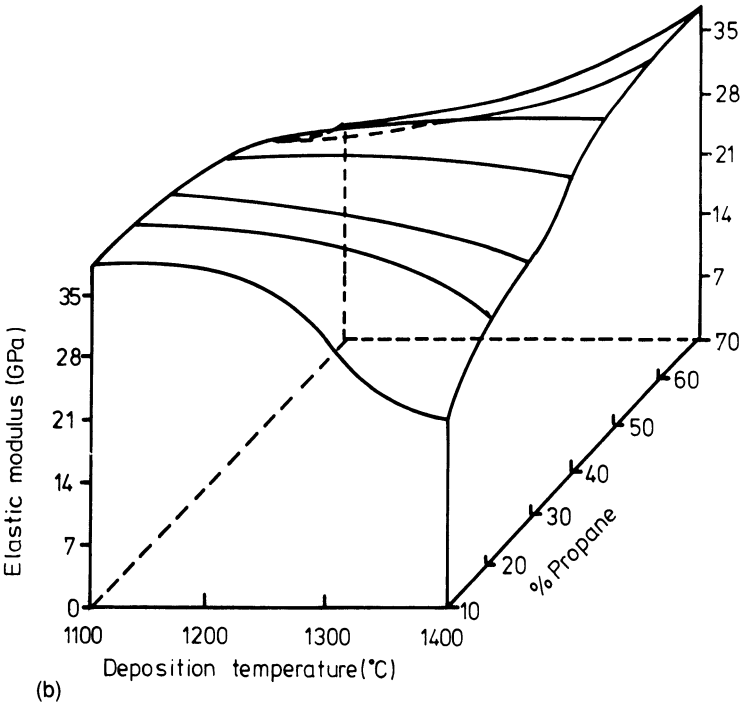
Elastic modulus (GPa)
35
28
21
14
7
0
1100
1200
1300
1400
Deposition temperature(°C)
35
28
21
14
7
70
60
50
40
30
20
10
% Propane

(b)

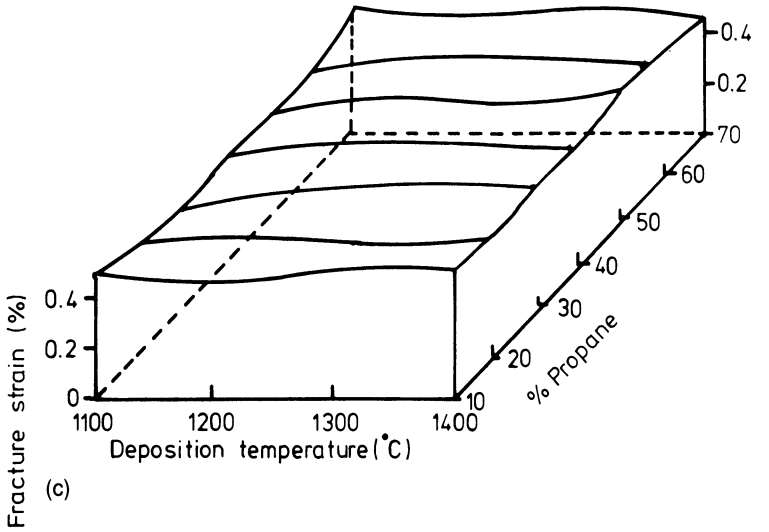

Fig. 8.18 3-D surface plots showing the complex relationships between processing conditions and mechanical properties of CVD carbon–carbon [51].

be due to a loosely bound interface between fibre and matrix. Figure 8.18 shows some 3-D surface plots illustrating the complex relationships between processing conditions and mechanical properties of CVD carbon–carbon.

8.4.3 Thermoset-derived carbon–carbon

The first requirement for a suitable thermoset resin matrix precursor is a high carbon yield which must be achievable under simple pyrolysis conditions. A second requirement is that the shrinkage of the matrix on carbonization should not damage the carbon fibres. Finally, the carbon matrix formed by pyrolysis of the precursor should contain open rather than closed porosity. Only under these preconditions can further improvement of density and mechanical properties be achieved by subsequent impregnation steps. Cross-linked aromatic resins with high molecular weights, such as polyimides, polyphenylene and acetylene-terminated aromatics, achieve a high initial strength after only one carbonization. This is a consequence of a high carbon yield and isotropic shrinkage without damage to the fibre. There is a tendency, however, to form closed porosity such that the mechanical properties achieved after one processing cycle are not significantly improved by further post-impregnation steps.

A second group of matrix precursors, which includes phenolic and furans, forms porous carbon matrices with low composite mechanical strength

after the first carbonization. The high accessible porosity allows strong increases in mechanical properties by repeated impregnation/recarbonization cycles.

The highest mechanical properties are achieved by using HM PAN or mesophase pitch-based fibres, preferably without surface treatment. If not surface treated, HM fibres show very low adhesion to the resin. The bulk cross-sectional shrinkage on pyrolysis is therefore very low. In the case of IM and isotropic fibres, especially those which have been surface treated, the first carbonization causes a bulk shrinkage as a result of good fibre/matrix adhesion. The shrinkage of the resin is resisted by the low compressibility of the fibres. As a result, a high degree of compressive pre-stress is built up in the fibres which reduces the strength of the composite.

The major influence on the mechanical properties of carbon–carbon produced from thermosetting resin precursors is the HTT [54]. At an HTT of below 2000 °C, the strength is low and brittle fracture the predominant failure mode. The matrix so formed is a brittle, isotropic glassy carbon in which propagating cracks readily sever the fibres without changing direction. At HTTs above approximately 2400 °C a graphite component begins to develop at the fibre/matrix interface. An apparent pseudo-plastic, 'ductile' fracture behaviour is the consequence. The strength and modulus increase up to an HTT of around 2750 °C.

Processing at 2800 °C and above tends to reduce the strength due to thermal damage to the fibres [9]. A graphical representation of the effect of HTT on the flexural strength of furan-based composites is shown in Fig. 8.19 [54]. The ductile behaviour of the graphitized composites may be illustrated by considering the energy of fracture [55]. At an HTT of 1000 °C this is measured at 0.3 kJ m^{-2} whereas at 2700 °C it is around 4 kJ m^{-2}, more than an order of magnitude higher.

Exotic high carbon yield resins are seldom used as matrix precursors in commercial operations due to their high cost, limited commercial availability and the formation of closed porosity. The thermosetting resins which are employed generally yield between 50 and 60% by weight of carbon on pyrolysis. A single impregnation carbonization treatment of a 2-D fabric reinforced composite would typically lead to a material with a low bulk density of 1.3–1.4 g cm^{-3}. The impregnation and carbonization thus require to be repeated several times in order to raise the densities to 1.7–1.8 g cm^{-3}. As previously discussed (Chapter 4), the density increase only follows the 1/2 power of the number of impregnation cycles due to blockage of the pores by the impregnant. Above a certain number of times, the density will hardly increase, such that four to six cycles are generally taken to be the optimum. Graphitization results in a shrinkage of the matrix, thus making the porosity more accessible, and is therefore routinely used as an aid to densification.

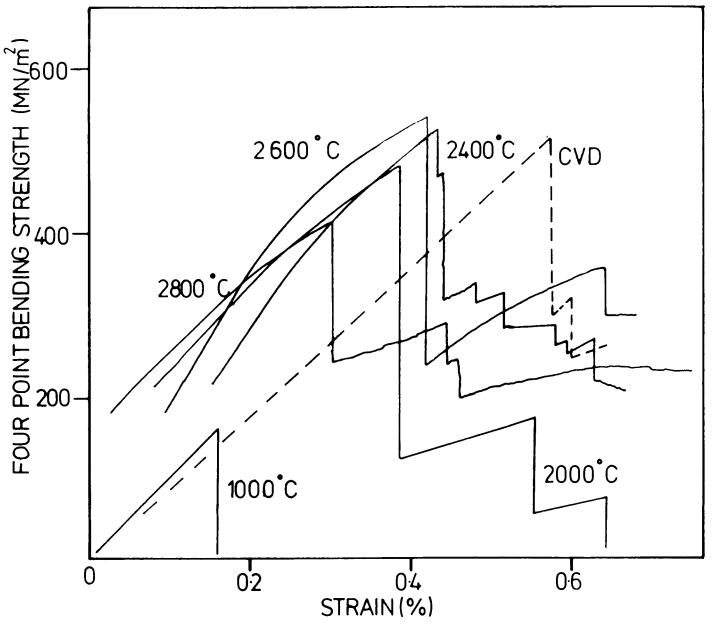

Fig. 8.19 Fracture behaviour of a carbon–carbon composite made from a furan precursor, with respect to HTT.

8.4.4 Mechanical behaviour of carbon–carbon with thermoplastic precursor matrices

The carbon yield of a mesophase pitch is increased from around 35% at ambient pressure to 80% by the application of 100 bar of inert gas pressure [56]. A gas pressure of 1000 bar may effect yields of up to 90% [57]. No systematic results are available in the open literature on the effect of high and ultra high pressures on the final mechanical properties of carbon–carbon. Generally, only an increase in bulk density up to 2 g cm^{-3} and a more rapid approach to 'desirable' mechanical properties is reported [58].

The properties of pitch-based carbon–carbon are not only controlled by the carbon yield of the matrix precursor, but also by the microstructure. Pitch carbonized under relatively low pressures results in a well graphitizable matrix carbon with a sheath structure parallel to the fibre surface and thus in anisotropic matrix properties [59]. A transverse oriented (TO) matrix structure has been observed when high pressures (≈1000 bar) have been applied during carbonization [60]. Such TO structures tend to produce a more isotropic matrix as is found in some CVD material. Preferred orientation of the carbon matrix has a significant influence on the mechanical bulk properties of the composite. This preferred orientation can be influenced by the heating rate during carbonization and the addition of

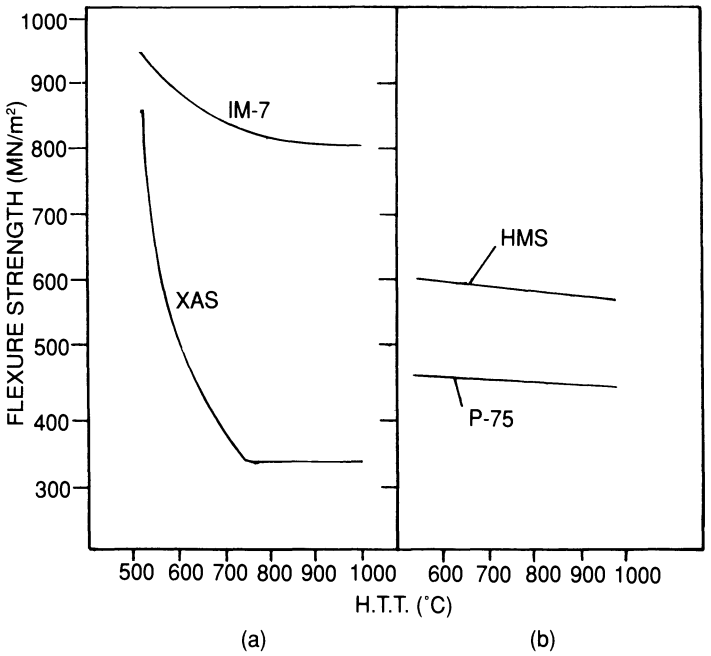

Fig. 8.20 Effect of HTT on the strength of pitch matrix carbon–carbon composites: (a) IM fibres; (b) HM fibres.

cross-linking agents such as sulphur to improve carbon yield. In the best cases (low heating rates ≈20 °C h^{-1} and no sulphur additions), complete matrix orientation parallel with the fibre surfaces results in a strong contribution of the matrix to the composite's modulus of the order of that of the fibres.

A carbon–carbon composite with a pitch-based matrix shows a pseudo-plastic fracture behaviour but the strength shows the reverse pattern of dependence on processing temperature to resin-based materials. Strength is observed to fall as the HTT is increased [61]. Figure 8.20 shows a typical strength/HTT relationship for pitch matrix composites with both IM and HM fibres. Figure 8.21 shows the increase in flexural strength and bulk density achieved as a function of the densification cycles for composites prepared from pitch [62]. As a general rule of thumb, four densification cycles generally increase the flexural strength of a pitch-based carbon–carbon composite by a factor of three to four times. A similar result is observed in thermoset-derived material [63]. A flexural strength of around 1000 MPa can be achieved after four impregnation/carbonization cycles. Four impregnation/graphitization cycles yield a strength of 700 MPa.

Microscopy shows that cracks between fibre and matrix and within the matrix are present in fully densified composites. The extent of matrix and interfacial cracking depends on the increasing anisotropy of the matrix

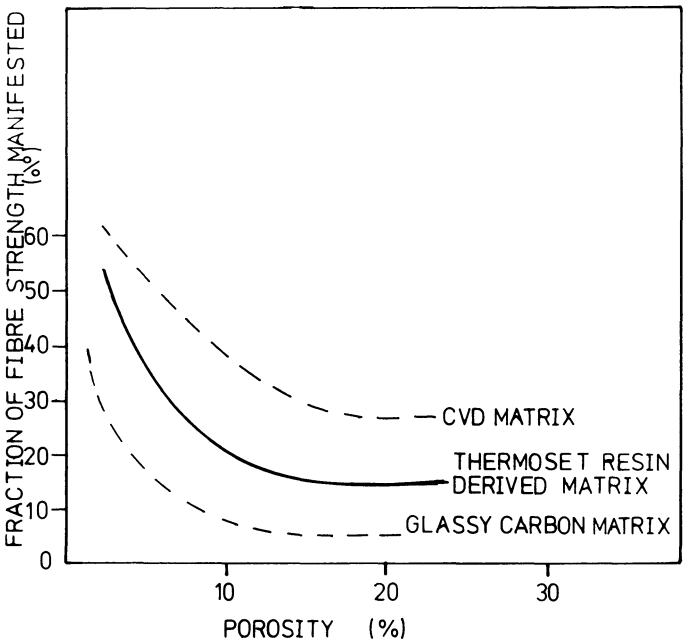

Fig. 8.21 The percentage of fibre strength manifested according to the percentage of open porosity in a carbon–carbon composite [66].

microstructure. In the case of a high degree of anisotropy, thermal contraction during cooling from the graphitization temperature matches that of the fibres and the oriented matrix. The shrinkage stresses resulting from a more isotropic matrix, on the other hand, cause crack formation. The bonding between fibre and matrix is very weak. This mechanical interlocking can be improved by repeated impregnation. Repeated graphitization cycles increase the size of the lens-shaped porosity between fibres and matrix. Graphitization thus aids densification but at the price of a lower 'ultimate' composite strength.

Recent studies by the author and co-workers [64] have concentrated on the production of carbon–carbon from high carbon yield thermoplastic resin precursors such as PEEK. Flexural strengths of close on 1000 MPa were obtained from a single carbonization cycle (IM fibre reinforcement). That is to say, the mechanical properties of the thermoplastic-based systems were equal or superior to those obtained from thermoset materials after four cycles. The thermoplastic precursor systems may well be viable as structural materials since their high raw materials costs are offset by lower processing costs. Of special interest are the composites made using ultra-high modulus pitch-based fibres. An optimum bond strength between fibres and matrix produced a flexural strength close to that of the polymer system whence it was derived, while an improved modulus was obtained due

Table 8.1 Mechanical properties of carbon–carbon derived from thermoplastics compared with those of their precursors

Property	*AS4/PEEK*	*P75/PEEK*	*AS4/PEEK (carbonized)*	*P75/PEEK (carbonized)*
Flexural strength (MPa)	1800	728	900	600
Flexural modulus (GPa)	150	280	190	300
Transverse flexural strength (MPa)	137	51.8	10	16

to the contribution of the matrix. A summary of the properties of the thermoplastic-based materials is given in Table 8.1 Ultra-high modulus materials of this type may well have a market niche in space structures which are lightly loaded, stiffness-critical and where high premiums are paid to save weight.

8.4.5 Porosity

One of the major factors determining the strength of carbon–carbon is the density of the material. The density may be considered as a description of the composites' porosity or void content. The strength of a ceramic material may be expressed in terms of its porosity by a simple empirical formula [65]:

$$\sigma = \sigma_0 \, e^{-BP} \tag{8.3}$$

where σ_0 is the strength of the material with zero porosity, B a constant and P the porosity.

A similar relationship has been observed in carbon–carbon composites as illustrated in Fig. 8.21 [66]. The upper curve shows a CVD material, the central curve a graphitized thermoset and the lower curve a carbonized thermoset with a glassy matrix. The change in strength due to differences in the type of matrix is thus clearly demonstrated. In flexural testing, cracks develop from the outer, tensile surface. In other words, the open pore content governs the strength, whereas in a tensile test a uniform stress field is generated such that the overall porosity will be the important factor. Microscopy shows that, even after four or more densification cycles, the composites still contain a large degree of porosity. Despite the inefficiency of the reimpregnation process, large increases in strength are obtained. This can be explained in part by a reduction in the porosity, but also because the reimpregnation tends to smooth the geometry and reduce the size of the voids thus lessening stress concentration.

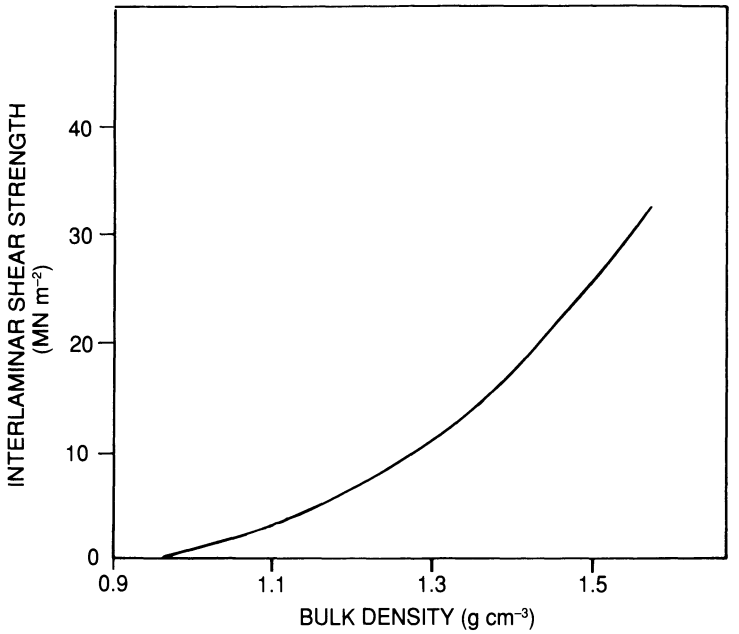

Fig. 8.22 Effect of increased composite density on the interlaminar shear strength of a pitch-based carbon–carbon composite [56].

8.4.6 Compression and shear properties

There are very few instances in which a carbon–carbon composite is used as a compression member [67]. The property which controls the compressive response is the interlaminar shear strength. The relationship between density and ILS of a pitch-based composite is shown in Fig. 8.22 [56]. The interlaminar shear strength increases with density in the same way as the flexural and tensile strengths. There is, however, an ultimate value of ILS of approximately 30 MPa. It is clear then that the shear strength of the matrix governs the shear strength of the composite. The same is true for a CVD-type matrix.

8.4.7 Effect of heat treatment temperature on the modulus of carbon–carbon

The modulus, like the strength of carbon–carbon, is dependent on the matrix type and HTT. Consider, for example, a UD material fabricated from a thermoset precursor as shown in Fig. 8.23. Increase in HTT causes a rapid increase in the modulus in the fibre axial direction. The specific modulus, along that axis, may reach a value three times that of steel for an HTT of ≈2800 °C [68]. In contrast, the modulus perpendicular to the fibre axis falls, albeit not so sharply as the increase in the parallel direction,

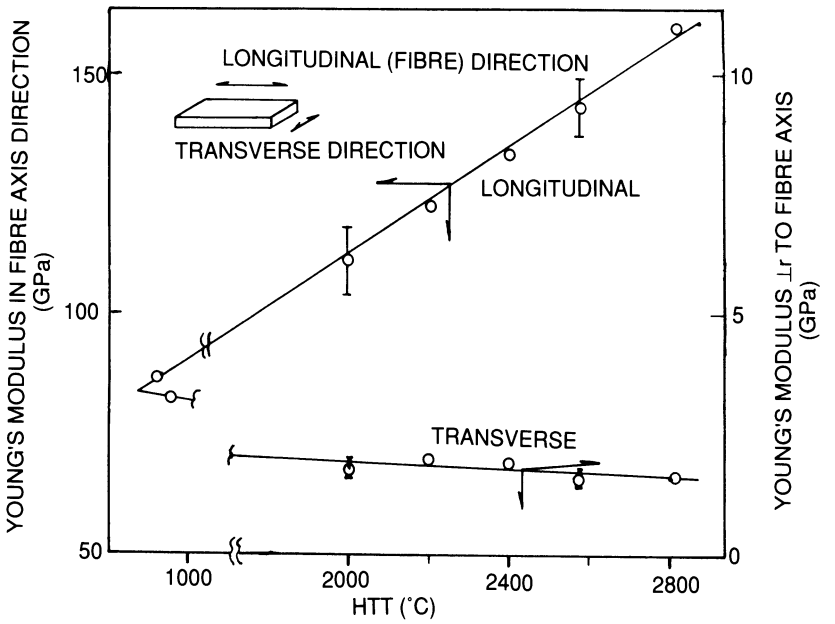

Fig. 8.23 Relationship between Young's modulus and HTT for a UD carbon fibre thermoset (furan) composite [68].

with increased HTT. These effects are due to the morphological changes in the matrix, the development of graphite crystallites and increase in the degree of preferred orientation.

8.4.8 Mechanical properties at high temperatures

One of the major assets of a carbon–carbon composite is that of retention of mechanical properties at high temperatures, as shown in Fig. 8.24 [69,70]. It can be seen from Fig. 8.24 that up to 1500 °C, there is a 10–20% increase in strength and modulus compared to ambient temperatures.

8.4.9 Fatigue properties

Very little work is presented in the open literature concerning the fatigue performance of carbon–carbon. Fitzer and Heym [71] showed a lifetime of 10^7 cycles at a stress of 40% of the static bending strength (Fig. 8.25). A Woeler diagram presented in the literature of Schunk [72] suggests the material shows a fatigue limit analogous to that of steel. An infinite fatigue life is predicted at 45–50% of the static strength (Fig. 8.26) under a cyclic, sinusoidal loading. The fatigue endurance properties of carbon–carbon appear, therefore, to be outstanding.

A question arises, however, as to whether the pore opening and closing

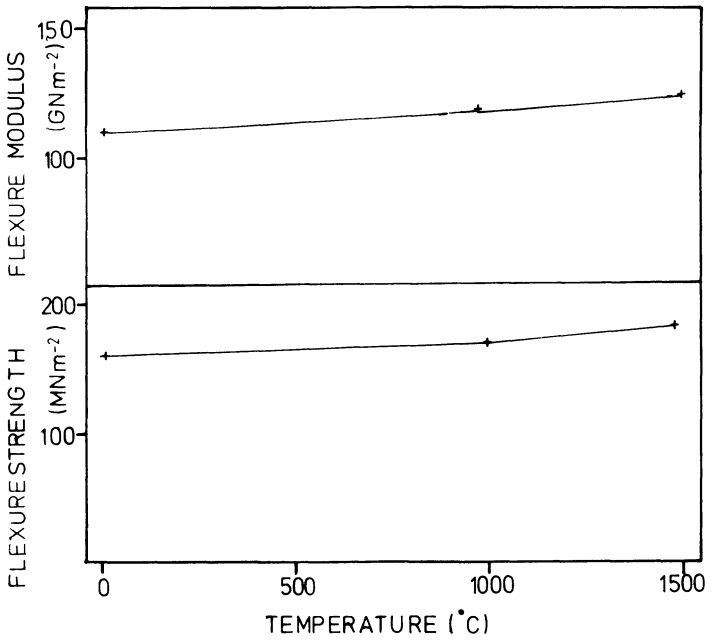

Fig. 8.24 Change in flexure strength and modulus of a carbon–carbon composite made from a thermoset precursor with respect to operating temperature [69].

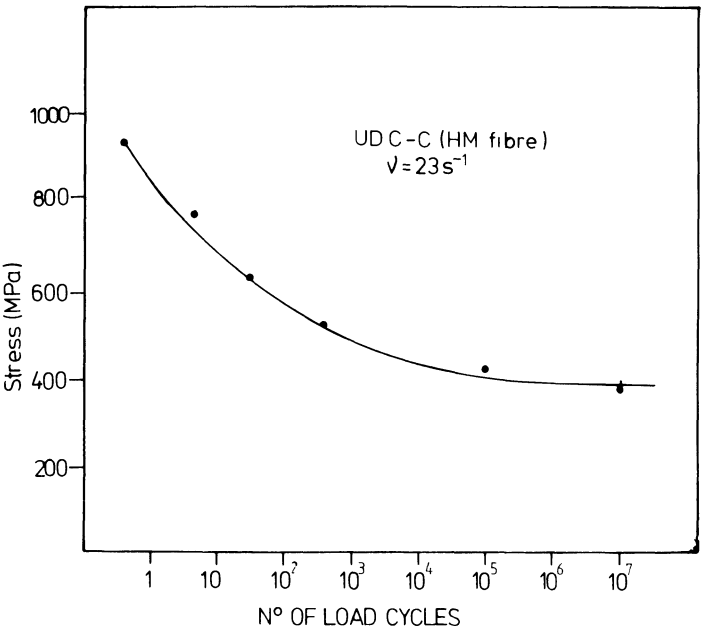

Fig. 8.25 Fatigue curve for a carbon–carbon composite [71].

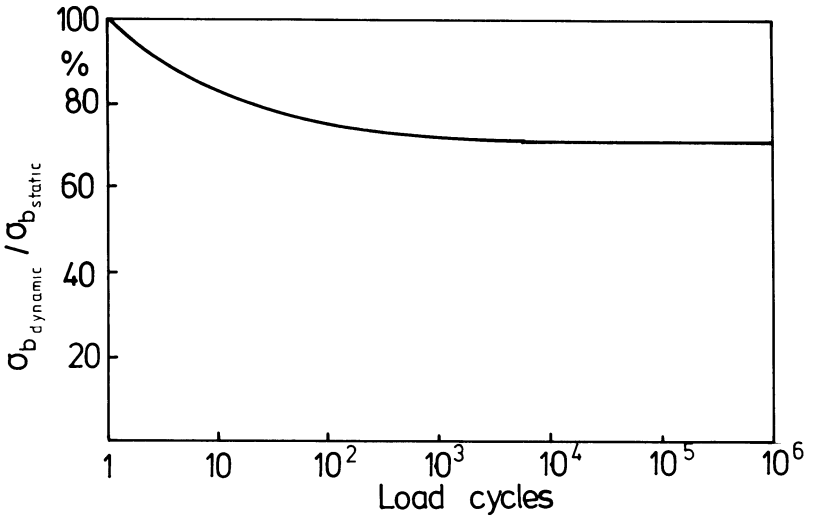

Fig. 8.26 Fatigue behaviour of carbon–carbon composites under alternating flexural load, suggesting a 'fatigue limit' as observed in ferrous metals.

mechanism, which must occur under fatigue loading, will continue indefinitely. The pore volume is increased during long time cycling. A probability exists that in local regions, the fracture strength of the matrix will be exceeded. The result will be the fracturing of the matrix in those areas and its loss as dust from the composite. This phenomenon, for obvious reasons, is known as 'dusting-out'. Dusting-out has been observed at high temperatures (≈1400 °C) in centrifugal loading operations (fan blades). There is therefore a severe limitation on the long time application of carbon–carbon under high alternating stresses.

8.4.10 Fracture toughness

Materials such as carbon–carbon which have internal flaws or voids as a consequence of fabrication processes must be evaluated for fracture toughness prior to consideration for a specific application. The toughness is interpreted as the ability of a material to resist crack propagation from existing voids. Very few data have been reported to date on the fracture toughness of carbon–carbon, due in the main to the difficulty in making accurate and meaningful measurements.

The various fracture toughness parameters are found to depend strongly on the type of carbon fibre used and the orientation of the initial crack with respect to the fibre reinforcement structure. In a two-dimensional, fabric-reinforced composite severe crack blunting and delamination are observed when crack propagation is perpendicular to the fibres [73]. K_{Ic}

values of around 7.6 MN $m^{-3/2}$ have been calculated in this orientation [63,68]. Such results are, however, invalid since linear elastic fracture mechanics is not applicable to pseudo-plastic failure. When crack propagation occurs collinear with the initial crack, such as between the layers of a 2-D material, fracture toughness parameters can be measured – 1- and 2-D laminates are particularly susceptible to this mode of failure. The interlaminar fracture toughness of a phenolic-derived material was found to be of the order of 0.11 kJ m^{-2}. This value is very low, around half that measured for even the most brittle epoxy composites [63]. The extremely brittle nature of the matrix and the presence of voids and shrinkage cracks may result in failure of components during processing. Cracks, etc. formed during the first pyrolysis cycle may grow as a result of thermal loading of subsequent cycles such that the materials are extremely unpredictable. A 2-D composite may thus fail by delamination without warning during the processing.

The interlaminar fracture toughness of 2-D ex-thermoset carbon–carbon may be increased by more than a factor of 2 by the introduction of a dispersed, third phase of particulate graphite. The graphite reduces the shrinkage of the matrix during carbonization, while increasing the G_{Ic} by a crack deflection and blunting mechanism. Optimization of filler content and particle size have resulted in G_{Ic}, values as high as 0.25 kJ m^{-2} being measured [63]. From a practical standpoint, 2-D composites containing graphite fillers were less prone to delamination during processing (in fact, in laboratory preparation this type of failure was totally eliminated) and easier to machine when finished.

As shown in Fig. 8.27, three-dimensional reinforcement leads to a pseudo-plastic fracture behaviour. The formation of stepwise cracks, as seen in the stress–strain diagram, results from a high degree of fibre pull-out during fracture and makes for an exceptionally tough material [72].

8.5 THERMAL PROPERTIES

Next to mechanical properties, the most important characteristics of a carbon–carbon composite are thermal conduction and thermal expansion. The number of papers in the literature relating to these is only exceeded by those on mechanical properties.

8.5.1 Thermal conductivity

Theory of thermal conductivity

Two mechanisms exist for thermal conduction in a solid; the first is via electron charge cloud drift (cf. electrical conductivity) and the second is

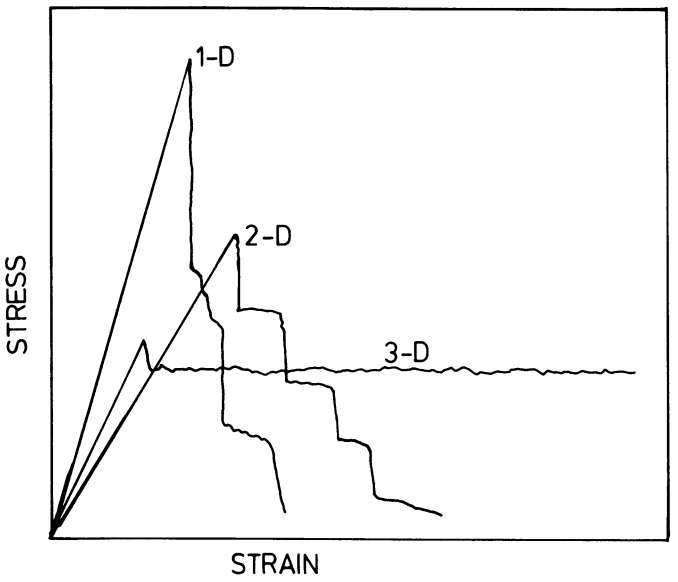

Fig. 8.27 Stress–strain behaviour of carbon–carbon showing increased 'pseudo-plasticity' with dimensions of reinforcement.

by lattice vibrations, known as phonons. The relative contributions from these two mechanisms have great implications for both the size and temperature dependence of thermal conductivity. The method for assessing the relative contributions of electronic and phonon mechanisms of thermal conductivity is by calculation of the Wiedmann–Franz ratio as a function of temperature [74]:

Wiedmann–Franz ratio

$$= \frac{\text{Thermal conductivity} \times \text{electrical resistivity}}{\text{Temperature}} (\text{in } \text{V}^2\,\text{K}^{-2}). \qquad (8.4)$$

A thermal conductivity dominated predominantly by the electronic component is signified by a near-constant Wiedmann–Franz ratio. Carbon-based materials have wildly varying Wiedmann–Franz ratios, indicative of a phonon-based thermal conductivity mechanism. The phonon mechanism is believed to be responsible for 99% of the thermal conductivity [75].

The thermal conductivity of a phonon-dominated material can be described by the Debye equation [76]:

$$K = bCvl, \qquad (8.5)$$

where K is the thermal conductivity, b a constant, C the specific heat per unit volume, v the phonon velocity and l the mean free path of phonons.

Phonons are scattered by two mechanisms; collision with other phonons

and collision with lattice defects, crystal boundaries or pores. The two contributions to phonon scattering can thus be expressed as

$$\frac{1}{l} = \frac{1}{l_e} + \frac{1}{l_d}, \tag{8.6}$$

where l is the mean free path of phonons, l_e the phonon–phonon scattering path length and l_d the spacing of inhomogeneities, defects grain boundaries, etc.

The diversity of different carbon structures gives rise to very different contributions from the two phonon-scattering mechanisms. For highly crystalline materials, such as natural graphite, there are few defects and grain boundaries, so the contribution from l_d is relatively small. Two factors influence the temperature dependence of the thermal conductivity of these highly crystalline materials. The phonon–phonon scattering path length, l_e, which dominates the overall phonon scattering, is inversely proportional to temperature. From intermediate to high temperatures, the thermal conductivity thus tends to decrease. At low temperatures, on the other hand, the specific heat rapidly decreases to zero despite an increase in the phonon–phonon scattering path length which aids thermal conduction. For less crystalline carbon materials inhomogeneity-induced phonon scattering is much more important than simple phonon–phonon scattering. This manifests itself in the relative temperature invariance of thermal conductivity, as shown in Fig. 8.28 [77].

Thermal conductivity in carbon–carbon composites

Carbon–carbon composites present the opportunity to 'tailor' thermophysical properties into carbon materials. The complexity of possible options can be gauged by brief consideration of the different fibre/matrix/processing permutations possible:

1. fibres – rayon, PAN, isotropic and mesophase pitch (plus variations in heat treatment);
2. matrix – Thermoset pyrolysis, CVD and thermoplastic/pitch pyrolysis;
3. fibre architecture – Felt, UD, fabrics and 3-D structures.

With such a range of options, a very wide range of thermal conductivities is possible.

CVD matrices

As previously discussed, a range of different carbon microstructures is possible from the CVD process, each of which has considerable influence over the thermomechanical properties of the composite. Liebermann and Pierson at the Sandia Laboratories have made several investigations into

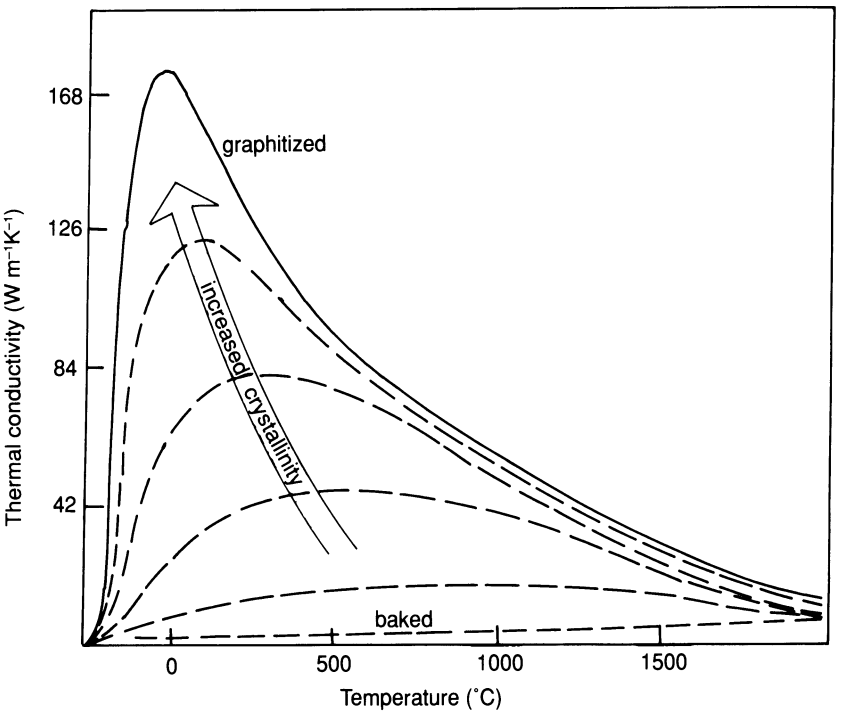

Fig. 8.28 The temperature dependence of thermal conductivity for crystalline and non-crystalline carbon material [77].

the CVD process/property relationships for different carbon–carbon composite materials [78]. Using a thermal gradient infiltration technique, they prepared a range of composites, based on a 0.1 g cm^{-3} felt preform, from CH_4/H_2 at 1250–1700 °C. Each composite was then given a final heat treatment at 3000 °C. The low density/volume fraction of the fibre preform allowed the assumption that the thermal conductivity property of the composite were matrix dominated.

The correlation of matrix microstructure with the thermophysical properties is relatively straightforward, as shown in Table 8.2. The rough laminar microstructure is clearly a good deal more 'graphitizable' than the smooth laminar and isotropic microstructures, and thus exhibits the highest thermal conductivity. A whole range of other studies validate Liebermann's theories on CVD matrix microstructure/property relationships. Curlee and Liebermann reported the thermal conductivity values for a filament-wound, CVD-densified tube where either CH_4 or C_6H_6 was used as the hydrocarbon feedstock [79]. While both matrices possessed the same smooth laminar microstructure, the composites prepared from benzene were found to have 80–120% higher thermal conductivity than the methane-derived matrix samples. This is again attributable to the

Table 8.2 CVD matrix microstructure/thermal conductivity relationships

Matrix microstructure	*Crystallite size* (Å)	*Thermal conductivity at 350 °C* (W m^{-1} K^{-1})
Smooth laminar	125	25
Rough laminar	385	96
Isotropic	90	25

relative graphitizability of the matrix. Curlee and Northrop prepared CVD-impregnated, filament-wound hoops from CH_4/H_2 mixtures at identifiable temperatures and pressures but with a different C/H feed ratio [80]. They produced both laminar and isotropic matrix microstructures. The laminar matrix material was found to possess roughly twice as great a value of thermal conductivity as the isotropic matrix composite (54 versus 22 W m^{-1} K^{-1} at 350 °C).

Thermoset-derived glassy carbon matrices

In these carbon–carbon systems, the fibres will dominate the thermal conductivity of the composite due to the fundamentally low thermal conductivity of glassy carbon. Fitzer and Heym [71] prepared UD composites from HM fibres and a phenolic precursor. Three reimpregnation–carbonization–graphitization cycles resulted in composites having a thermal conductivity of 40 W m^{-1} K^{-1} (at room temperature) parallel to the fibres and 3 W m^{-1} K^{-1} in the perpendicular direction. Their results were consistent with a 'rule of mixtures' basis, albeit a little on the low side. The surprisingly low transverse thermal conductivity probably results from the presence of porosity which will reduce the thermal conductivity.

McAllister and Lachmann have presented a range of thermal conductivity data for different carbon–carbon materials [81]. A lack of clear information on processing makes it difficult to discern, however, which factors influence the thermal conductivity. They present data for an early 3-D composite, based upon a 2-D graphitized rayon fabric pierced with HM PAN-derived fibres (T-50). The pseudo-3-D fibre structure was processed using repeated phenolic impregnation/pyrolysis/graphitization cycles to a final density of 1.65 g cm^{-3}. Thermal conductivity for this material is presented in Table 8.3 along with comparable data for a related Avco material called MOD-3 [82].

The Avco material was based on an unspecified woven carbon yarn and phenolic resin densified to approximately 1.6 g cm^{-3}. The two materials have almost identical thermal conductivities. Both materials show a relatively isotropic thermal conductivity when compared with the Fitzer/Heym UD

Table 8.3 Thermal conductivity of 3-D phenolic derived carbon–carbon materials

Thermal conductivity ($W\ m^{-1}\ K^{-1}$)	*McAllister–Lachmann*		*Avco*	*MOD-3*
	X–Y-plane	*Z-direction*	*X–Y*	*Z*
At 250 °C	830	55.4	83.0	55.3
At 2500 °C	27.7	24.5	29.4	24.2

material, a consequence of the 3-D fibre array. The authors of the Avco paper, however, point out that the thermal conductivities of these 3-D carbon–carbons are considerably lower than that of a premium grade aerospace graphite, such as the ATS grade.

Two conflicting reports have been published on the thermal conductivity of 2-D phenolic-derived carbon–carbon materials. Laramee *et al.* [83] (from Morton Thiokol) describe the thermophysical properties of 2-D carbon–carbon, from T-50 PAN fabric and phenolic processed to a density of 1.5 g cm^{-3}, proposed as a candidate material for rocket nozzle construction. In-plane conductivities in the range of 93 W m^{-1} K^{-1} (800 °C) were reported.

The high thermal conductivity value perpendicular to the ply direction – in comparison with Fitzer's previously discussed value of 3 W m^{-1} K^{-1} for transverse conductivity – seems a bit surprising. Curry, *et al.* have presented thermal conductivity data for the structural carbon–carbon used for the leading edge parts of the space shuttle [84]. The material is based on plain weave graphitized fabric/phenolic with three subsequent furan reimpregnation–pyrolysis steps, and then given a final SiC–$Si0_2$ oxidation protection coating. The thermal conductivity values quoted for this material are extremely low. At room temperature, the values are 5 W m^{-1} K^{-1} parallel to the plies and 3 W m^{-1} K^{-1} perpendicular. Oddly, the values of conductivity rise as the temperature increases, up to 14.5 and 6 W m^{-1} K^{-1} (parallel and perpendicular) at 1650 °C. This is very different behaviour from the other thermoset-derived carbon–carbons and leads one to question how much influence the SiC/$Si0_2$ coating plays on the thermal conductivity values.

Pitch-derived carbon matrices

Pitch-derived carbon matrix–carbon fibre composites are generally processed via the HIPIC technique (hot isostatic pressure impregnation and carbonization) of pitch into a dry carbon fibre preform. Repeated HIPIC cycles are required to build the composite matrix up to an acceptably high density/low porosity for deployment in severe ablative environments. Two sets of thermal conductivity data have been published on 3-D HIPIC-processed composites.

Table 8.4 Thermal conductivity of HIPIC-processed 3-D carbon–carbon materials

Thermal conductivity ($W\ m^{-1}\ K^{-1}$)	*Battelle 3-D carbon–carbon*		*Morton Thiokol 3-D carbon–carbon*	
	X–Y	*Z*	*X*	*Y*
At 30 °C	149	246	202	171
At 800 °C	—	—	91	80
At 1600 °C	44	60	—	—

Workers at the Battelle Institute [81] (the originators of the HIP process) fabricated a 3-D weave from T-50 fibre, with a 2–2–6 fibre distribution (*X–Y–Z*), and then used four HIPIC cycles with a coal-tar pitch impregnant to produce a composite of density 1.9 g cm^{-3}. The other documented 3-D composite is a body optimized for ring strength – a 9–2–9 *X–Y–Z* preform based on T-50 PAN fibre, HIPIC processed to a density of 1.9 g cm^{-3}; this material was described by workers at Morton Thiokol [83]. The thermal conductivity data are presented in Table 8.4.

The values are higher than those shown in Table 8.3 for phenolic-derived materials of similar fibre architecture. They reflect the more graphitic, thermally conducting nature of the HIPIC-derived matrix. It is worth noting, however, that the thermal conductivity of these materials is, at best, only a marginal improvement on those displayed by conventional synthetic graphites, despite their far superior mechanical properties.

Effect of heat treatment temperatures on thermal conductivity

Figure 8.29 shows the relation between the thermal conductivity and the HTT of a carbon–carbon composite where a thermosetting resin was used a the resin precursor, and Fig. 8.30 the relationship between HTT and L_a. High temperature treated composites based on pitch or on a thermosetting resin will have a high thermal conductivity [86].

Thermal conductivity at high temperatures

There are a number of reports in the literature concerning the high-temperature thermal conductivity of carbon–carbon [87,88]. Figure 8.31 shows the relationship between the measurement temperature and the thermal conductivity of a CVD-type composite material [87]. As the temperature is increased, so is the amount of phonon scatter due to vibration of the crystal lattice, and the thermal conductivity falls [89].

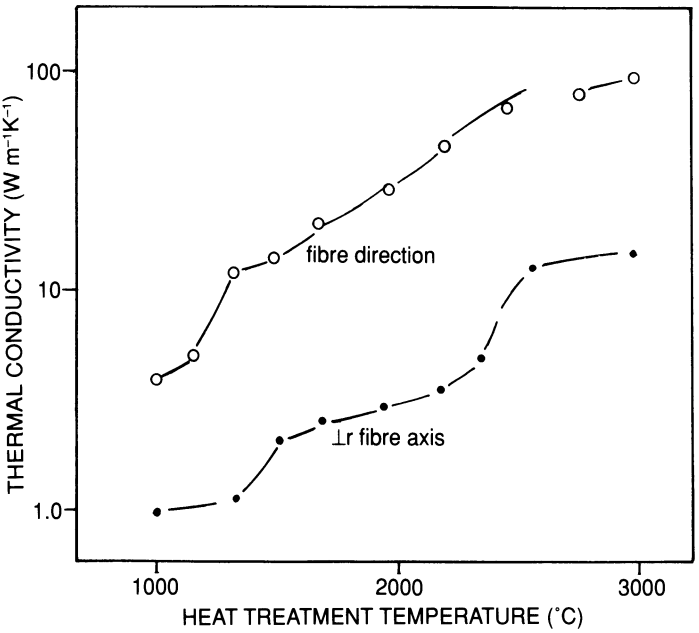

Fig. 8.29 Relationship between thermal conductivity and HTT for a thermoset resin derived composite [85].

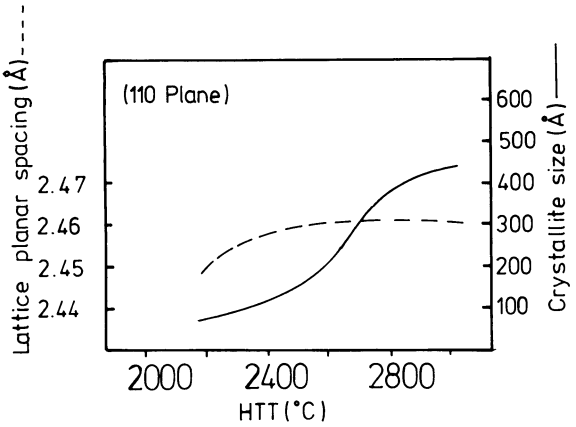

Fig. 8.30 Relation between X-ray pattern and the HTT for a furan resin matrix carbon–carbon composite [85].

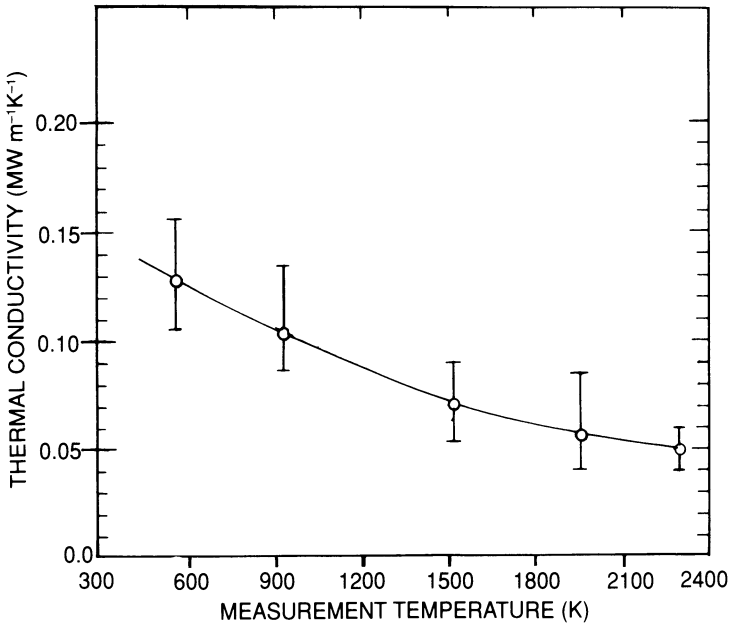

Fig. 8.31 High-temperature thermal conductivity of a CVD carbon–carbon material [87].

8.5.2 Thermal expansion

Thermal expansion is an important property when using materials at high temperatures. The thermal expansion in the fibre axis direction is chiefly governed by the thermal expansion of the fibre. That is to say, thermal expansion of a composite material in which a highly oriented PAN fibre is used resembles the expansion behaviour in the planar direction of graphite Fig. 8.32 [87,88].

8.6 ELECTROMAGNETIC PROPERTIES

When a thermoset-based carbon–carbon is heat treated to above 2800 °C, three-dimensional crystallite growth takes place such that L_{112} becomes very large. The electrical conductivity, as shown in Fig. 8.33, increases correspondingly [85]. The development of a three-dimensional structure is seldom, if ever, observed in carbon fibres. The electrical conductivity of a carbon–carbon composite is primarily governed by the density and the matrix microstructure, including porosity.

Magneto-resistance measurements have been used to investigate the graphitization process [90,91]. Tanaka *et al.*, [90] for example, report that the magneto-resistance of thermoset-derived composites changes from negative to positive values above an HTT of ≈2400 °C. The activation

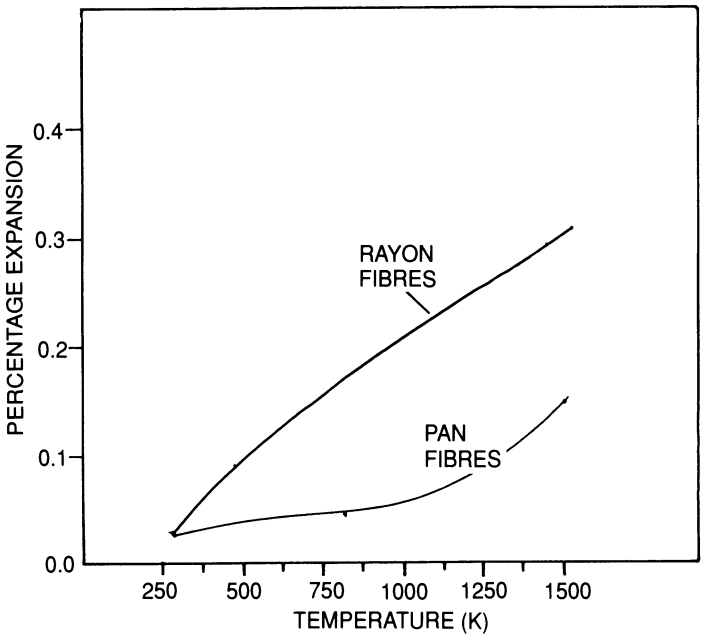

Fig. 8.32 Thermal expansion of a CVD carbon–carbon [87].

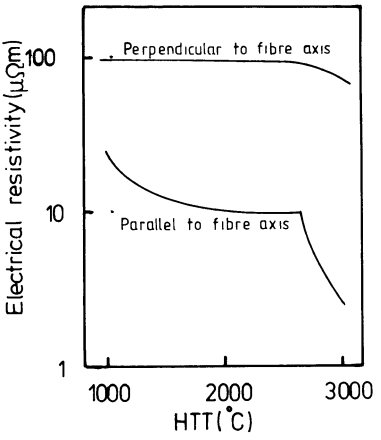

Fig. 8.33 Relationship between electrical resistance and HTT for a thermoset resin carbon–carbon [85].

energy obtained from the dependence on temperature was of the order of 1000 kJ mol^{-1}. They thus concluded that the rate-determining step in the graphitization of the matrix is the healing of defects. The three types of CVD microstructure show different magneto-resistances, especially following high-temperature heat treatment. It is shown that the rough laminar type is close to being a readily graphitized carbon [91].

REFERENCES

1. Liebermann, M. L. and Pierson, H. O. (1973) *Ext. Abst. 11th Biennial Conf. on Carbon*, p. 314.
2. Kotlensky, W. V. (1973) in *Chemistry and Physics of Carbon*, **9** (ed. P. L. Walker Jr), Marcell Dekker, New York, p. 174.
3. Kimura, S., Yasuda, E., Takase, N. and Kasuya, S. (1981) *High Temp. High Press*, **13**, 193.
4. Devillard, J., Berthier, J., and Clary, J. (1976) *Ext. Abst. 2nd Int. Carbon Conf.*, p. 489.
5. Ehrburger, P., Lahaye, J. and Bourgeois, C. (1981) *Carbon*, **19**, 1.
6. Pierson, H. O. and Liebermann, M. L. (1975) *Carbon*, **13**, 159.
7. Savage, G. M. (1985) PhD thesis, Univ. London.
8. Yamada, R. (1968) *The Science of New Industrial Materials* (eds Takei and Kawajima) Tokyo, p. 265.
9. Kimura, S., Yasuda, E., Tanaka, H. and Yamada, R. (1975) *J. Ceram. Soc. Jap.*, **83**, 122.
10. Yasuda, E., Kimura, S. and Shibusa, Y. (1980) *Trans. Jap Soc. Comp. Mat.*, **6**, 14.
11. Kimura, S. Tanabe, Y., Takase, N. and Yasuda, E. (1981) *J. Chem. Soc. Jap. (pure Chem. Sect.)*, **9**, 1474.
12. Saxena, R. R. and Bragg, R. H. (1978) *Carbon*, **16**, 373.
13. Marchand, A., Lespade, P. and Conzi, M. (1981) *Ext. Abst. 15th Biennial Conf. on Carbon*, Am. Chem Soc., Washington, DC, p. 282.
14. Tanaka, H., Kaburagi, Y. and Kimura, S. (1978) *J. Mat. Sci.*, **13**, 2555.
15. Marks, B. S., Mauri, R. E. and Bradshaw, W. G. (1975) *Ext. Abst. 12th Biennial, Conf. on Carbon*, Am. Chem Soc., Washington, DC, p. 337.
16. Fitzer, E., Geigle, K. H. and Huettner, W. (1979) *Ext. Abst. 14th Biennial. Conf. on Carbon*, Am. Chem. Soc., Washington, DC, p. 236.
17. Fitzer, E. and Huettner, W. (1981) *J. App. Phys.*, **14**, 347.
18. Gebhardt, J. J. (1979) *Ext. Abst. 14th Biennial. Conf. on Carbon*, Am. Chem. Soc., Washington, DC, p. 234.
19. Marsh, H. and Forrest, M. (1981) *Ext. Abst. 15th Biennial. Conf. on Carbon*, Am. Chem. Soc., Washington, DC, p. 270.
20. Tanaka, H., Mariyama, S. Yasuda, E. and Kimura, S. (1976) *Tanso (Carbon)*, no. 86, 107.
21. Fitzer, E., Heym, M. and Rhee, B. (1976) *Ext. Abst. 2nd Int. Carbon Conf.*, p. 508.

22. Fitzer, E., Huettner, W. and Manocha, L. (1979) *Ext. Abst. 14th Biennial Conf. on Carbon*, Am. Chem. Soc., Washington, DC, p. 240.
23. Gray, G., Hunter, A. and Savage, G. M. (1990) *Proc. Int. Iso. Press. Conf.*, Stratford-upon-Avon, 5–7 Nov, paper 25.
24. Gray, G. and Savage, G. M. (1991) *High Temp. Processing*, special edition, Butterworths, Oct. Oxford.
25. Gray, G. and Savage, G. M. (1992) submitted to *J. Mat. Sci.*
26. Payne, R., von Bradsky, G., Gray, G. and Savage, G. M. (1990) *Proc. Conf. Adv. in Elec. Mic.*, Seattle, p. 1024.
27. Peebles, L. H., Meyer, R. A. and Jortner, J. (1988) *Proc. 2nd Int. Conf. on Comp. Interfaces*, ICCI II, Cleveland, Ohio, USA, 13–17 June.
28. Jortner, J. (1976) *Proc. Army Symp. Solid Mech.*, US Army Mat. α Mech. Res. Ctr., AMMRC MS 76–2, Sept. p. 81.
29. Stouer, E. R., D'Andrea, J. F., Bolinger, P. N. and Gebhardt, J. J. (1977) *Ext. Abst. 13th Biennial Conf. on Carbon*, p. 166.
30. Diefendorf, R. J. and Tokarsky, F. M. (1971) *AFML-TR-72-133*, Parts I and II, US Air-force, Oct.
31. Gray, G. and Savage, G. M. (1992) submitted to *J. Mat. Sci.*
32. Zimmer, J. E. and White, J. L. (1983) *Carbon*, **21**, 323.
33. Meyer, R. A. and Gyetvay, S. R. (1986) in *Petroleum Derived Carbons* (eds J. D. Bacha, J. N. Newson and J. L. White), ACS Symp. 303, Am. Chem. Soc., Washington, DC.
34. Sheaffer, P. M. (1987) *Ext. Abs. 18th Biennial Conf. on Carbon*, p. 20.
35. McKee, D. W. (1987) *Carbon*, **25**, 551.
36. Jortner, J. (1986) *Carbon*, **24**, 603.
37. Fitzer, E. and Barger, A. (1971) *Proc. Int. Conf. on Carbon Fibres, their Composites and Applications*, London, Paper no. 36.
38. McAllister, L. E. and Taverna, A. R. (1971) *Proc. Am. Ceram. Soc. 73rd Ann. Mtg.*, Chicago.
39. Adams, D. F. (1976) *Mat. Sci. Eng.*, **23**, 55.
40. Hill, J., Thomas, C. R. and Walker, E. J. (1973) *Ext. Abst. 11th Biennial Conf. on Carbon*, Am. Chem. Soc., Washington, DC, p. 278.
41. Meyer, R. A. (1986) *Proc. Carbon 1986 Conf.*, Baden-Baden, Germany.
42. Evangelides, J. S. (1976) *Proc. Army. Symp. on Solid Mech.*, Sept., US Army, p. 98.
43. Jortner, J. *J R & E Rpt no. 8514*, p. 39.
44. Manocha, L. M. and Bahl, O. P. (1988) *Carbon*, **26** (1) 13.
45. Schmidt, D. L. (1972) *SAMPE J.*, May/June, 9.
46. Cristina, V. D. (1971) *Proc. AIAA Thermophys. Conf.*, Tullahoma, Tennessee, USA, April, Paper no. 71–416.
47. McDonald, J. E. (1971) *Mech. Eng.*, Feb., 21.
48. Pierson, O. H. and Northrop, D. J., (1975) *J. Comp. Mat.*, **9**, 118.
49. Delhaes, P., Trinquescoste, M. Pacault, A., Goma, J., Oberlin, A. and Thebault, J. (1984) *J. de Chem. Phys*, **81**, 809.
50. Oh, S. M. and Lee, J. Y. (1988) *Carbon*, **26**(6), 769.
51. Oh, S. M. and Lee, J. Y. (1989) *Carbon*, **27**(3), 423.
52. Marinkovic, S. and Dimitrijevic, S. (1985) *Carbon,* **23**, 691.

53. Parmee, A. C. (1972) *Carbon*, **10**, 333.
54. Adams, D. F. (1974) *J. Comp. Mats*, **8**, 320.
55. Zhao, J. X., Bradt, R. C. and Walker, P. L. Jr (1981) *Ext. Abst. 15th Biennial Conf. on Carbon*, Am. Chem. Soc., Washington, DC, p. 274.
56. Fitzer, E. and Terwiesch, B. (1973) *Carbon*, **11**, 570.
57. Chard, W. and Keck, H. (1977) *Proc. 13th Biennial Conf. on Carbon*, Soc., Washington, DC, p. 212.
58. Dietrich, H. and McAllister, E. (1978) *Proc. 8th Ann. Mtg Exp. Am. Ceram. Soc.*, Detroit.
59. Terwiesch, B. (1972) PhD thesis, Univ. Karlsruhe.
60. Evangelides, J. S. (1977) *Proc. 13th Biennial Conf. on Carbon*, Am. Chem. Soc., Washington, DC, p. 76.
61. Fitzer, E., Heym, M. and Karlisch, K. (1974) *Ext. Abst. 4th Lon. Int. Carbon and Graphite Conf.*, p. 39.
62. Fitzer, E. Huettner, W. and Manocha, L. M. (1980) *Carbon*, **18**, 291.
63. Savage, G. M. (1992) submitted to *J. Mat. Sci.*
64. Norton-Berry, P., Savage, G. M. and Steel, M. L. (1989) European Patent app. W35016/EP.
65. Ryshkewitch, E. (1953) *J. Am. Ceram. Soc.*, **36**, 65.
66. Kimura, S., Kasuya, S. and Yasuda, E. (1978) *Proc. Int. Symp. of Factors in Dens. and Sintering of Ceramics*, Japan, p. 229.
67. Hill, J. (1975). *Ext. Abst. 12th Biennial Conf. on Carbon*, Pittsburg, p. 287.
68. Yasuda, E. Tanaka, H. and Kimura, S. (1980) *Tanso (Carbon)*, no. 100, 3.
69. Kimura, S. Yasuda, E. and Tanabe, Y. (1982) *Proc. Int. Conf. Comp. Mats*, **IV**, p. 1601.
70. Fitzer, E. and Heym, M. (1977) *Ext Abst. 13th Biennial Conf. on Carbon*, p. 128.
71. Fitzer, E. and Heym, M. (1980) *Kunstofftechnik*, 85.
72. *Carbon Fibre Reinforced Carbon*, Schunk promotional brochure.
73. Kim, H. C., Yoon, K. J., Pickering, R. and Sherwood, R. J. (1985) *J. Mat. Sci.*, **20**, 3967.
74. Kelly, B. T., (1969) *Chem. Phys. Carbon*, **5**, 119.
75. Carbon and artificial graphite, in *Kirk-Othmer Dictionary of Chemical Technology*, 3rd edn, **4**, Wiley, New York.
76. Taylor, R., Gilchrist, K. E. and Poston, L. J. (1968) *Carbon*, **6**, 573.
77. Bokros, J. C., (1969). *Chem. Phys. Carbon*, **5**, 1.
78. Liebermann, M. L. and Pierson, H. O. (1973) *Proc. 11th Biennial Carbon Conf.*, p. 314.
79. Curlee, R. M. and Liebermann, M. L. (1973) *Proc. 11th Biennial Carbon Conf.*, Am. Chem Soc., Washington, DC, p. 280.
80. Curlee, R.M. and Northrop, D. A. (1973) *Proc. 11th Biennial Carbon Conf.*, Am. Chem. Soc., Washington, DC, p. 318.
81. McAllister, L. E. and Lachmann, W. (1983) in *Fabrication of Composites* (*Handbook of Composites*, **4**) (eds A. Kelly, and S. T. Millieko), North-Holland, p. 109.
82. Rolincik, P. G. (1973) *Proc. 11th Biennial Conf. on Carbon*, Am. Chem. Soc., Washington, DC, p. 343.

83. Laramee, P., Lamere, G., Prescott, B., Mitchell, R., Sottosanti, P. and Dahle, D. (1975) *Proc. 12th Biennial Conf. on Carbon*, Am. Chem. Soc., Washington, DC p. 74.
84. Curry, D. M., Scott, H. C. and Webster, C. N. (1979) *Proc. 24th SAMPE Symp.*, p. 1524.
85. Kimura, S., Yasuda, E. and Tanabe, Y. (1982) *Proc. Int. Symp. on Carbon in Japan*, p. 410.
86. Curlee, R. H. and Northrop, D. A. (1973) *Ext. Abst. 11th Biennial Conf. on Carbon*, Am. Chem. Soc., Washington, DC, p. 318.
87. Pierson, H. O., Northrop, D. A. and Smatana, J. F. (1973) *Ext. Abst. 11th Biennial Conf. on Carbon*, Am. Chem. Soc., Washington DC, p. 275.
88. Granoff, B. and Apodaca, P. (1973) *Ext Abst. 11th Biennial Conf. on Carbon*, Am. Chem. Soc., Washington, DC, p. 273.
89. Lamieq, P. Mace, J. and Perez, B. (1980) *Ext. Abst. 15th Biennial Conf. on Carbon*, Am. Chem. Soc., Washington, DC, p. 528.
90. Tanaka, H., Kaburagi, Y. and Kimura, S. (1978) *J. Mat. Sci.*, **13**, 2555.
91. Kimura, S., Hagis, N., Yasuda, E. Tanabe, Y., Hishiyama, S. and Kaburage, Y. (1983) *J. Ceram. Soc. Jap.*, **91**, 121.

Applications of Carbon–carbon Composites

9

9.1 BRAKES AND CLUTCHES

9.1.1 Introduction

Something like 63% by volume of the carbon–carbon produced in the world is used in aircraft braking systems. Carbon–carbon brake materials were originally developed by the Super Temp Division of B. F. Goodrich Inc. in the USA. Their process was licensed by Dunlop in the UK. Dunlop were the first company to manufacture and fit carbon–carbon composite brakes into regular service.

Trials were carried out in 1973 on a VC10 aircraft followed a year later by standard fitment to Concorde SST [1]. At the time when they were first introduced, the cost of the brakes was around £550 kg^{-1}. As a result, their use could only be considered economically viable on supersonic transports and high-performance military aircraft. Advances in technology have now reduced the cost of carbon–carbon suitable for brakes to around £100–£150 kg^{-1}.

It is now commercially advantageous to employ carbon–carbon brakes on civil subsonic aircraft. Furthermore, the use of carbon–carbon has been exploited or postulated for a number of land vehicles such as racing cars, high-speed trains and even main battle tanks (MBTs).

Today, probably the largest producer of carbon brakes is Hitco, based in California in the USA, who are owned by the UK's BP Corporation. Other major 'players' are the French company SEP, along with Bendix (Allied Signal) and Arcraft Braking Systems in the USA. Dunlop themselves still retain a market share, although not on the same scale as their competitors.

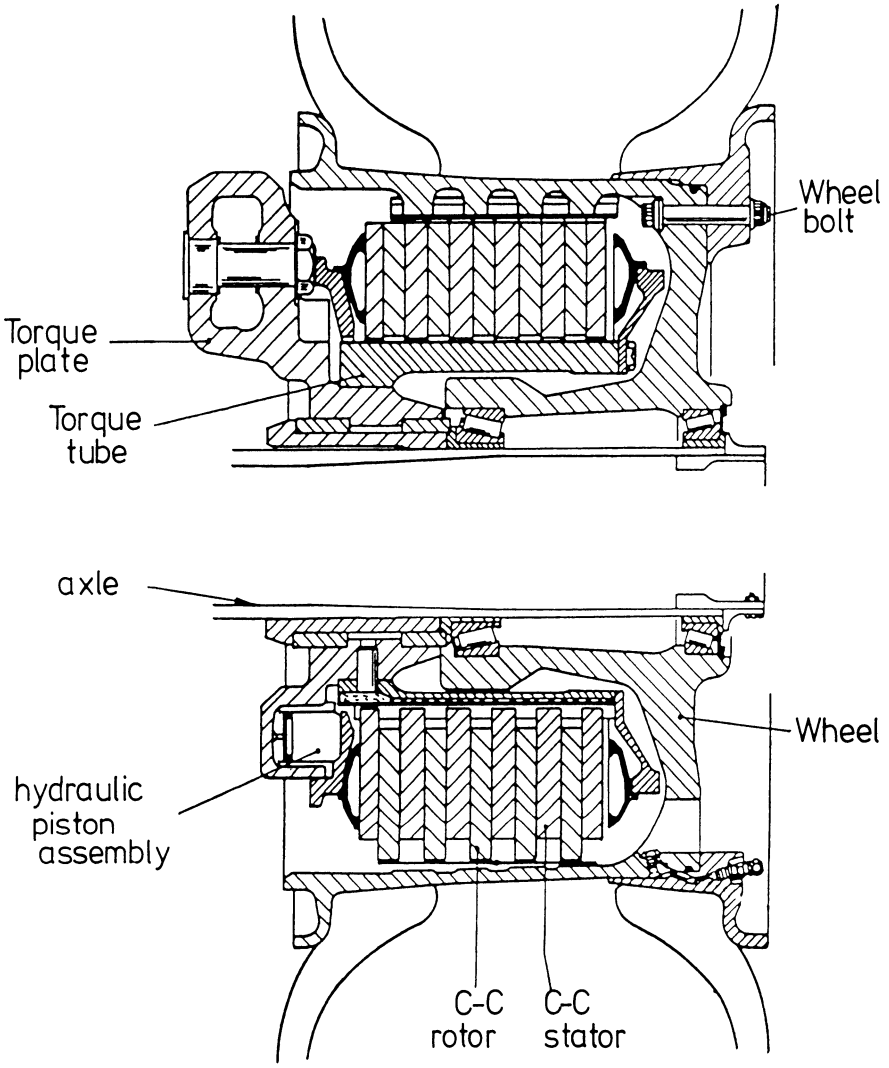

Fig. 9.1 Schematic diagram of a carbon–carbon aircraft disc brake system.

9.1.2 Aircraft brakes

Aircraft brakes are multiple disc brakes of rotors sandwiched between stators (Figs 9.1 and 9.2). The rotors are driven by the wheel and the stators held stationary by the brake structure. The braking action is performed by pressing the discs together using some form of hydraulic actuator system. The brake discs are required to provide the frictional torque which stops the aircraft, serve as a heat sink to absorb the heat generated during the braking action (of the order of several hundred MJ) and also act as a structural component. Friction between the rotating and stationary discs

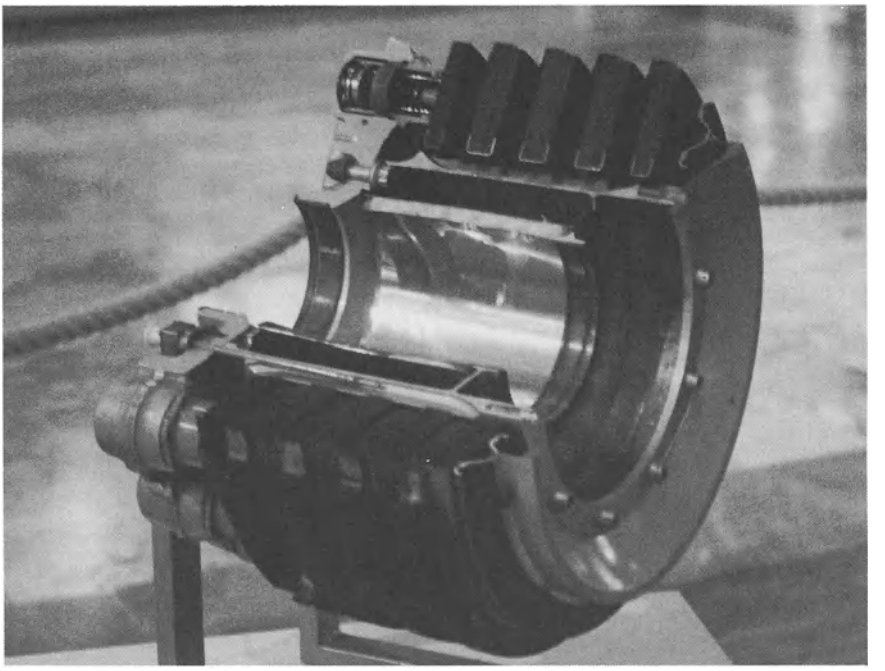

Fig. 9.2 Sectioned carbon–carbon brake from a commercial airliner (Airbus A320).

causes them to heat up to around 500 °C with surface temperatures reaching as high as 2000 °C as the kinetic energy of the aircraft is absorbed [2]. Consequently, the materials used in this environment must exhibit a good thermal shock resistance. The high thermal conductivity and very low coefficient of thermal expansion of carbon–carbon make it an ideal choice.

A number of performance parameters are important in aircraft brake design. These include peak torque, oxidation and stability. Such variables are controlled by engineering design, composition and processing conditions of the friction material. The two primary advantages of carbon–carbon are heat capacity (2.5 times greater than that of steel) and high strength at elevated temperatures (twice that of steel). The result is a 40% saving in weight compared to metal brakes and a doubling of their service life when measured as landings per overhaul (LPO). A wide-bodied airliner such as the Airbus A320 would expect to complete something like 2500 LPO when fitted with carbon brakes as opposed to around 1500 using a metal equivalent.

9.1.3 Materials and processing

Three distinct types of carbon–carbon composite are currently used in braking systems (Fig. 9.3). These are carbon fabric laminates, semi-random

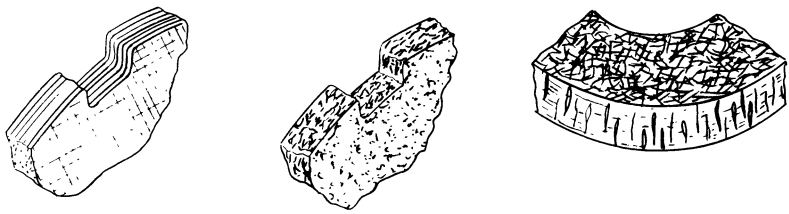

Fig. 9.3 The three types of carbon fibre reinforcement used in carbon–carbon composite brakes.

chopped carbon fibres (Hitco) and laminated carbon fibre felts with cross-ply reinforcement (SEP). The matrix consists exclusively of pyrolytic carbon or a combination of pyrolytic and glassy carbons. The pyrolytic carbon matrix is obtained via a chemical vapour deposition (CVD) process. The glassy carbon is produced from the carbonization of a high char yield resin, generally a phenolic. The resin is used in the consolidation of carbon fibres in the shape of a disc or in the densification of the porous disc by resin impregnation in the final stages of processing. A flow diagram showing a typical carbon–carbon brake manufacturing process is shown in Fig. 9.4.

Carbon–carbon composite brake discs must be protected from oxidation which occurs from repeated excursions to high temperatures during braking. Oxidation protection is achieved by the application of a 'trowelable' glass-forming penetrant to block the active sites on non-rubbing surfaces or by adding an inhibitor during fabrication.

9.1.4 Frictional properties and braking mechanisms

Brakes and clutches are devices for transferring rotating energy and may thus be considered together [3].

A schematic dynamic representation of a brake or clutch is shown in Fig. 9.5. Two inertias I_1 and I_2, travelling with angular velocities of ω_1 and ω_2 respectively, are brought to the same speed by engaging the clutch. In the case of a brake, one of the angular velocities will generally be zero. The two elements are rotating at different speeds thus resulting in slippage.

Energy dissipation during actuation causes a rise in temperature. When undertaking analysis of the performance of a device of this type, the factors of concern are:

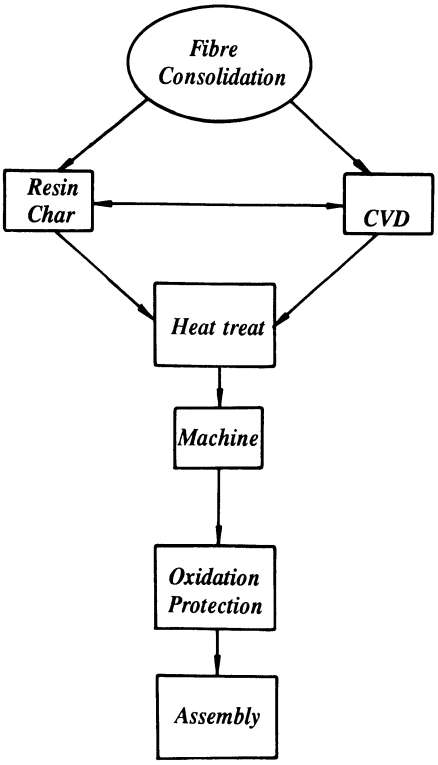

Fig. 9.4 Typical process flow chart for the manufacture of carbon–carbon composite brake discs.

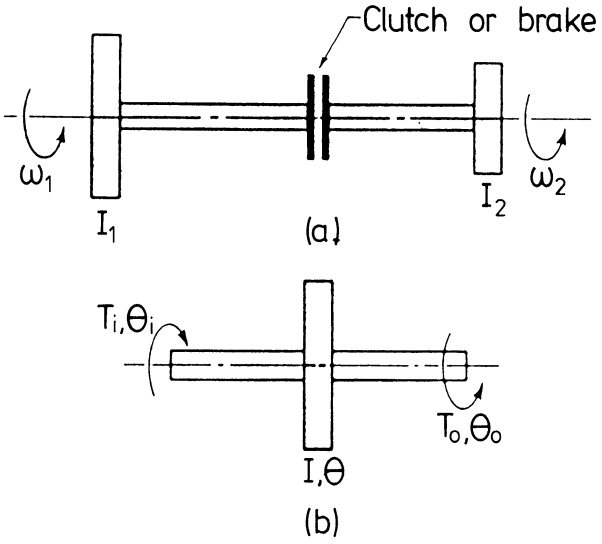

Fig. 9.5 Dynamic representation of a clutch or brake.

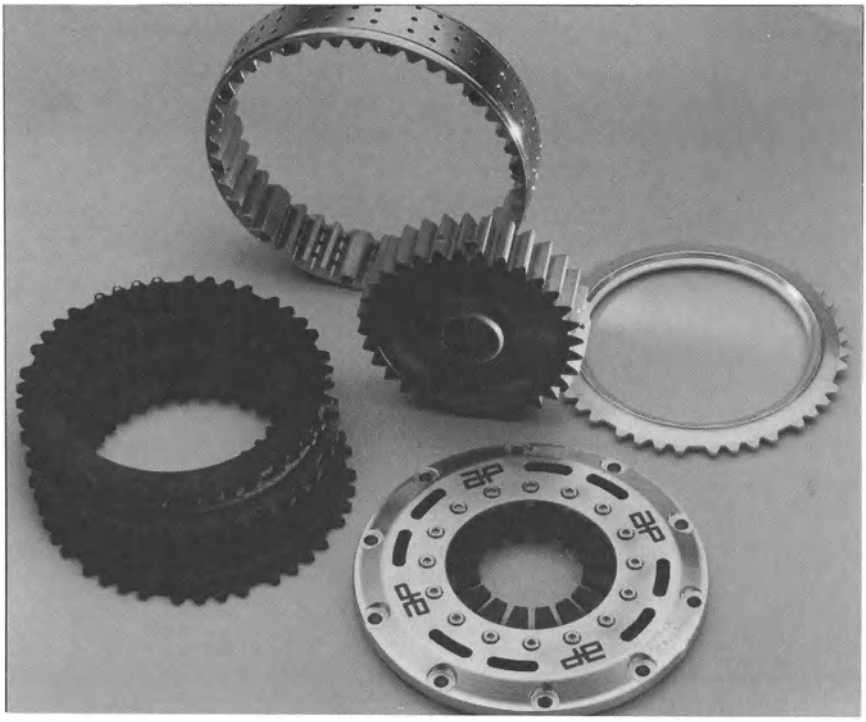

Fig. 9.6 Carbon disc clutch system from a Formula 1 racing car (courtesy AP Racing).

1. the actuating force;
2. the torque transmitted;
3. the energy loss;
4. the rise in temperature.

The torque transmitted must be studied individually for each geometric coefficient of friction (μ) and the geometry and *modus operandi* of the device. Temperature rise, on the other hand, is related to the energy loss which may be studied independently of the type of apparatus because the only geometry of concern is that of the heat-dissipating surfaces.

The disc–disc brake systems used on aircraft and the clutches of Formula 1 racing cars (Fig. 9.6) are examples of what is known as an 'axial clutch', that is to say that the mating frictional members are moved in a direction parallel to the shaft. Advantages of the disc system include the freedom from centrifugal effects, a large frictional area installed into a small space, a more effective heat dissipation from rubbing surfaces and a uniform distribution of applied pressure.

The capacity of a disc brake system can be analysed in terms of the

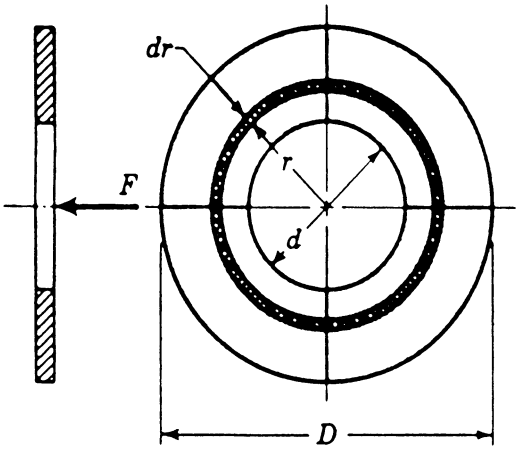

Fig. 9.7 Disc friction member.

material used and its dimensions. A friction disc of outside diameter D and internal diameter d is shown in Fig. 9.7. Two possible methods exist to calculate the axial force F necessary to produce a torque T and pressure p. The greatest wear on a rigid disc will initially arise in the outer areas, in which the work of friction is greatest. Once a degree of wear has taken place, the pressure distribution will change, permitting the wear to be uniform. The other solution is to employ devices such as springs, for example, to maintain a uniform pressure over the braking area.

Uniform wear

Uniform wear occurs once the discs have worn down to a point such that the greatest pressure occurs at $r = d/2$. By letting the maximum pressure be denoted p_a, we may derive the condition in which the same amount of work is done at radius r as is done at radius $d/2$:

$$p_r = p_a \frac{d}{2}, \quad \text{i.e. } p = p_a \frac{d}{2r}. \tag{9.1}$$

Now considering Fig. 9.6, we have an element of area of radius r and thickness dr. The area of this element, then, is $2\pi r$ dr. The normal force acting upon the element will be

$$\mathrm{d}F = 2\pi p r \mathrm{d}r. \tag{9.2}$$

The total normal (actuating) force acting on the disc may be calculated by integrating equation (9.2) between the limits $d/2$ and $D/2$:

$$F = \int_{d/2}^{D/2} 2\pi pr \, dr = \frac{\pi p_a d}{2} \int_{d/2}^{D/2} dr = \frac{\pi p_a d}{2} (D - d). \tag{9.3}$$

The torque is obtained by integrating the product of the frictional force and the radius:

$$T = \int_{d/2}^{D/2} 2\pi\mu pr^2 dr = \pi\mu p_a d \int_{d/2}^{D/2} r \, dr = \frac{\pi\mu p_a d}{8} (D^2 - d^2). \tag{9.4}$$

A more convenient expression of the torque may be obtained by substituting the value of F calculated from equation (9.3):

$$T = \frac{F\mu}{4} (D + d). \tag{9.5}$$

When designing a disc brake or clutch system, equation (9.3) is used to calculate the required actuating force per friction surface pair for the selected maximum pressure p_a. Equation (9.5) is then used to obtain the torque capacity per friction surface.

Uniform pressure

If uniform pressure can be assumed over the area of the disc, the actuating force is simply the product of the pressure and the area, i.e.

$$F = \frac{\pi p_a}{4} (D^2 - d^2). \tag{9.6}$$

The torque is found, as before, by integrating the product of the frictional force and the radius:

$$T = 2\pi\mu p \int_{d/2}^{D/2} r^2 dr = \frac{2\pi\mu p}{24} (D^3 - d^3) \tag{9.7}$$

since $p = p_a$

$$T = \frac{F\mu}{3} \frac{D^3 - d^3}{D^2 - d^2}. \tag{9.8}$$

In both solutions the torque has been calculated for a single pair of mating surfaces. In a complete braking system, this value must therefore be multiplied by the number of surfaces in contact.

Energy dissipation

When the rotating components of a vehicle or machine are slowed or brought to a halt by means of a brake, their kinetic energy must be absorbed by the brake. The energy is manifested in the form of heat

within the brake. Similarly, when the members of a machine which are initially at rest are brought up to speed, slippage must occur in the clutch until the driven members attain the same speed as the driver. It is this process of slippage by which kinetic energy is absorbed and appears in the appliance as heat.

The analysis in the previous two subsections showed how the torque capacity of a brake depends upon the coefficient of friction of the material and the safe, normally applied pressure. The nature of the braking load may be such however that, if the calculated torque value is permitted to develop, the device may be destroyed by its own generated heat. The performance of a brake or clutch is therefore limited by the friction characteristics of a material and its ability to dissipate heat. Should heat be generated quicker than it is dissipated, a temperature rise problem will result. It is apposite therefore to consider the amount of heat generated during the braking or clutch operation.

In order to model the events during a simple braking or clutch action, it is necessary to refer back to Fig. 9.5. Two inertias I_1 and I_2 possess angular velocities ω_1 and ω_2 respectively. Application of the clutch causes both angular velocities to change and eventually become equal. Assuming the two shafts to be rigid and a constant torque, the equations of motion relating the two inertias may be written:

$$I_1 \frac{d^2\theta_1}{dt^2} = -T \tag{9.9}$$

$$I_2 \frac{d^2\theta_2}{dt^2} = T, \tag{9.10}$$

where $d^2\theta_1/dt^2$ and $d^2\theta_2/dt^2$ are the angular accelerations of I_1 and I_2 respectively. T is the clutch torque.

The angular velocities at any time t may be found by integrating (9.9) and (9.10):

$$\frac{d\theta_1}{dt} = -\frac{T}{I_1}t + \omega_1 \tag{9.11}$$

$$\frac{d\theta_2}{dt} = \frac{T}{I_2}t + \omega_2. \tag{9.12}$$

The difference in velocities, $d\bar{\theta}/dt$, is known as the relative velocity:

$$\frac{d\theta_1}{dt} - \frac{d\theta_2}{dt} = \frac{d\bar{\theta}}{dt} = \frac{T}{I_1}t + \omega_1 - \left(\frac{T}{I_2}t + \omega_2\right)$$

$$= \omega_1 - \omega_2 - T\left(\frac{I_1 + I_2}{I_1 I_2}\right)t. \tag{9.13}$$

The clutching process is complete when $d\theta_1/dt = d\theta_2/dt$, i.e. when $d\bar{\theta}/dt = 0$. The time required to complete the operation, t, is therefore defined as

$$t = \frac{I_1 I_2 (\omega_1 - \omega_2)}{T(I_1 + I_2)}. \tag{9.14}$$

We may thus conclude that the time required to execute the braking or clutching operation is directly proportional to the velocity difference and indirectly proportional to the torque generated.

Throughout the analysis, the clutch torque is assumed to be constant. Using equation (9.13) therefore, the rate of energy dissipation (dE/dt) may be found:

$$\left(\frac{dE}{dt}\right) = T\frac{d\bar{\theta}}{dt} = T\left[\omega_1 - \omega_2 - T\left(\frac{I_1 + I_2}{I_1 I_2}\right)t\right]. \tag{9.15}$$

It is clear then that the greatest dissipation of energy occurs at the start of the action, i.e. when $t = 0$. The total energy dissipated may be found by integrating equation (9.15) between $t = 0$, and $t = t_1$.

$$E = \int_0^{t_1} \frac{dE}{dt}\,dt = T\int_0^{t_1}\left[\omega_1 - \omega_2 - T\left(\frac{I_1 + I_2}{I_1 I_2}\right)t\right]dt$$

$$= \frac{I_1 I_2 (\omega_1 - \omega_2)^2}{2(I_1 + I_2)}. \tag{9.16}$$

The energy dissipated is thus proportional to the velocity difference but independent of the torque.

Temperature effects

The temperature rise (ΔT) resulting from the braking action may be approximated using classical thermodynamics

$$\Delta T = \frac{E}{Cm}, \tag{9.17}$$

where C is the specific heat (J $kg^{-1}K^{-1}$), m the mass of device (kg) and E the total energy dissipated during braking operation (J). An equation of this form may be used qualitatively to explain events during the operation of the brake or clutch. There are, however, far too many variables involved for any useful or accurate quantitative information to be generated. The major advantage of a temperature rise analysis is the identification of the most important design parameters by experimental examination.

9.1.5 Experimental and in-service analysis of brake performance

Carbon–carbon friction materials are tested on a dynamometer using a ring-on-ring configuration. On a research scale it is performed with a small

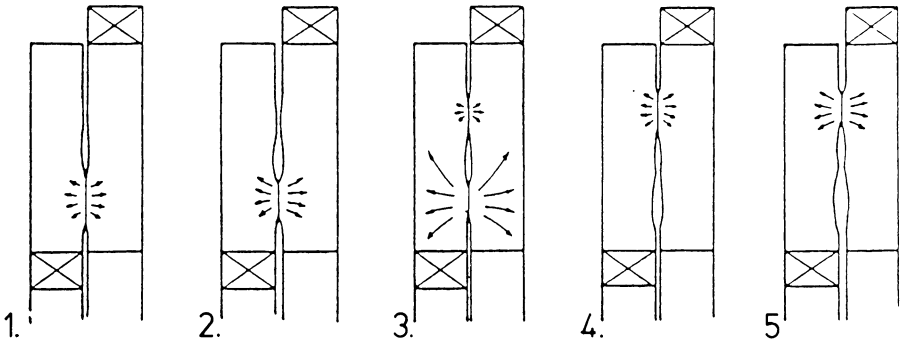

Fig. 9.8 Bands of contact formed during braking as a result of thermo-elastic and wear effects.

annular ring (around 5 cm OD × 3 cm ID) mounted on a rotating shaft and pressing against a similar, but stationary, ring positioned on the same axis. Full-scale testing is accomplished using a complete brake assembly mounted on a wheel with tyre. In both cases, test conditions are chosen to simulate in-service operation. The critical parameters are; relative sliding speed at the friction surface, pressure on the friction surface, kinetic energy loading per unit mass and per unit friction surface area and the rate of energy dissipation. The performance of the carbon–carbon brake is also considerably influenced by the ambient conditions, that is to say, the brake temperature and humidity. The final contributory factor is prior test history which establishes the condition of the friction surface.

The average coefficient of the friction (μ) in static or low-speed sliding configuration is generally low. When the brake is hot, however, μ can be very high, reaching as much as 0.6. Under wet conditions, μ is generally very low (around 0.1) due to the lubricating effect of absorbed water. The thermal loading on a disc is extremely severe and has a controlling influence on the brake design.

Frictional contact of brake components involves thermo-elastic and wear phenomena. The sliding surfaces initially contact one another at local points only. The work done at those points results in local expansion. Rotation of one of the surfaces causes the formation of a narrow annular band of contact. Further work and expansion take place at the radius until heat flow, wear at the band of contact and changes in mechanical loading in adjacent discs cause a new band of contact to become established. The work at the first band diminishes, the material cools locally and, because wear has taken place, that particular band of contact is unlikely to be re-established for some time. This mechanism, illustrated in Fig. 9.8, results in a very high rate of work per band of contact such that transient temperatures at the contact surface may exceed 2000 °C.

The micro-mechanism of braking involves the formation of a friction film from ground and compacted wear debris (Fig. 9.9). Repeated sliding

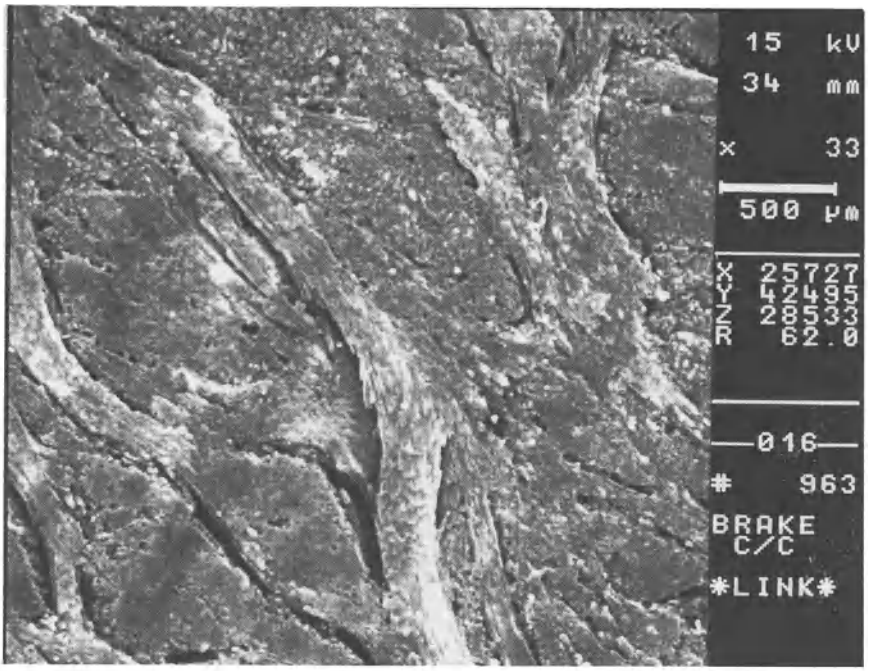

Fig. 9.9 Scanning electron micrograph of a fully developed friction surface in a carbon–carbon brake.

causes a delamination of part of the friction film resulting in the formation of new wear debris by abrasion of the substrate. The majority of this debris is compacted again, regenerating the friction film, while a small amount is lost to the atmosphere, contributing to wear. A schematic diagram of the wear process is shown in Fig. 9.10.

9.1.6 Racing car brakes

Carbon–carbon brakes were introduced into Formula 1 motor racing in the early 1980s by the Brabham team. Today, brakes of this type are universally used in the sport. In contrast to aircraft brakes, those employed in Formula 1 are of the disc and pad type, having evolved from the metal brakes they replaced. The brakes are operated by hydraulic callipers pressing the carbon–carbon pads against the ventilated discs (Figs 9.11 and 9.12) [4]. Disc systems are used, however, in the clutches of Formula 1 vehicles. The operation of the carbon–carbon brakes depends on their environment and on cooling. It is important that the geometry of the upright and cooling assembly complies with specifications concerning the disc assembly (Fig. 9.13). The essential requirement is to provide adequate passages for cooling air within the uprights, airflow being directed into the

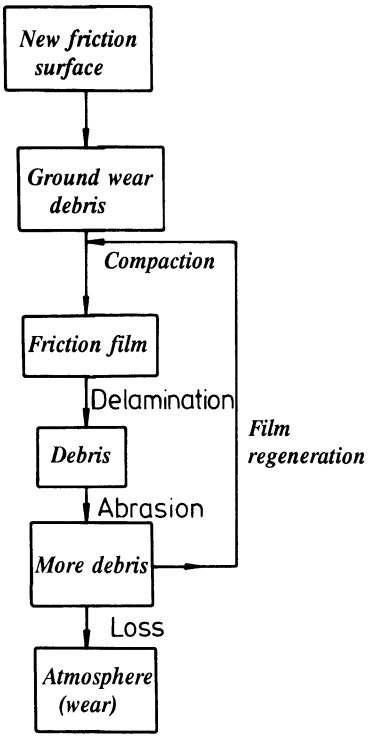

Fig. 9.10 Schematic flow diagram of the wear processes for carbon–carbon aircraft brakes.

vent holes in the disc. A cross-section of at least 70 cm^2 of air flow is generally required for each disc.

Referring to Fig. 9.11, a floating disc to bell assembly is necessary to avoid problems due to thermal expansion mismatch. The bells are made of titanium or a high-temperature aluminium alloy (e.g. alloy 2618) with a surface treatment to improve hardness and resistance to elevated temperatures. Dimensioning of contact surfaces between the sleeves and the bell is critical to prevent fretting. The brakes have an operation window of between 400 and 600 °C. Operating at too low a temperature results in poor performance due to a low coefficient of friction, whereas usage above 600 °C runs the risk of excessive oxidation.

It is important the driver run in and warm up his brakes correctly to develop an optimum friction surface and attain the operating window. During a practice lap he must brake firmly several times, but not during acceleration as this would cause glazing of the discs and pads caused by an absence of carbon dust on the rubbing surfaces. During pit stops the temperature of the brakes must be kept above 350 °C and is monitored constantly using an optical pyrometer to enable the determination of correct operation, brake balancing and temperature control on the callipers to prevent 'vapour lock' [4].

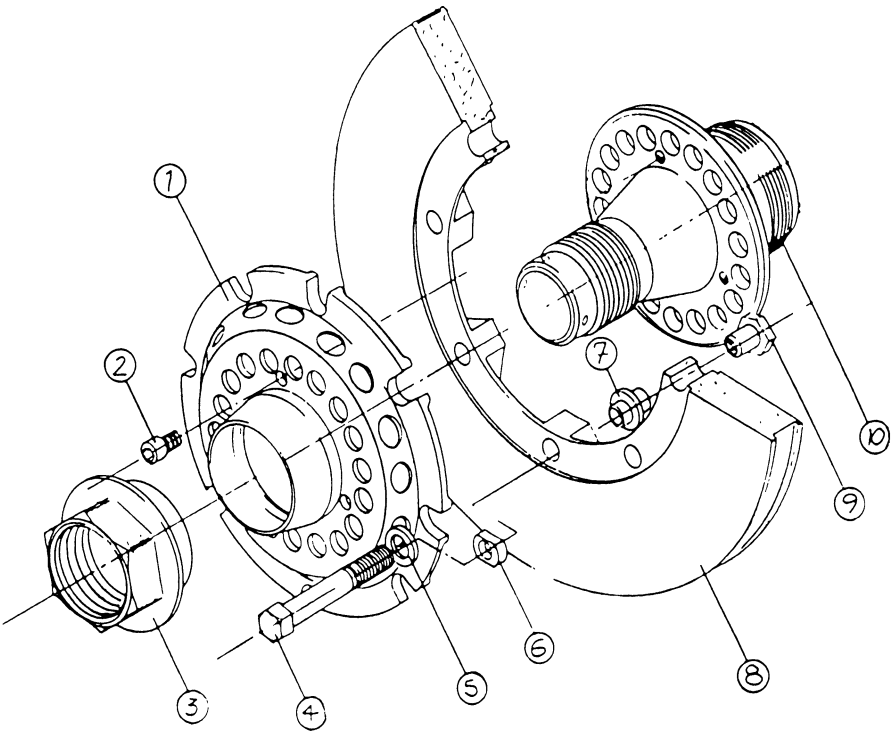

Fig. 9.11 Exploded diagram of Formula 1 carbon–carbon brake system: 1, disc bell; 2, bell-retaining screw; 3, extended wheel nut; 4, disc/disc bell bolt; 5, retaining washer; 6, drive lug; 7, mounting bush; 8, carbon–carbon disc; 9, mounting nut; 10, axle.

Ventilation of the discs plays an important role in cooling to avoid their mass temperature exceeding 600 °C. Location of the ventilation intakes is designed during aerodynamic studies of the vehicle in the wind tunnel. Brake ducts are placed in the zone where air flow is greatest. Determination of potential wear is carried out by regular measurement of disc and pad thicknesses by race engineers. Wear readings are taken using a precision (1/100 mm) micrometer. Measurements are taken at the centre of the friction surface of the disc and at both ends of each pad (Fig. 9.14).

Calculation of wear on discs and pads is carried out as follows. For measurement of maximum disc and pad wear at front and rear (D), let T_i = initial thickness and T_f = final thickness; then

$$D = T_i - T_f. \tag{9.18}$$

If the car travels X laps, in which the lap during which the car leaves the pit, plus the lap during which the car comes back to the pit is considered as one full lap, then wear per lap is

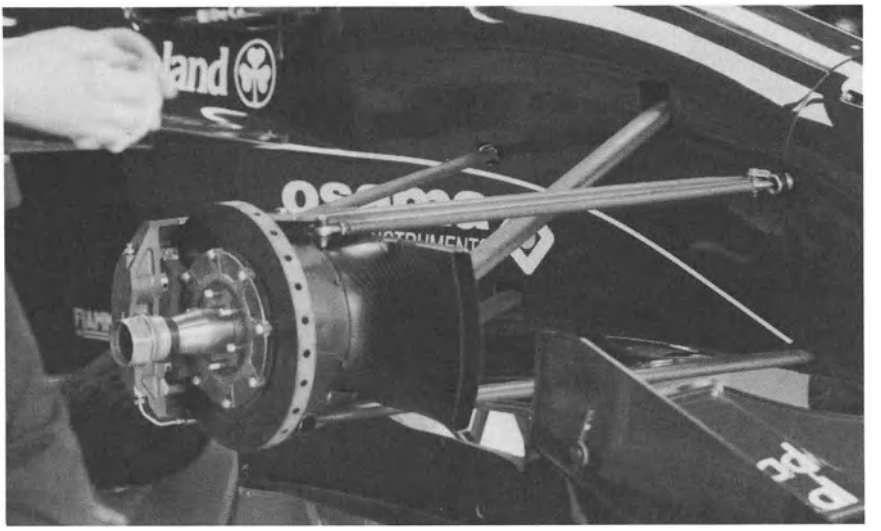

Fig. 9.12 Carbon–carbon brake fitted to a Formula 1 racing car.

$$W = D/X. \tag{9.19}$$

Average thickness of brake element is

$$T = \frac{T_i + T_f}{2}. \tag{9.20}$$

The potential of a new rubbing element, under identical conditions of use, can then be determined on a wear curve provided by the manufacturer (Fig. 9.15).

Two manufacturers provide products to the Formula 1 circuit, SEP and Hitco. The discs and pads used are generally made from the centre sections removed from aircraft brake discs to allow the fitting of the axle and are thus a good use of what might otherwise be scrap material – if anything as expensive as carbon–carbon could ever be thought of as such! Although nominally the same material, their characteristics are very different due to their different structures and processing routes.

Hitco brakes are made from phenolic resin, impregnated carbon fibres chopped into 38 mm lengths (known as 'matchsticks') which are compression moulded into discs. The resin is carbonized followed by resin reimpregnation and CVD densification to around 1.75 g cm^{-3}. SEP brakes, on the other hand, are a CVD-densified carbon fibre felt of roughly the same density. The performance characteristics of each can be explained using electron micrographs of pads tested on a Formula 1 car at a European

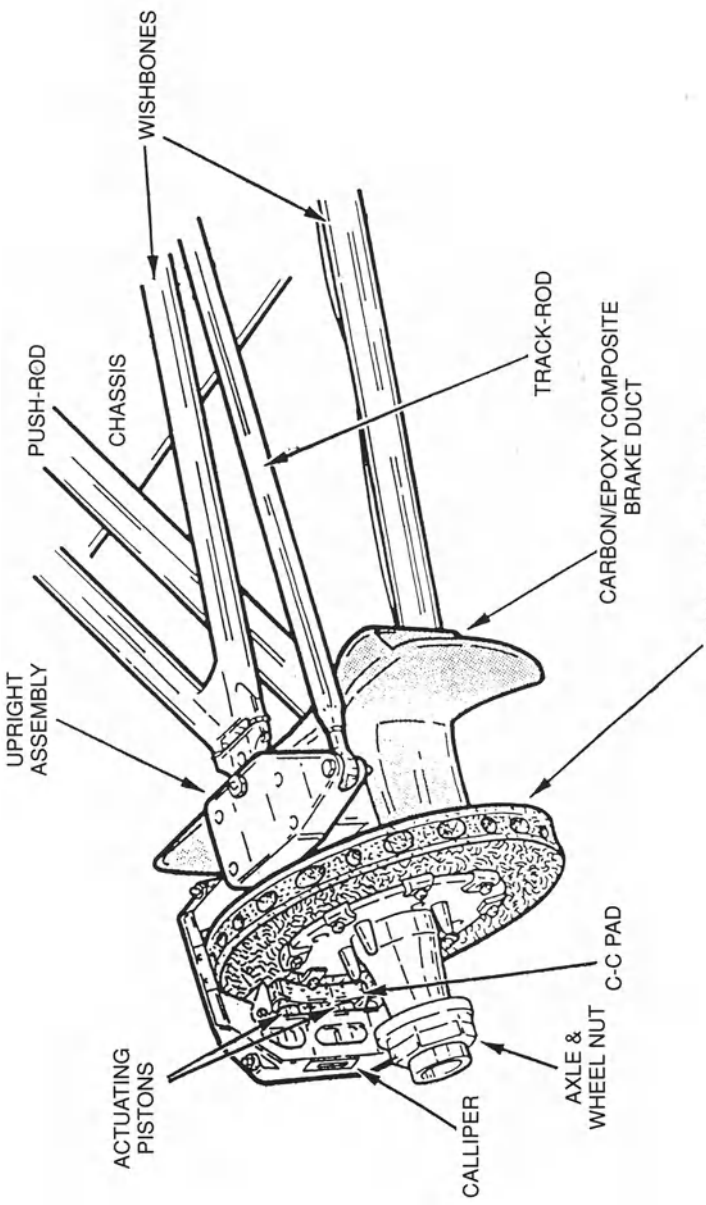

Fig. 9.13 Configuration of brakes and ventilation ducts on a Formula 1 racing car.

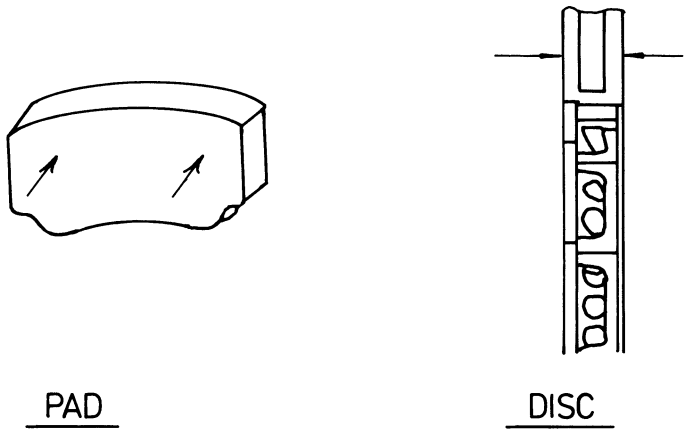

Fig. 9.14 Measurment points for calculation of carbon–carbon brake wear.

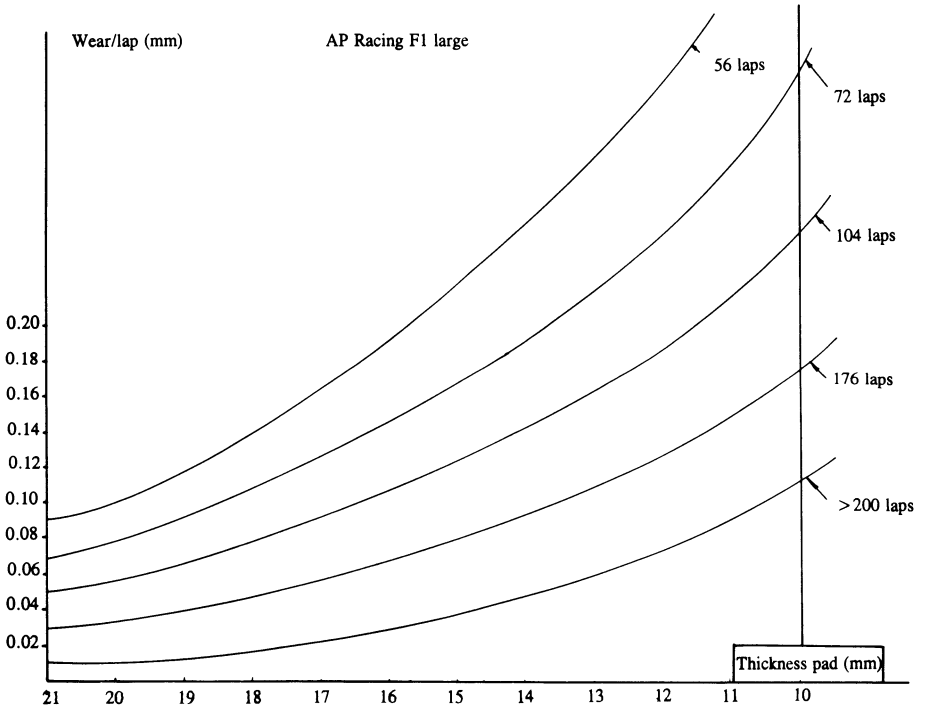

Fig. 9.15 Example of manufacturers' brake wear curves. (Courtesy of AP Racing).

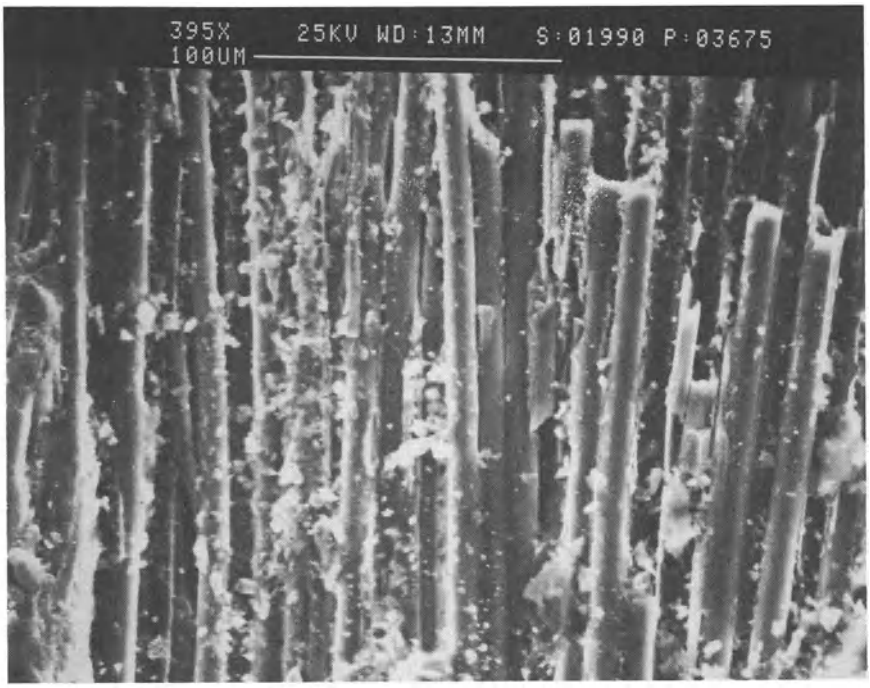

Fig. 9.16 Scanning electron micrograph of powdery isotropic carbon debris on the friction surface of a pad produced by resin pyrolysis.

circuit. As a prelude, it is interesting to note the driver's comments on the behaviour of each type of material and to correlate these with the microscopical observations. Resin based brakes heat up very quickly and perform excellently during the first couple of laps. Braking becomes increasingly difficult, however, with increasing time. Wear of the discs and pads is relatively slow. CVD brakes, on the other hand, are more difficult to heat up, requiring a great deal of care during the initial laps. Once up to temperature, performance remains fairly constant unless they become overheated. Wear is significantly faster than their competitors. Both types of brake were observed to become 'spongy' if overheated.

The friction surface of the thermoset resin based brakes heats up relatively quickly because of the essentially two-dimensional nature of the fibre reinforcement. Thermal conductivity is far greater along the fibres than through the glassy carbon matrix, thus the dissipation of heat energy away from the rubbing surface is relatively inefficient. The matrix is very brittle and only weakly attached to the fibre reinforcement. The friable isotropic carbon forms a characteristic 'powdery' debris which is subsequently compacted into the surface (Fig. 9.16). The resulting glazed

Fig. 9.17 Scanning electron micrograph of glazed friction surface of a resin based carbon–carbon brake pad.

surface thus loses a degree of breaking efficiency, but as a direct consequence, wear is reduced (Fig. 9.17).

Micrographs of an CVD brake's friction surface (Figs 9.18 and 9.19) illustrate the characteristics of a material densified by this technique. The surface is dominated by large pores as one would expect, since CVD is extremely efficient at filling small pores but very poor at filling large ones. The bond between fibres and matrix is much stronger than a resin-densified material so that debris is much larger and more irregularly shaped, producing a much rougher friction surface (Fig. 9.20). The observation that the CVD materials take longer to attain operating temperature can be explained by the microstructure of the carbon felt reinforcement and the insulating effects of the porosity. Although essentially lamellar in construction, the felt possesses a 'pseudo-three-dimensional' appearance such that fibres are available to conduct more heat away from the rubbing surface as it is being heated during operation. The maintenance of a rougher friction surface topography accounts for the more constant braking behaviour but also increases the wear. Overheating of the brakes results in oxidation. Oxidative attack takes place preferentially in the most thermodynamically unstable areas. In the case of carbon–carbon, as we have

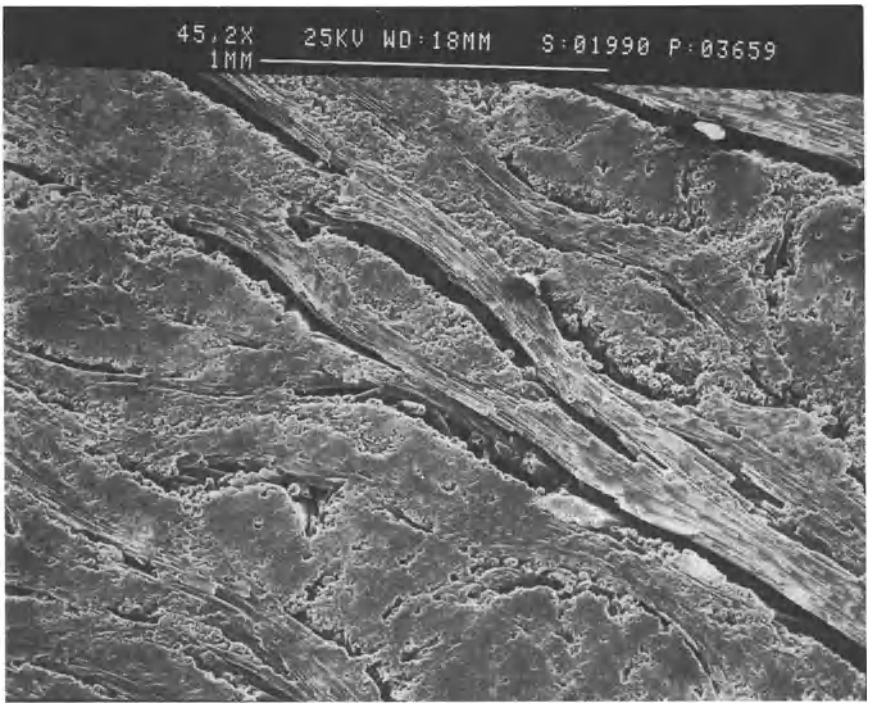

Fig. 9.18 Electron micrograph of CVD braking surface showing large-scale porosity.

seen in Chapter 6, this is in the matrix. Figure 9.21 shows an oxidized area at the corner of one of the pads, close to the rubbing face (i.e. the hottest part). Preferential attack of the matrix can clearly be seen. Degradation of the material in this way means that the support to the fibres is relaxed and stress transfer impeded, hence explaining the driver's observation that the brakes become 'spongy' as the material 'collapses' under the applied pressure. Oxidation protection is attempted using a trowelable 'paint' which does not penetrate the network of pores particularly well. Furthermore, the rubbing surfaces cannot be protected as this would impair their performance. Oxidation kinetics are reduced by ventilation due to the reduction in temperature. It should be remembered, however, that ventilation increases the partial pressure of oxygen available for reaction and the aerodynamics forces the oxygen into the pore structure in the interior of the material, eating it away from within. A number of teams prefer the CVD variety of brake, although they can result in severe problems of wear on some circuits. Other teams, in contrast, choose the thermoset resin derived brakes, sacrificing a little in performance to give improved longevity. It is indeed not uncommon for a mixture of both types of material to be used in the quest for the optimum set up.

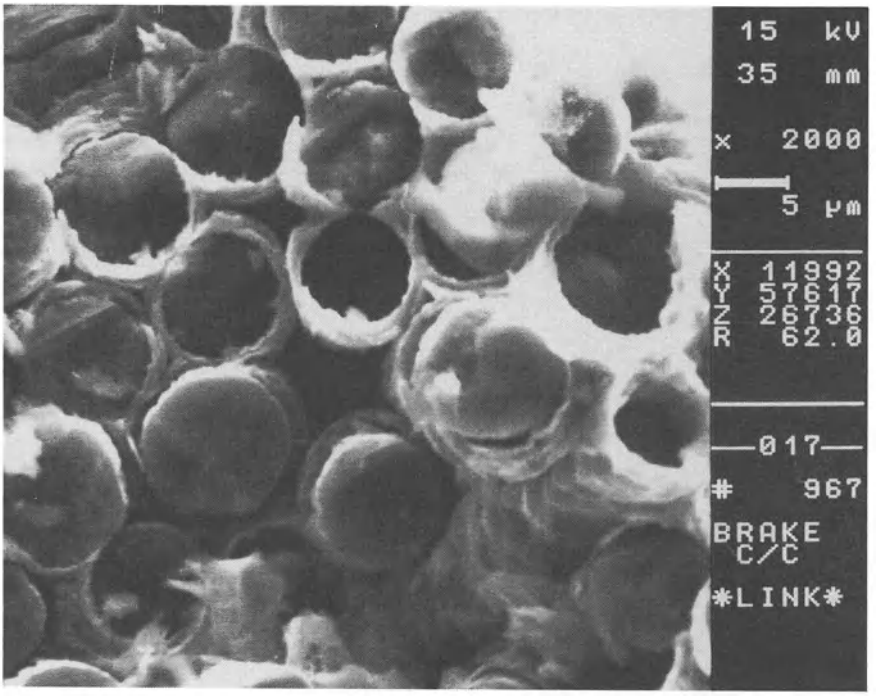

Fig. 9.19 Strong fibre matrix interface in CVD-densified carbon–carbon brakes.

9.1.7 Other braking applications

The major advantages of carbon–carbon braking materials are their light weight, excellent thermomechanical performance and inertness. Disadvantages are those inherent to all carbon–carbon applications, cost and oxidation. Aircraft and racing cars use carbon–carbon friction materials to obtain improved performance at lower weight than a metal alternative. The low density of carbon–carbon coupled with the tendency towards lower costs suggests possible applications in other forms of transport or machinery. The French have already tested such systems on their TGV Atlantique high-speed passenger trains. The thermomechanical stability of carbon–carbon allows it to absorb much more energy over a short period of time than a metal or organic brake. The use of carbon–carbon in emergency situations is a very important consideration. One could imagine the development of emergency brakes in high-momentum situations such as stopping trains and large road vehicles over short distances or preventing injury and damage due to the failure of lifting gear in mine shafts for example. Carbon–carbon brakes and clutches employed in military vehicles (mainly in Japan) improve airportability or allow a more

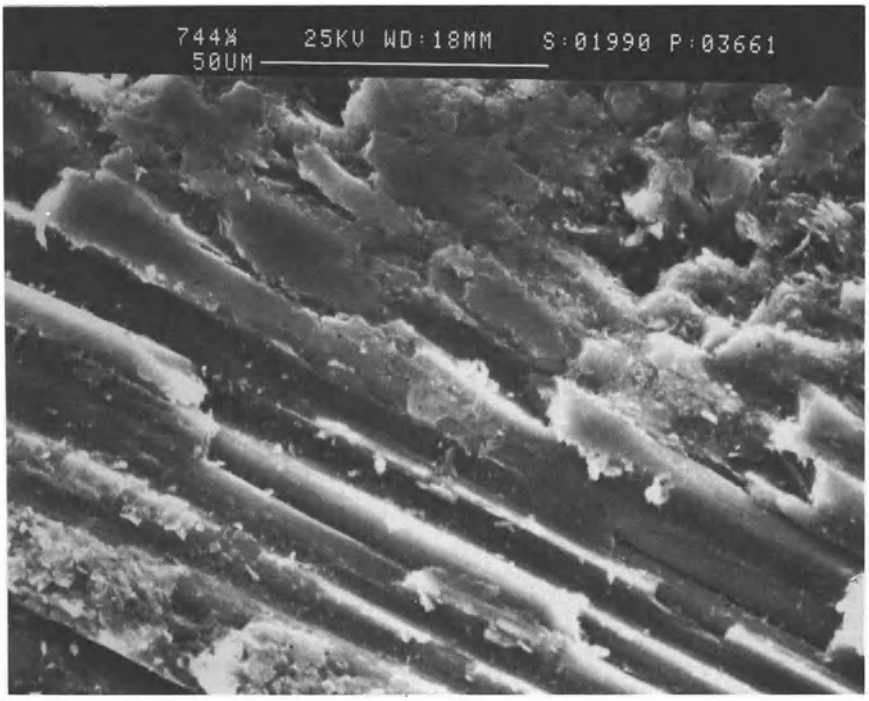

Fig. 9.20 Rougher friction surface developed in CVD brakes.

efficient distribution of the vehicle's weight into the area where it is most required, that of armoured protection. The cost of carbon–carbon would generally be considered prohibitive for use in domestic vehicles. Work has been carried out, with a degree of success, developing motor car brakes operating carbon pads on cast-iron discs [5]. It is difficult to foresee the introduction of carbon–carbon into the brakes and clutches of urban motor transport unless demanded by pollution control legislation, carbon–carbon particles being relatively harmless by comparison with the asbestos and organic materials presently used.

9.1.8 Design and optimization of carbon–carbon friction members

The firbre orientation within a carbon–carbon brake disc is determined by heat flow and structural requirements. Figure 9.22 illustrates the four criteria for preferred fibre orientation:

1. to conduct heat away from the friction surface and into the body of the disc;
2. to conduct heat radially;
3. to withstand shear forces at the drive slot;
4. to minimize the effects of the drive slot.

Fig. 9.21 Oxidation of carbon–carbon brakes occurs preferentially in the matrix phase.

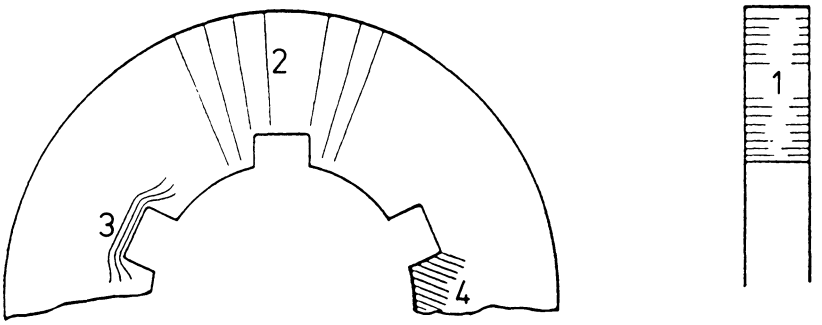

Fig. 9.22 Preferred fibre directions: 1, normal to friction surface (heat flow); 2, radially at surface (heat flow); 3, flow around notches (strength); 4, ± 45° to shear at slot (strength).

It is thus possible to identify a number of development objectives to improve the carbon–carbon composite materials.

1. an increase in thermal conductivity especially perpendicular to the friction surface;
2. an increase in the static coefficient of friction;

3. a greater strain to failure;
4. improved specific strength;
5. a reduction in costs.

One of the major reasons for adopting carbon brakes is a saving in weight. Designers are therefore reluctant to improve strength at the cost of increased weight. A critical design consideration is the material's strength in the 'fully worn' condition. An increase in specific strength is thus sought. Simultaneously, the volume of the heat sink is critical and hence a high-density composite is required which would possess the additional benefit of a higher thermal conductivity. Similarly, the use of continuous, three-dimensionally woven fibres would also increase thermal conductivity as well as specific strength and toughness. The improved toughness of a continuous fibre reinforcement network would be less sensitive to the non-uniform distribution of thermomechanical loading. An increase in the static coefficient of friction of the carbon–carbon would eliminate the unwanted high torques developed in aircraft brakes during taxiing, or racing cars when 'cold'. It is difficult to imagine, however, how this could be achieved.

Evidence suggests, then, that the optimum material configuration for brakes would be a 3-D polar weave with a high-density pitch-derived matrix. In reality, however, it is unlikely that such a material would be introduced since it would not be economically viable, costing of the order of £1000 kg^{-1} as opposed to £150 kg^{-1} for the essentially 2-D discontinuous material which, although not ideal, is adequate for the task. It is not inconceivable that such a product form will be introduced into the relatively cost-insensitive Formula 1 application, where the intrinsically more thermodynamically stable material would also alleviate oxidation problems. The brakes presently used in Formula 1 are somewhat inefficient in both materials and operation. High density 3-D material might perhaps allow later braking into corners. Furthermore, the development of a three-disc (two stators, one rotor) system along similar lines to an aircraft brake, would reduce the risk of oxidation to the friction surface, ensure a more uniformly distributed braking pressure and allow a greater friction contact surface area provided the thermal conductivity was sufficiently high to prevent overheating . The brake unit could then be packaged in a smaller configuration with a greatly reduced aerodynamic cross-section and lower inertia which would be manifest in improved acceleration out of a bend. Both discs and pads would benefit from improved oxidation protection to the non-rubbing surfaces, especially within ventilation holes.

9.2 ROCKET MOTORS

A rocket motor is essentially a venturi system, comprising a convergent portion which is embedded in the motor, a throat and an exit cone

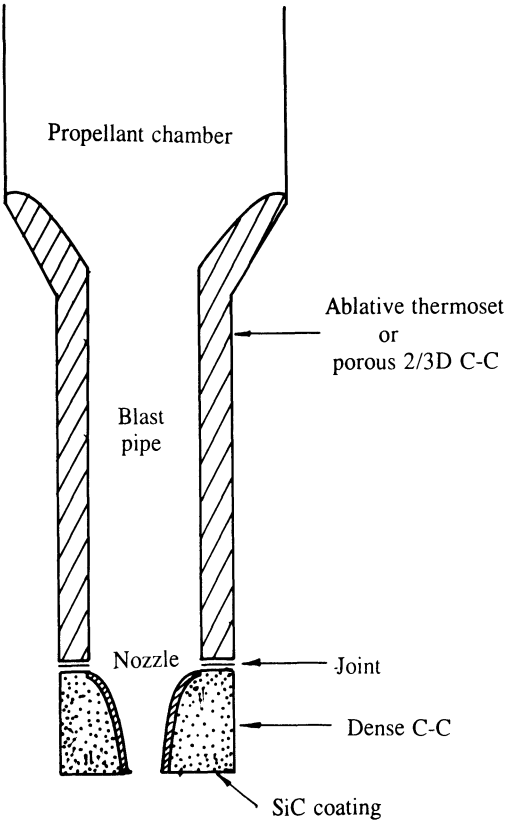

Fig. 9.23 Schematic diagram of a typical rocket motor construction.

(divergent). The exhaust gases from the propellant chamber pass out through the throat and then finally out of the exit nozzle. On average a rocket motor burns for around 30 s. The demands on the construction materials are relatively short-lived, but extremely intense. The size of components are dependent on the rocket's payload; British rockets typically possess a 75–200 mm diameter throat. The USA, of course, produce some much larger structures. A sketch of a rocket motor's construction is shown in Fig. 9.23.

Stress analysis conducted in the throat region has shown the thermomechanical loading regime to be approximately isotropic [6], thus necessitating the choice of 3-D material. A number of other concerns necessitate a preference for pitch-densified material; components are far too thick in cross-section to enable CVD to be a viable option, high-density pitch-based materials offer the best ablation resistance, mechanical stability and resistance to mechanical surface load at motor ignition. Orthogonally woven 3-D carbon–carbon has been successfully employed in rocket throat manufacture of small radius (up to a few tens of millimetres) for a number of years. Larger components require to be made from

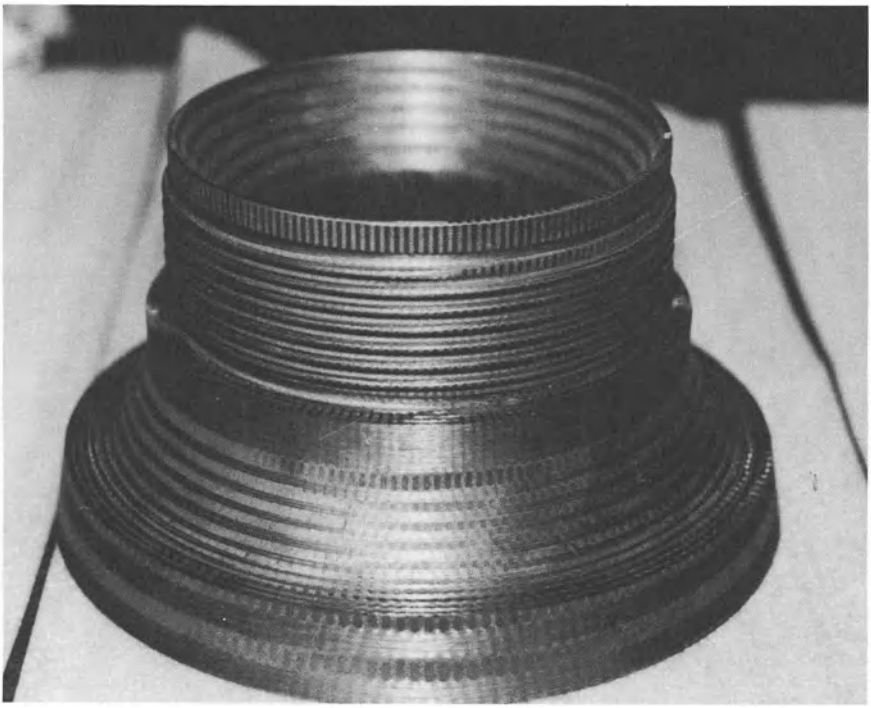

Fig. 9.24 3-D carbon–carbon ITE for nuclear missile (courtesy Hercules Inc.).

polar woven material, either machined from cylinders or contoured shapes. Components of this type have been test fired both in the USA and France since 1982. Ongoing research and development have resulted in a successive reduction in the number of parts required such that the whole of the entry and throat can now be made as a single component whereas previously, they were separate or a number of pieces. They are now integral so that gaps, joints or other weak points, which are sites for stress corrosion, are eliminated. Furthermore, there is no longer a difference in thermal expansion. Figure 9.24 shows a three-dimensionally polar woven single piece carbon–carbon throat, known as an ITE, for integral throat exit/entry. The threaded neck section is for attaching the exit cone or nozzle.

The criteria for selecting an exit nozzle material are even more stringent than those for the throat. The nozzle is generally constructed out of a dense carbon–carbon composite which may be coated with a ceramic, generally silicon carbide, to ensure good oxidation and wear resistance. It is important to note that although the burn time of the motor is relatively short, the nozzle must possess excellent dimensional stability, or else the direction of thrust cannot be properly controlled. Temperatures often

exceed 2000 °C, gas velocities are supersonic and the exit gases contain uncombusted fuel and water. Such an environment would obviously severely erode unprotected carbon–carbon composites, hence the requirement for a modicum of ceramic protection. Since rocket nozzles are not typically reused they do not necessarily require oxidation protection and may be allowed to burn partially. This burning must, of course, be taken into account at the design stage.

Dense carbon–carbon is preferred because of its superior ablation resistance. A number of companies operate the HIPIC process to manufacture the rocket motor components. These include Morton Thiokol [7], FMI, who also supply the UK's MoD with their carbon–carbon requirements, RTAC, Aerospatiale and Textron. The open literature reports the use of 2-D carbon–carbon exit cones in the USA, but such material may delaminate during manufacture and results in poor interlaminar properties and hoop strength.

The French aircraft company, Aerospatiale, have been involved in carbon–carbon composites since 1968. In order to compete successfully in the world market, the company has an industrial agreement with the carbon specialists Le Carbone-Lorraine under which they manufacture a family of products under the Aerolor banner. Aerospatiale are arguably the world leaders in the weaving of 3-D preforms. Their automated technology has been licensed to Hercules in the USA who produce rocket motor components in a joint venture with Rohr Industries under the name RTAC (Figs 9.25 and 9.26). Both Hercules and Aerospatiale produce 3-D parts up to 1200 mm in diameter for use in advanced missile systems such as Trident II.

9.3 HEATSHIELDS FOR RE-ENTRY VEHICLES

When a rocket blasts into space with velocities exceeding 17 000 mph (27 000 km h^{-1}) the heat generated at the leading edges can lead to temperatures as high as 1400 °C. Re-entry temperatures can be even higher, approaching 1700 °C, and well beyond the operation temperatures of metals [7]. Figure 9.27 shows a temperature profile across the surface of a trans-atmospheric space vehicle (such as the space shuttle) during re-entry. On a weight-for-weight basis, carbon–carbon can endure higher temperatures for longer periods of time than any other ablative material. Thermal shock resistance permits rapid transition from −160 °C in the cold of space to close to 1700 °C during re-entry without fracture. Although the space shuttle is perhaps the most well known example of a carbon–carbon re-entry heat shield, the greatest number of parts produced are used in the nose cones of ballistic missiles. All the British, French and American strategic nuclear missiles employ carbon–carbon heat shields which provide ablation and

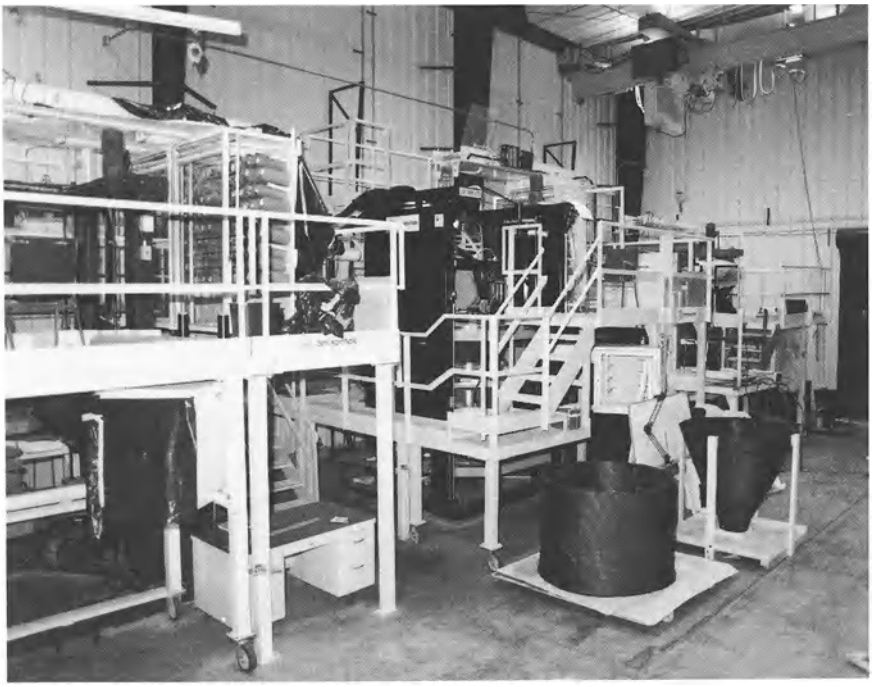

Fig. 9.25 Automated 3-D weaving facility producing fibre preforms for carbon–carbon rocket parts (courtesy Hercules Inc.).

heat resistance within a structural member. The primary purpose of the shield is to protect the crew (in the case of a manned vehicle) or instrumentation from the searing heat of re-entry.

The loading on a nose cone during re-entry is such that 3-D carbon–carbon is the most convenient material. The surface temperature rise occurs almost immediately the vehicle enters the earth's atmosphere. The thermal conductivity of the graphitic 3-D carbon–carbon is high enough to eliminate thermomechanical surface overload and avoid surface cracking. Additionally, the specific heat is so high that the component operates as a heat sink, absorbing the heat flux without any problems. The rate of ablation/erosion, driven by the air speed, depends critically on the grain size of the material. HIPIC-densified products are characterized by their fine grain morphology and low levels of porosity and are thus exceptionally ablation resistant. A problem arises, however, in constructing large-scale components such as those used in the leading edges and nose cone of the shuttle. Despite being the superior choice, 3-D HIPIC-fabricated materials, as we have discussed in previous chapters, are limited in the size that can be produced. It is not possible to make large thick pieces by CVD, so the only route available is that using thermosetting resins. The nose cone and leading edge of the space shuttle are formed from 2-D

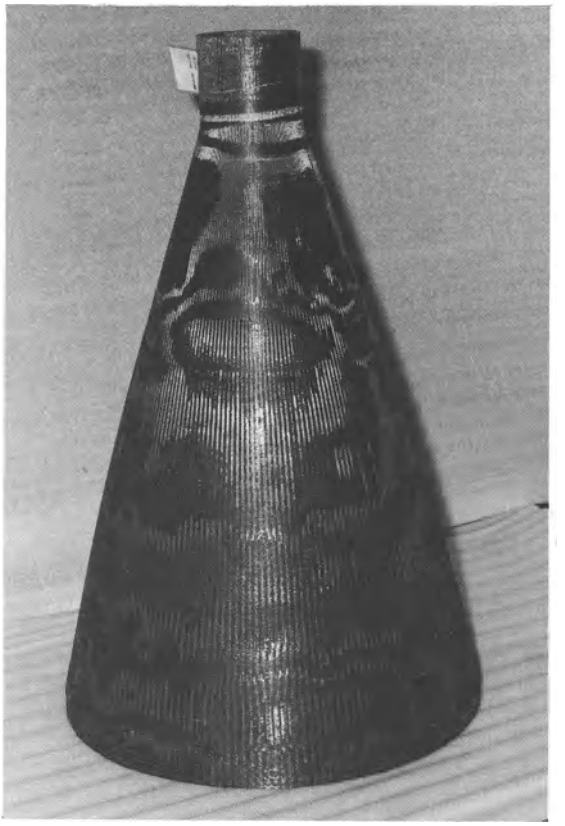

Fig. 9.26 Carbon–carbon rocket exit cone (courtesy Hercules Inc.).

carbon fabric impregnated with phenolic resins carbonized to around 1000 °C. Reimpregnation is carried out using furan or furan/pitch blends, and usually around four cycles are required. Figure 9.28 illustrates some of the re-entry loads on a typical ballistic warhead and a comparison between carbon–carbon and steel [6]. The superiority of the former is very obvious, especially in terms of ablation resistance and low density. Carbon–carbon re-entry vehicles are generally protected against oxidation, especially if, as in the case of the shuttle, the parts are designed to be reusable. Some warheads are, however, left unprotected with a controlled ablation input into the design calculations as this is believed to stabilize the missiles' flight path.

9.4 AERO-ENGINE COMPONENTS

The thermodynamic efficiency of heat engines such as gas turbines is greatly improved with an increase in operating temperature. There is therefore a

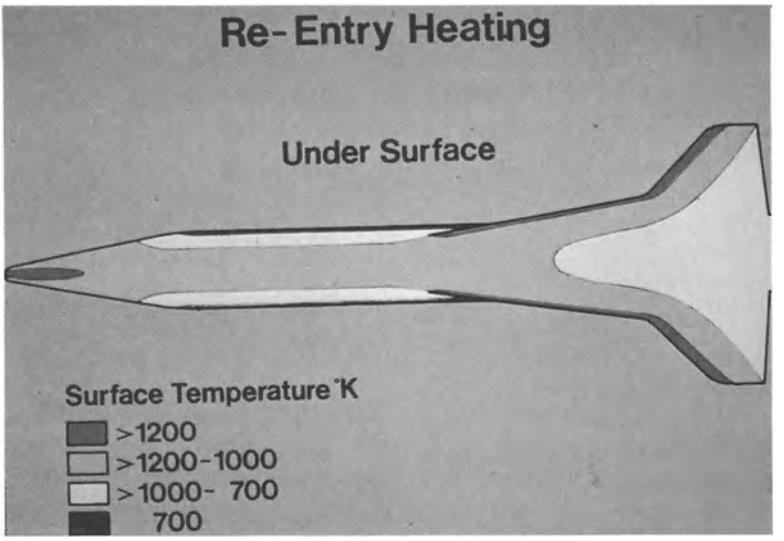

Fig. 9.27 Re-entry temperature profile across a transatmospheric space vehicle.

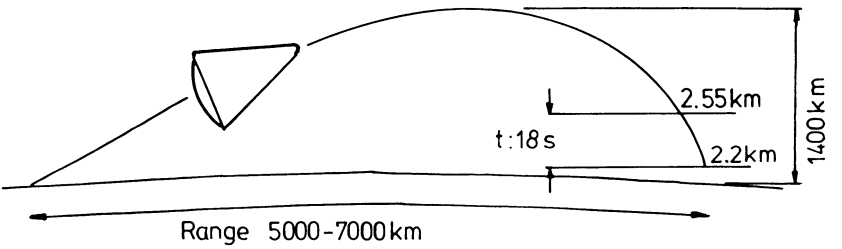

	Carbon/carbon	Steel
Wall temperature (°C)	3200	1500
Max flux (MWm^{-2})	65	80
Average flux (MWm^{-2})	15	35
Ablation ratio	1	7.5
Density(gcm^{-3})	2	7.8

Fig. 9.28 Material behaviour during re-entry.

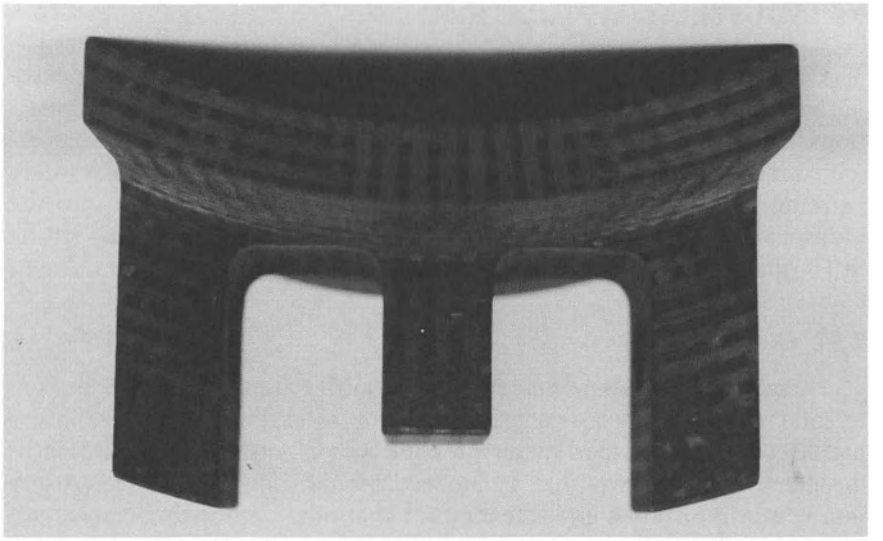

Fig. 9.29 3-D woven carbon–carbon jet engine component (courtesy Hercules Inc.).

driving force to develop carbon–carbon jet engine components. For the same power output the engines could then be made smaller, lighter and more fuel efficient. The toughness, most especially in impact, of carbon–carbon is two orders of magnitude greater than conventional ceramics. Jet engine motors can be made in single-piece format from carbon–carbon, thus saving fabrication and assembly costs. A number of countries are aiming to develop hypersonic aircraft over the next decade, capable of flying at speeds of up to mach 5. Carbon–carbon might well, therefore, be chosen as a structural material in the aircraft's basic airframe. In terms of properties, carbon–carbon is the ideal choice for hot engine components; its exploitation, though, is extremely limited due to the problems of oxidation. Until protective coatings, capable of withstanding extreme thermal cycling in aggressive oxidative atmospheres, are developed it is unlikely that the promise of carbon–carbon will ever be achieved in the theatre of jet engines. A number of materials producers are involved in joint venture research programmes with aero-engine manufacturers and a selection of prototypes have been made. To date, however, none has succeeded in fabricating a suitable flying component. In view of the high toughness requirements, it ought to be more likely that the 3-D configuration be preferred (Fig. 9.29). Having said that, production difficulties and costs may dictate a simple 2-D structure will be the first to be exploited.

9.5 INDUSTRIAL APPLICATIONS

The high price and secrecy surrounding carbon–carbon materials have in the past tended to restrict their use to aerospace and military applications. Commercial products do exist, however, such that there is an ever-increasing industrial exploitation of carbon–carbon, generally in areas where extreme heat would quickly destroy other materials. Research into the industrial applications of carbon–carbon components is especially strong in Germany [8].

9.5.1 Glass making

The machinery used to manufacture glass bottles dispenses a small amount of molten glass known as a 'gob'. The gob rolls down a channel into a mould where it is shaped by air pressure into a bottle. The equipment is designed in such a way that a damaged mould can be identified. A gob interceptor rejects the gob intended for that mould, diverting it so as not to clog up the machinery. Carbon–carbon gob interceptors, although approximately 100 times more expensive than the asbestos they replace, result in fewer replacements and less frequent shutdowns and so are exceptionally cost-effective. The two-dimensional carbon–carbon is inherently less bio-hazardous than the asbestos, and also acts as a heatshield protecting the underlying metallic components.

9.5.2 High-temperature mechanical fasteners

The tensile strength of most ceramics in, and refractory metals and alloys above 750 °C, is extremely poor. Hence mechanical fixing at high temperatures is often a cause of severe problems in engineering design. Screws, nuts and bolts, etc. made from carbon–carbon experience no loss in strength at high temperatures. The load-bearing ability of carbon–carbon is less than that of metals at low to moderate temperatures but a superior at high temperatures. Carbon–carbon nuts and bolts are shown in Fig. 9.30.

9.5.3 Hot press dies

High-quality ceramics and metals may be produced by sintering under mechanical pressure in a hot press operation [9]. The traditional material used in die manufacture is polycrystalline graphite. Such dies are required to be of considerable wall thickness due to the poor mechanical properties of the graphite. Carbon–carbon dies are specifically designed with high hoop strengths so as to reduce considerably the size of component required. A carbon–carbon die of, for example, 130 mm ID need only have a wall thickness of 15 mm. One may thus achieve shorter heating cycles and a more uniform temperature distribution in the hot pressed product [10].

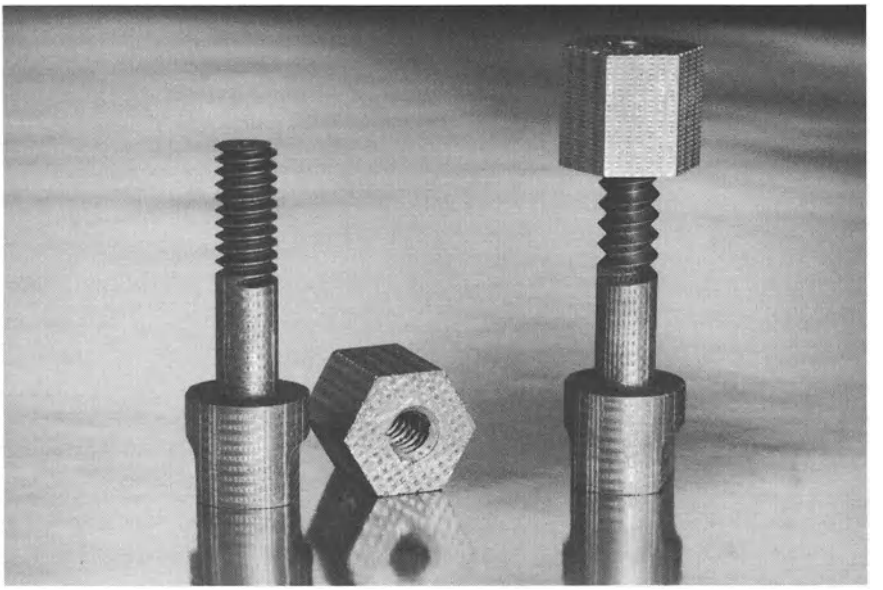

Fig. 9.30 High-temperature carbon–carbon fasteners (courtesy Hercules Inc.).

9.5.4 Hot gas ducts

High-temperature strength and resistance to thermal shock and temperature gradients make carbon–carbon tubes an ideal choice as the liners in the hot gas ducting in high-temperature nuclear reactors [11].

9.5.5 Furnace heating elements and charging stages

Furnaces operating between 1000 and 3000 °C in a non-oxidizing atmosphere tend to use graphite heating elements. The brittleness and moderate strength of graphite make such elements extremely difficult to handle and damage susceptible, especially considering the complex geometries often required. Carbon–carbon elements are far less fragile and are a considerable advantage in hot isostatic pressing equipment as only a small volume is needed, thus maximizing the working zone. Aside from its mechanical property advantages, the higher electrical resistance of carbon–carbon permits higher power operation and less voluminous electrical connections.

Charging stages allow a more effective use of furnace heating volume. Such stages have historically been produced from refractory alloys, ceramics or graphite depending upon operating temperature. The use of lightweight impact-resistant carbon–carbon serves to save volume and increase the lifetime of these stages. The lower thermal mass of the carbon–carbon component increases process efficiency and greatly reduces heating and cooling cycle times.

9.5.6 Moulds for forming superplastic metals

Superplastic forming of metals is a relatively new and extremely versatile route to the fabrication of complex shaped components especially in the aerospace industry. Titanium alloys in particular require temperatures in the region of 1000 °C and pressures of several atmospheres. Carbon–carbon moulds offer significant improvements over their 'opposition', mild steel. Being two orders of magnitude lighter their reduced thermal mass affords shorter processing cycles and much easier handling. Further, the negligible thermal expansion of carbon–carbon results in greater tolerances and eliminates folding of the titanium insert.

9.6 BIOMEDICAL DEVICES

Elemental carbon is known to have the best biocompatibility of all known materials [12]. It is compatible with bones, blood and soft tissue. The high cost of carbon–carbon compared with its competitors, be they metallic or polymeric, in the biomedical field may at first glance preclude its use. Consider, however, a rigid metal plate as frequently used in the repair of fractures. Such a device when firmly attached to a long bone such as the femur, will inevitably result in an altered stress distribution. The modulus of the bone is generally an order of magnitude lower than, say, a stainless steel plate of roughly the same cross-sectional area [13]. A plate made from this alloy will transmit around 90% of the load causing the underlying bone to become porotic. It is thus paramount that such plates be removed as soon as the fracture has healed. Failure to do so would most likely result in a spontaneous refracture at some later date.

Thus, although metals possess the required strength and toughness for use during the healing phase, they are far from satisfactory. With operating theatre charges running at around £10 000 per day, surgeons and hospital administrators would much prefer to avoid the second operation. Patients too would certainly wish to forgo the further trauma associated with the removal of the prosthesis. Carbon–carbon can be engineered in such a way as to possess mechanical properties identical to those of bone (Fig. 9.31), thus eliminating the need for removal once the healing is complete. There is a considerable interest in materials such as carbon–carbon, which are considered to be 'bio-active', in many areas of implant surgery. The objective is to use a material which is able to encourage the formation of bone rather than soft tissue at the interface. Carbon–carbon has been shown experimentally to be biodegradable in such applications – the body gradually replacing it with bone [7].

For obvious reasons, licenses to allow the use of materials take a long time to obtain. As a result the biomedical uses of carbon–carbon are very

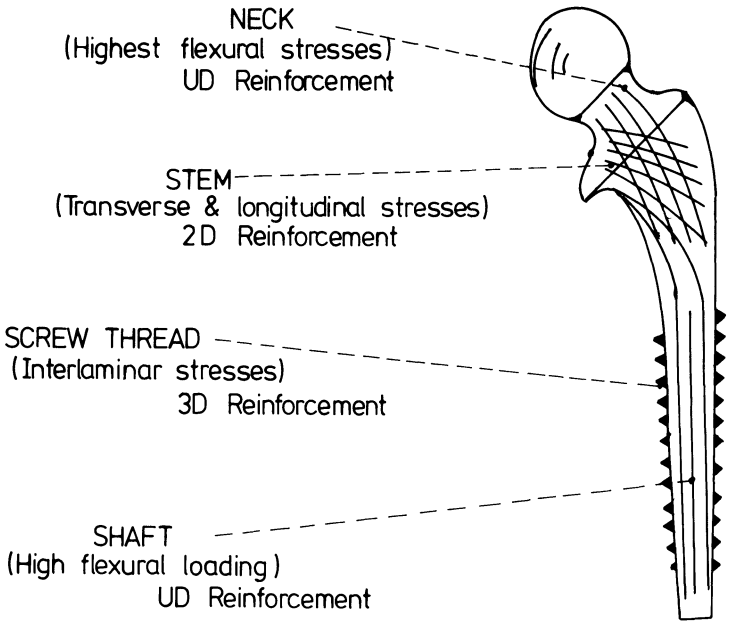

Fig. 9.31 Schematic diagram of carbon–carbon hip joint replacement designed to imitate the femur structure.

limited. There are reports in the literature, however, of its use in artificial hearts for animals [12], fixations for carbon fibre artificial ligaments [14] and bone plates in osteo-synthesis and as endoprosthesis [15].

9.7 SUMMARY

The most widespread use of carbon–carbon materials is in brakes. The rapid deceleration required for an aircraft on landing generates a considerable amount of frictional heat. Carbon–carbon composite brakes retain strength at high temperatures. Unlike steel brakes, carbon–carbon brakes maintain a more consistent performance over the life of the part, with no increase in stopping distance. The CTE of carbon–carbon composites remains fairly constant over a broad temperature range. Carbon–carbon has a high heat capacity so it can act as a lightweight heat sink. The material will slide against itself without galling, resisting wear and outlasting steel brakes 2 : 1. The lower wear rate means fewer overhauls and lower maintenance costs. Carbon–carbon brakes can endure thousands of thermal cycles with little or no fatigue. The brakes weigh far less than their metal equivalents, saving up to 800 kg on a Boeing 747. They are less prone to warping than metal and in racing cars carbon–carbon can reduce stopping distance by up to 30% compared to metal.

In a rocket throat and nozzle, hot gases rush through at high velocity, stressing and eroding the walls. A carbon–carbon composite will resist high-temperature erosion and abrasion without burning away. Rocket nozzles are typically not reused, so that they do not always require oxidation-protective coatings. They are thus allowed to burn partially. This burning must, however, be taken into account in the design of the part. In the past, the rocket motor entrance and throat were made up of a number of pieces. They are now integral such that a single-piece component is now the norm. This eases fabrication and eliminates the gap, joint or weak point, which is a site for stress corrosion. Further, there is no longer a difference in thermal expansion. Similar to a rocket nozzle, the nose cone and leading edge of the space shuttle and the heatshields of ballistic missiles must endure the searing heat of re-entry, up to 1700 °C. They must also endure solar radiation and the attack of atomic oxygen.

The USA and France have spent large sums on the development of carbon–carbon for military uses. In Germany the market focuses on the industrial applications of the material, albeit at a lesser stage of development. Carbon–carbon is widely used in glass bottle manufacture as push-outs, wear guides and transfer pads, in contact with the molten glass. It is not melted by molten glass and does not wet or require external cooling liquids. Its long life reduces maintenance and replacement costs. Other applications include hot press dies and heating elements.

The nuclear industry is interested in carbon–carbon for fusion reactors since it resists ultra high temperatures and thermal shock. If used in automotive pistons, carbon–carbon's low coefficient of friction would reduce drag and its light weight would increase engine efficiency. Higher combustion temperatures permit greater efficiency and performance while reducing engine size, weight and fuel consumption. In long-term engine use, most especially gas turbines, a ceramic coating for carbon–carbon is essential. The coating itself does not bear structural loads but it must adhere to the substrate to transfer loads.

Finally, because of its extremely good biocompatibility, controlled porosity and attractive Young's modulus which can be tailored to be close to that of bone, it is of interest as a replacement for metals used in implant surgery.

REFERENCES

1. Fisher, R. and Stimson, I. L. (1980) *Phil. Trans. R. Soc. Lond.*, **A294**, 583.
2. Awasthi, S. and Wood, J. L. (1988) *Ceram. Eng. Sci. Proc.*, **9**(7–8), 553.
3. Shigley, J. E. (1987) *Mechanical Engineering Design*, McGraw-Hill, New York.
4. *SEPCARB Brakes Assistance Manual*, Carbonne Industry France.
5. Fitzer, E., Fritz, W., Gkogkidis, A. and Mörgenthaler, K. D. (1986) *Proc. Carbon 86 Conf.*, Baden-Baden.

6. Grenie, Y. (1987) in *Looking Ahead for Materials and Processes* (eds J. de Bossu, G. Briens and P. Lissac, Elsevier, Amsterdam, p. 377.
7. Klein, A. J. (1986) *Adv. Mat. Process. Inc. Met. Prog.*, **130**(5), 64.
8. Von Gellhorn, E. (1986) in *HI-Tech – The way into the nineties* (eds, K. Brunsch, H. D. Gölden and C. M. Hekert), Elsevier, Munich, p. 67.
9. Richerson, D. W. (1982) *Modern Ceramic Engineering*, Marcel Dekker, New York.
10. Hütner, W. (1985) *Andernach*, **29**, Oct.
11. Von Gellhorn, E. and Grüber, H. (1986) *Proc. Carbon 86 Conf.*, Baden-Baden.
12. Lamicqe, P. J. (1984) *SEP Int. Carbon Conf.*, Bordeaux, France.
13. Williams, D. F. (1981) *Metals and Materials*, **7**(1), 24.
14. Burri, C. and Neugedauer, R. (1985) *Replacement of Ligaments by Carbon Fibres*, Springer-Verlag, Munich.
15. Claes, L. Fitzer, E. Hüttner, W. and Kinzl, K. (1980) *Carbon*, **18**, 383.

Technology Summary and Market Review

10

10.1 SUMMARY

Carbon–carbon composites consist of carbon fibres in a carbon matrix. The fibres may be chopped, continuous or woven and may be produced from rayon, polyacrylonitrile (PAN) or pitch (mesophase or isotopic). The carbon matrix may be deposited by chemical vapour deposition (CVD), by the carbonization of a thermosetting or thermoplastic organic material or by a combination of these. The result is a family of composites whose microstructures and properties may be multi-dimensionally tailored to a great degree for a range of applications. Unlike metals and ceramics, carbon–carbon composites retain their strength at very high temperatures. High thermal conductivity and low thermal expansion give carbon–carbon materials an excellent resistance to thermal shock. A high heat of sublimation and low CTE for carbon and graphite result in good ablation resistance. Other advantages include chemical resistance, excellent high-temperature wear characteristics, biocompatibility, shape stability and pseudo-plastic fracture behaviour.

High specific strength at high temperatures, excellent fracture toughness and thermal shock resistance have resulted in carbon–carbon composites finding use as aircraft and racing car brakes, heatshields for re-entry vehicles and rocket nozzles. All of these applications require the retention of properties to high temperatures. The excellent thermal shock resistance of carbon–carbon is, perhaps, best illustrated by rocket nozzles which can withstand a change in temperature from ambient to almost 3000 °C in the first few seconds of a missile launch. When carbon–carbon materials do break, they generally undergo a non-brittle, pseudo-plastic, type of fracture rather than catastrophic failure.

The deployment of carbon–carbons, despite their attractive properties, is severely limited, however, by two serious drawbacks. The materials are

extremely expensive to produce as a result of the very slow and inefficient processes currently used in the production. Furthermore, carbon–carbon composites oxidize at temperatures as low as 400 °C unless protected in some way. Oxidation is not such a great problem in limited-life components such as nose cones and rocket nozzles of military ordnance. The brakes of aircraft and racing cars are prone to oxidation in service but this can be minimized by design, and refurbishment after predetermined increments of time. When used for furnace insulation and heating elements the atmosphere is non-oxidizing, although they are attacked by high-temperature nitrogen. Oxidation is a serious problem in potential applications such as jet engine parts and reusable transatmospheric vehicles, requiring thermal cycling in oxygen-containing atmospheres. A great deal of research has been carried out and is ongoing into the protection of carbon–carbon using various coatings and inhibitors. As yet, however, no materials system has been sufficiently successful to allow in-service deployment in jet engines. In addition to the major problems of oxidation and cost, carbon–carbons exhibit low strain to failure, poor matrix properties, poor erosion resistance, lack of resistance to attack by moisture, and severe difficulties with joining. The properties of all carbon–carbon composites are influenced by the type, volume fraction and orientation of the fibres, the matrix microstructure, the method and conditions of processing, oxidation-protective coatings and inhibitors and any other additives.

10.2 THE STATE OF THE ART

10.2.1 Carbon fibres

As is generally the case with advanced composites, the mechanical properties of carbon–carbon composites are dominated by fibre properties and orientation. Most carbon–carbon composites are reinforced with continuous carbon fibres, so that their in-plane strength and stiffness are determined by the fibre strength and modulus, weave or lay-up geometry and fibre volume fraction.

The first carbon–carbons used rayon-based fibres, although their use is now limited to between 5 and 10% of the market as they have been largely superseded by the cheaper and superior PAN-based fibres. Rayon-based firbres are lighter ($\rho = 1.45$ g cm^{-3}) than PAN fibres and have higher CTEs than either PAN or pitch fibres. The disadvantages of rayon fibres are higher processing costs than PAN, lower strength and modulus, and severe shrinkage during heat treatment. Mesophase pitch-based fibres, which are more expansive and often possess higher moduli than PAN fibres, are widely used in aircraft brakes and non-aerospace applications. They do, however, exhibit lower strengths than PAN fibres.

Chopped fibres are used extensively in brakes and industrial applications. The composites thus formed offer considerable improvements in strength and toughness over monolithic carbons for relatively little added cost. The properties of chopped-fibre composites are not enhanced by fibre loadings in excess of 25% by volume. A number of brake manufacturers claim short fibres produce more uniform frictional properties which improve performance, although no data have been presented to substantiate this.

The purity of the fibres is of prime concern when the composites are used to make missile components. In such applications the fibres require to be greater than 99% carbon and contain less than 20 ppm of sodium and other alkali metals. Alkali metal flames result in an easily detectable signature from a rocket that may be readily discerned by an enemy's sensors. Furthermore, alkali metals catalyse the oxidation of carbon–carbon, thus decreasing the life.

The fracture toughness of a carbon–carbon composite is due, in part, to the deflection of cracks running through the matrix at the fibre/matrix interface as a result of the imperfect bonding therein. The sizing compounds, weaving lubricants and any other materials added to the surface of the fibres for ease of handling are generally removed prior to fabrication in order to avoid compromising the optimum bonding level. Crenulated or ribbed carbon fibres, such as those made from rayon, aid mechanical bonding or 'keying' of the fibre to the matrix, and often result in improved out-of-plane properties such as interlaminar shear strength.

The maximum use of the mechanical properties of the fibres is achieved by keeping them straight. Although some unidirectional (UD) fibres are used in carbon–carbon composites, the overwhelming majority of techniques employ woven fabric reinforcement. Fabrics only provide a two-dimensional plane of reinforcement, and for this reason the composites are referred to as 2-D composites. Should strength be required in three dimensions, fibres may be woven together in a 3-D configuration. It is customary to describe a three-dimensional weave in terms of the number of different **directions** in which the fibres are woven. The accepted nomenclature is n-D where n represents the number of directions. Clearly, as n increases so will the complexity of the weave, the cost of production and the difficulties in densification. The addition of multiple directions of reinforcement will of course proportionally reduce the strength in the primary x–y planes of the composite.

Lower modulus fibres are much easier to weave into fabrics or preforms. High modulus fibres have a tendency to break in the loom as a consequence of their low strain to failure. The cost of weaving tends to vary with the fibre properties, complexity of weave, the amount of material to be processed, fabric width and length of production run. Weaving is a relatively expensive process and may increase the price of the fibres by up to a factor

of 2 or 3. Three-dimensional weaving is very costly and can raise the cost of fibres by up to an order of magnitude. Ongoing research into automation, computer control and better weaving processes ought to reduce weaving costs. One would expect most of the reductions to arise in the three-dimensional sector since a great deal of work has already been done in two-dimensional weaving for the polymer composites industry.

10.2.2 The carbon matrix

The purpose of the carbon matrix is to hold the fibres in place and transfer the applied load to the fibres. The matrix controls the out-of-plane properties and, to a degree, the off-axis properties of the composite. Those properties depend upon the matrix precursor and the processing conditions. Possible precursors include pitches, thermosetting resins and hydrocarbon gases. Fractionated, modified pitches have carbon yields of up to 90% and are easily graphitized. Carbons thermosetting from resins are difficult to graphitize, and develop local graphitic structures. Crystalline graphite has very high strength in one plane, while strength in the other directions is low. Isotropic carbons, of course, have more isotropic properties. They generally exhibit higher strengths and lower strain to failure than graphitic matrices. Higher-density graphitic carbons have a higher resistance to ablation and oxidation than isotropic matrices.

Thermoset resins do not soften at high temperature, as does pitch. They can thus be used in low-pressure impregnation processes, especially in the form of prepregs which are easy to handle and process. Pitches are relatively easy to process in high-pressure carbonization processes, but the purity and reproducibility of these essentially 'natural' materials are extremely problematic. A great deal of research has been carried out into the use of high carbon yield polymeric precursors such as polyimides, polyphenylene and acetylene-terminated resins. Such resins have, as yet, only been used on a developmental basis. These resins, while much more expensive, allow the production of carbon–carbon with fewer processing cycles, thus reducing both the cost of fabrication and the chances of damaging a component during manufacture.

The strength of a carbon–carbon material increases with the reduction of the void content during processing. It may not be desirable to fully densify the composite, however, as it has been observed that uniform small-scale porosity can be effective as crack arrestors and in the attenuation of mechanical impulses. Pitch precursors are often purified and fractionated prior to use in order to separate high carbon yield fractions and improve product quality control. The blending of pitches with thermoset resins is often used to control grain size and degree of transformation from carbon to graphite.

10.2.3 Manufacturing processes

Chemical vapour deposition

Carbon fibre felts, 3-D preforms and porous 2-D carbon–carbon structures may be densified by chemical vapour deposition (CVD). In the CVD technique, the artefact is placed in a furnace where its pores are filled with carbon. The carbon is produced from the thermal decomposition (cracking) of a hydrocarbon gas, usually methane. Hydrogen is often added as a diluent in order to facilitate processing. As a general rule of thumb the carbon deposited at around 1100 °C has an isotropic structure and is referred to as pyrolytic carbon. Between 1000 and 1700 °C the carbon deposited has an 'intermediate' microstructure which becomes more graphitic with increasing temperature. Carbon deposited between 1700 and 2300 °C is graphitic in nature and known as pyrolytic graphite.

CVD carbon–carbon can have superior properties to composites made by any of the other routes as the matrix is built up layer by layer, thus ensuring good fibre/matrix bonding and minimizing the number of defects in the structure. CVD carbon–carbon often has a high degree of porosity, however, leading to low strength. A further advantage of the CVD process is that it can also be used to deposit non-carbon materials such as oxidation-protective coatings and inhibitors. Subtle changes in processing conditions enable the deposition of carbonaceous material of differing mechanical properties and oxidation resistance. However, CVD is an extremely slow and, therefore, expensive process requiring considerable operator skill. Processing conditions (temperature, system pressure, diluent partial pressure and gas flow rates, etc.) and even the placing of the component within the furnace all affect the manner in which the carbon is deposited. If the aforementioned conditions are not correctly achieved and controlled, the surface of the structure will overcrust, producing a weak, low-density area in the centre. In commercially operated processes it is generally necessary to compromise between an ideal system and one in which the rate of carbon deposition occurs at an economically viable rate. Consequently, parts usually require to be periodically removed from the furnace and the surface machined to open up the inner pores; the whole process commonly takes several months for completion.

Low-pressure carbonization of thermosetting resins

The low-pressure, thermoset, process commences with the lamination of a carbon fibre reinforced polymer structure using the techniques developed for the fibre-plastic composites industry. The resins are cured, usually in an autoclave, followed by a post-curing cycle to finish chemical cross-linking and expel any remaining volatiles. The composite is subsequently carbonized in an inert atmosphere at around 850–1000 °C, in a process that

may take up to a week. Following pyrolysis, the part may be further heat-treated depending upon its final operating temperature or required density. The most commonly used impregnating resins, phenolics and furans, have carbon yields of only 50–60% by weight. A number of higher-yield resins have been researched, but, to date none, have been commercialized because of problems such as excessive cost and processing difficulties. The part must therefore be reimpregnated, pyrolysed and heat-treated often three, four or more times before its final density and properties are achieved.

Reimpregnation/densification may be attained using more resin, a pitch/resin blend, CVD or a combination of these. The thermoset resin process is considerably cheaper than the CVD technique but the composites formed are sometimes of poorer quality. Relatively little initial capital investment in equipment is required and the techniques perfected in the polymer composites industry may be successfully transferred and modified to allow the production of large and complex structures. The technique is, however, labour intensive, especially in the laying-up of laminates, and again requires a good degree of operator skill and experience. Chopped fibres, impregnated with a thermoset, may be compacted in a die and heated to cure the resin. The part may then be removed from the die, then carbonized, graphitized and reimpregnated as required. Carbon–carbon made in this way is used in brake manufacture and in relatively inexpensive industrial applications such as dies for hot pressing.

High-pressure impregnation/carbonization using pitches and thermoplastic resins

In the hot isostatic pressure impregnation carbonization (HIPIC) technique, a 3-D woven fibre preform is impregnated with a thermoplastic resin or pitch and loaded into a processing can with excess matrix precursor. The can is evacuated and sealed and placed in a specially designed hot isostatic press (HIP) unit. The workpiece is heated so that the precursor (usually a pitch) melts and flows. Pressure is applied, by an inert gas via the sealed can, which forces the pitch into the pores of the preform. The artefact is then carbonized by increasing the temperature and pressure. The carbonized billet may, if required, be subsequently graphitized. Impregnation, carbonization and graphitization are repeated until the desired properties are achieved. Generally fewer cycles are required to process to the equivalent density than with the low-pressure technique owing to the higher carbon yields and the higher density of pitch carbon/graphite. Typically three to five cycles are used for the production of high-density materials ($\rho > 1.95$ g cm^{-3}).

The problems incurred in the HIPIC process include fibre distortion and breakage during processing and the inability to impregnate large structures. The difficulties arise from ineffective filling of the pores in the initial

preform, or partially densified substrate, with the molten pitch. Design limitations require carbonization and graphitization to be performed in separate furnaces. The size of articles which can be manufactured is also restricted to less than 2 m in diameter as the result of furnace technology limitations. HIPIC is, of course, extremely capital intensive because the high-temperature and high-pressure equipment required is very expensive, coupled with the need for materials handling equipment and safety requirements.

High-pressure carbonization without the need for metal cans may be carried out using 'exotic' thermoplastic resin precursors. These materials produce carbon–carbon composites with a unique range of microstructures but are prohibitively expensive. It is difficult to imagine, therefore, the widespread deployment of such materials except in very high added value products such as biomedical devices, space structures and fasteners. Chopped-fibre versions of such composites may be of value in brake systems as they represent a useful outlet for scrap recovery from their polymeric 'ancestors'.

10.2.4 Oxidation protection

The properties of carbon–carbon composites make them attractive for use in a great number of applications. Their usage to date has been restricted by high costs, poor matrix properties and high temperature oxidation. At the time of writing, only about 10–15% of carbon–carbon composites are protected from oxidation, but this is an area where a great number of market opportunities will arise should the technological problems be solved.

The rate at which carbon is oxidized depends upon temperature, oxygen partial pressure and the microstructure of the carbon. Oxidation of carbon starts at around 400 °C. Graphitic carbon with its denser, crystalline structure and lower proportion of reactive edge sites, does not begin to oxidize until slightly higher temperatures. Generally, a graphitic matrix microstructure will add between 50 and 100 °C to the onset of oxidation. Higher temperatures and partial pressures of oxygen result in faster oxidation rates.

Carbon–carbon composites are protected against oxidation by the use of refractory ceramic coatings and inhibitors which are generally glass-forming materials.

Oxidation-protective coatings

The coating process aims to protect carbon–carbon from oxidation by ensuring that it does not come into contact with high-temperature oxygen. The most common oxidation-resistant coating materials are silicon ceramics which are effective below 1700 °C. The coatings may be applied by a number of techniques such as pack cementation, CVD and thermal spraying. One of the most notable, coating process used to date is that developed by

Table 10.1 Thermal expansion coefficients for selected protective coating materials

Coating	*Linear CTE* (10^{-6} K^{-1})
SiO_2	0.55
SiC	4.3
Si_3N_4	3
Al_2O_3	7.5
$3Al_2O_32SiO_2$ (mullite)	5
TiC	9
TiB_2	8.5
ZrO_2 (partially stabilized)	10
Carbon–carbon	0.32–2.66

LTV missiles to protect the leading edges and nose cone of the space shuttle. The pack cementation process is executed by immersing the composite in a bed of silicon carbide, alumina and silicon powders. The bed is heated in an inert argon atmosphere to 1760 °C in order to allow a diffusion reaction between the silicon vapours and the carbon–carbon which converts the composite's outer layers to SiC. In the LTV technique, the coated component is subsequently impregnated with tetraethyl orthosilicate (TEOS) which is hydrolysed and heat-treated to produce a silica (SiO_2) residue within the coating. Any remaining surface inhomogeneities such as cracks and pores are sealed using a sodium silicate–silicon carbide mixture to produce a final coating, roughly 0.5 mm thick. A number of organizations such as GA Technologies have used CVD techniques to apply SiC and silicon nitride (Si_3N_4) coatings. These materials, along with boron nitride, are applied in layers of which a minimum thickness of 0.2–0.6 mm is required to afford adequate protection.

Silicon ceramic coatings provide protection by reacting with oxygen at high temperatures to form silica. The liquid silica flows into cracks in the coating and seals them. Unfortunately, below 1000 °C the carbon–carbon substrate is very prone to oxidation because the silica is too viscous to flow into the cracks and does not wet the carbon very well. Furthermore, thermal cycling and impurities may result in devitrification of the silica. Devitrification is a phase transformation which increases the rate of oxidation and causes the coating to lose strength and crack. The major problem with the materials used to coat carbon–carbon is that their CTEs are generally much higher than that of the substrate (Table 10.1). Under extreme thermomechanical loading it is obvious that two materials of very different CTE will eventually 'part company', resulting in spallation of the coating. Certain carbon–carbon composites will be easier to coat than others since the materials may have significantly different CTEs depending on

the type of fibre and matrix. Unfortunately it is the high strength and high modulus composites, which are the most attractive for structural purposes, that are the most difficult to coat. Finally, care must be taken to ensure that processing and operating temperatures are not high enough to allow a carbothermic reduction reaction between coating and substrate to take place which would reduce the mechanical properties of the composite.

Inhibitors

Inhibitors are glass-forming materials used to protect carbon–carbon in the intermediate temperature range (450–1000 °C). Boron, silica and oxygen form borate glasses that will flow into cracks at these relatively low temperatures. Unlike silicates, borate glasses wet and adhere well to carbon fibres. Inhibitors such as boron, zirconium boride or silicon carbide powders may be added to thermoset resins prior to prepregging, or may be placed in a porous substrate by impregnation with a pre-ceramic polymer during densification or by chemical vapour infiltration (CVI). All are oxygen 'getters', forming molten borate, silicate or borosilicate glasses at high temperatures. The glasses flood into cracks and pores to prevent oxygen from penetrating the matrix. Above 1000 °C, however, oxygen will diffuse through irrespective of the method of coating. It should be noted that boron compounds can result in a decrease in composite strength by reacting with the carbon fibres to produce boron carbide at high temperatures (≈2000 °C). Additionally, boron compounds are often very brittle and may adversely affect the fracture toughness of the carbon–carbon especially when present in large amounts. A number of materials, such as lithium, zirconium and phosphorous oxides, may also be added which have the effect of lowering the viscosity of silica in the intermediate temperature range.

In addition to inhibitors, a number of other compounds have been added to carbon–carbon either to improve performance or aid fabrication. Carbon black and graphite powders are sometimes used to increase the carbon yield and reduce the pyrolysis shrinkage of thermoset resins. Milled carbon fibres have also been added to resins in order to improve the interlaminar shear strength. The milled fibres, unfortunately, tend to orientate themselves parallel to the fabric plane thus affording little, if any, improvement. Finally, some mention is given in the patent literature to the addition of ceramic powders in an attempt to improve ablation resistance.

10.3 THE CARBON–CARBON MARKET

Despite having the highest specific strength of all known materials at high temperatures, carbon–carbon composites are used in only three major

applications: aircraft and racing car brakes, rocket nozzles and heatshields for re-entry vehicles. A number of minor applications also exist such as biomedical devices, space equipment and a few specialized industrial uses. Aside from their high-temperature strength, carbon–carbon composites possess a number of other desirable properties but are dogged by two glaring weaknesses: poor oxidation resistance and expensive fabrication costs. Oxidation problems severely limit the exploitation of the relatively 'cost-insensitive' jet engine market, while costs of what is essentially an inefficient labour-intensive batch process prevent deployment in a number of non-military applications. A further problem arises in that the ambient temperature properties of carbon–carbon are very mediocre. While they are stiff, strength is relatively low. They are brittle, although they fail pseudo-plastically, and are very porous with a tendency to spallation. Operators tend to circumvent such problems by periodically replacing components as is the case with brakes, or by designing for short life spans (rocket components).

Carbon–carbon is a relatively small business area accounting for around £100m. sales in 1990. The only published market survey predicts an annual growth of roughly 11% towards £200m. at the turn of the century [1]. It should be remembered, of course, that this survey was written in 1985, i.e. prior to recent sweeping political changes in the Eastern Bloc. The great majority of carbon–carbon purchases are for military use and military technology development, many of which may be curtailed or shelved in the present political climate. One would therefore expect the demand for carbon–carbon to be somewhat less than predicted. There will, however, be a significantly increased requirement for strategic materials such as carbon–carbon from emerging nations which strive to develop sophisticated weapon systems. Exploitation of such markets by Western producers would, of course, be illegal and therefore extremely hazardous! Most carbon–carbon technology is of a strategic nature, especially in the USA. Furthermore, it is not inconceivable that those nations would choose to set up their own facilities since, as Chapter 7 shows, it is not too difficult to do so provided one is prepared to bear the initial capital investment and high fabrication costs.

At the time of writing (1992), 75% of the world demand for carbon–carbon is in the USA as a result of the large aerospace and defence industry. France, again because of its aerospace and defence interests, is the leading European producer, whereas Germany leads in the limited industrial market.

The largest producer of carbon–carbon in both volume and money terms is the British company BP, by virtue of its acquisition of the Hitco corporation. Hitco manufacture both brakes and rocket parts. Second in volume, and third in sales, is the Bendix Division of the Allied-Signal Corporation who specialize in brake production. The French company

Table 10.2 Breakdown of carbon–carbon market by application

	% *of total*	
Application	*Volume*	*Value*
Aircraft brakes	63	31
Rocket nozzles	14	31
Nose cones and ablatives	11	37
Other	12	1

SEP splits its business between rocket parts and brakes, and ranks third in the world in volume of material produced and second in sales. The company has recently entered into a technology-licensing agreement with the chemical giant Du Pont. Other significant 'players' include Avco, Dunlop, FMI, Goodrich, Kaiser Aerotech, Schunk and Sigri. A fuller listing of the various companies involved in the carbon–carbon industry is given in Section 10.6.

The major application for carbon–carbon composites are **aircraft brakes**, accounting for between 60 and 70% of the total volume (Table 10.2). Carbon brakes are several times the price of the sintered metal brakes they replace in commercial aircraft. The cost of the discs is, however, only a fraction of the cost of a completed undercarriage system. Their advantages far outweigh the increased cost. Weight savings of up to 30% may be achieved, which accounts for up to 900 kg on a Boeing 747–400 aircraft, thus making large savings in fuel costs. Carbon–carbon brakes also possess extended service lives compared with metal brakes. Almost all military aircraft now use carbon brakes. The market for commercial airliners is, of course, much larger. All of the airbus family of aircraft (A-300, 310 and 320) fly carbon brakes as do Boeing 747–400, 757, 767, McDonnell Douglas MD-11 and, of course, Concorde. Most new commercial aircraft programmes are now specifying carbon brakes.

The military brake market is now fairly mature. Aside from the introduction of new aircraft, the bulk of the market will be for refurbishment of worn brakes. Brakes are smaller on military planes as they are much smaller aircraft. Therefore less energy has to be dissipated. Carbon–carbon brakes in commercial aircraft, on the other hand, is an emerging and expanding market expected to mature by the turn of the century. Carbon–carbon composites are also used in the brakes and clutches of Formula 1 racing cars. This is not, however, considered a prime market since the majority of teams aim to receive their materials free of charge or at least at a considerable discount as a focus of advertising and PR. It is unlikely that carbon brakes will be used in passenger cars in the foreseeable future because of costs. A more likely opportunity would arise for large trucks

and, especially, high-speed trains, provided technological advancements can reduce the cost of the material to around £100 kg^{-1}. Environmental safety, improved performance and lower maintenance requirements would be the driving force of these applications.

The first applications of carbon–carbon composites were in high-temperature **rocket components**. Oxidation protection is not a critical issue in what are generally short-lived parts due to the fixed period of rocket burn. Life spans are sufficiently brief to enable 'state of the art' coatings to overcome oxidation problems, or else a 'controlled ablation' may be designed into the structure. Composites for rocket components are the most expensive, requiring a very high (graphitized) density of 1.9–2.0 g cm^{-3} to provide ablation resistance. Materials costs in excess of £1000 kg^{-1} are not uncommon.

Each of the USA's space shuttle vehicles employs roughly 750 kg of silicon carbide protected carbon–carbon in its leading edges and nose cone. Although the USA only plans to replace the *Challenger*, the EC, the former Soviet Union and Japan all have plans for similar vehicles. Doubtless, all of these vehicles would use carbon–carbon leading edges, as would any of the proposed transatmospheric airliner projects should they come to fruition.

Carbon–carbon composites could be used very effectively in high-performance jet engines to improve efficiency by reducing weight and increasing operating temperatures. The jet engine market could easily mature into a £100m. per annum business by the turn of the century provided the oxidation problem can be solved. The technological problems of providing a truly reusable high-temperature carbon–carbon system are further amplified by funding which, in the main, is provided by the military and therefore subject to the whims and discretion of politicians. Although actively researched, the only carbon–carbon to date in this application are vectoring nozzles for the afterburner of jet fighter aircraft engines produced by Pratt and Whitney, which proved unsuccessful due to material inconsistency.

Carbon–carbon has the potential for widespread use in biomedical prosthetics devices. Composites may be fabricated to possess similar stiffness to bone and can be demonstrated to be not only biocompatible but **bioactive** being porous enough for bone and tissue to grow into and anchor. The German company Schunk has carried out a great deal of work into the fabrication of carbon–carbon hip joints. Carbon–carbon prosthetics are limited by their brittleness, difficulties in effective stress analysis and cost. Further, gaining approval and qualification from the various national medical authorities is a very slow process. World sales of prosthetics account for sales of some £150m. but carbon–carbon will face stiff opposition from thermoplastic resin matrix composites which, although less biocompatible, are cheaper and easier to work with.

Table 10.3 Breakdown of production costs for a mid-price-range (£300 kg^{-1}) carbon–carbon composite

	Percentage of cost
Carbon fibres	17
Weaving	17
Matrix precursor	2
Fabrication	40
Protective coating	12
Pretax profits	12

Carbon–carbon composites are far too expensive to find use in passenger cars in the foreseeable future. They may find a limited use in racing car engines, however, as for example, pistons, provided oxidation and erosion can be overcome. Reciprocating carbon–carbon engine parts would improve efficiency by allowing higher operating temperatures coupled with dimensional stability and self-lubrication. Finally, a small market could arise for carbon–carbon structures in the space industry – lightly loaded, stiffness-critical components such as satellite and space telescope trusses. Carbon–carbon would also be a useful armour material against laser weapons as a result of its high thermal conductivity.

10.4 COMMERCIALIZING A PRODUCT

At the present time, the number of applications of carbon–carbon composites is extremely limited. To meet the requirements for current and new uses, the materials must be competitively priced, possess attractive property and performance characteristics, be able to be fabricated efficiently to high standards of quality and provide a library of well-understood design data.

The price of carbon–carbon varies considerably, depending on the end use and method of production, etc. Aircraft braking materials are the cheapest at around £120 kg^{-1} whereas high-density three-dimensional composites used in rocket nozzles may cost in excess of £1000 kg^{-1}. Fabrication costs account for a significant proportion of the price of carbon–carbon. A lowering of fabrication costs by the introduction of more efficient technology would therefore significantly reduce the price of finished articles. Table 10.3 shows a rough breakdown of a medium-priced composite costing, say, between £300 and £400 kg^{-1}. The apportioning of costs will vary considerably as a result of the wide variety of carbon–carbon parts which may be fabricated. The data do, however, serve to illustrate how finished component prices may be reduced by improvements in the various contributing factors.

Carbon–carbon raw material costs vary according to the type and geometries of fibres and matrix precursor. Carbon fibres range in price from around £10 kg^{-1} for chopped low-strength fibres to over £300 kg^{-1} for continuous high modulus (HM) types. Liquid matrix precursors cost from around £1 to £1.50 kg^{-1} for phenolic resins, and up to in excess of £50 kg^{-1} for exotic high-yield polymers such as PEEK and polyphenylene. Reductions in raw materials costs only offer a relatively small potential drop in the price of the finished composite. There currently exists an overcapacity in carbon fibre production so one would expect prices to drop significantly in the foreseeable future as the suppliers fight for market share. Even when they do, only 15–20% decreases can be expected when equated to carbon–carbon production. The most widely used liquid matrix precursors are phenolic resins which are very cheap and would not be thought to change much, if at all, in price. It is possible that the cost of the more exotic precursors such as acetylene-terminated resins will be reduced significantly over the next decade. Matrix precursors make very little direct contribution to the overall cost, but indirectly, in terms of how they influence fabrication, their effects are very noticeable. Resins possessing improved processability and/or carbon yield might well be introduced, despite what might be higher initial raw materials costs.

A reduction in weaving costs would correspondingly reduce composite prices. The cost of weaving varies according to weave geometry, number of dimensions and type of fibre. Two-dimensional fabrics add, on average, £5–£50 kg^{-1} to the cost of the fibres, whereas 3-D weaves may increase costs by up to an order of magnitude with angle interlocks falling somewhere between the two. It is doubtful whether the cost of fabrics will fall significantly since the processes are fairly advanced from the polymer composites industry. Three-dimensional weaving, on the other hand, ought to fall by a large amount as the technology develops.

Aside from brakes, all current applications may be described as **price-insensitive** in that they are in the main military applications where high performance can demand high premiums. In biomedical usage, materials costs can often be lost in surgical costs. Jet engines are another area in which high costs can be justified by improved performance and lower density. Prices ought to remain high in these theatres, although end-user protests and competition between manufacturers may lead to a reduction.

Carbon–carbon brake manufacturers must compete with lower-performance sintered metal and phenolic resin based brakes as well as each other. As a direct result, their costs have reduced steadily over the years. Prices vary according to quality and performance. Composites for fighter aircraft braking systems may cost up to £300 kg^{-1} while prices as low as £100 kg^{-1} have been quoted for inferior materials. Motor car brakes sell for less than £5 kg^{-1}. Even the cheapest carbon–carbon systems could not compete with this price unless their usage becomes mandatory due to

governmental edicts on safety and environmental protection. Reduction of composite costs to around £60 kg^{-1} is, however, an attainable target, making carbon–carbon economically viable for truck and train brakes. Industrial grade composites retail at around £150 kg^{-1}. Reduction in costs would lead to corresponding increases in applications such as furnace elements, high-temperature moulds, dies and machinery.

The most important properties of carbon–carbon composites are high-temperature strength coupled with low density. Design strengths and operating temperatures vary with application, many of which are extremely sensitive both militarily and commercially. Materials requirements in terms of performance are steadily increasing with respect to both thermal and mechanical properties. Developments in carbon fibres, fabrication technology and oxidation should allow carbon–carbon to meet those demands. In missile applications and, to a lesser extent, in brakes, the ablation resistance of the material is important. Such components are generally made from high-density composites with graphitic matrices. The high density and heat of sublimation of graphite allow large amounts of energy to be absorbed when a missile re-enters the earth's atmosphere or an aircraft is brought to a halt. More important for brakes are wear and frictional properties.

Carbon–carbon brakes have a coefficient of friction of around 0.5 under low energy stop conditions. The brakes wear uniformly and are not only lighter than their metal competitors they can endure longer lifetimes before they need to be replaced. Lifetime is generally not of prime concern for missile components since they will only be used once. By contrast, jet engines require part-lives in excess of 1000 h at temperatures between 1000 and 1400 °C in an oxidizing atmosphere. Any company able to solve the oxidation problem on temperature cycling will clearly have a large potential business in this area. Furthermore, the engines required for the proposed 'hypersonic' aircraft will demand even higher temperatures, perhaps in excess of 2000 °C.

Fabrication expertise, most especially the achievement of strict quality control, is a crucial requirement for the commercialization of a carbon–carbon product range. A manufacturer must clearly understand, qualitatively at least, the complex relationships between raw materials, process variables and materials properties. A more quantitative understanding will be preferable so as to allow for efficient optimization of his operations. Carbon–carbon parts may take anything up to 9 months to produce. The high-temperature equipment required will necessitate a large initial capital investment in both hardware and highly skilled personnel. It is pertinent to consider the carbon–carbon business as a highly specialized, 'bespoke' fabrication operation, where customer contacts are therefore an important key to success. The materials supplier must understand in detail the end user's requirements and applications so that the various weaving,

densification and protection processes may be tailored best to meet those requirements.

The carbon–carbon supplier must have good relations with the national government, since the majority of parts are used in military applications. Government contracts are often very lucrative and can be used to finance R&D costs and provide capital for expenditure on plant. Funding from government allows a manufacturer to develop an expertise which may, at a later date, be transferred into civilian markets. Military funding does, however, have one or two pitfalls associated with it. Difficulty may often be incurred in exporting carbon–carbon artefacts as a result of the strategic nature of the material. The administration in the USA, through its 'United States Law Preventing Export of Military Sensitive Products (ITAR) regulations', requires that all carbon–carbon researchers and manufacturers be registered with the Defence Logistics Service Centre (DLSC). The export of carbon–carbon is forbidden unless an export licence is obtained from the aforementioned organization. Indeed, no information, with respect to carbon–carbon composites, may be passed to a foreign national without government approval. The regulations have thus proved very difficult for the European companies who have entered the market via a US acquisition.

Finally, it is important that carbon–carbon producers research carefully the properties of their products and in tandem with the designers who will ultimately employ them. Design data for carbon–carbon are very limited so many designers feel very uncomfortable in specifying such unpredictable anisotropic materials. There is no typical carbon–carbon composite, rather a whole family of materials. The fabricator and designer must therefore work closely together in order to design and tailor a specific product to a specific application.

10.5 ORGANIZATION OF THE CARBON–CARBON BUSINESS

The carbon–carbon business may be divided into seven different sectors:

1. carbon fibre suppliers;
2. matrix precursor suppliers;
3. weavers;
4. prepreggers;
5. manufacturers;
6. coaters;
7. end users.

The ways in which the various sectors interact are illustrated in the flow diagram in Fig. 10.1. Carbon fibre suppliers sell products to weavers or prepreggers. Matrix precursor suppliers sell to prepreggers or directly to manufacturers. Prepreggers also supply manufacturers. Weavers may also

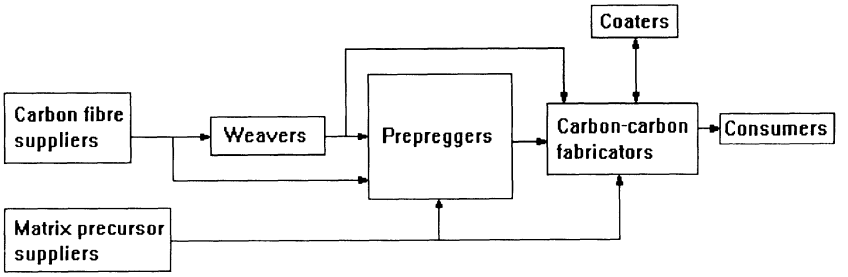

Fig. 10.1 Integration of companies involved in the carbon–carbon industry.

supply direct to the fabricators, especially 3-D preforms. Manufacturers generally contract protective coatings to outside specialist companies, although a few do coat composites in-house. Fabricators, of course, sell the completed composites to the end user. Companies active in the business often compete within a number of the market sectors. ICI (Fiberite), for example, are both a weaver and prepregger, while FMI is a fibre supplier, weaver and manufacturer. Furthermore, a number of end users are believed to be contemplating producing their own materials, unhappy at the poor quality of the raw materials with which they are supplied.

Firms generally enter the carbon–carbon market by acquiring an expertise in one of the seven business sectors. They may choose to specialize in that area, or by various processes of backward and forward integration, enter one or more of the other sectors. There are essentially three routes of entry into the business: internal development, technology licensing and acquisition or joint venture. The majority of carbon–carbon producers all have products that were originally developed internally. There is a high mobility of personnel within the business as firms 'poach' experts from their competitors in order to take a 'short cut' in development. Great care must be taken that a company has more than one expert otherwise he may be enticed elsewhere taking with him his knowledge! Generally 25% or more of the investment into a product will be required to go into R&D. Government contracts are usually used as funding and products will take at least 5 years to commercialize.

Latecomers into the market, or those with a limited technology base, may license technology from outside. Table 10.4 shows a number of firms known to be licensing aspects of their expertise to others. The US government will license its patents free of charge to firms who sell their products back to the government.

A quick entry into the business may be attained via acquisition although it is not without its problems. The acquiring company is generally required to pay a substantial premium, perhaps 20 or more times the annual earnings of the company it wishes to buy. The opportunities to acquire

Table 10.4 Licensing activity in the carbon–carbon business

Licenser	*Technology*	*Licensee(s)*
Vought	Oxidation protection	BP (Hitco)
Aerospatiale	Three-dimensional weaving	Hercules
GA Technologies	Oxidation protection	Chromalloy B.F. Goodrich Kaiser Aerotech Rohr Industries

carbon–carbon concerns are extremely limited and subject to government veto should it be deemed to 'endanger national security'. Most of the organizations involved in the business are small components of larger companies and thus difficult to capture. The purchase of smaller, privately owned, firms such as FMI would generally be easier. Notable acquisitions in recent years include Fiberite by ICI during its take-over of Beatrice Chemicals, BP's purchase of Hitco from Owens-Corning for $240m. and Amoco's acquisition of the Union Carbide carbon fibre operations. A number of firms have entered joint ventures to pool their respective resources especially in the theatre of jet engine components, most notable being the teaming of Pratt and Whitney and Hitco, and RTAC with General Electric.

10.6 MAJOR COMPANIES IN THE CARBON–CARBON MARKET

ABS (Aircraft Braking Systems) grew from Goodyear Aerospace and is one of the largest carbon–carbon brake suppliers after Hitco and Bendix. They are based in Akron, Ohio and have material on some A320 and Fokker 100 programmes.

Aerolor from France is a joint venture formed between Aerospatiale and Le Carbone-Lorraine in 1975. The company's products are densified by a variety of methods and their technology has been licensed to a number of other companies such as Hercules. Aerospatiale are particularly expert in 3-D weaving technology.

Amoco, the American oil company, has acquired the carbon fibre business formally owned by Union Carbide. They produce fibres from rayon, PAN and pitch precursors and are the dominant fibre suppliers to the carbon–carbon industry in the USA. Sold under the Thornel brand name, Amoco fibres range in price from £20 to £500 kg^{-1}.

Ashland Carbon Fibres based in Ashland, Kentucky produce pitch-based carbon fibres and fractionated pitches for use as matrix precursors. Ashland fibres are sold under the trade name of Carboflex in the form

of mat, chopped and milled grades. Aerocarb pitch, costing around £6–10 kg^{-1}, has a theoretical yield of close on 90% by weight. Ashland are engaged on a programme of research aiming to improve the quality and reproducibility of their pitches, and methods of blending them with thermosetting resins.

AVCO's speciality materials division from Lowell, Massachusetts produces PAN-based carbon fibres, called Avcarb, which are woven into satin fabrics. Carbon–carbon composites are densified using the thermoset resin and CVD processes. The company has filed a number of patents around the addition of ceramic powder to improve ablation resistance.

BASF from Germany acquired the Celion line of carbon fibres from Celeanese in the USA in 1985. These fibres are used both in polymer and carbon matrix composites. BASF also own the prepregger Narmco, situated in Anneheim in California. Narmco produce phenolic and bismaelamide precursor prepregs in addition to epoxy prepregs and other advanced materials.

The Bendix Aircraft and Strut Division is based in South Bend, Indiana and forms part of the Allied-Signal Corporation. The company produces carbon–carbon brakes from phenolic resin impregnated, chopped pitch based fibres.

BF Goodrich (Super Temp Division) produce carbon–carbon composites for use in brakes, by CVD at their plant in Alto Pueblo in Colorado. The brakes are used on the space shuttle and Boeing 747–400 aircraft. In an attempt to diversify beyond brakes they have licensed oxidation protection know-how from GA Technologies.

Borden chemicals from Columbus, Ohio produce the phenolic resin SC-1008. Originally developed by Monsanto, SC-1008 is the most commonly used thermoset resin matrix precursor, selling for between £1 and £1.50 kg^{-1}. The resin is supplied in the form of a solution containing 60% solids.

Carbon–carbon Advanced Technologies (CCAT) is owned by Alco Standard and located in Fort Worth, Texas. The company was founded by former employees of Vought Missiles and produces 2-D composites from phenolic prepreg precursors. CCAT is active in the jet engine market, producing oxidation-protected composites by impregnating partially densified substrates with pre-ceramic polymers which decompose to silicon carbide on pyrolysis.

Chromalloy Research hail from Orangeburg in New York State and are one of the largest coaters of carbon–carbon components using technology licensed from GA Technologies.

Dunlop in the UK produce carbon–carbon brakes by the isothermal CVD method which are used on Concorde and by Boeing.

Fiberite have production and research facilities in Winona, Minnesota and Tempe, Arizona and are owned by the UK's ICI. They supply a variety

of phenolic matrix precursor prepregs along with a chopped fibre brake moulding compound. In addition, Fiberite weave their own fabrics at their plant in Greenville, Texas.

Fibre Materials Inc. (FMI) are based in Biddeford, Maine, and are primarily a manufacturer of carbon–carbon substrates for use in rocket nozzles and nose cones. They also produce carbon fibres on a limited scale and have developed proprietary 3-D weaving technology. FMI were the first people commercially to exploit the HIPIC process.

The Garrett Turbine Engine Company is a division of Allied-Signal and based in Los Angeles. Garrett are evaluating carbon–carbon jet engine components supplied by LTV's Vought Missiles Division.

General atomic (GA) Technologies are located in San Diego, California and are a subsidiary of the Chevron Oil Corporation. GA undertake protective CVD coating of carbon–carbon and licenses its technology to a number of other organizations. BF Goodrich, Kaiser Aerotech and Rohr industries have all licensed complete oxidation protection systems, while Chromalloy have acquired only coating technology. The system is based on boron inhibitors, a boron-containing 'paint' and CVD-deposited silicon carbide.

General Electric from Philadelphia is yet another engine manufacturer engaged on carbon–carbon research. GE have teamed with Rohr Industries and SAIC in order to further their research.

Hercules have an outstanding reputation as a supplier of advanced composites and carbon fibres. The company are based in Salt Lake City, Utah and produce a number of carbon fibres and fabrics under their Magnamite trade name. Most notable for carbon–carbon are their range of intermediate modulus (IM 6, 7 and 8) and high modulus (HMU and UHMS) fibres made from PAN precursors. IM-6 in particular has a very high tensile strength and good dimensional stability at extreme temperatures. HMU fibres have been found to be especially suited for use in carbon–carbon. The propulsion systems division of Hercules assemble rocket motors. Historically they have bought in carbon–carbon components made elsewhere, but recently in-house production facilities have been constructed. Their plant contains HIPIC and CVD equipment along with 3-D weaving apparatus using a process licensed from Aerospatiale. In 1989 Hercules and Rohr Industries formed a joint venture company, Refractory Technology Aerospace Components (RTAC). RTAC develops and manufactures carbon–carbon rocket motor, turbine engine, missile and aerospace components.

Hitco from Gardena in California are arguably the world's largest producer of carbon–carbon. Purchased from Owens Corning by BP, Hitco concentrate mainly on brake materials which they sell almost exclusively to Aircraft Braking Systems. The majority of Hitco's production is 2-D, employing all the densification techniques except HIPIC, although this

is being extensively researched by the parent company (BP). Hitco are involved with Pratt and Whitney in developing oxidation-resistant jet engine parts.

Kaiser Aerotech from San Leandro in California produce a 2-D carbon–carbon composite called K-Karb which is used in industrial applications such as glass making.

Kobe Steel Company of Japan manufacture very high quality, high-density carbon–carbon by the HIPIC route.

Mitsubishi Kasei Corporation, based in Tokyo, produce a range of ultra-high modulus coal-tar pitch-based fibres. These fibres possess very high thermal conductivity and are used in aircraft, motor racing, passenger train and main battle tank (MBT) brakes. Mitsubishi carbon–carbon is also used in fusion reactors, space vehicles and an number of other applications. They possess expertise in all aspects of production (CVD, thermoset resin and HIPIC).

Rhône-Poulenc from France market Kerimid 601, a polyimide precursor resin with a carbon yield of 80% which is cited in a number of patents.

Rohr Industries are based in Chula Vista, California. They are teamed with general Electric for the manufacture of jet engine components. They have worked closely with SAIC in the past and are presently involved with Hercules in their joint venture company RTAC.

Schunk from Germany produce brakes, industrial and biomedical components at their plant in Giessen.

Science Applications Incorporated (SAIC) are based in San Diego in the USA, producing rocket parts and inhibited composites. SAIC are not a production company but, rather, a development house concerned with R&D for other companies and government agencies. SAIC generally employ low-pressure resin techniques and the HIPIC process.

Sigri hail from Munich and supply industrial products such as heat exchanger tubes, metal-forming moulds and furnace elements etc.

Société Européene de Propulsion (SEP) are located in France and are one of the world's leaders in carbon–carbon technology. SEP's carbon–carbon business has evolved from its work on the rocket nozzles and warheads for France's independent nuclear deterrent. The materials are marketed under the trade name SEPCARB for use in aircraft and racing car brakes and missile parts. The company is also reported to be actively researching bioimplants although, as yet, boasts no commercial products. CVD, HIPIC and low-pressure resin technologies are all employed in their various densification processes. A range of carbon–ceramic and ceramic–ceramic composites are produced, the most notable of which are C–SiC and SiC–SiC (SEPCARBINOX) which are densified by CVD.

Textron, based in Massachusetts, is a leading supplier of 3-D carbon–carbon materials for rocket nozzle integral throat entrances used in tactical, strategic and space propulsion systems.

Tonen from Tokyo in Japan, produce a range of ultra-high modulus pitch-based fibres which are used in brake manufacture.

United Technologies Corporation (UTC), in the guise of their Pratt and Whitney Division, are actively researching jet engine components. A well-documented programme involved fabrication of carbon–carbon 'afterburner' flaps for their F-100 jet engine. The parts were rejected not on cost grounds, but rather due to poor quality and reproducibility. UTC's research laboratories have demonstrated a degree of success in silicon ceramic coatings of oxidation protection using pack cementation and CVD techniques.

Vought Missiles are a division of the LTV Corporation from Dallas, Texas. They developed the 2-D carbon–carbon composite used in the leading edges and nose-caps of the space shuttle. Vought no longer produce carbon–carbon on a large scale but are engaged in extensive research programmes funded by the US government and the Garrett Turbine Company.

10.7 CONCLUSION

Carbon–carbon composites are a unique family of composite materials, retaining their mechanical properties to extremely high temperatures. This, along with a high degree of toughness and inertness, makes them ideal candidates for application in a large theatre of advanced engineering. There are, however, two major drawbacks limiting the widespread development of carbon–carbon; firstly, the fabrication processes used are extremely inefficient and secondly, they tend to oxidize quickly in air at temperatures as low as 400 °C. The cost of carbon–carbon varies from around £100 kg^{-1} to well in excess of £1000 kg^{-1} with an average of the order of £300–400 kg^{-1}. As a result, markets are limited mainly to military applications where high premiums are paid for improved performance. Surveys of the carbon–carbon business prospects have generally predicted an increasing usage of the materials well into the next century. With recent changes in the political climate, however, it remains to be seen how much of this military spending will come to pass. A number of companies are already 'feeling the pinch', finding that defence contracts are not the 'blank cheque' they once believed them to be!

It is possible to be extremely simplistic in describing the future market prospects of carbon–carbon, splitting the business into two distinct sectors. In the 'commercial' sector, usage, such as brakes, heat exchangers and furnace elements, is constrained simply by cost. There are a whole host of applications ideally suited to the properties of carbon–carbon provided the price is lowered as a result of more efficient fabrication. In the 'military' sector it is performance rather than price which is of concern. Efforts to

Table 10.5 Predicted growth for the carbon–carbon market (sales in £m.)

Business area	*1985*	*1990*	*1995*	*2000*
Brakes				
Aircraft	20	45	60	75
Land transport	—	—	5	10
Rocket components				
Exit cones	20	25	25	30
Nose cones/ heatshields	20	25	25	25
Jet engine parts	—			
Space	—	0.5	1	2
Biomedical	—	—	0.5	1
Total	60	95	117.5	143

develop oxidation-resistant carbon–carbon parts for heat engine components and the heatshields of hypersonic aircraft are intensive in the drive towards a truly reusable system. The long-term reality, however, is that carbon–carbon composites will remain highly specialized performance materials at least until the turn of the century. It is very doubtful that there will be sufficient reduction in price or advances in technology in the short to medium term to bring carbon–carbon into widespread use. Table 10.5 shows projected estimates for carbon–carbon sales up to the year 2000.

REFERENCES

1. '*Advanced Materials Technologies Report 8, Carbon–Carbon Composites*, C. H. Kline & Co. (1987).

Index